Characterisation of calcium channels

in human immune cells

A thesis submitted for the degree of PhD

Hannah Elizabeth Wajdner

Department of Biomedical Science

University of Sheffield

October 2015

Author's declaration

I hereby certify that all writing and scientific figures presented in this thesis are original works by the author, unless otherwise stated in figure legends. All research displayed was carried out and processed by the author unless directly specified. All research findings, concepts and diagrams obtained from other sources have been clearly referenced with no infringement of copyright. Permission to re-use figures from published work was sought where appropriate; figure legends when permission was granted. This statement is true at the date of submission.

Hannah Wajdner

Acknowledgements

Firstly I'd like to thank my supervisors; Liz, Karen and Malcolm for giving me the opportunity to undertake this PhD. Liz, thank you for your support, wisdom, and great ideas. Thank you for helping me to become a better scientist and for being so understanding throughout my moves to and from Sheffield. Karen and Malcolm thank you for your encouragement, training, advice and for the invaluable contributions you've made to my project. Thanks for welcoming me to GSK and giving me the opportunity to experience the industrial research environment.

Thanks to all the members of the Seward & Grundy lab, past and present, I've really enjoyed working with you all! Jasmine, you've been my go to girl from day one; I'm indebted to you for much of what I learned during my first and second year. Thank you for all your help with my project; from teaching me how to do cell culture to sharing Kreb's coffee with me on stressful days. Claudia, thank you for all your support, training and wisdom. Thanks for listening to my moaning on bad days and for your helpful ideas about experiment issues. Reuben, thank you for all the LAD2 help over the years and for showing me how to stay chilled whilst doing a PhD! Marta, it's been lovely working with you, thanks for the many lunch break chats and for instigating communal cafeterie coffee! Finally, Donna, although not a Seward lab member you've also been a great support from day one. Thanks for your wise words and encouragement throughout the past 4 years.

I've greatly benefited from help and training from many friendly faces at GSK. Thanks for everyone in AI and RRI DPU for being so willing to help me with my experiments and for making me feel at home during my placements. In particular, thanks to Simon, Ben, Aga and Katie who have taught me a lot about the world of macrophages. I'm looking forward to working with you all again soon!!

Finally, I'd like to thank my friends and family. Thanks to Mum, Dad, Becky and James for listening to my PhD woes and calcium channel chat. Dad, thank you for challenging me to think logically and to Mum thanks for calm advice during experiment freak outs. Thanks to all my friends in Sheffield, York and Leicester who've reminded me that there's more to life than science and thanks to those who have prayed for me over the years. Last but not least, thank you to Ben. Despite what you say, I couldn't have done any of this without your support and prayer. Thank you for your unwavering confidence in me, for making me smile when things were tough and for being so understanding whenever I had to work late or over weekends. Here's to our next adventure ;-)

Abstract

The aim of the work described in this thesis was to investigate and characterise novel aspects of calcium (Ca^{2+}) signalling in human immune cells. Ca^{2+} influx has important roles in directing intracellular signalling, therefore controlling cellular functions, consequently delineating the channels mediating Ca^{2+} influx is important. My work has focused on Ca^{2+} signalling in mast cells and macrophages, two cell types which have been demonstrated to be important contributors to respiratory disease such as asthma and COPD, respectively. Advancement in understanding of the signalling factors regulating mast cell and macrophages has an important application. The results from my study encompass three separate research areas and I report three novel contributions that further the understanding of Ca^{2+} signalling in immune cell biology.

Inappropriate activation of the FcεRI, found predominantly on mast cells, is a crucial link between mast cells and allergic disease. Inappropriately activated mast cells release proinflammatory mediators leading to symptoms of allergic disease. Consequently mediators locally released in the lung contribute to symptoms of asthma such as bronchoconstriction, mucus production and inflammation (Barnes, 2008). A store-operated Ca^{2+} channel (SOCC), Orai, has recently been implicated in IgE-mediated Ca^{2+} signalling in rodent and human mast cells and importantly, the Orai channel was shown to be crucial for mast cell mediator release (Ashmole *et al.*, 2012). These recent findings therefore implicated Orai as a potential therapeutic target for the treatment of IgE-mediated allergic disease. Another cation channel family, also shown to be capable of mediating Ca^{2+} signalling downstream of the FcεRI are TRPC channels. Previous studies have implicated TRPC channels as coupled to Orai in their activation and studies in rodent mast cells have implicated TRPC channels with a role in FcεRI-mediated mediator release (Ma *et al.*, 2008; Sel *et al.*, 2008; Cohen *et al.*, 2009; Suzuki *et al.*, 2010b; Yildirim *et al.*, 2012; Medic *et al.*, 2013). However there is limited research focused on the contribution of TRPC channels to IgE-mediated signalling in human mast cells. Novel work in this thesis has shown that although TRPC channel family members are expressed in human mast cells, TRPC channels make no contribution to IgE-mediated Ca^{2+} signalling in human mast cells. These data have provided important evidence to suggest that unlike the Orai channel, TRPC channel(s) do not represent a therapeutic target for the treatment of IgE-mediated allergic disease, such as asthma. Similarly this work has provided important information which has increased the current understanding of the signalling components involved in allergic mast cell activation.

In comparison to other immune cells such as the T cell and mast cell, the study of Ca^{2+} signalling in macrophages has been neglected. Macrophages have important roles in innate immune defence; directing phagocytosis and inflammatory cytokine release to protect the body following pathogen attack. Therefore identifying modulators of macrophage biology is a crucial component in understanding how macrophages are regulated. Ca^{2+} channels such as Orai could represent vital components involved in aspects of macrophage activation. Store-operated Orai Ca^{2+} channels have been indicated to be active in rodent macrophage cells, however to date the role of Orai channels in human macrophage biology has not been studied. This study addresses this gap in the current knowledge. My results have shown

that Orai (and its crucial activator protein, STIM) are expressed at mRNA level in human monocyte derived macrophages (hMDMs), importantly I demonstrate the functional activity of Orai-mediated Ca^{2+} signalling and identify Orai-mediated Ca^{2+} signalling as a contributor downstream of Immunoglobulin-G receptor (FcγR) activation. Interestingly, Orai was shown to be a significant contributor to the regulation of pHrodo® labelled *Escherichia coli* (*E. coli*) phagocytosis by interferon-γ (IFNγ) primed hMDMs. Orai inhibition however, had no effect on the cytokine release induced by lipopolysaccharide (LPS) or LPS + Anti-Immunoglobulin G (Anti-IgG). This work has provided important evidence for Orai activity in aspects of human macrophage biology and has given key evidence to direct further work in the field. Similarly in respect to respiratory disease, as Orai has been implicated as a potential therapeutic target for treatment of allergic disease such as asthma, understanding how Orai inhibition would affect other immune cells resident in the lung represents a crucial aspect of identifying the risk of Orai inhibition.

Macrophages have been implicated as crucial contributors in the pathogenesis of COPD, with an increase in macrophage numbers seen in COPD patients as well as an inappropriate release of proinflammatory mediators caused in response to cigarette smoke. Another regulator of Ca^{2+} signalling, the purinergic receptor family member has also been associated with COPD. P2X7 and its ligand ATP have been linked in the pathogenesis of COPD, with attenuation of P2X7 activity showing protective effects against symptoms associated with COPD and increased P2X7 expression and ATP concentrations in COPD patients (Lommatzsch *et al.*, 2010 ; Cicko *et al.*, 2010 ; Mortaz *et al.*, 2009 ; (Eltom *et al.*, 2011). Despite the evidence suggesting P2X7 inhibition is a potential therapeutic target to treat COPD, evidence from rodent models suggest there is an implicit risk in interfering with macrophage regulated bacterial handling by P2X7 inhibition. Therefore my study has sought to further investigate the role of P2X7 in human macrophage Ca^{2+} signalling and bacterial handling in order to increase understanding about the consequences of P2X7 inhibition. The results show that P2X7 does not significantly contribute to purinergic Ca^{2+} signalling in hMDMs and similarly that P2X7 inhibition had no effect on the phagocytosis of *E. coli*. However, preliminary evidence suggests P2X7 does contribute to ATP mediated Ca^{2+} signalling in human alveolar macrophages (hAMs). These results have provided data which has emphasised the importance of the translation of findings into human tissue resident cells, in particular for therapeutic target validation studies.

In sum, the work described in this thesis shows novel findings which make significant advancements in the knowledge of ion channels in immune cell biology. Importantly the results of this thesis also provide strong evidence to aid direction for further work in the field.

Abstract

Abbreviations

(5-LO) 5-lypoxygenase
(ADCC) antibody-dependent cell-mediated cytotoxicity
(Akt) protein kinase B
(Anti-IgG) anti-Immunoglobulin G
(ARDS) acute respiratory distress syndrome
(ASM) airway smooth muscle
(ATP) adenosine triphosphate
(BALF) broncho-alveolar lavage fluid
(BBG) brilliant blue G
(BMDMs) murine bone marrow derived macrophages
(BMMCs) bone marrow-derived murine mast cell
(BSA) bovine serum albumin
(Ca^{2+}) calcium
(CAD) CRAC activating domain
(cADPR) cyclic ADP Ribose
(CaSR) Ca^{2+} sensing receptor
(Cav1) Caveolin-1
(CCL) chemokine C-C motif ligand
(CLL) chronic lymphocytic leukemia
(Co-IP) co-immunoprecipitation
(COPD) chronic obstructive pulmonary disease
(COX) cyclooxygenase isoenzmes
(CR) complement receptors
(CRAC) Ca^{2+} release-activated Ca^{2+}
(Csf1) colony-stimulating factor 1
(Csf1op/op) colony stimulating factor-1 osteopetrotic mice
(CST) cytometer set-up and tracking
(CXCL) C-X-C motif chemokine ligand
(CXCR) C-X-C motif chemokine receptor
(DCs) dendritic cells
(DMEM) Dulbecco's modified eagles media
(*E. coli*) escherichia coli
(ECM) extracellular matrix
(EDTA) ethylenediaminetetraacetic acid
(EGF) epidermal growth factor
(ER) endoplasmic reticulum
(ERK) extracellular-signal-related-kinase
(FCS) foetal calf serum
(FcyR) Immunoglobulin-G receptor
(FFA) flufenamic acid
(FLIPR) fluorometric Imaging Plate Reader
(GAB2) GRB2-associated-binding protein 2
(GM-CSF) granulocyte-macrophage colony-stimulating factor
(GPCR) G-protein coupled receptor
(GRB2) growth receptor-bound protein 2
(GWAS) genome wide association study
(hAMs) human alveolar macrophages

(HBSS) Hank's buffered salt solution

(HDAC-2) histone deacetlyase

(hMDMs) human monocyte derived macrophages

(HSCs) haematopoeitic stem cells

(HSG) human salivary gland

(ICS) inhaled corticosteroids

(IFNγ) interferon γ

(IgE) immunoglobulin E

(IL) interleukin

(IP$_3$) inositol trisphosphate

(IRAK) interleukin-1 receptor-associated kinase

(ITAM) immunoreceptor tyrosine based activation motifs

(IκBα) nuclear factor of kappa light polypeptide gene enhancer in B-cells inhibitor, α

(JNK) c-Jun N terminal kinase

(KC) keratinocyte-derived chemokine

(LABA) long acting β 2 adrenoceptor agonists

(LAMA) long acting muscarinic antagonists

(LAMP) lysosomal-associated membrane protein 1

(LAT) linker for activation of T cells

(LPS) lipopolysaccharide

(LTC) leukotrienes

(M. bovis BCG) mycobacterium bovis bacillus calmette–guérin

(*M. tuberculosis*) mycobacterium tuberculosis

(MAPK) mitogen-activated protein kinase

(MCP-1) monocyte chemoattractant protein-1

(M-CSF) macrophage colony-stimulating factor

(MFI) mean fluorescent intensity

(Mg^{2+}) magnesium

(MHC) major histocompatibility complex

(MIP-2) macrophage inflammatory protein-2

(MIP3α) macrophage inflammatory protein-3α

(MMP-9) matrix metalloproteinase-9

(MyD88) myeloid differentiation primary response gene 88

(M-β-CD) methyl-β-cyclodextrin

(Na$^+$) sodium

(NAADP) nicotinic acid adenine dinucleotide phosphate

(NFκB) nuclear factorκB

(NFAT) nuclear factor of activated T cells

(NLRs) nucleotide binding oligomerisation domain like receptors

(NMDG) N-methyl-d-glucamine

(NMMHC-IIA) non-muscle myosin heavy chain IIA

(NO) nitric oxide

(oATP) oxidised ATP

(ORMDL3) orosomucoid like 3

(PAGE) polyacrylamide gel electrophoresis

(PAMPs) pathogen-associated molecular patterns

(PBS) phosphate buffered saline

(PDGF) platelet-derived growth factor

(PE) phycoerythrin

(PGD) prostaglandins
(PGN) peptidoglycan
(PI3K) phosphoinositide 3-kinase
(PIP2) phosphatidylinositol-4, 5-bisphosphate
(PKC) protein kinase C
(PLA2) phospholipase A2
(PLCγ) phospholipase γ
(PM) plasma membrane
(PPADs) pyridoxalphosphate-6-azophenyl-2', 4'-disulfonic acid
(PPARγ) peroxisome proliferator-activated receptors
(PRRs) pattern recognition receptors
(RLRs) retinoic acid inducible gene like receptors
(RNS) reactive nitrogen species
(ROS) reactive oxygen species
(SAM) sterile α motif
(SARAF) SOCE associated regulatory factor
(SCF) stem cell factor
(SCID) severe combined immunodeficiency
(SDS) sodium dodecyl sulfate
(SelK) selenoprotein
(SERCA) sarcoendoplasmic reticulum Ca^{2+} transport ATPase
(SH2) src homology 2
(SNAP) soluble NSF attachment protein
(SNARE) soluble N-ethylmaleimide-sensitive factor Attachment Protein Receptor
(SNP) single nucleotide polymorphism
(SOAR) STIM-Orai activating regions
(SOCC) store-operated Ca^{2+} channels
(SOCE) store-operated Ca^{2+} entry
(SR) sarcoendoplasmic reticulum
(Syk) spleen tyrosine kinase
(TGF-β) transforming growth factor-β
(Th2) T-helper type 2 cells
(TIRAP) toll/interleukin-1 receptor domain-containing adapter protein
(TIRF) total internal reflection fluorescence
(TLR) toll like receptor
(TM) transmembrane
(TNFα) tumour necrosis factor α
(TRAM) TRIF–related adaptor molecule
(TRIF) TIR-domain-containing adapter-inducing interferon-β
(TRP) transient receptor potential
(TSLP) thymic stromal lymphoprotein
(VAMP) vesicle-associated membrane protein
(V-ATPase) vacuolar type ATPase
(VEGF) vascular endothelial growth factor
(VSMCs) vascular smooth muscle cells
(WT) wild-type
(Zn^{2+}) zinc

Table of Contents

List of Figures

Chapter 1: Introduction

Chapter 2: Materials and methods

Chapter 3: TRPC in human mast cells.

Chapter 4: P2X7 in human macrophages

Chapter 5: Orai in human macrophages

1 Chapter 1 – Introduction

1.1 General introduction

1.1.1 Respiratory disease & key immune cells involved

Ca^{2+} signalling has been demonstrated to have key roles in the control of immune cells. The studies described in this thesis addressed three novel aspects of research on Ca^{2+} signalling in immune cells, with the intention of increasing the understanding of immune cells associated with respiratory diseases such as COPD and asthma. Ca^{2+} channels found to have important functional roles could represent novel drug targets as a way to modulate aberrant immune cell activity in immune disease or conversely could be identified as channels whose activation are crucial to maintain for immune system homeostasis. COPD and asthma are both characterised by airway obstruction, with a progressive and irreversible obstruction in COPD and a variable and reversible obstruction in asthma. Coupled to airway obstruction is chronic inflammation of the respiratory tract caused by the release of proinflammatory mediators from a number of cell types.

Asthma has a global prevalence of up to 18% and is expected to affect up to 400 million people worldwide by 2025 (McIvor, 2015), it therefore represents a significant burden on healthcare providers. One of the main cells implicated in the pathogenesis of asthma is the mast cell; other key cells involved are T-helper type 2 cells (Th2) and eosinophils. Allergens are heavily implicated with the symptoms of asthma – with an inappropriate immune response occurring to normally innocuous stimuli. Mast cells express a receptor involved in detecting antibodies made against allergic stimuli, the high affinity immunoglobulin E receptor (FcεRI). It is activation of this FcεRI which culminates in the production of proinflammatory mediators associated with bronchoconstriction. For example, preformed mast cell mediators such as histamine and newly synthesised mediators such as prostaglandins (PGDs) and leukotrienes (LTCs) have direct bronchoconstrictory functions. There are two stages of asthma reported, with the first driven by the preformed mediators and the second later and longer lasting response caused by the release of newly synthesized mediators (O'Byrne et al 2009). Cytokines such as interleukin -4, -5 and -13 (IL-4, IL-5 and IL-13) are typically associated with asthma and are crucial for driving B cells to undergo immunoglobulin class switching to produce immunoglobulin E (IgE) and in driving eosinophilic differentiation (Barnes, 2008). Key cells and mediators implicated in the pathophysiology of asthma is showed in ***Figure 1.1.*** Activation of the FcεRI represents a crucial step in the initiation of asthmatic symptoms, therefore understanding the signalling associated with this receptor is crucial if receptor modulation is desired.
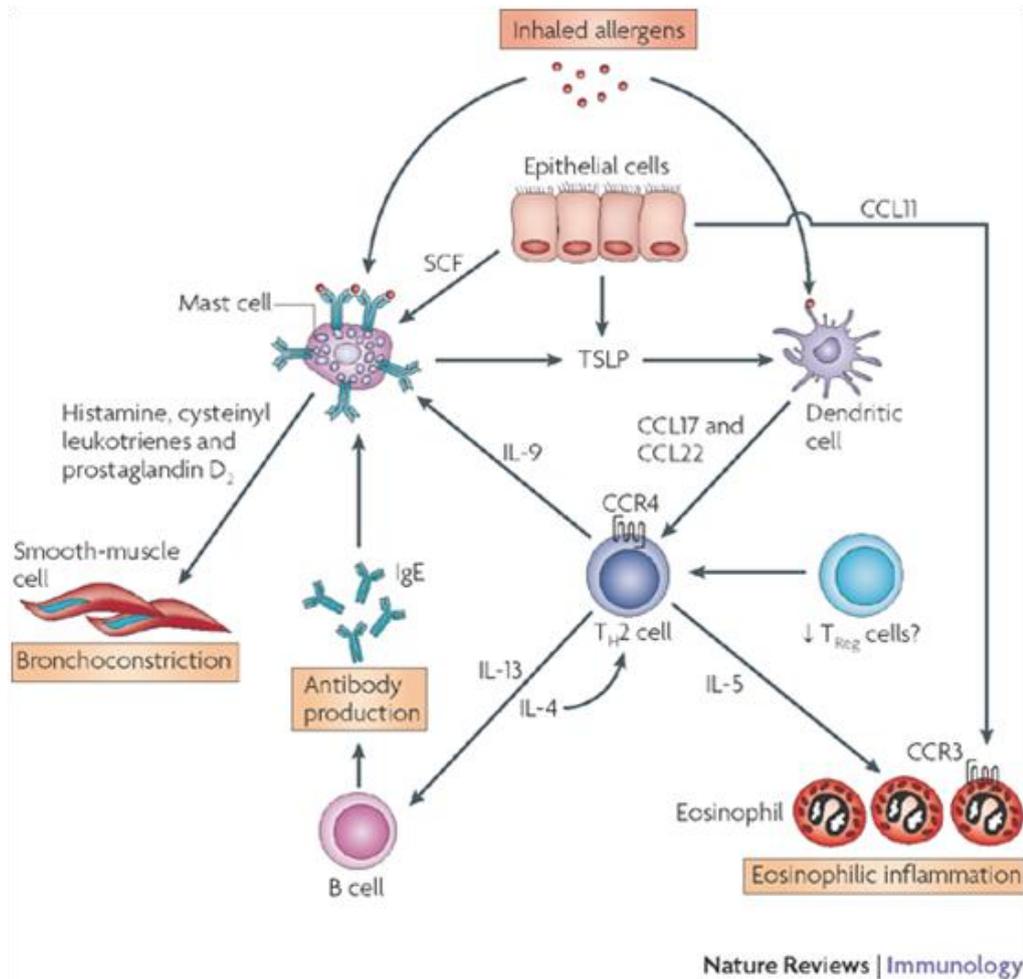
Figure 1.1   Schematic diagram showing key cells implicated in the pathophysiology of asthma

Reproduced with permission from (Barnes, 2008).

COPD encompasses a group of airway pathologies; chronic bronchitis, bronchiolitis and emphysema. COPD affects 8% of the world's population and is the 3rd leading cause of death worldwide (Barjaktarevic *et al.*, 2015). COPD pathogenesis is largely associated with smoking, as components from cigarette smoke are implicated in the activation of lung resident cells and subsequent release of inflammatory mediators such as IL-1β and IL-8 and chemotactic mediators to attract circulating neutrophils and monocytes in the lung. Whilst asthma is associated with Th2 cytokine response, COPD is typically Th1 mediated. Several cells are implicated in the pathogenesis of COPD including: macrophages, DCs, epithelial cells, neutrophils, eosinophils and T & B lymphocytes. A key cell implicated is the macrophage, which is shown to be increased by 5-10 fold in the lung of COPD patients. Macrophages contribute to symptoms of COPD through the release of proinflammatory mediators but are also have impaired capability in phagocytosis of bacteria and apoptotic cells. This suggests they also contribute to the increased susceptibility to bacterial infections as seen in COPD patients, which is the main cause of disease exacerbations

(Barnes, 2014). A diagram summarising the key cells and mediators that contribute to COPD pathophysiology is shown in **Figure 1.2.**
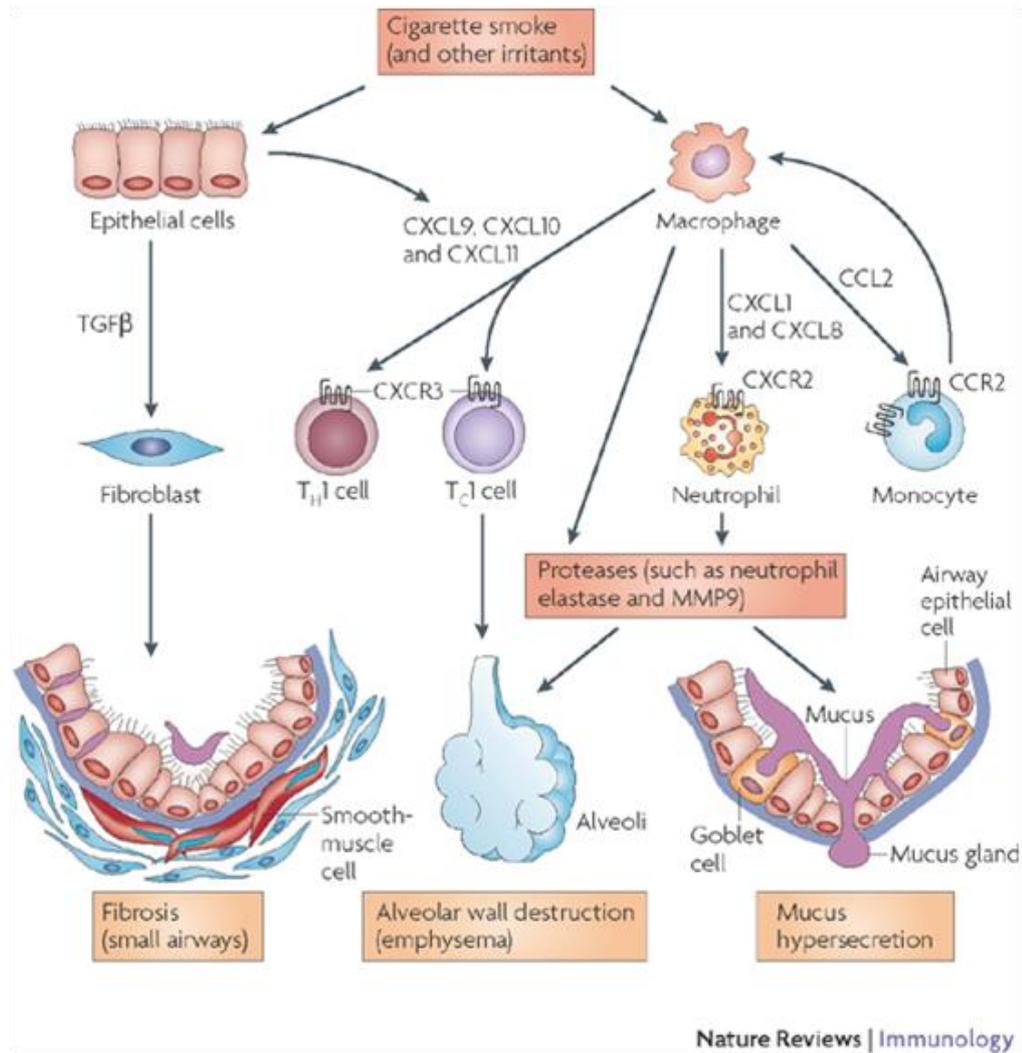
Figure 1.2　　　　**Schematic diagram showing key cells implicated in the pathophysiology of COPD**

Reproduced with permission from (Barnes, 2008).

Current pharmacological treatments for asthma and COPD include short or long acting bronchodilators and inhaled corticosteroids (ICS), which act to relax and open the airways and to decrease chronic inflammation, respectively. Long acting bronchodilators can be classified into long acting muscarinic antagonists (LAMA) and long acting β 2 adrenoceptor agonists (LABA), a wide range of LAMA and LABA monotherapies are available and similarly combination therapies of LABA and LAMA and LABA-ICS have been approved. Novel inhalers to improve delivery and treatment compliance are being marketed alongside these compounds (Barnes, 2010; Barjaktarevic *et al.*, 2015; Weinstein, 2015). Notably, ICS are largely inadequate in the suppression of chronic inflammation in COPD and asthma (Marwick *et al.*, 2010). It is thought that this is a consequence of oxidative stress which

impairs the glucocorticoid co-repressor histone deacetylase (HDAC-2) and subsequently prevents ability of glucocorticoids to mediate transrepression of proinflammatory genes. In COPD it is shown that cigarette smoke is involved in reducing HDAC activity (Marwick *et al.*, 2010; Barnes, 2011).

Despite progress in therapeutics for respiratory diseases there remains a need for more effective therapies. In order to find new medicines to treat asthma and COPD, a better understanding of pathophysiology of the disease and the biology of the key cells implicated with roles in disease progression is required. To this end, Ca^{2+} channels were characterised in two immune cell types, mast cells and macrophages, which are implicated with key roles in asthma and COPD, respectively. Although theoretically Ca^{2+} channels could represent targets to treat both asthma and COPD, there is equal value in characterising Ca^{2+} channels in immune cells as a way to discharge or identify the risk associated with modulating Ca^{2+} channel activity common to both cell types. Similarly as there are many areas of Ca^{2+} signalling biology in mast cells and macrophages that have not yet been investigated, research to complete gaps in the current knowledge provides important information from a basic science perspective.

1.1.2 Importance of Ca^{2+} signalling in immune cell function

Studies investigating human patients with mutations in ion channels, gene-targeted mouse models and the use of ion channel inhibitors have demonstrated how important ion channels are in immune cells; both in their development and in regulating innate, adaptive and allergic immune responses (Feske *et al.*, 2015). Ca^{2+} influx is a critical second messenger in intracellular signalling cascades and is involved in directing functions ranging from the production of enzymes and transcription factors to regulated secretion. Other divalent cations such as Mg^{2+} and Zn^{2+} also have similar signalling roles. The membrane transport of other ions such as Na^+ and K^+ are responsible for the control of the cell's membrane potential, which is indirectly responsible for immune cell signalling through control of ion channel electrochemical gradients (Feske *et al.*, 2015). Although the role of Ca^{2+} is to direct intracellular signalling events, Ca^{2+} influx following receptor activation also causes depolarization of the cell membrane which can lead to a disruption to the electrochemical driving force for further entry. It is largely the efflux of K^+ through K^+ channels that is responsible for hyperpolarizing the membrane potential and providing the driving force to maintain Ca^{2+} influx (Vig & Kinet, 2009; Feske *et al.*, 2015).

There are many different types of Ca^{2+} channels, which, depending on their mode of activation, are classified as ligand-gated ion channels, voltage-gated ion channels, capacitative (store-operated) ion channels and stretch-activated ion channels. Generally speaking, voltage-gated Ca^{2+} channels are predominantly expressed in electrically excitable cells such as neurons and cardiomyocytes. Ligand and store-operated ion channels are ubiquitously expressed but are the main ion channel type reported in non-excitable cells such as immune cells. Even within the ligand and store-operated ion channel subgroup there are numerous distinct Ca^{2+} channels families with differing modes of activation and

signalling roles. The diagram below *(Figure 1.3)* shows examples of different Ca^{2+} channel families and some of the key proteins involved in modulating Ca^{2+} signalling (From Vig and Kinet 2009).
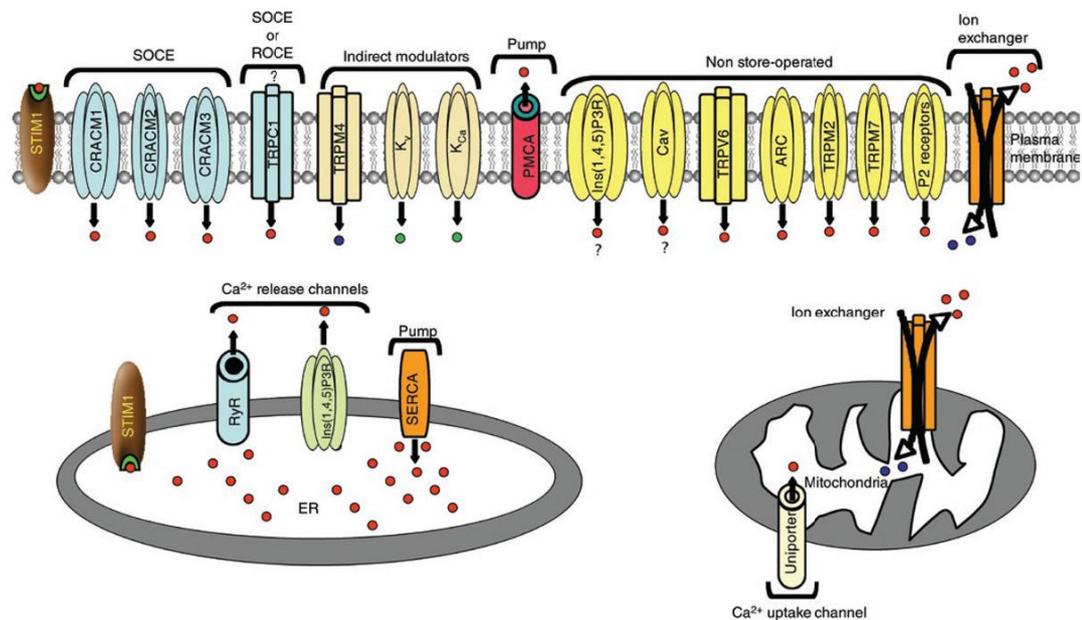
Figure 1.3   **Schematic diagrams showing common routes of Ca^{2+} influx and efflux**

Routes with similar mechanisms of activation are grouped together here. Reproduced with permission from (Vig & Kinet, 2009)

Red dots, Ca^{2+}; blue dots, Na+; green dots, K+. ROCE, receptor-operated Ca^{2+} entry; Kv, voltage-gated K+ channel; KCa, Ca^{2+}-activated K+ channel; PMCA, plasma membrane Ca^{2+} ATPase; Ins(1,4,5)P3R, Ins(1,4,5)P3 receptor; TRPV6, transient receptor potential, vanilloid, member 6; ARC, arachidonate-regulated, Ca^{2+}-selective; P2 receptors, purinergic receptors; RyR, ryanodine receptor; SERCA, sarco-endoplasmic reticulum Ca^{2+} ATPase; ER, endoplasmic reticulum.

Ca^{2+} signalling has been recognised to have critical roles in immune cells, ranging from the degranulation of preformed mediators from mast cells (Vig & Kinet, 2009), to T lymphocyte induced cytokine production (Feske, 2009) and neutrophil chemotaxis (Lindemann *et al.*, 2013), to give a few examples.

Aberrant Ca^{2+} signalling and homeostasis are known to be contributing factors to the pathophysiology of immune disease. For example; an endoplasmic reticulum (ER) resident transmembrane (TM) protein, orsomucoid like 3 (ORMDL3). This gene regulates ER homeostasis by sarcoendoplasmic reticulum (SR) Ca^{2+} transport ATPase (SERCA2b) inhibition and was identified through a genome wide association study (GWAS) study as a gene with a gain of function single nucleotide polymorphism (SNP) commonly found in

sufferers of childhood asthma (Moffatt *et al.*, 2007). In Jurkat T cells, over expression of ORMDL3 was shown to reduce store-operated Ca^{2+} entry (SOCE), however the basal Ca^{2+} levels were increased and there was an enhanced unfolded protein response (Carreras-Sureda *et al.*, 2013). ORMDL3 over-expression has since been shown to increase levels of airway remodeling and airway hyper responsiveness in mice models (Miller *et al.*, 2014). This shows the potential implication of the dysregulation of a protein associated with Ca^{2+} homeostasis.

Similarly, enhanced intracellular Ca^{2+} ion concentration has been reported in airway smooth muscle (ASM) cells from asthma patients, with an effect on enhanced bronchoconstriction and an association with ASM cell proliferation and extracellular matrix (ECM) deposition. The G-protein coupled receptor (GPCR) Ca^{2+} sensing receptor, (CaSR) is traditionally associated with its role in the regulation of parathyroid hormone secretion and is known to be activated by extracellular Ca^{2+} concentration, it can also respond to other stimuli such as polyvalent cations, amino acids and pH. A recent study has implicated the CaSR with a potential role in asthma. CaSR was shown to be expressed in human and mouse airways with an increased expression in asthmatic donors. Notably polycations were shown to activate the human CaSR in human ASM cells as assessed by Ca^{2+} signalling and CaSR inhibitors, calcilytics were demonstrated to abrogate the signalling pathways characteristic of airway contractility in asthma, whilst knockout of CaSR in ASM cells was protective against polycation induced bronchoconstriction. Calcilytics were also shown to reduce AHR and inflammation in an ovalbumin allergic mouse model (Yarova *et al.*, 2015). Together these studies emphasise how aberrant Ca^{2+} homeostasis is linked to immune and respiratory disease.

There are also direct examples of where anomalous Ca^{2+} channel activity has been implicated as a cause of disease. The members of the transient receptor potential (TRP) channel family have long been recognised as capable of mediating Ca^{2+} influx and increasingly of being associated with respiratory disease. TRP family members such as TRPA1, TRPV1, TRPV4 and TRPM8, although originally principally associated with neuronal cells, have now been shown to be expressed in mouse and human lung. Interestingly many of the activators of TRP channels; for example low pH, osmolarity changes, temperature alteration and factors associated with reactive oxygen species (ROS), are altered in airway disease. This indicates that aberrant activity of TRP channels and related inappropriate Ca^{2+} signalling may be a contributing factor to respiratory disease. A recent study demonstrated TRPA1 to have a role in mediating cough associated with environmental and occupational exposure (Grace *et al.*, 2014). The highlights the importance of TRP channel family members in respiratory disease, although there is a lack of understanding regarding TRPC family contribution of immune disease, something my study aims to address.

An immune disease caused directly by impairment of a plasma membrane Ca^{2+} channel was shown in a subset of patients with a severe combined immunodeficiency (SCID) like phenotype. SCID is most often associated with defective development of functional T and B cells, leaving patients with a severe susceptibility to infections. The X-linked form of SCID is associated with mutations in the γ chain of cytokine receptors and this is common to

around half of the cases of SCID. However autosomal recessive mutations in the Orai1 and stromal interaction molecule 1 (STIM1), two proteins shown to be crucial for conducting SOCE were also shown to have a SCID like phenotype and immunodeficiency symptoms manifested as recurrent severe infections with viral, bacterial, mycobacterial and fungal pathogens (Feske, 2009). T cells from patients with mutations in Orai1 were shown to be defective in SOCE and T cell activation was impaired. Lymphocyte numbers were normal however, suggesting Orai1 and STIM1 are not crucial for lymphocyte development. Patients with mutations in Orai1 and STIM1 were reported not to survive past their first year of life, STIM1 and Orai1 deficient mice were shown to die perinatally. Orai1 and STIM1 were also associated with a role in skeletal muscle function and development, with myopathy reported as a severe symptom in Orai1 or STIM1 mutation patients (Feske *et al.*, 2010). This illustrates a direct example of Ca^{2+} channel impairment causing immune disease. Together, these studies emphasise the importance of Ca^{2+} homeostasis for immune cell regulation and illustrate the impact of research in this area.

1.1.3 Thesis summary

The important role of Ca^{2+} signalling in maintaining immune homeostasis is emphasised by the studies described above. However there are numerous gaps in the current understanding regarding the role of Ca^{2+} in immune cell control. With the application of respiratory disease in mind, my work has focused on three specific original research areas:

1. Identification and characterisation of TRPC channel contribution to FcεRI-mediated signalling in human mast cells

2. Investigation of P2X7 contribution to purinergic Ca^{2+} signalling and bacterial handling in human macrophages.

3. Identification and characterisation of Orai channels to Ca^{2+} signalling and function in human macrophages

A summary of these three studies is described in the **Abstract**, however the key novel findings of these pieces of research can be summarised as followed. Firstly TRPC1 & 6 channels are expressed in human mast cells but are not significant contributors to FcεRI-mediated signalling. Secondly, P2X7 channels do not significantly contribute to purinergic Ca^{2+} signalling or *E. coli* phagocytosis in hMDMs nevertheless preliminary data suggests P2X7 is a functional contributor to purinergic signalling in hAMs. Thirdly, Orai-mediated Ca^{2+} signalling is active in IFNγ primed hMDMs and a significant contributor to Anti-IgG signalling. Orai-mediated Ca^{2+} signalling is involved in the control of *E. coli* phagocytosis in IFNγ primed hMDMs.

The rest of this introduction will summarize the current knowledge of the cell types and ion channels that is relevant to this investigation namely; mast cells and macrophages, Orai, TRPC and P2X channels.

1.2 Introduction to mast cell biology

Since their discovery in the 1800s there has been much learned about mast cell biology, *Section 1.2* summarises some key areas of mast cell biology that are pertinent to this thesis.

1.2.1 Mast cells; discovery, derivation and heterogeneity

Mast cells were first identified by Paul Ehrlich in the 1800s; his identification was based on their characteristic and distinctive cytoplasmic granules. Ehrlich gave mast cells their name 'mastzellen', after the Greek meaning of mast – 'to feed', as he had mistakenly characterised the cells as cells with phagocytic ability. Mast cells develop from CD34+/CD117+ pluripotent progenitor cells found in the bone marrow. In order to undergo full maturation, human mast cells require KIT activation – through binding of the stem cell factor (SCF) ligand to the c-KIT receptor. This translates that mast cells kept in culture conditions require SCF supplementation for their survival. Interestingly, mouse mast cells can be cultured in the presence of IL-3 instead of SCF; this iterates some of the differences seen in rodent and human immunology. For full differentiation *in vivo*, mast cells migrate to their final location in peripheral tissues. Once there, cytokines released from cells in the surrounding milieu initiate the final differentiation process. As long as a supply of SCF is maintained, mast cells *in vivo* are relatively long lived (Gilfillan *et al.*, 2011a). Mast cell heterogeneity is based on the tissue of residence, however broadly speaking mast cells are classically characterised according to the levels of chymase and tryptase present:

- MC_T mast cells = tryptase only. Most frequently found in respiratory and intestinal mucosa
- MC_{TC} mast cells = tryptase and chymase. Most frequently found in the skin, synovium, conjunctiva, lymph nodes, sub mucosa, stomach and intestine.
- MC_{Cc} mast cells = chymase only. Found in mucosal tissue of stomach, intestine and colon.

Although mast cell maturation is dependent on peripheral tissue location, it is likely that mast cells retain phenotypic flexibility in order to respond to changes in the environment (Beaven, 2009).

1.2.2 Mast cell functions in innate and adaptive immunity

Mast cells have a wide range of functions in the immune system, largely instigated by mediator release. Although more commonly known for their role in allergic disease and hypersensitivity, mast cells also have role in innate and adaptive immunity and in angiogenesis, wound healing and tumor growth. Their ability to have such wide ranging functions is a consequence of their flexible and diverse expression of activating receptors.

This enables them to secrete mediators selectively in given situations (Gilfillan & Beaven, 2011).

Mast cells were first demonstrated to have roles in innate immunity, in particular in the detection of invading organisms, through studies into mast cells and helminth infection. Woodbury *et al.* demonstrated that mast cells accumulate and degranulate at locations of helminth infestation in the intestine of rats (Woodbury *et al.*, 1984). In support of this data, another study showed that mice with deficient mast cells have impaired ability for worm expulsion (Nawa *et al.*, 1985), in combination this work demonstrates the importance of mast cells for protection against helminths.

Mast cells have also been shown to have a protective role against bacterial infection; one study demonstrated that mast cell deficient mice were 20-fold less effective in the clearance of enterobacteria than the wild-type (WT) controls, here tumour necrosis factor α (TNFα) production by mast cells was implicated as key for neutrophil recruitment in mounting the immune response to clear this bacteria (Malaviya *et al.*, 1996). Subsequent studies have implicated mast cells with a role in the control of viral infection. In the HMC-1 human mast cell line, following infection with respiratory syncytial virus HMC-1 cells were shown to release several chemokines which could be involved in immune cell recruitment to help tackle this viral infection *in vivo* (Al-Afif *et al.*, 2015). Importantly, in allergic disease such as asthma, allergic symptoms are commonly reported to be exacerbated during bacterial/viral infections. A recent study compared the mediator release of mast cells following either IgE stimulation or simultaneous activation with IgE and toll like receptor (TLR) ligands. Interestingly they found that TLR+ IgE activation greatly enhanced cytokine production. This observation gives important evidence in support of the mechanism behind the augmented allergic symptoms seen during an infection (Suurmond *et al.*, 2015).

1.2.3 Mast cells and allergic disease

Charles Blakely noted the first scientific report of allergic disease in 1869, when he performed a skin prick test to demonstrate that pollen was the causative agent for his hay fever (Beaven, 2009). Following this, the first links that mast cells were contributors to allergic disease were upon discovery that histamine could cause anaphylactic shock and that there was a correlation between histamine levels and mast cell counts in urticaria lesions (Riley 1953, Riley and West 1952). However, it was the discovery of the IgE class of antibodies by (Bennich *et al.*, 1968) that signified a crucial breakthrough in the understanding of the immunological basis of allergy. It is now known that for antigen-IgE production to occur, IgE antigens are taken up by antigen presenting cells that present the processed antigen to naïve T cells to cause an acquired Th2 cell phenotype. Through the action of B cell major histocompatibility complex (MHC) class II molecules/IL-4 and IL-13, B cells then undergo class switch recombination to become IgE producing B cells. Once produced antigen-IgE mediates its biological functions through binding to FcεRI and CD23 receptors which are predominantly expressed on mast cells but also on some other hematopoietic cells. Due to the primary expression of the FcεRI being on mast cells, this

shows how the link between IgE and allergy implicates mast cells as the effector cell type (Galli & Tsai, 2012).

It is now well recognised that in allergic individuals, re-exposure to an antigen specific IgE causes FcεRI receptor cross linking on mast cells and basophils. This initiates a complex signalling cascade culminating in the secretion of mediators which leads to an immediate hypersensitivity reaction. If this release occurs in the airways then the symptomatic response is characterised by an increased vascular permeability, smooth muscle contraction and mucus secretion, if there is a systemic activation and mediator release anaphylaxis can occur (Beaven, 2009; Galli & Tsai, 2012). However, what predisposes some people to develop IgE antibodies towards allergens is unclear.

1.2.4 Mast cell mediators

Preformed mediators in granules

Following mast cell activation, degranulation occurs within seconds and is complete after around 5-10 minutes. The main components of mast cell granules include; proteases such as tryptase, chymase and carboxypeptidase. However histamine is arguably the most well known degranulated mediator as it has a key role in the contribution to mast cell mediated disease. Lysosomal enzyme, β-hexaminidase is released from mast cell granules and is frequently used as a way to measure mast cell degranulation using *in vitro* assays (Lundequist & Pejler, 2011). Once released, histamine acts through histamine GPCR receptors located throughout the body. Histamine activation of H1 receptors located on the bronchial smooth muscle and endothelial cells are responsible for bronchoconstriction – one of the main symptoms of allergic asthma. In sum, the release of histamine from mast cells can lead to; increased vascular permeability, vasodilatation and bronchial constriction (Lundequist & Pejler, 2011).

Mast cell degranulation occurs via regulated exocytosis. Exocytosis is mediated through Soluble *N*-ethylmaleimide-sensitive factor Attachment Protein Receptor (SNARE) proteins which can be classified into; t-SNARES, located on the target membrane, and v-SNARES, located on the vesicle membrane. There are numerous members of each of the vesicle and target located SNAREs and work in the Seward lab has characterised which SNAREs are expressed in human mast cells and to link SNARE expression to distinct cytokine release (Reuben Friend thesis). Of the v-SNARE family, vesicle-associated membrane protein (VAMP)-8 deficient mast cells have been shown to have impaired FcεRI-mediated exocytosis. Similar studies have implicated Syntaxin and Soluble NSF Attachment Protein (SNAP)-23 (t-SNARES) in FcεRI-mediated exocytosis. Other regulators of exocytosis have been shown to be required for successful degranulation of mast cell mediators. For example, the bone marrow-derived murine mast cell (BMMCs) from Doc2α (a Ca^{2+} sensing protein involved in exocytosis regulation) deficient mice were shown to have reduced levels of FcεRI induced exocytosis (Kalesnikoff & Galli, 2008).

Eicosanoids

Activated mast cells release newly generated eicosanoids in relatively large quantities over a short time period. Eicosanoids are lipid mediators that comprise PGDs and LTCs. The de novo production of eicosanoids occurs downstream of arachidonic acid production, and involves a combination of phosphorylation of mitogen-activated protein kinase (MAPK) and intracellular Ca^{2+} flux are required. LTCs are generated from 5-lypoxygenase activity (5-LO) and PGDs from cyclooxygenase isoenzmes (COX) (Funk, 2001). Following release, eicosanoids can act through specific GPCRs to exert effects on the local environment; the effects of PGD2 and LTC4 have been shown to cause bronchoconstriction and potentiation of airway hyper responsiveness. Consistent with mast cell hyperactivity, in broncho-alveolar lavage fluid (BALF) from asthmatics the levels of PGD2 and LTC4 are enhanced compared to healthy controls (Boyce, 2007).

Cytokines and chemokines

Mast cells can produce a wide range of cytokines and chemokines including: IL-3, IL-4, IL-5, IL-6, IL-10, IL-13, granulocyte-macrophage colony-stimulating factor (GM-CSF) and TNFα and chemokine (C-C motif ligand (CCL)-2, 3, 5 and chemokine C-X-C Motif ligand (CXCL)-8 (Galli *et al.*, 2005). Cytokine and chemokine release occurs much later than that of the granulated and eicosanoid mediators, taking place several hours after mast cell activation. TNFα is an exception to this, as evidence has shown that this cytokine is also present in preformed granules, therefore its release can occur in two phases. Thymic stromal lymphoprotein (TSLP) is a member of the IL-2 cytokine family and has been shown to have a role in contribution to allergic asthma. The primary producers of TSLP are epithelial cells, keratinocytes and stromal cells but DCs and mast cells have also been shown to be capable. IL-4 primed mast cells were demonstrated to produce TSLP following FcεRI stimulation in a study by (Okayama *et al.*, 2009). In health, TSLP has been largely thought to have roles in maintenance of Th2 type homeostasis at barrier surfaces, however in disease it is a contributor to the development of Th2 type inflammatory responses that lead to allergic asthma (Ziegler *et al.*, 2013).

1.2.5 Mast cell surface receptors

Mast cells express a vast array of endogenous receptors giving them the ability to respond to a range of stimuli. A list of the commonly reported mast cell receptors is summarised in *Figure 1.4* whilst further details regarding the signalling downstream of the mast cell receptors relevant to this study is given below.

Table 1 | **Ligands and their receptors that influence mast-cell activation**

Receptor	Species	Ligand	Source of ligand	Initiating signals	Mast-cell response	Refs
Fc						
FcεRI, FcγRI, FcγRIII	Mouse, rat, human	IgE-bound antigen	B cells	SRC-family kinases and SYK	• Induced degranulation • Induced eicosanoid, cytokine and chemokine release	106–111
G-protein coupled						
C3aR	Human	C3a	Hepatocytes	$G_{\alpha i}$	• Induced degranulation and chemokine production • Increased FcγRI-dependent degranulation	101,102
A_3R	Mouse	Adenosine	Mast cells, pro-inflammatory cells	$G_{\alpha i}$	• Increased and sustained FcεRI-dependent degranulation	89
CCR1	Mouse	CCL3	Mast cells	$G_{\alpha i}$	• Induced degranulation • Increased FcεRI-dependent degranulation	98
CCR3	Human	CCL11	Epithelial cells, pro-inflammatory cells	$G_{\alpha i}$	• Increased FcεRI-dependent IL-13 secretion	112
$S1P_2$	Mouse	S1P	Mast cells	$G_{\alpha i}$	• Induced degranulation	78
Cytokine						
IL-3R	Human	IL-3	Mast cells, T cells	JAK–STAT	• Increased FcεRI-dependent histamine and LTC_4 release	113
IL-4R	Mouse	IL-4	Mast cells, T cells	JAK–STAT	• Inhibited FcεRI-dependent cytokine release • Increased FcγR-dependent degranulation and cytokine production • Inhibited FcεRIβ expression and increased FcγRIIIα expression	114,115
	Human	IL-4	Mast cells, T cells	JAK–STAT	• Increased FcεRI-dependent histamine, LTC_4 and IL-5 release	116,117
IL-5R	Human	IL-5	Mast cells, T cells	JAK–STAT	• No effect on FcεRI-dependent degranulation • Increased FcεRI-dependent cytokine release	117
IL-10R	Mouse, rat, human	IL-10	Mast cells, T cells	JAK–STAT	• No effect on FcεRI-dependent degranulation • Decreased FcεRI-dependent cytokine release • Decreased FcεRIβ expression	118–120
TGFβR1	Mouse, rat	TGFβ	Mast cells, pro-inflammatory cells	JAK–STAT	• Decreased FcεRI-dependent degranulation • Decreased FcεRI-dependent TNF production • Decreased FcεRIα and FcεRIβ expression	121,122
KIT	Mouse, rat, human	SCF	Fibroblasts, endothelial cells, bone-marrow cells, stromal cells	KIT, SRC-family kinases and PI3K	• Induced cytokine and chemokine release • Induced growth, differentiation and adhesion • Increased FcεRI-dependent degranulation • Increased FcεRI-dependent cytokine release	36,91–94,97
Other						
TLRs	Mouse, rat, human	PAMP	Bacteria, viruses	MyD88, IRAK and TRAF	• Induced degranulation • Induced eicosanoid and cytokine release	5

A_3R, A_3 adenosine receptor; C3a, complement component 3a; C3aR, C3a receptor; CCL, CC-chemokine ligand; CCR, CC-chemokine receptor; FcγRI, high-affinity receptor for IgG; FcεRI, high-affinity receptor for IgE; FcγRIII, low-affinity receptor for IgG; $G_{\alpha i}$, α-subunit of inhibitory G protein; IL, interleukin; IL-3R, IL-3 receptor; IL-4R, IL-4 receptor; IL-5R, IL-5 receptor; IL-10R, IL-10 receptor; IRAK, IL-1-receptor-associated kinase; JAK, Janus kinase; LTC_4, leukotriene C_4; MyD88, myeloid differentiation primary-response protein 88; PAMP, pathogen-associated molecular pattern; PI3K, phosphatidylinositol 3-kinase; S1P, sphingosine 1-phosphate; $S1P_2$, S1P receptor 2; SCF, stem-cell factor; STAT, signal transducer and activator of transcription; SYK, spleen tyrosine kinase; TGFβ, transforming growth factor-β; TGFβR1, TGFβ receptor 1; TLR, Toll-like receptor; TNF, tumour-necrosis factor; TRAF, TNF-receptor-associated factor.

Figure 1.4   Common mast cell receptors and their ligands and effect on mast cell function

Reproduced with permission from (Gilfillan & Tkaczyk, 2006)

FcεRI receptors

The FcεRI is a heterotetrameric receptor consisting of the IgE binding α subunit, the membrane tetraspanning β-subunit and two identical disulphide linked-γ subunits. It is the γ subunits that initiate the signalling events downstream through the immunoreceptor tyrosine based activation motifs (ITAM)s attached (Gilfillan & Beaven, 2011). Activation of FcεRI results in the stimulation of a complex signalling cascade with a number of signalling axes which branch off following the initial receptor cross linking. The principal signalling cascade activated following FcεRI activation is depicted in **Figure 1.5**; from the first steps

following receptor cross linking, the signalling is initiated by a SRC family kinase, Lyn, which is located in lipid membrane rafts along with the FcεRI receptors. Lyn phosphorylates tyrosine residues present in the β and γ chain associated ITAMs leading to tethering of spleen tyrosine kinase (Syk) and subsequent activation of the TM adaptor molecule, linker for activation of T cells (LAT) (Gilfillan *et al.*, 2011b). Importance of LAT for FcεRI-mediated degranulation were demonstrated by (Saitoh *et al.*, 2000) where profound defects in FcεRI-mediated degranulation were seen in LAT deficient BMMCs. LAT regulated phospholipase-γ (PLCγ) regulation has been shown to be key for initiation of the downstream signalling necessary for degranulation. Similarly, following activation of LAT-growth receptor-bound protein 2 (GRB2) pathways, signalling involving MAPK and extracellular-signal-related-kinase (ERK) leads to activation of transcription factors involved in cytokine production. In addition to the Lyn directed signalling pathways, another alternative signalling pathway downstream of FcεRI activation was also proposed. (Rivera & Gilfillan, 2006) showed that another SRC family kinase, Fyn, was involved in mast cell mediator release and was involved in crosstalk with Lyn to initiate FcεRI regulated mast cell degranulation. Fyn was shown to activate phosphoinositide 3-kinase (PI3K) following GRB2-associated-binding protein 2 (GAB2) phosphorylation. Notably, FcεRI activation culminates in a signalling cascade that causes Ca^{2+} mobilization, the known Ca^{2+} channels mediating this Ca^{2+} flux are discussed in **Section 3.1**.
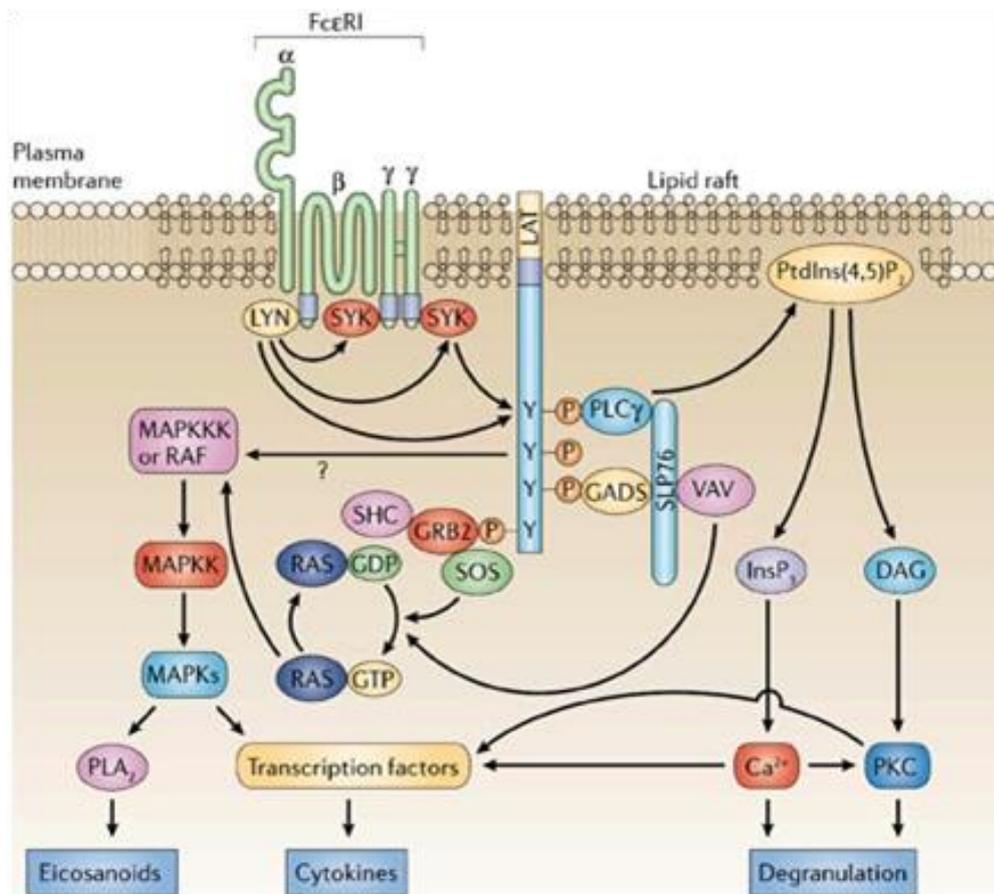
Figure 1.5 **Schematic diagram showing key components of the principal FcεRI signalling cascade**

For clarity, only one high-affinity receptor for IgE (FcεRI) is shown. Reproduced with permission from (Gilfillan & Tkaczyk, 2006).

c-kit receptor

The c-kit receptor is a single chain receptor with five extracellular immunoglobulin-like domains. In order for receptor activation to occur, ligand binding by SCF needs to occur to induce dimerization and activation of the downstream signalling cascade. SCF has been shown to have a substantial modulatory effect of Anti-IgE induced degranulation and cytokine production. However, c-kit signalling alone seems insufficient to induce degranulation but studies have demonstrated the release of cytokines and PGDs (Lewis *et al.*, 2013a). The c-kit signalling cascade is similar to that induced by FcεRI; c-kit signalling induces activation of Src kinases, PLCy1, PI3K and MAPK but it does not appear to initiate Syk, LAT or protein kinase C (PKC) signalling, perhaps explaining the lack of degranulative capacity (Gilfillan & Tkaczyk, 2006). A schematic diagram depicting the c-kit receptor activation cascade is shown in ***Figure 1.6.***
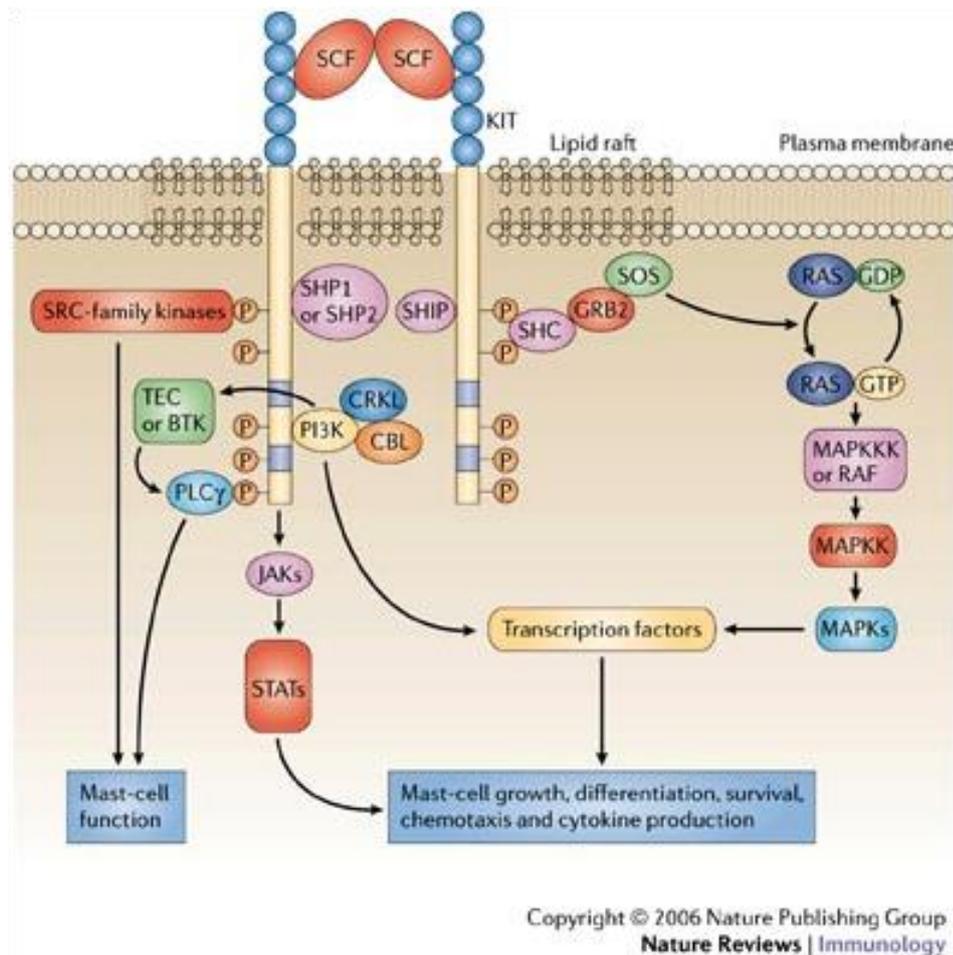
Figure 1.6 **Schematic diagram showing key components of the c-kit signalling cascade**

1.2.6 Mast cell models

Due to the difficulty in obtaining a source of primary tissue from which to isolate primary mast cells, frequently mast cell models are used instead. There are several mast cell models from human and rodent origins available. The oldest mast cell model is the RBL-2H3 cell line, derived from rat basophilic leukaemia cells. Originally this cell line was derived from a tumour in Wistar rats by (Eccleston *et al.*, 1973), these RBL cells were defined as RBL-I-RBL-IIII, and although they were demonstrated to have a good FcεRI expression they were not significant releasers of histamine in response to FcεRI activation. It was in 1981 when sub lines of the original RBL cells were cloned in order to produce the RBL-2H3 cell line which was subsequently shown to be strong histamine releasers (Barsumian *et al.*, 1981). Although characterisation has shown that RBL cells function as would be expected for a mast cell, caution should always be taken in the translation from rodent to human studies. In this regard, the use of later established human mast cell lines may prove more relevant in most research scenarios.

Two major human mast cell lines are referenced in mast cell research papers; namely the laboratory of allergic disease 2 (LAD2) mast cell line and the HMC-1 mast cell line. Another human mast cell line called the LUVA cell was also described in 2011, although the use of this latter cell line has not been widely verified (Laidlaw *et al.*, 2011). LAD2 cells were first obtained from bone marrow aspirates from a patient with mast cell leukemia. Analysis of these cells once in culture found that they expressed FcεRI, stained with the characteristic mast cell kimura marker and had intracellular granules. Importantly they were shown to release β-hexaminidase in response to FcεRI activation showing their scope for mast cell research (Kirshenbaum et al 2003). The HMC-1 mast cell was first described in 1988 and was originally derived from peripheral blood of a patient with mast cell leukemia. Upon initial characterisation of the cells, it was found that they bear similarities to immature mast cells but importantly they do not possess FcεRIs (Butterfield *et al.*, 1988). This therefore limits the scope of the mast cell research that can be undertaken with this model cell. A more recent comparison study of HMC-1 and LAD2 cells to primary skin mast cells stated that HMC-1 cells showed a very immature mast cell phenotype, whereas LAD2 cells were more intermediately differentiated as compared to the primary skin mast cells (Guhl *et al.*, 2010). This highlights that LAD2 cells are a superior human mast cell model to HMC-1 cells.

Section 1.2 has covered key aspects of mast cell biology pertinent to my study, further information about the importance of Ca^{2+} in mast cell biology and the current knowledge of specific Ca^{2+} channels with defined roles in mast cell activation is discussed in ***Section 3.1***.

1.3 Introduction to macrophage biology

1.3.1 Macrophage – discovery and key characteristics

Metchnikoff first described macrophages in 1882 - macrophages were described as cells that migrated to punctured starfish larvae and were able to uptake particles from the larvae digestive tract (Gordon, 2007). Over the last 100 years there has been a wealth of research into macrophages, delineating the important roles of macrophages in many different tissues. A wide functional diversity has been reported from macrophages taken from different tissue sites *in vivo*, phenotypic characterization of macrophages has led to the genesis of the rigid definitions of classical and alternatively activated macrophages otherwise denoted as M1 and M2 macrophages. M1 and M2 macrophages are defined due to distinct proinflammatory and anti-inflammatory effects when naïve macrophages are cultured with LPS/IFNγ or IL-4 and IL-13, respectively. It is increasingly apparent that these binary classifications represent two extreme states which are not representative of the complex *in vivo* tissue resident macrophage phenotypes (Mosser, 2003; Gordon, 2007). Macrophages are perhaps best described for their key role as cells of innate immune function and inflammation; they direct phagocytosis of pathogens and produce proinflammatory cytokines to initiate an immune response to aid host defense. Conversely, macrophages have been shown to have important roles in wound healing and repair (Murray & Wynn, 2011) and in other aspects of biology. For example macrophages have crucial roles in regulating development and metabolic homeostasis. Macrophages have also been shown to be key contributors to the pathogenesis of several types of disease; in particular cancer and inflammatory diseases, including respiratory diseases (Wynn *et al.*, 2013).

1.3.2 Macrophage derivation

Following from the identification of macrophages by Metchnikoff, it was commonly thought that tissue-resident macrophages originated from blood derived monocyte precursors. However, recent fate mapping experiments have demonstrated that some tissue resident macrophages arise from the yolk sac, which occurs before development of haematopoeitic stem cells (HSCs) (Dey *et al.*, 2014). Macrophages resident in the liver, brain, epidermis and lung originate from colony-stimulating factor 1 receptor (Csf1r) erythro-myeloid progenitor cells, that are distinct from HSCs. Interestingly, throughout ageing in steady state conditions, lung AMs were shown to be replaced over time by cells of HSC origin, whereas the other macrophage subtypes were only marginally replaced by HSC cells and Csf1r+ve cells yolk sac derived were largely maintained throughout the time period assessed (Gomez Perdiguero *et al.*, 2015). The transfer of bone marrow HSCs into lethally irradiated recipients with ablate tissue macrophages has demonstrated that monocyte precursors can differentiate into functional macrophages under certain conditions, for example in cardiac macrophages, the replenishment of macrophages has been shown to occur from blood monocyte cells following cardiac insult (Dey *et al.*, 2014). Together these recent findings illustrate that although not all macrophages are originally

derived from blood monocyte precursors; further work is required to understand the contribution and in the replacement of tissue resident macrophage cells following immune insult or cell death.

1.3.3 Macrophage functions

The wide receptor expression on cell surface of macrophages enables them to detect a number of invading pathogens and act among the first line of defense in a pathogen attack. For example TLR and scavenger receptors alone can bind a large range of ligands which are present on the surface of microorganisms e.g. lectins, lipoproteins, proteins, oligonucleotides, polysaccharides, and other molecules.

Mediator release

Macrophages can direct inflammation through the release of a panel of proinflammatory mediators differentially released dependent on the activating ligand. In response to inflammatory stimuli, endogenous macrophage receptor activation leads to the release a range of proinflammatory cytokines including TNFα, IL-6, IL-8 and IL-2. Similarly they can release proinflammatory mediators such as PGDs, LTCs and complement. This panel of proinflammatory mediators have a range of functions dependent on the local environment they are released into, but are also known to direct specific components of the inflammatory immune response (Arango Duque & Descoteaux, 2014). Macrophages can also release ROS, reactive nitrogen species (RNS), hydrolytic enzymes and chemokines. Macrophages skewed towards an M2 phenotype can release anti-inflammatory/tissue healing mediators such as IL-10, transforming growth factor-β- (TGF-β), platelet-derived growth factor (PDGF), vascular endothelial growth factor (VEGF) and epidermal growth factor (EGF) (Laskin, 2009).

Phagocytosis

Phagocytosis is carried out by effector cells of the innate immune system, such as macrophages and neutrophils. Phagocytosis is essential for the clearance of microbes, apoptotic cells and foreign particles and is initiated through ligands found on the surface of the particles binding to receptors on the phagocytic immune cells. Upon particle ingestion, macrophages can process and present the antigens for the foreign particle which can be recognised by T helper cells. This culminates in the release of cytokines from T-lymphocytes to cause B cell activation and initiate antibody production specific to the foreign antigen. Specific antibodies then bind to the antigens located on the pathogen surface. These opsonized pathogens can then be detected again by macrophages through the FcγR which can initiate FcγR mediated phagocytosis (Arango Duque & Descoteaux, 2014). Phagocytosis also encompasses processing of the particle to cause phagosomal maturation; this is a key step in effective destruction of pathogens. Following engulfment of the particle, into a

membrane enclosed phagosome, the phagosome undergoes a maturation process which involves a process of lipid remodelling, fusion with endosomes or lysosomes, acidification and ROS generation to kill/destroy the particle (Nunes & Demaurex, 2010). Phagosomal acidification is involved in limiting bacterial growth and enhancing the effectiveness of microbicial components such as the activity of hydrolytic enzymes (Steinberg *et al.*, 2007), and is also important in the contribution of phagosomal maturation due to its involvement in membrane traffic regulation.

Dependent on the particle type, different ligands are found therefore a range of receptors can be activated. Examples of receptors involved in the initiation of phagocytosis include: FcγR, complement receptors (CR), scavenger receptors. Depending on the receptor initiating phagocytosis, there are differences in how the phagocytic engulfment can occur. For example, following FcγR or Dectin-1 receptor activation, an extension of the pseudopodia occurs and engulfment of the target. However the CR-mediated phagocytosis initiates 'sinking phagocytosis' where a force is applied on the particle to cause it to be pulled into the cell (Aderem & Underhill, 1999; Goodridge *et al.*, 2012). Other differences between the phagocytosis initiated by FcγR and CR are that FcγR phagocytosis is tightly coupled to the release of inflammatory mediators whereas no release of mediators has been demonstrated through CR phagocytosis. FcγR-dependent phagocytosis is seemingly a Syk-dependent process with PI3K signalling initiated downstream, demonstrated by the inhibitory effects of wortmannin of FcγR mediated phagocytosis (Aderem & Underhill, 1999). Although FcγR mediated phagocytosis is largely thought to occur through the binding of IgG opsonized particles, (Salmon *et al.*, 1987) have also demonstrated a specific FcγR on human neutrophils initiates opsonin-independent phagocytosis of non-opsonized *E. coli* through the binding of mannose-binding adhesions to FcγRs. It was shown that blocking FcγR with a 3G8 anti –FcγR antibody led to inhibition of internalisation of *E. coli*. However the attachment of *E. coli* to the cell surface was not affected. There has been shown to be a large similarity between the phagocytic and endocytic pathways, and a lot of mechanistic understanding has been gained from knowledge of the endocytic pathway (Stenmark, 2009; Flannagan *et al.*, 2012). For example, phagosomal maturation requires endolysosomal protein machinery to regulate the membrane targeting and fusion, SNARE proteins and RabGTPases have been shown to be involved (Dayam *et al.*, 2015). Similarly, although the typical definition of phagocytosis is defined by the uptake of particles larger than 0.5μM in size and endocytosis of particles smaller in size, the utilisation of endosomal pathways by pathogens, in non phagocytic and phagocytic cells has been described – often in the context of foreign pathogens evading detection by the immune system (Bonazzi & Cossart, 2006). As such an important role regulated by macrophages, research to delineate further details regarding the mechanisms controlling phagocytosis is important.

1.3.4 Macrophage heterogeneity

Tissue resident macrophages exist at a number of locations within the body, e.g. in the skin, spleen, lung, liver, gastrointestinal tract, CNS, blood and bone. Whilst the majority of tissue resident macrophages have roles in immune surveillance there are key differences

between other functions dependent on the tissue location. For example, whilst CNS located macrophages, microglia, have additional roles promoting neuronal survival, alveolar macrophages from the lung clear airway surfactant (Davies *et al.*, 2013). An in-depth gene expression profile study has characterised the differences between tissue macrophages isolated from lungs, spleen, brain and peritoneum has been performed by (Gautier *et al.*, 2012). Further information regarding AMs and MDMs, the macrophage types used in the present study is provided below.

Alveolar macrophages (AMs)

AMs are located on the epithelial surface of the lung which puts them in immediate contact with the environment, and therefore exposed to inhaled pathogens and host-epithelial derived factors. Due to this location, AMs have a critical role in regulating the pulmonary immune responses in response to inhaled pathogens. It has been demonstrated that AM differentiation is dependent on GM-CSF; with GM-CSF driving peroxisome proliferator-activated receptor (PPARγ) mediated AM maturation. A cell selective PPARγ knockout mouse (CD11c-CrePpargfl/fl mice) was shown to have a significantly reduced number of mature AMs when isolated from the BALF and lungs (Schneider *et al.*, 2014). Similarly, PPARγ was shown to confer the transcriptomic profile specific to AMs (Gautier *et al.*, 2012). The functional niche of AMs compared to other macrophage types may be explained by their residing in a tissue where marked changes in the environment occur on a frequent basis. For example, the partial O_2 pressure, tissue oxygenation and microbial flora vastly change during periods of distinct microbial contact (Hussell & Bell, 2014). Although macrophages from the lung are generically referred to as AMs, in fact there are at least three types of macrophages resident in the lung: bronchial macrophage, interstitial macrophages and AMs. AMs are located in the air space and form 90-95% of the cells in the steady state (Kopf, Schneider and Nobs 2015).

Monocyte derived macrophages

In the original model of macrophage differentiation, macrophages were thought to originate from CD34+ myeloid progenitor cells in the bone marrow and upon stimulation with GM-CSF or macrophage colony-stimulating factor (M-CSF) differentiate into promonocytes, with further division leading monocytes released into the bloodstream for circulation for a 3 day period. It was originally believed that monocytes migrated to varying tissue locations to become mature tissue resident macrophages (Andreesen & Kreutz 1991). The differentiation cascade as understood from these studies led to the development of *in vitro* protocols to create monocyte derived macrophages. Human Ab serum was shown to induce monocyte to macrophage differentiation in culture over a period of 7 days (Musson, 1983; Andreesen *et al.*, 1990). Monocyte to macrophage differentiation was originally characterised by: a change in morphology - around a 10 fold increase in size with decrease in nucleus to cytoplasm ratio and multinucleation, an increase in ability to phagocytose particles and to perform antibody-dependent cell-mediated cytotoxicity (ADCC), and expression of 'maturation' markers, some of which e.g.

CD16 have since been shown to be present on monocytes too (Andreesen and Kreutz 1991). M-CSF and GM-CSF have been shown to have important roles in driving monocyte to macrophage differentiation *in vitro* (Brugger *et al.*, 1991); (Eischen *et al.*, 1991). In 2004, it was shown that M-CSF and GM-CSF mediated differentiation led to two distinct groups of macrophages based on their phenotype and cytokine based responses was shown. M-CSF differentiation of human CD14+ monocytes produced macrophages that subverted the Th1 response in face of mycobacterial infection and did not respond by releasing IL-23 or IL-12 but did release IL-10. Conversely GM-CSF driven differentiation produced macrophages that promoted Th1 immunity in response to mycobacterial infection with secretion of IL-23 and IL-12 in cells that had also been primed with IFNγ (Verreck *et al.*, 2004). Further work by (Fleetwood *et al.*, 2007) corroborate Verreck's work in murine bone marrow derived macrophages (BMDMs). Experiments to attempt to characterise the transcriptomic and surface expression of M1 and M2 macrophages have since been described (Jaguin *et al.*, 2013; Vogel *et al.*, 2014); (Martinez *et al.*, 2006). Characterisation of polarised human macrophages *in vitro* of human macrophages cells differentiated *in vitro* with M-CSF or GM-CSF (with and without IFNγ/LPS, IL-4, dexamethasone and IL-10) showed that CD64 and CD40 were stereotypical M1 markers whereas CD163 was a characteristic M2 marker (Vogel *et al.*, 2014). From this area of investigation, the coined M1 and M2 phenotypes have largely been interpreted in the macrophage field as somewhat rigid groups with distinct immune functions. However it has since been reiterated that these M1 and M2 phenotypes do not strictly mirror tissue specific macrophage types and are merely examples of how differing lineage determining cytokines can lead to macrophages with vastly different roles.

1.3.5 Macrophage surface receptors

Macrophages express a variety of surface receptors, that upon ligand – receptor binding can lead to activation of the cell to initiate an immune response e.g. cytokine release or phagocytosis. Receptors endogenously expressed by macrophages include: pattern recognition receptors (PRRs), FcγRs, CRs, lectins and scavenger receptors (Taylor *et al.*, 2005). PRRs can be separated into 3 groups; TLRs, retinoic acid inducible gene like receptors (RLRs) and nucleotide binding oligomerisation domain like receptors (NLRs). A list of the key receptors and their functional roles is summarised in ***Figure 1.7***. The macrophage receptors focused in my study are the FcγR and TLR families therefore more information on these families is provided in this ***Section (1.3.5)*** to provide the necessary context for the work of this thesis.

Receptor family	Example	Function (example)
Scavenger (collagenous)	SR-A	Phagocytosis of bacteria and apoptotic cells, endocytosis of modified LDL, adhesion
Scavenger (noncollagenous)	CD36	Phagocytosis of apoptotic cells, diacyl lipid recognition of bacteria
GPI-anchored	CD14	LPS-binding protein/interactions MD2/MyD88, TLR signaling, apoptotic cell recognition
Integrin	CR3 (CD18/11b)	Complement receptor (C3bi) mediated phagocytosis Adhesion to endothelium
Ig Superfamily	FcR (ITAM/ITIM)	Antibody-dependent binding, uptake, killing
	TREM-1 (ITAM)	Regulation of inflammation
Seven transmembrane	CCR2	Receptor for MCP-1
	C5aR	Chemotaxis, degranulation
	EMR2 (EGF-TM7)	Myeloid cell adhesion Chondroitin sulphate binding
NK-like C-type lectin-like	Dectin-1 (ITAM-like)	β-glucan receptor, fungal particle ingestion TNFα release/interaction TLR2
C-type lectin (single CTLD)	DC-SIGN	Mostly DC, pathogen recognition, ICAM adhesion
Multiple CTLD	MR	Clearance, alternative activation, antigen transport?
Toll-like receptors (Leucine-rich repeats)	TLR2 TLR4	Response to Peptidoglycan Response to LPS

[a]MØ express multiple receptors belonging to major structurally defined families. Examples shown are referred to in text.

Figure 1.7   Overview of macrophage receptors implicated in immune recognition

Reproduced with permission from (Taylor et al., 2005)

TLR receptors

The TLR receptor family includes 9 members and TLR receptor activation can lead to the propagation of a signal which can involve four types of adapter molecules; myeloid differentiation primary response gene 88 (MyD88), toll/interleukin-1 receptor domain-containing adapter protein (TIRAP), TIR-domain-containing adapter-inducing interferon-β (TRIF) and TRIF–related adaptor molecule (TRAM). Broadly speaking, the TLR signalling cascade can be split into either MyD88 or TRIF-dependent pathways, with different TLR family members utilizing different pathways and adapter molecules. MyD88-dependent signalling can modulate NF-κB and MAPK transcription whereas TRIF- dependent signalling is more commonly associated with NF-κB and interferon regulatory factor 3 (IRF3)

activation (Kawai & Akira, 2010) *(Figure 1.8).* TLR receptor activation is crucial for mediating innate immune response following pathogen attack.
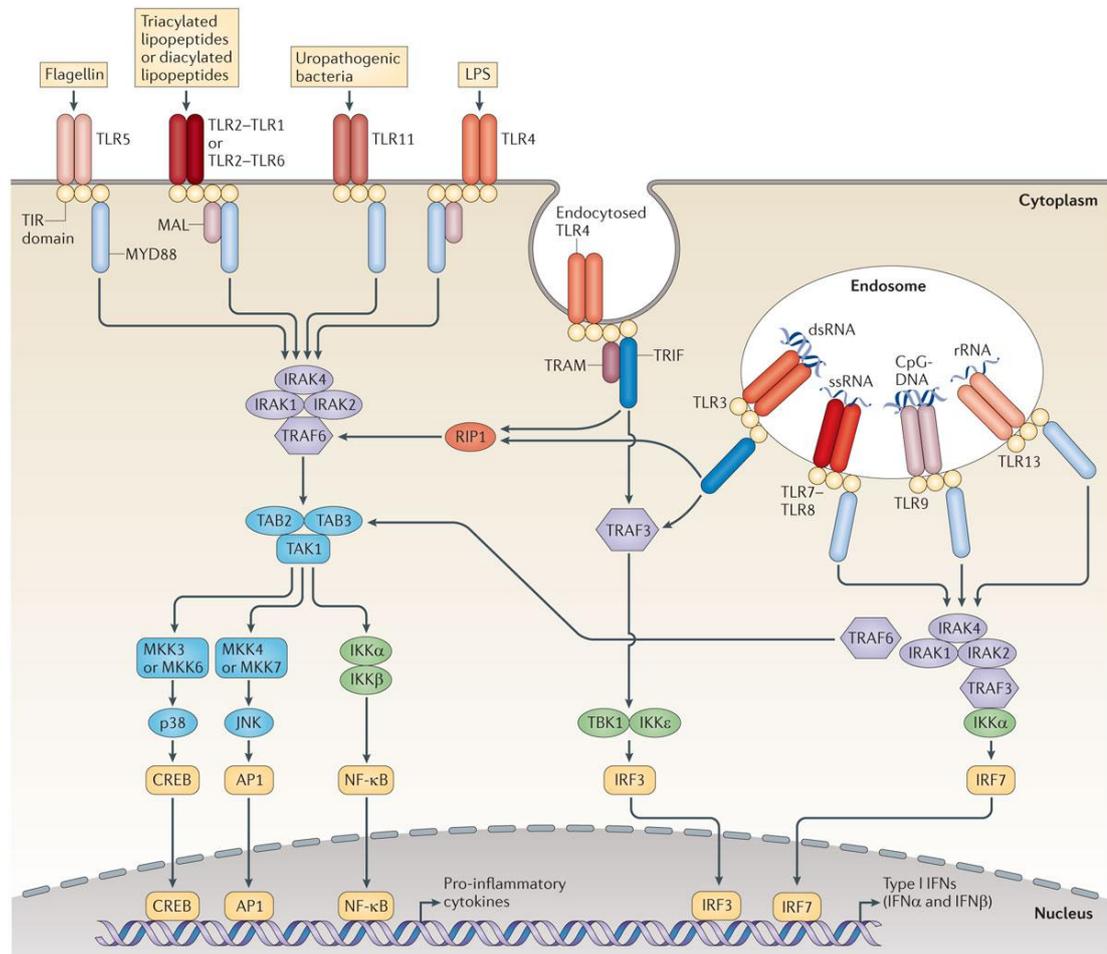
Nature Reviews | Immunology

Figure 1.8   Schematic diagram showing signalling downstream of TLR receptor activation

Figure reproduced with permission from (O'Neill et al., 2013).

Signalling downstream of the TLR adapter molecules involves signalling messengers such as interleukin-1 (IL-1) receptor-associated kinase (IRAK) and TRAF contrary to the Syk/PI3K-dependent signalling cascades as seen in Fc and T cell receptors (TCR). However, a number of studies in immune and non immune cells alike, have demonstrated the involvement of PLC and subsequent Ca^{2+} influx following TLR4 receptor activation. A selection of this work has implicated the potential for SOCC as components of the TLR4 signalling cascade, details of these studies are provided in *Section 5.1*. Although the work summarised in *Section 5.1* provide evidence to support to activation of SOCE downstream of TLR activation, none of these studies address SOCE and TLR signalling in human macrophages identifying a gap in current knowledge. Similarly the details of LPS induced Ca^{2+} mobilization varies in each study, where different macrophage type and non immune cells were used, indicating

differential activity dependent on the cell type and associated microenvironment. In summary it is clear that translation of work into human macrophages is important and there is a gap in the current knowledge that this study aims to address.

FcγR

FcγRs for IgG were recognised over 50 years ago and two general classes of IgG Fc receptors are now recognised; activation receptors characterised by ITAM motifs and inhibitory receptors characterised by ITIM motifs (Gessner *et al.*, 1998). In the Fcγ receptor signalling cascade; following ITAM phosphorylation, Syk and LYN pathways are initiated leading to the PLCγ production (Crowley *et al.*, 1997; Wen *et al.*, 2002) and therefore inositol trisphosphate (IP_3) production and store depletion. Conversely, inhibitory FcγR subtype activation mediated by ITIM motifs leads to production of SRC kinase, promoting the recruitment of Src homology 2 (SH2) domain containing phosphatases such as SHIP, SHIP then acts to degrade phosphatidylinositol-4,5-bisphosphate (PIP2) which prevents PLC and IP_3 production (Goodridge *et al.*, 2012). The full signalling cascade initiated by Fcγ receptors is shown in ***Figure 1.9***. The 5 subtypes of the FcγR can be classified as activatory or inhibitory based on whether they are associated with an ITAM or ITIM motif. FcγR include 4 main family members in *Homo sapiens*; FcγRI, FcγRIIa, FcγRIIb and FcγRIII. Each differs in their affinity for the ligand, IgG. FcγRI is the high affinity activatory receptor subtype and leads to activation of the ITAM-Syk/LYN-PLC pathway. FcγRIIa and FcγRIII represent lower affinity activatory subtypes with differential preference for IgG subtypes. ***Figure 1.10*** shows the different FcγR subtypes, their relative affinity for IgG and the expression profile in a number of immune cell types. Activation of FcγR *in vivo* occurs following cross linking of the receptor by IgG immune complexes. Downstream functions associated with FcγR activation include phagocytosis, ADCC, transcription of cytokine genes and release of proinflammatory mediators (Dijstelbloem *et al.*, 2001). FcγRs are often described as the linkers between the innate and adaptive immune system: they are expressed largely on innate effector cells however they are activated by immunoglobulins binding to the Fc part of the receptor (Nimmerjahn & Ravetch, 2008b). Due to the activation by IgG, FcγRs are also associated with autoimmune disease, when IgG is inappropriately made against self-antigens. Similarly, FcγRIIb acts an important negative regulator of auto immune disease as it helps to balance the FcγR immune response by preventing overactivity (Brownlie *et al.*, 2008).

As described in detail in ***Section 5.1***, there have been several studies that demonstrate a robust Ca^{2+} influx in cells following FcγR activation; this has been coupled to phagocytic ingestion in a selection of these studies. Due to the components of the signalling cascade initiated by FcγR, the Ca^{2+} influx is likely to be predominantly controlled from Ca^{2+} mobilisation the ER stores and subsequent SOCE from plasma membrane channels. There are reports which suggest a contribution of SOCE to FcγR signalling in murine macrophage cells, however there is a lack of knowledge regarding the direct involvement of Orai in FcγR signalling and of the Ca^{2+} signalling in human macrophages – again highlighting another gap

in knowledge that my study aims to address. Further details regarding SOCE contribution to FcγR signalling is covered in *Section 5.1.3*
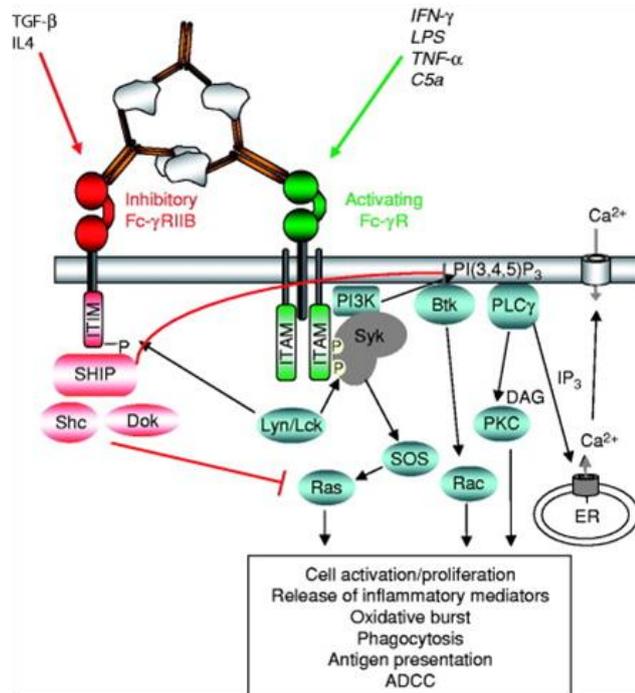
Figure 1.9   **Schematic diagram showing the co-regulation of activating and inhibitory FcR signalling**

Red lines indicate points where inhibitory signalling pathways interfere with their activating counterparts. Moreover, factors that change the balanced expression of activating and inhibitory FcRs are shown at the top. See text for further details. Reproduced with permission from (Nimmerjahn & Ravetch, 2007)

Structure	Name	CD	Gene	Alleles*	IgG1	IgG2	IgG3	IgG4	Major function
ITAM—γ₂	FcγRI	CD64	*FCGR1A*	–	6×10^7¶	No binding	6×10^7¶	3×10^7¶	Activation
α	FcγRIIA	CD32A	*FCGR2A*	His131 Arg131	5×10^6 3×10^6	4×10^5 1×10^5	9×10^5 9×10^5	2×10^5 2×10^5	Activation
ITIM— α	FcγRIIB	CD32B	*FCGR2B*	Ile232 Thr232	1×10^5 1×10^5	2×10^4 2×10^4	2×10^5 2×10^5	2×10^5 2×10^5	Inhibition
α	FcγRIIC	CD32C	*FCGR2C*	Gln13 Stop13	1×10^5	2×10^4	2×10^5	2×10^5	Activation
γ₂	FcγRIIIA	CD16A	*FCGR3A*	Val158 Phe158	2×10^5 1×10^5	7×10^4 3×10^4	10×10^6¶ 8×10^6¶	2×10^5 2×10^5	Activation
GPI anchor	FcγRIIIB‡	CD16B	*FCGR3B*	NA1, NA2 or SH	2×10^5	No binding	1×10^6	No binding	Decoy; activation?
β₂m α	FcRn§	None assigned	*FCGRT*	ND‖	8×10^7¶	5×10^7¶	3×10^7¶	2×10^7¶	IgG recycling and transport
	TRIM21§	None assigned	*TRIM21*	ND	5×10^6¶	5×10^6¶	2×10^6¶	5×10^6¶	Activation and proteasome targeting
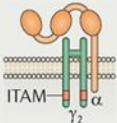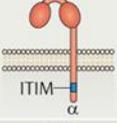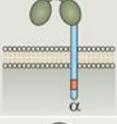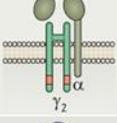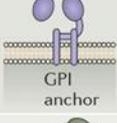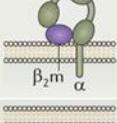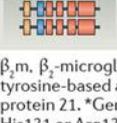
β₂m, β₂-microglobulin; FcγR, Fc receptor for IgG; FcRn, neonatal FcR; GPI, glycosyl phosphotidylinositol; ITAM, immunoreceptor tyrosine-based activation motif; ITIM, immunoreceptor tyrosine-based inhibitory motif; TRIM21, tripartite motif-containing protein 21. *Gene polymorphisms identified either by the position in the protein and the amino acid substitutions (for example, His131 or Arg131), or by the name of the allele (NA1, NA2 or SH). ‡Associates with integrins[140]. §Intracellular receptor[50,52]. ‖No alleles have been described to date that affect binding affinity or that are linked with disease. ¶Affinity value corresponding to a high-affinity interaction. The binding affinity values of the FcγRs for the various immunoglobulin subclasses are depicted in M^{-1} unit.

Figure 1.10   Table showing human receptors for IgG

Table reproduced with permission from (Guilliams et al., 2014)

Section 1.3 has covered areas of macrophage biology with relevance to my study, further information about the importance of Ca^{2+} in macrophage biology and the current knowledge of specific Ca^{2+} channels with defined roles in macrophage activation is discussed in **Section 4.1 & 5.1**.

1.4 Orai channels

This section provides an overview of the key properties of Orai channels and the critical associated proteins. Topics covered have been selected to provide appropriate context for the work of this thesis.

1.4.1 Discovery of SOCE, I_{CRAC} and distinctive biophysical properties

SOCE is now a well described activation mechanism to direct Ca^{2+} signalling through SOCCs (Smyth *et al.*, 2010). However it was Berridge in 1983 that first identified IP_3 as the second messenger responsible for Ca^{2+} release from the ER, subsequently the process of SOCE as a consequence of IP_3 regulated ER Ca^{2+} release was proposed by Putney in 1986. Further research by Hoth and Penner in 1992 revealed the first unequivocal evidence for a Ca^{2+} current in non-excitable cells. Their experiments performed in rat mast cells demonstrated Ca^{2+} release activated Ca^{2+} current (I_{CRAC}). I_{CRAC} was shown to be activated following ER store depletion, mediated either by IP_3 or also through the action of Ca^{2+} chelator, BAPTA (Hoth & Penner, 1992). Together these studies provided evidence to elucidate the process of SOCE.

From the work of Hoth and Penner, several defining characteristics of I_{CRAC} were observed. I_{CRAC} was shown to have characteristic current-voltage relationship, with the current amplitude greater at negative potentials and often zero during positive potentials (Hoth & Penner, 1993). When the standard voltage protocol was performed in electrophysiology experiments (voltage ramps of -100 to +100mV), the current-voltage relationship showed an inward rectification at negative voltages (Parekh & Putney, 2005). A high Ca^{2+} selectivity of the I_{CRAC} current was demonstrated through the observation that I_{CRAC} current was at zero at positive voltages when Ca^{2+} was the charge carrier (Parekh & Penner, 1997). Similarly, when fura Ca^{2+} dye was used to measure Ca^{2+} entry into a cell over time as a measure of Ca^{2+} permeability, rat mast cells were shown to be more Ca^{2+} selective than voltage-gated Ca^{2+} channels (Hoth, 1995). Ca^{2+} release-activated Ca^{2+} (CRAC) channels were shown to lose their selectivity for Ca^{2+} in a divalent free external solution; in DVF conditions Na^+ permeation shows corresponding store-operated currents that were 5-8 fold larger than Ca^{2+} (Parekh & Putney, 2005). Studies by Hoth and Penner were unable to distinguish single channel I_{CRAC} activity however their predicted single channel conductance to be significantly lower than 1pS (Hoth & Penner, 1993). Other defining characteristics of the I_{CRAC} current include fast Ca^{2+}-dependent inactivation (CDI) which occurs within tens of milliseconds following Ca^{2+} influx into the cytosol. This was first observed in Jurkat T cells and subsequently in RBL cells (ZWEIFACH & LEWIS, 1995; Fierro & Parekh, 1999). Evidence supporting fast CDI of I_{CRAC} was supported by data showing that hyperpolarising voltage steps reduced the current amplitude; the inactivation seen was greater in the presence of EGTA but was limited by the presence of BAPTA. This suggested dependence on the local Ca^{2+} concentration. I_{CRAC} can also undergo slow CDI (ZWEIFACH & LEWIS, 1995). In summary, these distinct biophysical characteristics of I_{CRAC} have been used to identify the current in a number of cell types and have allowed distinction of I_{CRAC} activity prior to identification of selective I_{CRAC} antagonists.

SOCE has been most commonly studied following activation of the immunoreceptors; TCR, BCR, FcεR and less commonly the FcγR. However SOCE can also be activated through G-protein coupled chemokine receptors and some PRRs e.g. Dectin-1. ER Ca^{2+} release and therefore SOCE can also occur following production of second messengers such as cyclic ADP ribose (cADPR) and nicotinic acid adenine dinucleotide phosphate (NAADP)(Feske *et al.*, 2015).
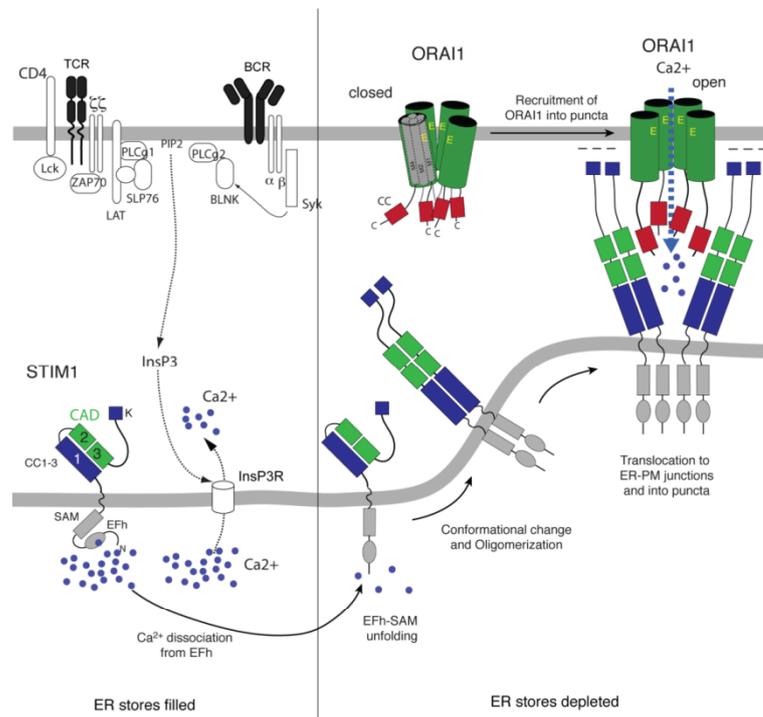
Figure 1.11   Schematic diagram showing the molecular choreography of Orai1 channel activation

TCR and BCR-signalling cascades are shown as examples of receptors whose activation culminates in the production of IP3. Depletion of ER Ca^{2+} concentration causes dissociation of Ca^{2+} from STIM1 EF hand and initiates multimerization and translocation of STIM1 to junctional ER sites in close contact with the plasma membrane. STIM1 multimers form puncta where they recruit Orai1 channels. Green boxes of STIM1 represent the C terminus where the minimal CRAC activation domain (CAD or otherwise known as SOAR). This region of STIM1 interacts with the CC domain in the C-terminus of Orai1 (red boxes) and additional domains in the N-terminus of Orai1 (not shown). Reproduced with permission from (Feske et al., 2012).

1.4.2 Identification of the proteins critical for SOCE/I$_{CRAC}$

Although I_{CRAC} was first described in 1992, it was only over ten years before the identity of the channel mediating I_{CRAC} was found. The pore forming component directing I_{CRAC} was first described in 2006, three studies simultaneously discovered the molecular identity of the pore forming protein. It had previously been observed that T cells from a subset of SCID like patients were deficient in SOCE and I_{CRAC}, therefore a study by (Feske *et al.*, 2006) performed linkage analysis of mutations in SCID patients, alongside a drosophila siRNA screen to find that the mutated protein causing this SCID/SOCE was a 4 TM protein they named Orai. Importantly they demonstrated that expressing WT Orai1 in SCID T cells caused a rescue of the SOCE and I_{CRAC}. Also published in 2006 (Vig *et al.*, 2006b; Zhang *et al.*, 2006) described work where a drosophila RNAi screen was performed with the aim of identification of proteins that inhibited SOCE. Both of these studies proposed CRACM or Orai as the pore forming protein mediated the I_{CRAC} current (the channel mediating I_{CRAC} will be referred to as Orai throughout this thesis).

The ER Ca^{2+} sensor protein responsible for the detection of ER Ca^{2+} depletion and subsequent activation of the I_{CRAC} was identified as ER resident protein, STIM. Again, an RNAi screen in drosophila was the first indication that *Stim* or the mammalian homologue STIM1 was involved in SOCE (Roos *et al.*, 2005). Similarly, a siRNA screen in HeLa cells identified STIM1 and another STIM family member (STIM2) as proteins required for SOCE mediated Ca^{2+} influx (Liou *et al.*, 2005). Heterologous expression of Orai1 or STIM1 individually had no effect on I_{CRAC}, however when expressed together a significant amplification of the I_{CRAC} was seen, thus demonstrating the functional interaction of the two proteins to mediate I_{CRAC} (Peinelt *et al.*, 2006; Soboloff *et al.*, 2006a). The choreography of STIM and Orai proteins to initiate SOCE is illustrated in ***Figure 1.11***. Identification of Orai and STIM as the critical proteins mediating I_{CRAC} represents a significant breakthrough in the field.

1.4.3 Orai1

Orai channels are highly selective Ca^{2+} channels with four TM domains. They are now well recognised as the pore forming subunit of the I_{CRAC} channel. The glutamate residue at the extracellular end of TM domain1 has been described as the region important for determining Ca^{2+} selectivity; this has been corroborated by several independent studies (Vig *et al.*, 2006a; Yeromin *et al.*, 2006). A point mutation of this glutamate region (E180 in Drosophila orai and E106 in Orai1) led to a significant change in the ion selectivity of the channel. Through the implicated role of the glutamate residue in Ca^{2+} selectivity it was hypothesized that the Orai channel selectivity filter was composed of a ring of glutamates to make a pore with a diameter in the region of 3.5anstrum. Indeed (McNally *et al.*, 2009), demonstrated through cysteine scanning mutagenesis that the entire pore region of Orai1 is lined by TM1 residues. The effect of the point mutation of the glutamate region is therefore proposed to affect the permeability by increasing the pore size to allow permeation of larger monovalent cations such as Cs^+.

Original studies suggested that Orai channel stoichiometry was tetrameric (Mignen *et al.*, 2008; Penna *et al.*, 2008). Studies of total internal reflection fluorescence (TIRF) photobleaching were used to count the number of photobleaching steps of single molecular entities and suggested that the tetrameric complex formation was most likely. However, the crystal structure of drosophila Orai was discovery was a hexameric assembly indicated; with a closed state with 3 Orai dimeric units organised around a central pore (Hou *et al.*, 2012). A subsequent study has shown that a concatenated hexameric Orai channel structure is reflective of the Ca^{2+} selectivity of a native I_{CRAC} channel (Yen et al 2014). However not all subsequent studies have validated the hexameric structure as seen in dOrai crystal; (Thompson & Shuttleworth, 2013) found that only a tetrameric concatener assembly of Orai channel subunits produced the Ca^{2+} selective I_{CRAC} like channel, a hexameric assembly showed non-selective cation currents. The reasons behind these discrepancies are possibly due to limitations in techniques to determine channel structure, or could be explained by a difference in stoichiometry in a resting or active state. In general, the other suggested functional residues of the Orai channel have been authenticated by the crystal dOrai structure. For example; the E106 region as selectivity filter, V102 as the hydrophobic gate, G98 as the gating hinge and R91 as basic gate, the structure of Orai1 and the key functional residues is shown in ***Figure 1.12*** (Amcheslavsky *et al.*, 2015).
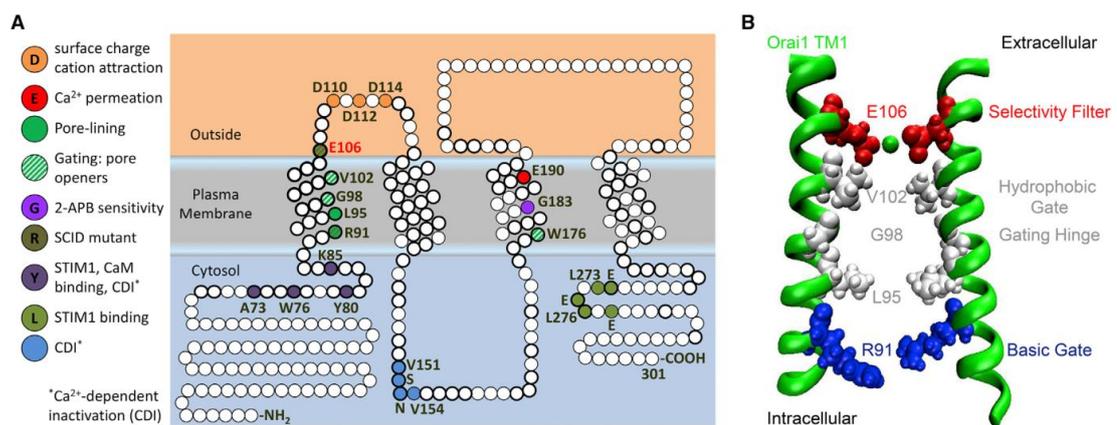
Figure 1.12   **Diagram illustrating Orai1 structure-function mapping**

A.) Annotated sequence of Orai1. (Circles) Residues; (bold) conservation in the three human Orai channels. Color-coded channel functions defined by mutational analysis are highlighted from N- to C-terminus: N-terminal STIM1 and CaM binding; Ca2þ-dependent inactivation (CDI); mutation that causes human SCID; constitutively active channel mutants; Ca2þ permeation; cation electrostatic attraction; second CDI site; TM3 residues that contribute to permeation and gating; and C-terminal STIM1 binding. B.) TM1 residues lining the Orai1 store-operated pore elucidated by functional analysis: selectivity filter E106, hydrophobic gate V102, gating hinge G98, L95, and basic gate R91. For clarity, only two TM1 domains, from two Orai1 monomers, are represented. Reproduced with permission from (Amcheslavsky et al., 2015).

1.4.4 STIM1

STIM1 and STIM2 have a single TM region with a putative Ca^{2+} binding domain in the ER lumen. STIM1 was shown to sense ER store depletion through its luminal EF-hand through mutagenesis assays. Notably following store depletion, STIM1 was shown to translocate to punctate regions near the plasma membrane (Liou *et al.*, 2005). Further definition of the role of the EF- sterile α motif (SAM) domain was performed by (Stathopulos *et al.*, 2008), where the EF-SAM domain was recombinantly expressed in *E. coli* and biophysical functional characterisation performed. Here the authors find that the EF-SAM binds Ca^{2+} and is monomeric when loaded with Ca^{2+} but upon Ca^{2+} depletion forms dimers and oligomers. Corroborating studies by (Zhang *et al.*, 2005) identified STIM1 as a Ca^{2+} sensor and showed EF-hand mutants of STIM1 to cause constitutive activation of Orai in T-lymphocytes without store depletion, thus implicating the EF hand as the region of STIM required for control of Orai activation. Importantly immunofluorescence, EM localisation and surface biotinylation showed the translocation of STIM1 from the ER to the plasma membrane upon store depletion. Further demonstration of the oligomerisation and translocation of STIM1 to form puncta at the plasma membrane upon store depletion was shown using FRET analysis of fluorescently tagged proteins expressed in HeLa and RBL cells (Liou *et al.*, 2007). A schematic diagram illustrating the key functional domains of the STIM1 protein is shown in ***Figure 1.13A***.
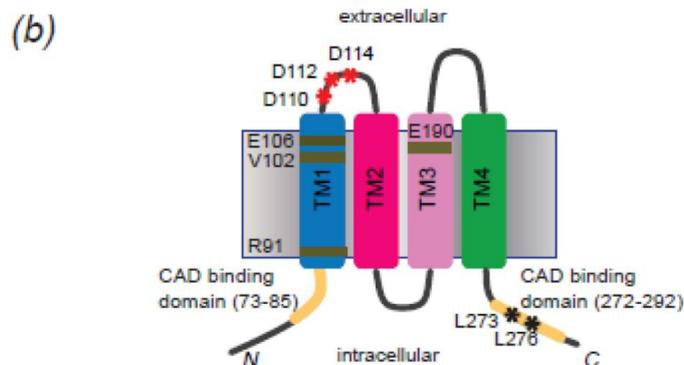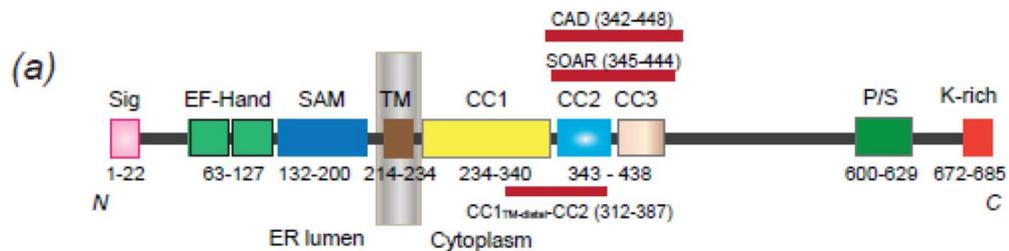
Figure 1.13 **Schematic diagram showing the topology and functional domains of STIM1 and Orai1**

> *A.) Topology of STIM1 and its functional domains. The domains include: signal peptide (Sig), EF-Hand (canonical and non-canonical EF-hand), sterile α motif (SAM), transmembrane domain (TM), coiled-coil domain (CC), CRAC Activation Domain (CAD), STIM Orai1-Activating Region (SOAR), Proline-Serine-rich domain (P/S), Lysine-rich domain (K-rich). The STIM1312–387 fragment is shown as a red bar below. B.) Topology of Orai1. Each Orai1 monomer includes four transmembrane domains (TM1–4). Residues important for Orai1 function are marked, and CAD binding regions of N- and C- termini are highlighted in golden yellow. Figure reproduced with permission from (Shim et al., 2015)*

1.4.5 STIM2

Since the initial discovery of STIM proteins as ER Ca^{2+} sensing proteins responsible for Orai activation, numerous studies have elaborated on the function of STIM1. Whilst STIM1 and STIM2 are co-expressed in most cell types (Thiel *et al.*, 2013), until recently the function of STIM2 was largely unknown. In 2006 STIM2 was reported to have an inhibitory effect on SOCE (Soboloff *et al.*, 2006b), however it was later shown that STIM2 was capable of activating SOCE but in response to smaller decreases in ER Ca^{2+} concentration (Brandman *et al.*, 2007). Interestingly subsequent work has shown that STIM2β, a splice variant of STIM2, does have an inhibitory effect on SOCE through proposed allosteric interaction with Orai (Rana *et al.*, 2015).

A structural difference between STIM1 and STIM2 was described by (Wang *et al.*, 2014b); here it was shown that, Phe394, part of the SOAR gating region of the protein was present in STIM1 but not STIM2. Subsequent studies have revealed that STIM2 has a role in the detection of more subtle levels of ER Ca^{2+} depletion, and that it aids the normal translocation and clustering of STIM1 at ER-plasma membrane junctions following a mild stimulus, thus increasing the sensitivity of SOCE to occur following weaker agonist signals (Ong *et al.*, 2015). Ong *et al.*, showed the knockout of STIM2 in mice salivary glands decreased fluid secretion predominantly following relatively low stimulus intensity activation, demonstrating how modulation of STIM2 signalling can affect functions *in vivo*. STIM2 is also capable of clustering with Orai1 following its translocation to the plasma membrane from the ER, however relative to STIM1 is a very poor activator of Orai1. Studies by (Thiel *et al.*, 2013) showed that STIM2 drives Ca^{2+} oscillations following low agonist concentrations and therefore mild store depletion. Another explanation for the differential activation thresholds for STIM1 and STIM2 could be due to STIM2 having a role in the regulation of Ca^{2+} entry in unstimulated cells or in the homeostatic maintenance of cytosolic Ca^{2+} concentrations.

1.4.6 STIM1-Orai1 interaction

Identification of the CRAC activating domain (CAD) or STIM-Orai activating regions (SOAR) of STIM1 was found in independent studies. Indication that the C-terminal coiled-coil motif of Orai1 was key for dynamic coupling to STIM1 was shown in fluorescence resonance energy transfer (FRET) studies by (Muik *et al.*, 2008). Subsequent investigations in HEK-293 cells identified a 107aa region of the C-terminus of STIM1 as key for Orai1 activation. (Kawasaki *et al.*, 2009) used a screen to assess the affect of Cherry-tagged fragments of STIM1 C-terminus to identify the crucial region, a finding that was confirmed by (Park *et al.*, 2009). Direct gating of Orai1 and STIM1 was shown by (Zhou *et al.*, 2010). (McNally *et al.*, 2012) delineate the features of STIM1-Orai1 gating and identify V102 in the extracellular region of the Orai pore as a candidate. When V102 was mutated, Orai was shown to be constitutively active, independently of STIM1, thus showing the importance of V102 in gating regulation.

1.4.7 Orai2

Orai2 has been demonstrated to form a functional SOCC with largely similar I_{CRAC} properties as originally described for Orai1. These include, a high selectivity for Ca^{2+} over sodium and an enhanced current in DVF solution (DeHaven *et al.*, 2007; Lis *et al.*, 2007). Subtle differences were shown in the Ba^{2+} and Na^{+} permeation between the Orai subtypes, observed through an in-depth biophysical characterisation of Orai1, 2 and 3 expressed in HEK-293 cells (Lis *et al.*, 2007). Notably, Orai2 mediated currents were not susceptible to CDI. Presently the functions of Orai2 are not well known, however the expression of Orai2 has been reported to coincide with that of Orai1 in a number of tissues and cell types (Hoth & Niemeyer, 2013).

1.4.8 Orai3

Like Orai2, Orai3 is able to conduct a typical I_{CRAC} current following store depletion with similar properties as described above (DeHaven *et al.*, 2007; Lis *et al.*, 2007). However, Orai3 was reported to have a prominent fast CDI in comparison to Orai1 and 2. Notably Orai3 has been shown to be activated by 2-APB independently of STIM1 (Lis *et al.*, 2007; Peinelt *et al.*, 2008). It has been demonstrated that E81 is homologous to Orai1 E106 in the control of Orai3 Ca^{2+} selectivity.

Orai3 is perhaps best known for its activity as an arachidonate-regulated Ca^{2+} channel (ARC) channel. A pentameric arrangement of Orai1 and Orai3 was shown to form a distinct Ca^{2+} channel that can be activated by arachidonic acid. ARC activated Ca^{2+} currents are similar to I_{CRAC} and have been shown to require STIM but are store independent (Mignen *et al.*, 2008). Interestingly LTC4 was shown to activate Orai1/Orai3 channels in vascular smooth muscle cells (VSMCs), whether LTC4 could activate Orai1/Orai3 channels in other cells types is not yet known (González-Cobos *et al.*, 2013). Orai3 has been implicated with a role in cancer,

with increased Orai3 expression seen in cancer tissue and MCF-7 breast cancer cells (Faouzi *et al.*, 2011). siRNA of Orai3 reduced expression of proto-oncogene, c-myc (Faouzi *et al.*, 2013).

1.4.9 Interacting proteins

A number of regulatory proteins have been associated with Orai channels since their molecular identification in 2006. A comprehensive list of other interacting proteins is summarised in *Figure 1.14*. These interacting proteins can modulate Orai activity and must be considered as potential influencers of Orai-mediated signalling.

Regulator name	Cellular localization	Effect on SOCE	Binding partner(s)/possible mechanism	References
Septin	Resides at the ER-PM junctions. Organizes membrane domains to facilitate STIM1-Orai1interactions at the ER-PM junctions	Enhances SOCE	STIM1:Orai1complex	[81]
CRAC regulatory protein 2A(CRACR2A)	Resides in the cytoplasm. Facilitates clustering of STIM1 and Orai1 at the ER-PM junctions.	Enhances SOCE. Regulates SOCE in[Ca^{2+}]$_i$ dependent manner	STIM1 Orai1 N-terminus	[82]
Junctate	Resides in the ER membrane. Recruits STIM1 to the ER-PM junctions	Ensures efficient and timely assembly of STIM1/Orai1 complexes at the ER-PM junctions.	STIM1	[84]
SOCE-associated regulatory factor(SARAF)	Resides in the ER membrane. Translocates to ER-PM junction in STIM dependent manner and facilitates dissolution of STIM1 clusters to turnoff SOCE.	Diminishes SOCE	STIM1 STIM2	[85]
Calmodulin	Resides in the cytoplasm. Site of action not established.	Reduces SOCE through Ca^{2+}-dependent inactivation.	Orai STIM	[83,86,87]
Golli	Anchored at the plasma membrane. Cellular function unknown.	May inhibit SOCE, mechanism unknown.	C-terminal domain of STIM1	[88,89]
Partner ofSTIM1(POST)	Resides primarily in the ER membrane. Binds to STIM1 and co-migrates to the ER-PM junction after store depletion. Organizes signalling molecules around the CRAC channel.	No direct effect on SOCE but thought to organize signalling molecules around the CRAC channel.	STIM1	[90]

Figure 1.14   Table summarizing key regulators of SOCE

1.4.10   Orai channel pharmacology

Before molecular characterisation of the proteins comparing the channel mediating Orai Ca^{2+} influx, finding compounds to selectively inhibit Orai was challenging. However a number of compounds were reported to confer inhibitory activity to SOCE; the compounds most commonly reported were La^{3+}, Gd^{3+}, 2-APB, BTP2, SK&F96365. Although these compounds were largely effective in Orai Ca^{2+} influx they were also shown to confer activity against a wide range of other ion channels and signalling processes.   For example, lanthanides (La^{3+} and Gd^{3+}) have been shown to inhibit a number of TRPC subtypes in addition to Orai channels, (Jung *et al.*, 2003; Putney, 2010), SKF96365 has been shown to inhibit voltage-gated Ca^{2+} channels and 2-APB has been shown to inhibit K^+ channels and TRP channels whilst also activating TRPV6 (Lievremont *et al.*, 2005). The inhibition of Orai channels by 2-APB is complex; at low concentrations (1-5µM) 2-APB has been shown to enhance Orai activity however at concentrations higher than 10µM it completely blocks Orai activity. At high concentrations, 2-APB has been shown to inhibit the cluster formation of STIM1 which could be altering the effectiveness of its ability to activation Orai channels (DeHaven *et al.*, 2008). The reasons for this dual profile are unclear.

Identification of the crucial proteins required for SOCE has allowed more accurate identification experiments to be performed to identify novel antagonists, using recombinant proteins expressed in a model system as a way to validate compounds. As summarised by (Sweeney *et al.*, 2009), Orai channel selective antagonist development has been led by pharmaceutical companies. Initially this was in the form of pyrazole based compounds which were discovered through screening for immunosuppressive agents, for example compounds by Astellas were shown to inhibit IL-2 production from Jurkat T lymphocytes. In 2005 Synta pharmaceuticals first reported the discovery of inhibitors of Orai channels, as shown in human primary T cells, Jurkat T lymphocytes and RBL cells. After the development of these initial Synta compounds a novel antagonist; 3-fluoro-pyridine-4-carboxylic acid (2', 5'-dimethoxy-biphenyl-4yl)-amide, otherwise known as Synta66 was published through patent application WO2005/009954. Synta66 was supplied to several research groups who confirmed its action as a selective Orai antagonist in several cell types.

Synta66 was first described by (Ng *et al.*, 2008), in this study Synta66 was found to inhibit thapsigargin induced Ca^{2+} signal in RBL cells by 90%, similarly pre-treatment with Synta66 for 5 minutes was sufficient to abolish I_{CRAC} currents. A concentration-response experiment revealed an IC50 of 3µM. Later the effectiveness of Synta66 as a selective Orai channel antagonist was described by (Di Sabatino *et al.*, 2009) in RBL cells they reported the IC50 to be 1.4µM. Di Sabatino used a panel of radio-ligand binding assays (CEREP) to show Synta66 did not significantly affect the activity of other ion channels, receptors and enzymes at a concentration of 10µM. (Li *et al.*, 2011) demonstrated the activity of Synta66 against SOCE

in VSMCs, interestingly the potency of the compound was far greater in this cell type (IC50 26nM) compared to a parallel experiment performed in leukocytes (showing IC50 of 1.76µM).

Distinct Orai selective inhibitors were then developed by GSK, the structure of these compounds (named GSK-7975A and GSK-5503A) compared to Synta66 is shown in (Derler *et al.*, 2013). Functional patch clamp electrophysiology experiments demonstrate that the action of GSK-7975A, GSK-5503A and Synta66 exhibit similar inhibitory profiles. The potency of GSK-7975A for inhibition of Orai1 and Orai3 currents was shown to be ~4µM (IC50), indicating it has a lower potency than Synta66. Importantly, (Derler *et al.*, 2013) also provides the first indication of mode of action the GSK-7975A. FRET assays demonstrated that GSK-7975A does not interfere with STIM1/STIM1 oligomerization or STIM1/Orai1 interaction. However experiments with an Orai1 E106D pore mutant showed that GSK-7975A no longer inhibited the Ca^{2+} currents. The explanation for the altered Orai pore geometry preventing the action of GSK-7975A could be: A) GSK-7975A binds to a site close or allosterically linked to the Orai pore selectivity filter in order to prevent ion permeation B) GSK-7975A inhibits permeation through Orai through enhancing the process of Ca^{2+}-dependent inactivation. Due to the lack of a concentration-dependent change in the Ca^{2+}-dependent inactivation seen through GSK-7975A this option is less likely. Notably Derler and colleagues also studied the selectivity profile of GSK-7975A against 16 other recombinantly expressed ion channels. The majority of ion channel activity was not modulated by 10µM GSK-7975A, including TRPC3 and TRPC6 importantly. However, GSK-7975A showed a slight inhibitory effect on Cav1.2 Ca^{2+} entry and also showed minor inhibition of TRPV6 with a profile similar to that shown by La^{3+}. A potential explanation for these two non specific effects could be due to similarities in the selectivity filter structure between the three channels, further research would be necessary to confirm such speculation. Given the difference in the mode of activation of TRPV6 and Cav1.2, it is unlikely that these singular off target effects would be a problem when GSK-7975A is used to study SOCE *in vitro*. Taken together, the work described in ***Section 1.4.10*** illustrates that great progress has been made in the discovery of selective Orai channel antagonists. As work by the Seward lab and others have shown, availability of selective Orai inhibitor tools has allowed work to be performed to elucidate the function of Orai channels in primary human immune cells, where genetic manipulation is a significant technical challenge.

In sum, ***Section 1.4*** has revealed that there is a wealth of knowledge regarding the characteristic properties of Orai and STIM. However, as discussed in ***Section 5***, there is a lack of understanding in the functional role of Orai channels in aspects of immune biology, in particular that of human macrophages.

1.5 TRPC channels

1.5.1 Discovery, background and overview

TRP channels are a super family of structurally related channels of which the majority are classified as cation channels with Ca^{2+} permeability (Venkatachalam & Montell, 2007). TRP channels were first discovered in Drosophila photoreceptors, mutations in TRP were shown to have a transient response to light with a 10-fold decrease in Ca^{2+} influx mediated by the light. Further experiments showed that Ca^{2+} channel inhibitor lanthanum (La^{3+}) mimicked the TRP mutant phenotype in drosophila photoreceptors, and that there was no further effect of La^{3+} on mutant TRP cells, indicating the TRP protein encoded a Ca^{2+} channel (Montell & Rubin, 1989). Subsequent heterologous expression studies indicated that TRP was a novel type of Ca^{2+} permeable channel (Hardie & Minke, 1992).

The TRP super family of cation channels has 7 subfamilies which can be split into two further groups based on sequence similarity. Within the group 1 subfamily are the: TRPC, TRPV, TRPM, TRPN and TRPA channel families, although TRPN channels are not found in mammalian tissues. These subgroups all have 6 putative TM domains. Within the group 2 subfamily are the TRPML and TRPP channel families, these TRP channels are distantly related to those in group 1 due to their large extracellular loop between the 1st and 2nd TM domain (Montell, 2005).

In general the TRP channel structure consists of 6 TM segments with a pore region loop between TM S5 and S6. At the NH2 terminal are 3-4 ankyrin repeats which are involved in mediated protein-protein interactions (Minke & Cook, 2002). TRP channels can form homomeric and heteromeric channel formations, the frequency of heteromeric channel formations reported means that there is a possibility for more ion channels each with their own characteristics. Although some correlation between the channel sub grouping and activation mechanism is seen, in general the subfamily assignment is not a reliable indicator of the activation mechanism. For example there are thermally activated TRP channels found in the TRPV, TRPM and TRPA subfamilies and TRPV1 can respond to numerous stimuli ranging from proinflammatory mediators to heat. The majority of the TRP channel families have low selectivity for Ca^{2+} over other monovalent and divalent cations. Exceptions to this are TRPM4 and M5 which are not permeable to Ca^{2+}, and TRPV5 and V6 which have a high selectivity for Ca^{2+} (Birnbaumer, 2009).

My study focuses on TRPC channels and the rest of **Section 1.5** covers details of TRPC biology relevant to this thesis.
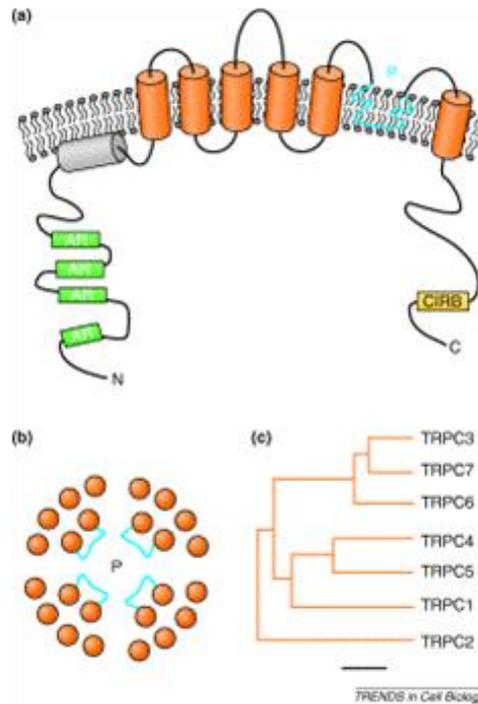
Figure 1.15   Diagram showing the structure of canonical transient receptor potential (TRPC) channel proteins

A.) Structure of TRPC channel subunits (represented by TRPC3) - consists of six transmembrane segments (orange) and one hydrophobic segment (P) that does not span the membrane completely and is thought to comprise the channel pore (blue). There is another hydrophobic domain (gray) that does not seem to span the membrane at all. The N-terminal region contains four ankyrin-like repeats (ARs). Near the C terminus, there is a region (CIRB) that binds both calmodulin and the inositol (1, 4, 5)-trisphosphate receptor, and is important for proper trafficking of the protein to the plasma membrane. B.) The formation of a functional TRPC channel requires four subunits to come together. The image shows how four TRPC subunits with their transmembrane segments (orange) and pore sequences (blue) might be seen from above the plasma membrane. C.) Structural relatedness of the TRPC channel family. Scale bar=10 PAM units. Reproduced with permission from (Putney, 2004).

1.5.2 TRPC activation

There are 7 TRPC family members, with TRPC1, 3, 4, 5, 6 and 7 expressed in humans and in other mammalian cells TRPC2. TRPC2 is a pseudogene is human but is expressed in other species (Vannier *et al.*, 1999). The structure of TRPC channels is denoted in *Figure 1.15*. In addition to Ca^{2+}, TRPC channels also show permeability to K^+, Na^+, Cs^+ and Ba^{2+} (Parekh & Penner, 1997). Classically the TRPC family was divided into 2 subgroups based on the sequence similarity and also largely correlating to their mode of activation. The TRPC1, 4 and 5 channels form subgroup 1 and have been shown to be activated by PLC-dependent signalling processes; there is increasing evidence for activation of this subgroup by store depletion (Birnbaumer, 2009). TRPC3, 6 and 7 are subgroup family 2, these channel members share 70-80% amino acid homology and are sensitive to activation by DAG – a

component further down the PLC signalling cascade (Hofmann *et al.*, 1999; Okada *et al.*, 1999). Whether TRPC3/6/7 also contributes to SOCE is controversial (discussed further in **Section 1.5.8**). A large proportion of the early work into TRPC activation mechanisms was performed using HEK over-expression systems; the emerging evidence of the influencing nature of the co-expression of other TRPC channels and STIM/Orai families suggests that TRPC mode of activation may be variable in different native systems dependent on the expression profile of such proteins.

1.5.3 TRPC1

(Zhu *et al.*, 1995) identified TRPC1 through a screen to identify homologues of Drosophila TRP channels. TRPC1 has been demonstrated to be widely expressed in tissues including the brain, heart, lung, smooth muscle, salivary gland and liver (Wu *et al.*, 2010). There are 5 splice variants of TRPC1 at mRNA level, with three translated into functional proteins (Dietrich *et al.*, 2014). Of all the TRPC family members, TRPC1 has been most consistently described to be a SOCC. (Zitt *et al.*, 1996) report the first study of TRPC1 activity; CHO cells were transfected with TRPC1A, a splice variant of TRPC1. Significant currents were induced by thapsigargin and IP$_3$ in TRPC1A expressing cells, with sensitivity to 10µM Gd^{3+}; indicating TRPC1 is a SOCC. The current-voltage relationship of the store-operated TRPC1 currents was linear with the reversal potential close to zero indicating a channel with distinct biophysical properties than I$_{CRAC}$ currents. Substitution experiments ascertained that the TRPC1A channels were supporting Na$^+$ and Ca^{2+} flux and noise analysis of currents predicted single channel amplitude of 1.1pA at -70mV and a single channel conductance of 16pS. Comparable currents were induced by store depletion in Xenopus oocytes and Sf9 insect cells providing further evidence to corroborate the channels activation mechanism.

The first evidence for endogenous TRPC1 involvement in SOCE was described in human submandibular gland ductal cells (Liu *et al.*, 2000), here it was shown that knockdown of TRPC1 led to a decrease in the SOCE. Native TRPC1 mRNA and protein expression and Ca^{2+} signalling activity was demonstrated in arterial smooth muscle cells (Xu & Beech, 2001). Since this discovery, TRPC1 has been linked with SOCE in a number of cell types including; keratinocytes, platelets, smooth, skeletal and cardiac muscles, HEK-293, salivary gland, neuronal, intestinal and endothelial cells (Cheng *et al.*, 2013). Contrary to the store-operated mode of activation, TRPC1 can also be mechanically gated, with activation occurring through tension across the lipid bilayer, as demonstrated by heterologous expression studies in CHO-K1 cells and in Xenopus oocyte cells (Maroto *et al.*, 2005).

Notably, TRPC1 was demonstrated to have an intracellular expression in HEK cells, when expressed alone. However, co-expression of TRPC1 with TRPC3, 4, 5 and 6 or dual expression of TRPC1 and TRPC4 was shown to be capable of altering TRPC1 localisation to the plasma membrane (Hofmann *et al.*, 2002). TRPC1 localisation at plasma membrane and intracellular sites has been described in sinus endothelial cells (Uehara, 2005). (Lockwich *et al.*, 2000) show TRPC1 localises with cholesterol rich lipid rafts in the plasma membrane in human salivary gland (HSG) cell membranes, suggesting plasma membrane

localization. Emerging evidence, as covered in **Section 1.5.10**, suggests that TRPC channel localization is dependent on the expression levels of associated proteins and the activation state of the cell. Further details regarding TRPC1 activity as a SOCC and its reported role in mast cells is covered in **Section 1.5.8** and **3.1**, respectively.

1.5.4 TRPC3

TRPC3 was first described by (Zhu *et al.*, 1996) as a channel activated by PLC. (Zitt *et al.*, 1997) later showed that TRPC3 expressed in CHO cells exhibited constitutive activity. TRPC3 channels showed permeability for Ca^{2+} and sodium and were not enhanced by store depletion protocols. Notably, TRPC3 currents were enhanced by an increase in intracellular Ca^{2+} concentration, indicating a Ca^{2+}-dependent activity. (Dietrich *et al.*, 2003) suggest that TRPC3 constitutive basal activity is caused by the glycosylation status. When the glycosylation of TRPC3 and TRPC6 (TRPC6 a subfamily member without basal activity) were compared, TRPC3 was shown to be glycosylated on the 1st extracellular loop whereas TRPC6 has 2 glycosylated extracellular sites. Mutagenesis studies to impair the 2nd glycosylation site of TRPC6, gave TRPC6 a constitutive basal activity like TRPC3.

Despite original heterologous expression studies showing no store-operated TRPC3 currents, over-expression of TRPC3 in HEK-293 cells has been shown to cause increase in SOCE, similarly knockdown of TRPC3 in mouse models decreases SOCE (Kim *et al.*, 2006); (Zagranichnaya *et al.*, 2005). As discussed in **Section 1.5.8** it is likely that the co-expression of STIM1 may be responsible for modulating the activation status of TRPC channels.

1.5.5 TRPC4 and TRPC5

TRPC4 was initially cloned from the bovine adrenal gland (Philipp *et al.*, 2000) whereas TRPC5 was initially cloned from mouse brain (Okada *et al.*, 1998). TRPC4 and TRPC5 have a high level of structural similarity and have a number of similarities. Unique to TRPC4 and TRPC5 channels is the expression of a PDZ-binding domain - where protein-protein interactions occur to direct signalling complexes (Tang *et al.*, 2001). Evidence suggests the PDZ binding domain is crucial for localization of TRPC4 with signalling complexes at the plasma membrane – deletion of PDZ from TRPC4 expressing cells caused impairment in TRPC4 plasma membrane expression (Mery *et al.*, 2002).

Histamine and carbachol induced currents in HEK TRPC4 and TRPC5 expressing cells – with a current voltage relationship demonstrating a double rectifying form and reversal potential close to zero. IP_3 did not induce any significant current. Notably, the basal Ca^{2+} concentration was higher in TRPC4 and TRPC5 expressing cells compared to that of control HEKs (Schaefer *et al.*, 2000). The double rectifying current-voltage relationship is characteristic of TRPC4 and 5 and caused by Mg^{2+} block that occurs at negative membrane potentials (Blair *et al.*, 2009). HEK cells expressing cloned murine TRPC5 revealed a Ca^{2+}

influx in response to 100μM carbachol which was sensitive to inhibition through PLC inhibitor U73122 demonstrating the dependence on PLC. However, in addition to activation by PLC-coupled receptors, some reports have shown TRPC5 to be activated/potentiated by increase in intracellular Ca^{2+} concentration and by high concentrations (10-100μM) of lanthanides (Jung *et al.*, 2003; Blair *et al.*, 2009). Studying the effect of lanthanides on TRPC5 in HEK cells, (Jung *et al.*, 2003) reported a dual effect of La^{3+}, with an inhibitory and activatory effect reported dependent on concentration. This was observed both through whole cell and single cell electrophysiological analysis; potentiation was predicted to occur through an increase in the channels open probability. A corroborating study in TRPC5 expressing HEK cells using whole cell and single channel patch clamp recordings showed 1μM $[Ca^{2+}]I$ caused a 25 fold increase in agonist activated TRPC5 current (Blair *et al.*, 2009). Together these studies show that TRPC4 and TRPC5 can be activated by PLC coupled receptor mechanisms but also are sensitive to Ca^{2+}-dependent activation.
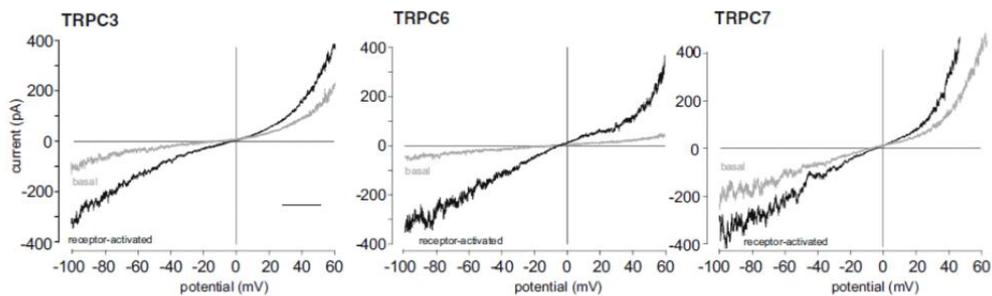
Figure 1.16   Current-voltage relationships of TRPC3, 6 and 7 channels

Channels were expressed in HEK-293 cells and activated downstream of receptor stimulation. TRPC3 and TRPC7 have high basal activity compared with TRPC6 (see grey traces). Note that voltage is displayed to 100mV in the negative direction and only +60mV in the positive direction; all channels are outwardly rectifying with a reversal potential close to 0mV. Reproduced with permission from (Dietrich et al., 2005).

1.5.6 TRPC6

TRPC6 is widely expressed throughout a number of tissue types; brain, kidney, lung, heart, ovary and testis (Garcia & Schilling, 1997). A number of physiological roles for TRPC6 have been delineated (Dietrich & Gudermann, 2007). Notably, gain of function TRPC6 patients present with focal segmental glomerulosclerosis, a kidney disease causing progressive loss of kidney function (Winn *et al.*, 2005). Over-expression of TRPC6 in COS-7 cells was shown to cause an enhanced Ca^{2+} influx, indicating Ca^{2+} permeability through this channel (Boulay *et al.*, 1997). CHO-K1 cells transfected with hTRPC6 and H1 histamine receptors exhibited histamine sensitive TRPC6 currents with dual inward and outward rectification, and a reversal potential of -3.6 mV, unitary single channel amplitude was estimated to be -1.5 ±

0.1pA at -60mV and TRPC6 was shown to be permeable to Ca^{2+}, Cs^+, Na^+ and K^+ (Hofmann *et al.*, 1999). Example current-voltage traces from cells expressing TRPC3, 6 and , 7 are shown in ***Figure 1.16.*** Interestingly, Hofmann and colleagues also showed that as opposed to TRPC1, TRPC6 was not activated by thapsigargin. This study revealed for the first time that the DAG analogue, OAG (100µM) caused Ca^{2+} influx via TRPC6 channels. Notably, OAG was also shown to activate hTRPC3 and hTRPC6 expressing cells but not hTRPC4 and hTRPC5. Further work by (Estacion *et al.*, 2006) shows that TRPC6 activation can be regulated by the membrane potential of the cell, with a dual role of TRPC6 suggested based on the membrane potential. OAG mediated Ca^{2+} influx was shown to be impaired in HEK-TRPC6 cells with a membrane potential close to zero, induced by high K^+ however a Ca^{2+} influx was observed in cells with a negative resting membrane potential. DAG is a product downstream of PLC-linked receptors, and physiological activation of PLC-linked receptors in heterologous expression systems have been shown to activate TRPC6 currents (Boulay *et al.*, 1997; Hofmann *et al.*, 1999; Inoue *et al.*, 2001; Venkatachalam *et al.*, 2003; Cayouette *et al.*, 2004; Estacion *et al.*, 2004; Bousquet *et al.*, 2010). Other reported activators of TRPC6 include a main constituent of St John's Wort: hyperforin. Through studies for the treatment of depression, hyperforin has been demonstrated to reduce monoamine uptake by elevating the Na^+ concentration and therefore decreasing the driving force for neurotransmitter transporters, this activity lead to the prediction of the mechanism of action occurring through a non-selective non voltage activated cation channel. Hyperforin was shown to drive driving Na^+ and Ca^{2+} influx in a lanthanide and SK&F96365 dependent manner. PC12 cells transfected with a TRPC6 dominant negative mutant, exhibited a significant decrease in hyperforin induced Ca^{2+} entry and in PC12 WT cells, single channel properties of TRPC6 like channels were observed after hyperforin application (Leuner *et al.*, 2007).

Despite original work demonstrating TRPC6 to be insensitive to store-operated activation, subsequent studies in platelet cells report contrary results. Platelet cells from double TRPC6$^{-/-}$ and Orai$^{-/-}$ show a greater reduction in SOCE than in Orai$^{-/-}$ cells, suggesting a contribution or supporting role of TRPC6 to SOCE (Chen *et al.*, 2014). It must be considered that this study is considering TRPC6 activation in combination with Orai, as discussed in more detail in ***Section 1.5.8*** evidence suggests STIM/Orai can regulate TRPC activation and receptor/store-operated preferences.

1.5.7 TRPC7

TRPC7 is also a non-selective Ca^{2+} permeable cation channel with two splice variants reported. TRPC7 expression has been shown in the heart, lung, eye, brain, spleen and testis (Okada *et al.*, 1999). Like TRPC3, TRPC7 has a high constitutive activity. It has been shown to be activated by DAG, similarly to TRPC3 and TRPC6, through work in HEK cells expressing murine TRPC7. TRPC7 activity has also been demonstrated following activation of ATP activated P2Y receptors (Shi *et al.*, 2004).

1.5.8 TRPCs as SOCCs

A wealth of evidence supporting TRPC channels as SOCC comes from work looking into TRPCs-STIM1-Orai interaction. An in depth and comprehensive review of this subject is summarized by (Choi *et al.*, 2014), however **Section 1.5.8** covers a few key studies which have provided important contributions to the understanding of TRPC-STIM1-Orai interaction and TRPC as SOCCs. Whilst initial homomeric expression studies in HEK cells suggested that TRPC3/6/7 are not store-operated, it appears that store-operated activation of TRPC channels is largely dependent on the expression and/or interaction with other SOCE machinery, STIM and Orai.

There are a number of studies which suggest a functional interaction of Orai and TRPC channels, Experiments in over-expression HEK cell models demonstrate that thapsigargin induced Ca^{2+} entry in TRPC1, TRPC3 and TRPC6 stably expressing cells is enhanced by over-expression of Orai1 (Liao *et al.*, 2007). HEK cells expressing Orai1 R91W (a mutant that results in inactive Orai channels) in combination with TRPC3 and TRPC6 caused a reduction of Ca^{2+} response to OAG in comparison to TRPC3 TRPC6 expression alone (Liao *et al.*, 2009). GST pull down assays and co-immunoprecipitation (co-IP) experiments provided evidence for physical interaction between TRPC/Orai proteins in HEK cells and similarly in human platelets (Jardin *et al.*, 2008). Co-localisation of TRPC with Orai1 was reported in endogenously in HSG cells (Ong *et al.*, 2007). Taken together these results suggest either a direct interaction of Orai and TRPC channels to explain the combination of phenotypes seen, or TRPC channel being dependent on Ca^{2+} signal through Orai channels for its activation.

Notably, TRPC channel store-operated activation has also been shown to be dependent on the co-expression of certain TRPC subtypes or STIM expression. TRPC3 only functioned as a STIM1-dependent channel in the presence of TRPC1, and TRPC6 only functioned STIM1-dependently with co-expression of TRPC4. However, TRPC channels were active in a receptor-operated manner irrespective of co-expression partner (Yuan *et al.*, 2007). In HEK-293T cells, TIRF experiments demonstrated that in the absence of STIM1, TRPC1 does not reside in membrane lipid rafts and acts as a ROCC, responding to carbachol but not thapsigargin. Cholesterol reducing agent, methyl-β-cyclodextrin (M-β-CD) also inhibited thapsigargin induced currents, even with STIM1 present, M-β-CD caused TRPC1 to act as a ROCC not a SOCC, demonstrating the integrity of the lipid raft is requisite to allow TRPC1-STIM1 SOCC activity (Alicia *et al.*, 2008). Substantiating studies to support a model of STIM1 regulation of TRPC activity was shown in 2010. Mutagenesis of TRPC/STIM electrostatic interaction site in the TRPC channels led to a defective store-operated Ca^{2+} signal, whilst receptor-operated (carbachol activated) Ca^{2+} signalling was left intact (Lee *et al.*, 2010). These studies show the mode of TRPC activity is influenced by co-expression of TRPC and STIM proteins.

Progress in understanding the complex interaction of Orai and TRPC channels was aided by investigation into the functional domains of STIM1. STIM1 can interact and cause activation

of both TRPC and Orai channels, however the regions of STIM1 mediating Orai and TRPC interaction are independent (Zeng *et al.*, 2008). Whilst STIM1 binds to TRPC1 through the ERM domain, this region was not required for TRPC activation (Huang *et al.*, 2006). Subsequent work by (Zeng *et al.*, 2008) showed that the K domain of STIM1 regulated gating and activation of TRPCs through electrostatic interaction. Expression of STIM1 KK$^{684-685}$EE mutant in HEK-293 cells caused impairment of TRPC1 activity but had no effect on STIM1 interaction. Co-expressing a TRPC1 mutant with mutation in same electrostatic interaction region caused a rescue of the phenotype. This demonstrated that it was the electrostatic regulated gating that was the crucial factor for STIM1 regulated TRPC1 activation (Zeng *et al.*, 2008). Subsequent studies by (Lee *et al.*, 2010) showed that STIM1 electrostatic interaction occurs in TRPC3, TRPC4, TRPC5 and TRPC6 channels in addition to TRPC1. Corroboration of distinct regulation of TRPC1 and Orai1 by STIM1 is demonstrated in studies in exocrine secretory cells. Expression of Orai1 and STIM1 in stimulated cells was demonstrated to co-localise around 50%, whereas localization of TRPC1 expression was indicated to be in the regions of STIM1 where Orai1 is not present (Hong *et al.*, 2011). The distinct regions of STIM1 utilised for TRPC and Orai activation illustrate that whilst there is an overlap in the mode of activation of TRPC and Orai channels, the channels are regulated independently.

(Cheng *et al.*, 2011b) convincingly demonstrated that TRPC1 is a component of SOCE in HSG cells, using the STIMKK$^{684-685}$EE mutant as a way to differentiate between Orai and TRPC-mediated SOCE. Thapsigargin induced Ca^{2+} entry was attenuated in cells expressing the STIM1 KK$^{684-685}$ mutant. Patch clamp analysis showed that the characteristic properties of an Orai-mediated I_{CRAC} current were hidden in WT HSG cells, but following STIM1 KK$^{684-685}$ mutant expression, I_{CRAC} current was revealed. Through analysis of biotinylated membrane fractions, it was shown that TRPC1 plasma membrane insertion was dependent on thapsigargin mediated local Ca^{2+} influx through Orai channels but that the co-clustering of STIM1 and TRPC1 was unaffected by Orai1 knockdown. Together these findings illustrate a distinct activity of Orai and TRPC in HSG SOCE, but that TRPC activity is dependent on Ca^{2+} entry through Orai channels (Cheng *et al.*, 2011b). The model of TRPC activation proposed by Cheng is shown in ***Figure 1.17***.

In contrast to the studies described above, (DeHaven *et al.*, 2009) report that TRPC channels function independently to STIM1 and Orai1. In this study STIM1 was co-expressed with TRPC channels in HEK-293 cells with the aim to delineate whether STIM1 potentiated TRPC Ca^{2+} influx. DeHaven and colleagues reported no enhancement in the carbachol induced TRPC Ca^{2+} signal by STIM co-expression. However these results could be explained by the methodology used. Experiments were performed in the presence of 5μM Gd^{3+}, with the aim to remove a contribution of Orai Ca^{2+} influx from the signal recorded. However based on work by (Cheng *et al.*, 2011b), it is clear than Gd^{3+} block of Orai-mediated Ca^{2+} influx would prevent a STIM regulated contribution of TRPC, therefore providing an explanation for why no enhancement in the signal was reported by STIM1 co-expression. The work of (DeHaven *et al.*, 2009) has not considered the investigation of TRPC in respect to their dependence on Orai/STIM for store-operated activity. Consequently it is not

surprising that TRPC and STIM/Orai were found to function independently based on the assay used.

Together these studies exhibit the modulating role STIM and Orai proteins can have on TRPC channel activity. Although TRPC channels may be commonly activated through PLC or DAG, increasing evidence supports that in native systems, co-expression and functional interaction of STIM and Orai proteins leads to TRPC activation in a store-dependent manner.
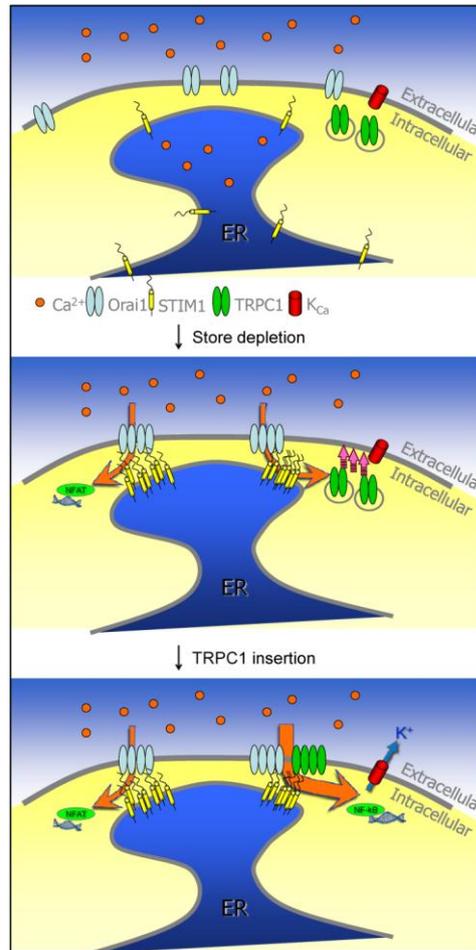
Figure 1.17   **Proposed model for TRPC1 activation**

In resting cells Orai1 and STIM1 have diffused localization in the PM and ER membrane, respectively. We predict that TRPC1 is localised in recycling vesicles (top panel). Following Ca^{2+} store depletion, STIM1 aggregates and translocates to the ER/PM junctional domains. Orai1 is recruited to the STIM1 puncta resulting in CRAC channel activation. The resulting [Ca^{2+}]i increase leads to activation of NFAT and insertion of TRPC1-vesicles into the plasma membrane (middle panel). TRPC1 is then gated by STIM1 resulting in enhancement of Ca^{2+} entry, higher [Ca^{2+}]i, and activation of KCa channels and NFκB (lower panel). Reproduced with permission from (Cheng et al., 2011a)

1.5.9 TRPC heteromerisation

TRPC family members are known for their heteromeric channel interactions with each other and other distinct TRP channel members. FRET analysis and co-IP studies in HEK over-expression models, revealed that TRPC channels were able to heteromultimerize with other channels within their subfamily (i.e. TRPC3/6/7 partners and TRPC1/4/5 partners). All homomultimeric TRPC channel combinations displayed a FRET signal (Hofmann *et al.*, 2002). In contrast to (Hofmann *et al.*, 2002), (Yuan *et al.*, 2007) described co-IP of TRPC3 with TRPC1, in the presence of STIM1, similarly interaction between TRPC4 and TRPC6 was reported. Although this work does not determine direct interaction, it is possible that the co-expression of STIM1 is crucial for an alternative heteromeric partner formation. Heteromeric store-operated TRPC1/TRPC4 channels have been reported in endothelial cells with interaction of Orai1 upon store depletion (Cioffi *et al.*, 2012a). Using electrophysiological techniques, TRPC1 was shown to form heteromeric channel complexes with TRPC3, 4, 5, 6 and 7 (Storch *et al.*, 2012). TRPC1 channels have also been shown to form heteromers with TRPV4, with current-voltage relationships distinct from TRPV4 homomers (Ma *et al.*, 2011a) and TRPP2 (Tsiokas, 2009; Ma *et al.*, 2010). These studies highlight that consideration of the heteromeric capacity of TRPC channels in interpretation of TRPC data is important.

1.5.10   TRPC supporting proteins

TRPC channel function and plasma membrane localisation is regulated by a variety of trafficking, scaffolding and regulatory proteins. A comprehensive list of the trafficking and scaffolding proteins shown to interact with TRPC channels is shown in ***Figure 1.18.*** It is possible that TRPCs mode of activation is also dependent on the expression of these regulatory proteins.

For example the lipid raft scaffolding component, Caveolin-1 (Cav1) has been shown to have a crucial role in TRPC localisation at the plasma membrane. (Brazer *et al.*, 2003) use immunocytochemistry, co-IP, GST-pull down and yeast-two hybrid assays to demonstrate an interaction between TRPC1 and Cav1. Mutagenesis studies in HSG and Madin darby canine kidney cells showed that TRPC and Cav1 interaction occurs through the N-terminus of TRPC1. A disruption to the TRPC1-Cav1 binding domain (TRPC1aa271-349 deletion) impaired translocation to the plasma membrane and similarly decreased the Ca^{2+} influx in response to thapsigargin. Similarly a mutation to alter the corresponding TRPC1-Cav1 binding domain region in Cav1 caused the same phenotype. This study revealed the importance of lipid raft scaffolding proteins such as Cav1 with roles in localisation and activation of TRPC1 channels. Similarly, TRPC6 channel localisation has been shown to be regulated by Gq-protein mediated receptor activation, ER store depletion and PI3K activation (Cayouette *et al.*, 2004; Monet *et al.*, 2012). These examples demonstrate the

regulative capacity of TRPC channels by interacting proteins and highlight that a number of factors must be considered when studying TRPC activity. Some of the contradictory results seen in the literature could be a result of differences in the regulatory protein expression in the model systems used.

Channel	Other channels	Signalling proteins	Scaffolding and trafficking proteins
TRPC1	TRPC1a, TRPC3 (Xu et al.1997), TRPC4, TRPC5 (Strubing et al.2001), TRPC6 (Strubing et al.2003), TRPC7 (Zagranichnaya et al.2005), TRPV4 (Ma et al.2010), TRPV6 (Schindl et al.2012), Orai1 (Cheng et al.2008)	IP3R, CaM, Gq/11 (Lockwich et al.2000), PLCγ (Tu et al.2005), PMCA (Singh et al.2002), SERCA (Redondo et al.2008), STIM1 (Huang et al.2006)	β-tubulin (Bollimuntha et al.2005a), Cav-1 (Lockwich et al.2000), Enkurin (Sutton et al.2004), Homer (Yuan et al.2003), MxA (Lussier et al.2005), RhoA (Mehta et al.2003), SNAP-25, VAMP(Redondo et al.2004)
TRPC6	TRPC1, TRPC4, TRPC5 (Strubing et al.2003), TRPC3, TRPC7, (Hofmann et al.2002), Orai1 (Liao et al.2007)	IP3R, CaM, Calcineurin (Tang et al.2001), FKBP12 (Kim and Saffen 2005), Fyn (Hisatsune et al.2004), Gαq/11 (Bandyopadhyay et al.2005), mAChR,PKC (Kimand Saffen2005), PLCγ (Hirschler-Laszkiewicz et al.2009), SERCA (Redondo et al.2008)	Clathrin, dynamin (Goel et al.2005), MxA (Lussier et al.2005), PI(3)K, PTEN (Monet etal.2012), Rab9, Rab11 (Cayouette et al.2010), RhoA (Tianetal.2010), Syntaxin (Bandyopadhyay et al.2005)

Figure 1.18   TRPC1 and TRPC6 interacting and scaffolding proteins. Adapted with permission from (Ong *et al.*, 2014)

1.5.11   TRPC channel pharmacology

In general there is a great lack of selective compounds to activate or inhibit specific TRPC family members. The discovery of such compounds has not been aided by the lack of a crystal structure for TRPC proteins to date. Classically non-selective Ca^{2+} antagonists such as: lanthanides, 2-APB, flufenamic acid (FFA) and SKF-96365 have been used to characterise TRPC channels activity. The wide inhibitory ability of lanthanides: Gd^{3+} and La^{3+} and SK&F-96365 and 2-APB has been summarised in *Section 1.4.10*. FFA, an N-phenyanthranilic acid, has been shown to stimulate TRPC6 but inhibit other TRPC and TRPM channels (Kraft & Harteneck, 2005; Foster *et al.*, 2009). In the absence of more selective tools the concentration variable effects of Lanthanides, 2-APB and FFA have previously been utilised as a way to distinguish between different channel activities. A few novel TRPC inhibitors

have been described over the past 6 years (Miller *et al.*, 2011; Schleifer *et al.*, 2012; Richter *et al.*, 2014); however these newly described TRPC inhibitors have a range of off target effects and are not selective for individual TRPC family members.

Recently (Washburn *et al.*, 2013) described a high throughput screen with the aim to identify highly potent and selective TRPC3/6 blockers, with a good oral PK to provide small molecule blockers to be put forward for lead optimization and target validation. Due to the association of TRPC3 and TRPC6 with cardiac hypertrophy, these channels have been identified as novel targets to treat cardiac disease. Screening was performed using HEK cells over expressing TRPC3 or TRPC6 and using carbachol as an agonist to measure the resulting change in electrical potential using membrane potential dyes measured on a FLIPR machine. This study identified a number of compounds with a proven high selectivity for TRPC3/6; assay results showed that there was no effect of the compound on a number of other ion channels including: TRPA1, TRPV4, Cav1.2, hERG and Nav1.5. One of these GSK compounds, GSK-3503A (example 19 in the publication) has been used in experiments described in ***Section 3.2.6*** of this thesis. Subsequent publications validated the use of these compounds with endogenous TRPC3/6 receptors as the TRPC3/6 antagonist was shown to dose dependently block cell hypertrophy signalling triggered by angiotensin II or endothelin II in (Seo *et al.*, 2014a).

Whilst the work of Washburn and Seo represent a significant advance in the development of selective TRPC antagonists, it is clear there is a still great need for development of TRPC selective antagonists against all subtypes. ***Section 1.5*** has described the intricacy of TRPC activation; the availability of robust potent and selective TRPC antagonists would aid further research to delineate TRPC function.

1.6 P2X7 receptors

1.6.1 Purinergic receptors history and overview

Purinergic receptors were first classified into P1 and P2 subtypes based on their activation by either adenosine or ATP (Burnstock, 1978). However a few years later the P2 receptor subtype was categorized again, into the P2X and P2Y family, this time based on their selectivity for ATP and ADP, respectively (Burnstock & Kennedy, 1985). Following the first receptor cloning in 1994 (Brake *et al.*, 1994) it was found that P2X receptors are ligand gated ion channels, whereas the P2Y receptors are G protein coupled receptors (Webb *et al.*, 1993). P2X receptors are activated by ATP and function as non-selective ion channels that are permeable to Na^+, K^+, Ca^{2+}, Sr^{2+} and Ba^{2+} (North, 2002).

P2X receptors are widely expressed throughout the body, for example P2X has been shown to be expressed in; macrophages, DCs, monocytes, lymphocytes, erythrocytes, osteoblasts, fibroblasts, endothelial and epithelial cells, as well as cells from the central and peripheral nervous systems (Bartlett *et al.*, 2014). P2X7 has been shown to be implicated in a number

of diseases, most of which have been elucidated through P2X7 single nucleotide polymorphisms, further details of the involvement of P2X7 in immune disease is provided in *Section 4.1* however a full review covering the involvement of P2X channels in a range of diseases is provided by (Bartlett *et al.*, 2014).

1.6.2 P2X family distinct characteristics

There are 6 other members of the P2X family all of which can also be activated by ATP. However there are distinguishing characteristics which can be used to discern between family members in the absence of selective antagonists. Differences in the pharmacological profile of the P2X family are summarised in *Figure 1.19*. Other defining characteristics of the P2X receptor family members are there desensitization properties following agonist application, these are summarised in *Figure 1.20*.

Receptor	ATP	ADP	αβmeATP	βγmeATP	2meSATP	BzATP
P2X1	1	30	1-3	10	1	3
P2X2	10	~300	>100	>300	3	30
P2X3	1	~50	1	>300	0.3	
P2X4	10	>>100	>>100		10-100	
P2X5	10	~300	>>100		10	>500
P2X7	100/**1000**	>>300	>>300	>100	10	3/**30**
P2X4/P2X6	10		30			

Figure 1.19   Agonist sensitivities of cloned P2X receptors

> *Numbers denote EC50 (µM). Values are taken from rP2X7 data, however rP2X7 and hP2X7 EC50s are shown for P2X7, with the latter in bold type. Table adapted from North and Surprenant 2000 reproduced with permission*
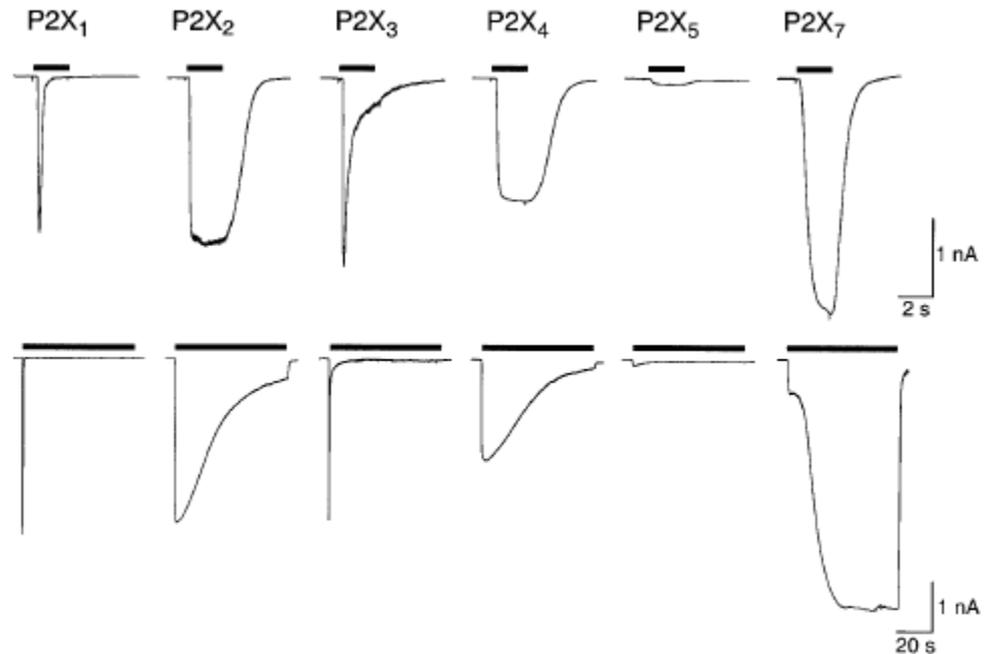
Figure 1.20 Whole cell currents in HEK293 cells expressing P2X channels

P2X2 and P2X4 exhibit slow desensitization whereas fast desensitization was observed for P2X1 and P2X5. P2X7 shows no desensitization over the duration of ATP application. Graph shows the fast (top) and slow (bottom) desensitization of homomeric rat P2X receptor subtypes, caused by a brief application (2-s duration) or prolonged application (60-s duration) of ATP. HEK293 cells were transfected with P2X cDNA 48hr prior to whole cell recordings - 30µM of ATP was applied or 1µM ATP for P2X7. Figure reproduced with permission from (North & Surprenant, 2000; North, 2002)

1.6.3 P2X7 structure

P2X7 receptors are membrane proteins that consist of oligomers of 3 subunits with two membrane spanning domains per subunit. P2X7 is characterised by its short N-terminus and longer C-terminus. Since the elucidation of the crystal structure of the drosophila P2X4 (Kawate *et al.*, 2009) it was suggested that 3 ATP molecules bind to the P2X receptors at locations between each subunit. P2X7 receptors in monomeric confirmation has a total of six helical transmembrane domains (TMDs) (2 from each subunit) with TM2 responsible for forming the physical gate to allow ion flow (Bartlett *et al.*, 2014). A diagram illustrating the structure of P2X7 receptors is shown in ***Figure 1.21***. Through the identification of loss-of-function single polymorphisms in motifs of the P2X7 protein, the regions responsible for certain P2X7 channel functions have been described. A rare polymorphism in the R307Q of human P2X7 was shown to cause a reduction in the affinity of ATP binding to the P2X7 channel and therefore has an inhibitory functional effect on the P2X7 current (Gu *et al.*, 2004). Similarly as shown in studies in HEK-293 cells and Xenopus oocytes, residue 551 in the carboxy terminus of P2X7 when mutated leads to an attenuation in receptor function

and cell surface expression, indicating this motif is important for regulation of the surface expression of the pore forming part of the P2X7 receptor (Smart *et al.*, 2003).
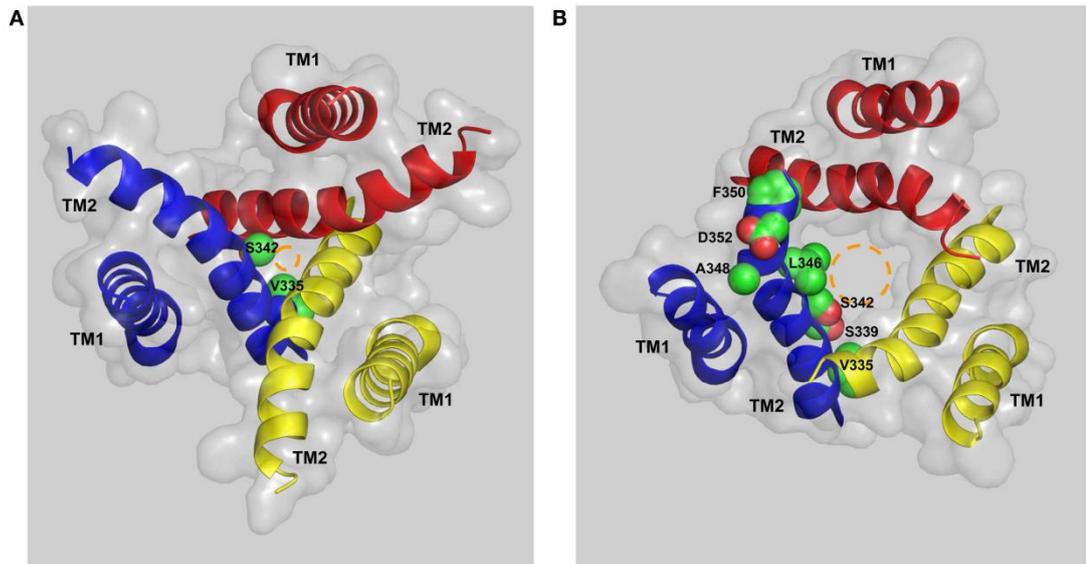
Figure 1.21 **Structural model of P2X7: the transmembrane ion-conducting pathway in the human P2X7**

1.6.4 P2X7 defining characteristics

P2X7 was originally known as P2Z and was first characterised in 1996 (Surprenant *et al.*, 1996). Cloned rat P2X7 receptor were heterologously expressed in HEK-293 cells, using whole cell patch clamp electrophysiology Surprenant and colleagues showed bzATP induced currents reversed at -2mV and exhibited a linear current voltage relationship. This was contrary to other P2X channels which showed no rectification between -90 to 50mV. A sustained nonselective conductance was observed following repeated application of agonist. The EC50 for ATP and bzATP were shown to be 115μM and 7μM respectively. The magnitude of the current amplitude and the duration of the current were increased in low divalent solution (removal of Mg^{2+}/Ca^{2+} or both), however switching to low divalent solution had no major effect on the EC50 for bzATP and ATP. (Rassendren *et al.*, 1997) subsequently described the cloning and expression of human P2X7, characterisation of endogenous P2X7 currents in hMDMs was compared alongside heterologously expressing hP2X7 in HEK-293 cells. Notably, the properties of the heterologously expressed hP2X7 in HEK-293 cells were largely similar with those observed in the hMDM cells, suggesting that hMDM used in Rassendrens study express homomultimeric P2X7 assemblies. When compared to rat P2X7 it was seen that higher concentrations of agonist were required to activate hP2X7 in normal divalent conditions, the EC50 for bzATP was around 50μM and for ATP was around 1000μM (compared to 7μM and 115μM respectively). Similarly the removal of extracellular Mg^{2+} led to a greater potentiation of the current compared to rat P2X7. A sequence homology similarity of 80% between rat and human P2X7 may account for the functional differences observed. The rank of potency of agonists for P2X7 is as

follows: bzATP>>ATP>2,methylthio ATP > ATPγS>>adenosine diphosphate (Surprenant *et al.*, 1996). bzATP is around 10-30 times more potent than ATP to P2X7 receptors and P2X7 channels are less responsive to ATP than other P2X channels, with ATP concentrations over 100μM required to cause receptor activation (North 2002).

The P2X7 channel opens following ATP application within a millisecond timeframe, following removal of the extracellular ATP the channel then closes within tens of milliseconds. However unlike other P2X channels, P2X7 has a slower desensitization rate – ATP application can be present for minutes with only a very small decrease in the P2X7 current. Following P2X7 receptor activation there is an initial fast influx of monovalent and divalent cations, predominantly Na^+ and Ca^{2+}, however following continual agonist application to the P2X7 receptor, a large permeability pore opens that permits the entry of large organic molecules up to 900D in size. There are conflicting results in the literature about whether the pore opens through P2X7 channel dilation or whether there is the activation of a secondary channel such as the hemichannel, pannexin. P2X7 mediated pore formation is associated with a rapid lowering in cytoplasmic K^+ through the large pore, therefore P2X7 activation leads to a complete collapse in the normal ionic gradients (Qu *et al.*, 2007). Experiments to study P2X7 mediated pore formation can be undertaken through the measurement of the uptake of dyes such as ethidium and YO-PRO. Lower levels of YO-PRO uptake were seen hP2X7 expressing cells compared to rP2X7, with higher agonist concentrations required for hP2X7 mediated permeabilisation (Rassendren *et al.*, 1997).

Early studies indicated P2X7 had a bifunctional role, mediating ion influx and pore formation by distinct mechanisms. Truncation of the COOH region of P2X7 was demonstrated to inhibit dye uptake without altering ion channel currents (Surprenant *et al.*, 1996; Rassendren *et al.*, 1997). This was followed by a breakthrough paper in 2006 that demonstrated a hemichannel; pannexin-1 was connected to P2X7 and the mediator of large pore formation. siRNA knockdown of pannexin-1 was shown to inhibit P2X7 mediated dye uptake without altering the associated membrane current or Ca^{2+} influx, whilst P2X7 expression was left intact (Pelegrin & Surprenant, 2006). However despite this seemingly clear cut hypothesis of a secondary channel directing P2X7 mediated pore formation, later work has disputed this conclusion. Macrophages from pannexin-1 knockout mice and following siRNA knockdown of pannexin-1 were shown to have no defect in P2X7-mediated dye uptake (Qu *et al.*, 2011; Alberto *et al.*, 2013), similarly the pannexin-1 inhibitor, CBX had no effect on dye uptake in HEK-P2X7 and human monocyte cells (Bhaskaracharya *et al.*, 2014). It seems further work is necessary to determine the mechanism involved in P2X7 mediated pore formation.

In relation to P2X7 mediated pore formation, P2X7 activation has been linked to directing the production and release of IL-1β in macrophage cells (Ferrari *et al.*, 1997b; Solle *et al.*, 2001). IL-1β secretion and release can often be separated into two different steps; with the first requiring an inflammatory signal from a pathogen-associated molecular pattern (PAMP) or damage-associated molecular pattern (DAMP) to initiate the gene expression of the IL-1β precursor and inflammasome components. The second step is characterised by

the ATP P2X7 receptor mediated inflammasome assembly, caspase-1 activation, IL-1β maturation and secretion. K^+ efflux through P2X7 channels is initiated following pore formation and is shown to be important for P2X7 mediated caspase-1 mediated IL-β maturation. There are conflicting results about whether Ca^{2+} influx is also required (Brough *et al.*, 2003; Franchi *et al.*, 2007; Qu *et al.*, 2007; Piccini *et al.*, 2008; Katsnelson *et al.*, 2015).

1.6.5 P2X7 splice variants and single nucleotide polymorphisms

There have been 9 splice variants of P2X7 described for the human P2X7 (Cheewatrakoolpong *et al.*, 2005; Feng *et al.*, 2006) and numerous SNPs causing either a gain or loss of function to human P2X7 (Gu *et al.*, 2001; Wiley *et al.*, 2003; Cabrini *et al.*, 2005; Dardano *et al.*, 2009). For example the analysis of two splice variants expressed in hHEK293 cells, one with a lacking 1st TMD and the 2nd missing the entire cytoplasmic tail revealed a resulting non-functional channel or channel with reduced functionality, respectively (Cheewatrakoolpong *et al.*, 2005). Subsequently (Feng *et al.*, 2006) report a novel hP2X7 variant (P2X7j) which lacks the entire intracellular carboxy terminus, the 2nd TMD and the distal 3rd of the extracellular P2X7 loop. P2X7j expressed in human cervical epithelial cells and HEK cells was shown to be defective bzATP induced Ca^{2+} mobilisation, pore formation and apoptosis. Notably, co-IP experiments revealed a potential interaction between P2X7j and WT P2X7 which led to the hypothesis that P2X7j can hetero-oligomerise with the full length P2X7 to form non-functional P2X7 oligomers. These two examples reveal the significant impairment seen in certain P2X7 splice variants

A number of SNPs in human P2X7 have been associated with disease, for example a P2X7 489C>T allelic variant leading to His 155 into Tyr change in extracellular receptor domain causes a gain of function to the P2X7, this mutation was seen in lymphocytes from patients with chronic lymphocytic leukemia (CLL). Notably P2X7 489T expression in HEK cells caused a higher functional activation than WT P2X7, as observed by the Ca^{2+} mobilisation in response to bzATP and the rate of EtBr uptake. Other loss of function SNPs such as 1513C caused a loss of function to P2X7; this SNP was seen 3-fold greater levels in patients with CLL than in controls. It was hypothesised that the combined presence of loss of function variants with 489T in CLL individuals increased P2X7 function to variable extents (Cabrini *et al.*, 2005). A SNP present at a low frequency within the causasian population is A Glu-496 to Ala. This SNP produces non-functional P2X7 when expressed homozygously and reduces P2X7 mediated function in heterozygous expression. In particular this was shown by a reduction in the ATP induced Ca^{2+} signal, EtBr uptake and bzATP induced cytotoxicity of T-lymphocytes (Gu *et al.*, 2001). These examples illustrate the impact of the impaired function of P2X7 in human biology.

1.6.6 P2X7 heteromultimerization

The P2X channel family is well reported to interact and form heteromultimeric channel complexes, despite this, the involvement of P2X7 as a heteromeric channel is less clear. Original data showed P2X7 was the only member of the P2X family unable to form hetero-oligomeric channels. Investigation into the protein-protein interactions between P2X family members using co-IP assays showed that a number of interacting partners were found for members P2X1-6; however no interactions were detected in any combinations for the P2X7 channel. The possibility of this result being caused by interference of their unique long intracellular carboxy terminus was proven not to be the case through co-IP experiment repeated with a P2X7 channel with a deletion of the carboxy tail (Torres *et al.*, 1999).

In subsequent studies a conflicting result was found (Guo *et al.*, 2007). Here evidence was produced that indicated P2X4 and P2X7 channels formed heteromeric channels. For example, co-IP and functional assays showed that P2X4 and P2X7 are able to interact, similarly, a non functional P2X4 mutant expressing cell inhibited P2X7 mediated current. The differences in the results of the co-IP in this study and in (Torres *et al.*, 1999) could be explained by the difference in detergents used. (Guo *et al.*, 2007) used DDM which has a better ability to preserve proteins, therefore the harsher detergent used in the Torres study could have led to degradation of part of the P2X7 interacting region. However taken on its own the study by (Guo *et al.*, 2007) is not direct proof of P2X4 and P2X7 forming a heteromeric channel assembly, interaction as assessed by co-IP could occur due to an interaction between the two channels but with them both remaining in their homomeric forms, i.e. homotrimeric interaction.

Further work by (Nicke, 2008) used antibodies and sodium dodecyl sulfate (SDS) polyacrylamide gel electrophoresis (PAGE) to investigate the interaction of P2X4 and P2X7 and concluded there was no evidence for heteromeric channel formation. Instead they proposed that previous reports of channels with a combined P2X4/P2X7 functional phenotype could be due to homotrimeric complexes. This conclusion is supported by later work by (Boumechache *et al.*, 2009) who performed experiments to cross-link solublized proteins with DSS and resolved through SDS-PAGE to show that P2X7 can assemble as monomers, homodimers and homotrimers, but not heteromeric formations. As homotrimers of P2X7 were able to co-immunoprecipitate with P2X4 this suggests that interaction of the channels occur between the receptor complexes rather than within. This hypothesis was confounded in work by (Antonio *et al.*, 2011), who performed *in situ* proximity ligation, co-immunoprecipitation, co-isolation using affinity beads, chemical cross-linking and atomic force microscopy to conclude that P2X7 and P2X7 interact in the form on homotrimers but not in a heteromeric assembly. Notably, although there have been inconsistencies in the conclusions regarding the channel subunit formation of P2X receptor families, there are a number of corroborating studies that show convincing evidence for a functional interaction between P2X7 and P2X4 and thus investigators should consider the possibility of P2X7/P2X4 functional interaction in the analysis of experiment (Casas-Pruneda *et al.*, 2009); (Ma *et al.*, 2006).

1.6.7 P2X7 pharmacology

The first generation of P2X7 antagonists were described in between 1980 and 1990, namely; suramin and brilliant blue G (BBG) (Dunn & Blakeley, 1988; Soltoff *et al.*, 1989) this was closely followed by the introduction of pyridoxalphosphate-6-azophenyl-2',4'-disulfonic acid (PPADs), oxidised ATP (oATP) and KN-62 (Lambrecht *et al.*, 1992; Murgia *et al.*, 1993; Gargett & Wiley, 1997). These classical P2X7 receptor antagonists are largely non-selective between purinergic receptor family members (Jacobson *et al.*, 2002). PPADs is an irreversible P2X7 blocker and has been shown to have the highest potency at human P2X1, P2X7 and P2Y1 receptors and is largely ineffective in rP2X4R inhibition however was found to have an IC50 of 27.5μM ± 3.4 at hP2X4R expressed in HEK 293 cells (Garcia-Guzman *et al.*, 1997). Similarly Suramin is a weak antagonist of P2X4 and P2X7 receptors. Suramin was shown to have an IC50 of 178μM ± 46.9 to hP2X4 expressed in HEK 293 cells whereas it P2X1, 2, 3 and 5 with an IC50 in the range of 1-10μM (Garcia-Guzman *et al.*, 1997; North & Surprenant, 2000). Suramin has also been demonstrated to antagonize G-proteins and proteases such as the HIV reverse transcriptase (Jacobson *et al.*, 2002). oATP has been more frequently described as a P2X7 selective antagonist, however this compound has too been shown to inhibit other targets; P2X2 and P2X3 (Evans *et al.*, 1995) and to attenuate proinflammatory signalling in a model where P2X7 had been deleted (Beigi *et al.*, 2003). oATP is an irreversible blocker of P2X7.

BBG and KN-62 are non competitive P2X7 antagonists, with BBG being demonstrated to have off-target effects on voltage gated sodium channels, similarly KN-62 also shows activity as an antagonist of Ca^{2+}/calmodulin-dependent protein kinase II (North & Jarvis, 2013). Interestingly KN-62 is inactive at the rat P2X7 receptors, but active at hP2X7, whereas BBG has been described as a rat selective P2X7 antagonist and inactivate at hP2X7 (Donnelly-Roberts *et al.*, 2009). These examples demonstrate the differential activity of P2X7 antagonists observed at receptors from different species.

Subsequent development of more selective P2X7 antagonists has been aided by the high throughput screening of large chemical libraries. This work has largely been driven by realisation of the therapeutic potential of selective P2X7 compounds in the treatment of pain and inflammation. Importantly these second generations of P2X7 antagonists have been developed with the profile of a therapeutic compound in mind, whereas the classical antagonists largely did not have the properties that would aid pharmacokinetics and dynamics *in vivo* (Bartlett *et al.*, 2014). Examples of these novel P2X7 selective compounds are summarized by (Nelson *et al.*, 2006; Donnelly-Roberts *et al.*, 2009). One example is A740003 which was shown to have an IC50 of 40nM at human P2X7 and 18nM at rat p2X7. A740003 was shown to be ineffective in the blockage of other P2X and P2Y receptors (at concentrations up to 100μM) and a CEREP panel gave further confirmation of its lack of activity at other common ion channels and receptors (Honore *et al.*, 2006). Certain novel P2X7 antagonists have also been shown to have the potential in the treatment of inflammatory pain; GSK314181A and A389977 had dose-dependent effects on rodent models of inflammatory pain (Broom *et al.*, 2008; Honore *et al.*, 2009).

The P2X7 selective antagonists used in the present study were developed by GlaxoSmithKline. The validity of the GSK-2160A and GSK-3583A compounds in the inhibition of P2X7 currents has been demonstrated through robust studies FLIPR, electrophysiology and functional assays with rat and human P2X7 expression systems to confirm the compounds selectivity and potency for the P2X7 target. Similarly, published use of the GSK-2160A compound was reported in (Ali *et al.*, 2013) where an in depth pharmacokinetic and pharmacodynamic profiling first in human study was performed. Although the results shown in (Ali *et al.*, 2013) led to the decision to halt the use of the compound for clinical use, the results do give convincing proof that the compound is active against P2X7 in native cells as well as over-expression models. This gives confidence that these P2X7 antagonists will be effective tools in this study.

There are also a number of naturally derived compounds which have been shown to block P2X7 activity, for example the Chinese herb emodin, plant derived alkaloids and estrogen hormone 17-β estradiol (Bartlett *et al.*, 2014). A gout treatment therapeutic, probenecid, has been demonstrated to block the P2X7 channel function and pore formation (Bhaskaracharya *et al.*, 2014). Importantly, probenecid is also frequently used as a component of FLIPR imaging buffer in order to prevent dye extrusion from the cell, therefore this publication reveals that caution is needed in the design of Ca^{2+} imaging assays to monitor P2X7 activation.

It is known that SNPs and splice isoform variants of P2X7 can respond differently to P2X7 inhibitors. For example, GSK1370319A was shown to have a 7 fold greater potency in individuals with a gain of function A348T SNP compared to individuals with the E496A loss of function SNP (McHugh *et al.*, 2012). This emphasises care is needed in translation of results using P2X7 antagonists, there may be stark differences seen within species based on variation in P2X7 expression.

As introduced in ***Section 1.6.7*** cations can act to inhibit P2X7 activation. (Virginio *et al.*, 1997; Virginio *et al.*, 1998) provide a detailed study of the inhibition of P2X7 by divalent cations. Here they show the IC50 for Ca^{2+} and Mg^{2+} is around 2-3mM, an increase in divalent cations causes a rightward shift in the agonist concentration response curve and Virginio propose that the divalent cations act in an allosteric way to change the affinity of ATP for the P2X receptor. The reported reduction in P2X7 mediated Ca^{2+} influx under physiological concentrations of Ca^{2+} and Mg^{2+} could suggest that this is a mechanism by which P2X7 activity is regulated.

2 Chapter 2 materials and methods

2.1 Cell culture

All cell types described below were incubated at $37^{o}C$ in a 5% CO_2 humidified atmosphere.

2.1.1 LAD2 cell culture

LAD2 cells were a kind gift from Dr. D Metcalfe at the National Institute of Allergy and Infectious Diseases, National Institute of Health, Bethesda, MD. The cell line was originally derived from a patient with mast cell leukemia. LAD2 cells were cultured in StemPro-34 media supplemented with StemPro-34 nutrient supplement and 2mM L-glutamine (all Gibco Life Technologies) in addition to 100ng/ml rhSCF (R&D systems). Cells were passaged weekly; and media was added to maintain a density of 400,000-500,000 cells/ml. To re-thaw cells from frozen stocks, a total of 1.5ml of media + 100ng/ml SCF was added to the cell vial. The cell suspension was transferred to a 6-well plate and rocked continuously at room temperature for 6 hours, every 30 minutes the cells were gently pipetted to disperse any clumps. At the end of these steps, the cells were transferred to a $12.5cm^2$ Nunclon surface tissue culture flask. To freeze cells, 10 million cells were spun at 100g for 5 minutes and then resuspended in PZerve cryopreservation supplement (Protide) with 200ng/ml rhSCF. The cells suspension was transferred to a cryovial and placed in a cryocontainer for 30 minutes at room temperature, 1 hour at $-20^{o}C$, 1 hour at $-80^{o}C$ before being placed into liquid nitrogen for long term storage.

2.1.2 HEK-293 cell culture

HEK-293 cell culture media - Dulbecco's modified eagle media (DMEM) (Gibco 31331-028) containing 10% foetal calf serum (FCS)

HEK-293 TRPC6 cell culture media – DMEM (Gibco 31331-028) containing 10% FCS and 400µg/ml geneticin (Gibco)

HEK-293 cells were split twice weekly, or when 90% confluency was reached. Cell Dissociation Solution (CDS – Sigma C5914) was used to free adherent cells. 1ml of CDS was used per $25cm^2$ Nunclon tissue culture flask and was incubated at $37^{o}C$ for 1 minute followed by addition of 2ml of HEK media to wash out the flask; the cell suspension was transferred into a 15ml tube and was spun at 110g for 4 minutes. Cells were resuspended in fresh media and 20% of the cell suspension was re-seeded into a $25cm^2$ Nunclon surface tissue culture flask, containing 5ml of culture media.

A stable HEK-TRPC6 cell line was a generous gift from Professor Guylain Boulay. TRPC6 was cloned from mouse brain RNA and amplified using PCR. A stable cell line was then created by transfecting HEK-293 cells with mTRPC6-pcDNA3 using a Ca^{2+} phosphate-based protocol. The pcDNA3 plasmid conferred resistance to geneticin to allow for selection of TRPC6 expression (Boulay et al. 1997). HEK-TRPC6 cells were therefore cultured with geneticin.

2.1.3 HLMC isolation and purification

Culture media used throughout the HLMC isolation purification and culture:

- **HLMC media** : DMEM Gibco Cat: 32430---027, 10% heat inactivated FCS Gibco cat: 10108, 1% antibiotic/antimycotic solution – (containing 10 units/ml penicillin, 10 units/ml streptomycin and 25μg/ml amphotericin B) and 1% MEM non-essential amino acids (NEAA) Gibco Cat: 11140--- 035.
- **HLMC culture media**: DMEM Gibco Cat: 32430---027, 10% heat inactivated FCS Gibco cat: 10108, 1% antibiotic/antimycotic solution – (containing 10 units/ml penicillin, 10 units/ml streptomycin and 25μg/ml amphotericin B) and 1% MEM non-essential amino acids (NEAA) Gibco Cat: 11140--- 035, Rh-IL-10 R&D systems Cat 217-IL, Rh-IL-6 R&D systems Cat 206-IL & Rh-SCF R&D systems Cat 255-SC - at concentrations of 10ng/ml, 50ng/ml and 100 ng/ml respectively.
- **DMEM wash media:** DMEM (Gibco Cat: 32430---027) +2% heat inactivated FCS (Gibco cat: 10108)
- **Hank's Balanced Salt Solution (HBSS) wash media:** HBSS w/o Ca^{2+} or Mg^{2+} Gibco 14170 HBSS + 2% FCS
- **HBSS protein solution:** 85% HBSS w/o Ca^{2+} or Mg^{2+} Gibco 14170, 2% FCS, 10% horse serum, 1% BSA
- **Kimura stain:** 0.05% Toludine blue solution, 0.03% Light green, Saponin saturated in 50% ethanol, 0.067M/6.4pH Phosphate buffer. (0.05% Toludine blue contained: 0.05g toludine blue dissolved in 50ml of 1.8% NaCl solution, 22ml EtOH and 28ml dH2O.)

Antibody coating of dynabeads

Magnetic Dynabeads (Dynabeads Sheep anti-mouse IgG Invitrogen Cat 110.31) were coated with mouse anti human CD117 antibody (BD Pharmingen Cat 555713) so they could be used to isolate CD117+ cells from a mixed cell population using positive magnetic selection. 100μL of the bead solution was initially rinsed with HBSS wash media using the MPC-1 magnet to retain the magnetic beads in-between each wash/removal of the supernatent. Following the washing steps, the beads were resuspended in 400μL of HBSS protein with 8μL of the CD117 antibody. The bead mixture was then incubated for 2hours at 4°C under continuous rotation. Following the incubation period, the magnetic beads were then washed 3x using the MPC-1 magnet as described previously. Finally the CD117 coated beads were then resuspended in 100μL HBSS protein solution, ready for immediate use.

HLMC isolation and purification

The provision of human lung tissue and the use of the tissue in this study were approved by the National Research Ethics Service (REC reference: 10/H1010/50). All human subjects gave written informed consent for the use of their tissue. Human lung tissue samples were obtained from patients undergoing lung resection surgery at the Northern General Hospital, Sheffield. Dr Peter Peachell obtained the ethical consent for the use of human tissue in research.

Lung tissue was collected no longer than 24 hours after surgery. Upon receipt of the tissue in the lab, the mast cell isolation protocol was carried out using aseptic technique throughout. The lung tissue was cut into a fine pulp and then transferred to 100µM gauze fixed over a sterile screw top pot and was rinsed with DMEM wash media to remove any unbound cells. The chopped tissue was then transferred into a fresh 200ml sterile pot containing HLMC media, 4mls of this media was used per 1g of tissue and the resulting cell mix was left at 4^0C overnight.

The following day, the tissue was equilibrated to room temperature before adding collagenase (Sigma C2674) and, hyaluronidase (Sigma H3506) enzymes to digest the tissue. 3mg of collagenase and 3.75mg per 1g of tissue was added and left stirring continuously at 37^oC for 75 minutes. To further liberate cells from the connective tissue, the cell suspension was forced through a sterile 50ml syringe 30 times, followed by filtering the cell suspension solution through 100µM gauze whilst rinsing with DMEM wash media. The cells were then washed, by centrifuging three times for 8 minutes at 160g at 4^oC, re-suspending in fresh DMEM wash media after each spin. Before the last spin, a 10µL sample of the cell suspension was collected and added to 45µL of Kimura stain. Mast cells were identified as cells that had taken up the kimura stain and counted using a haemocytometer. After the last wash step, the pelleted cells were resuspended in 2ml of HBSS protein solution and incubated at 4^0C for 30 minutes under continuous rotation - this step acts to block non-specific binding of the CD117 antibody used subsequently. Following the blocking step, the cells in HBSS protein solution were diluted in HBSS wash media to obtain a 50ml volume and the diluted cell suspension was filtered through 100µM gauze to remove any excess mucus remaining at this stage. The cell suspension was spun at 160g for 5 minutes at 4^oC and the pellet was resuspended in 4ml HBSS wash media.

Isolation of mast cells from the mixed cell population was then performed using a Dynal magnetic bead purification system. The CD117 antibody coated magnetic beads (prepared as described previously) were added to the cell suspension at a ratio of 1:5 which equates to 125µL of beads to 10×10^6 mast cells. The bead/cell mixture was transferred to a sterile 2ml tube (or numerous tubes if had more cells) incubated at 4^oC under continuous rotation for 90 minutes. The bead/cell mixture was transferred to a fresh 15ml tube, made up to 10mls in HBSS wash media and was connected to the MPC-1 magnet and left for 3 minutes. The supernatent which contains only CD117-ve cells was discarded. The CD117+ cells were

left attached to the surface of the tube in contact with the magnet and two further washes of the CD117+ve cells were performed using HBSS wash buffer, the CD117+ve cells were resuspended in 1ml of HLMC culture media and counted – CD117+ve cells were cultured at a final density of 500,000 cells/ml.

2.1.4 Human lung mast cell (HLMC) cell culture

Purity of the HLMCs was verified using kimura staining, a well described mast cell marker that binds to peptidoglycans; when taken up by mast cells the stain takes on a cerise/purple colour whereas eosinophils stain green, for (Kimura, 1973). HLMC isolated and cultured using the present methodology was shown to have 97% ± 3 purity of mast cells, as determined by kimura stain. Similar purity levels were seen in HLMCs isolated using the same methodology by (Oskeritzian *et al.*, 2005) – 95%, and (Sanmugalingam *et al.*, 2000) – 99.4%.

HLMC purity was further confirmed by staining cells with an anti-CD117 (c-kit receptor) antibody, (phycoerythrin (PE) - tagged anti-CD117 IgG1 antibody (Miltenyi Biotech, Surrey UK)). Representative data in **Figure 2.1** shows the cells stained with the anti-CD117 antibody and the corresponding isotype control (PE-tagged mouse IgG1 isotype). Staining was performed in a selection of donors, following Ca^{2+} imaging experiments. Cells were excited at 488nm to visualize staining with PE anti-CD117 and PE-mouse IgG1 isotype followed by excitation at 340nm to visualize all cells loaded with fura-2AM. The number of fura-2AM loaded cells were used to calculate the total cell number, then the cells with positive staining for CD117 were calculated as a % of this total. Over 97% of cells showed c-kit antibody staining providing further evidence to support high HLMC purity when using the isolation methodology stated here. Although CD117 is present in a number of cells throughout the body, of the mixed cell population obtained from lung tissue, CD117 expression is exclusive to mast cells except from one study suggesting a small population of pulmonary fibroblasts exhibited CD117 expression also (Ding *et al.*, 2013). However, based on the stark morphological differences between HLMC and fibroblast cells, the contamination of the culture with fibroblast cells would be evident.

HLMCs were cultured once a week, the cells in media were spun down at 100g for 5 minutes at room temperature, and then resuspended in fresh HLMC culture media.
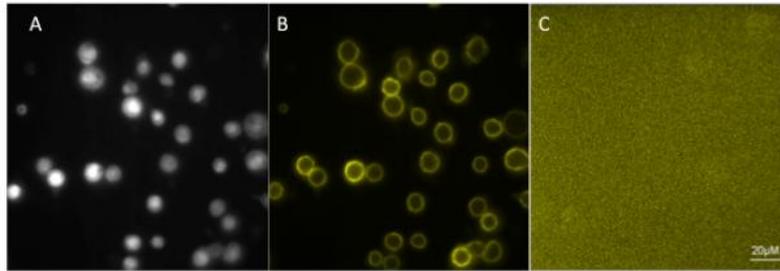
Figure 2.1   **HLMC cells stained with CD117 antibody**

A.) HLMCs stained with fura2-AM, excited at 340nm. B.) HLMCs stained with CD117, excited at 488nm C.) HLMCs stained with isotype control antibody, excited at 488nm. Pictures were taken by Reuben Friend.

2.1.5 PBMC isolation and hMDM differentiation

Fresh whole blood supplemented with heparin anti-coagulant was collected from the GSK Blood Donation Unit. Typically 100mls of blood was used per isolation experiment with a final hMDM yield of 16-40 million cells. Blood was diluted 1:1 with sterile PBS; it was then added to accuspin tubes containing 15ml of histopaque (Sigma 10771). 25ml of diluted blood was added to each tube. Tubes were spun at 350g for 25minutes (brake =1). The buffy coats were then combined and volume was made up to 50ml before another spin was performed (350g for 5minutes). The supernatant was removed and pellet resuspended in PBS, making the volume up to 50ml, at this stage the cells were counted using a haemocytometer. Cell suspension was spun and the pellet resuspended in miltenyi buffer (Phosphate buffered saline (PBS) w/o Ca and Mg, 0.05% bovine serum albumin (BSA), 5mM ethylenediaminetetraacetic acid (EDTA) with MACS CD14+ microbeads (#130-050-201) ($80\mu L/10^7$ cell) and incubated for 15minutes at 4^oC before positive selection of CD14+ cells through the use of a LS column (Miltenyi 130-042-401) and magnet. CD14+ cells were spun at 350g for 5 minutes in a volume of 15mls of miltenyi buffer and cell culture media, cells were then resuspended in media (Iscove's Modified Dulbecco's Media (IMDM) Thermofisher 12440, 10% human Ab serum (Sigma H4522), 1% L-glutamine (Gibco 25030), 1% Pen/Strep (Gibco 15140)) at an assay specific density of 300,000 - 750,000 cells/ml. Cells in suspension were plated out into a 96well plate – 100μL per well to give a density of 75,000 cells/well. The 36 external wells were filled with PBS to circumvent evaporation. rhGM-CSF (R&D systems) (5ng/ml) was applied to each well and cells were left for 7 days to differentiate into MDMs.
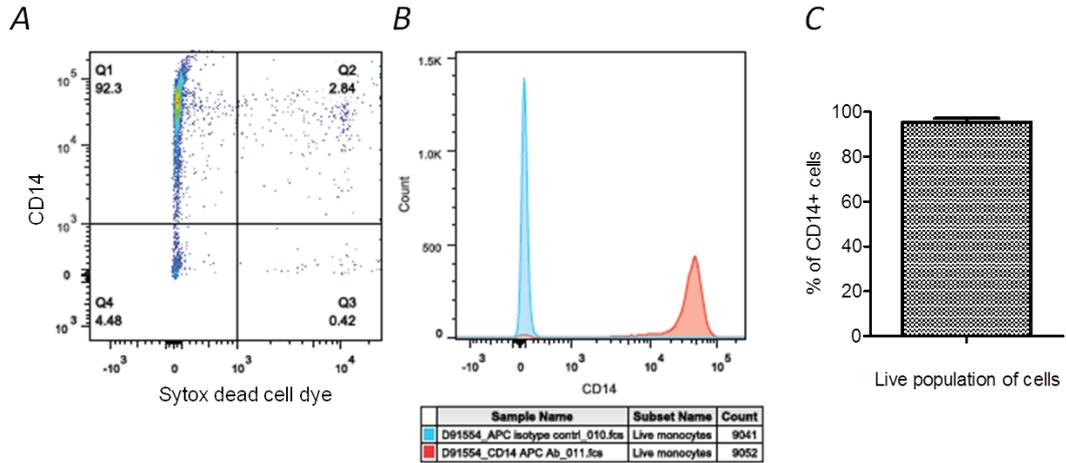
Figure 2.2   **Flow cytometric assessment of CD14+ monocytes**

Flow cytometry was performed in CD14+ monocytes following their isolation from a blood PBMC experiment. ***A.)*** *Scatter plot with % of CD14+ cells,* ***B.)*** *Histogram to show representative mean fluorescent intensity (MFI) for isotype control and CD14+ stained cells,* ***C.)*** *Mean ± SEM of CD14+ cells in a live cell population (95.4 ± 0.9%) of 3 donors randomly tested. For methodology used for Figure 2.2 see* ***Section 2.16****.*

As part of the present study, some experiments were performed to support that monocytes had been isolated correctly and that monocyte differentiation had occurred. Flow cytometry experiments were performed to assess the percentage of CD14+ cells obtained following magnetic bead isolation. It was considered that contaminant CD14- cells could impact on the differentiation process, so validation of the purity of the starting material was required. As shown in ***Figure 2.2*** these experiments demonstrated that over 90% of day0 blood monocytes were CD14+ve, which provided confidence in the starting material. Notably, morphological analysis of the cells at day0 and day7 of the culture process showed cells that were in line with the predicted morphology for monocytes and macrophages, respectively. The cells at day0 were around 3µm in diameter, spherical in space with a uniform interior. Conversely, the cells at day 7 were around 20µm in diameter, showing around a 10 fold increase in size. The cells displayed a spherical shape with the stereotypical 'fried egg' morphology, a ring like actin cytoskeleton surrounding the main cell body ***(Figure 2.3).***

Day0: CD14+ monocytes   Day 7: monocyte derived macrophages
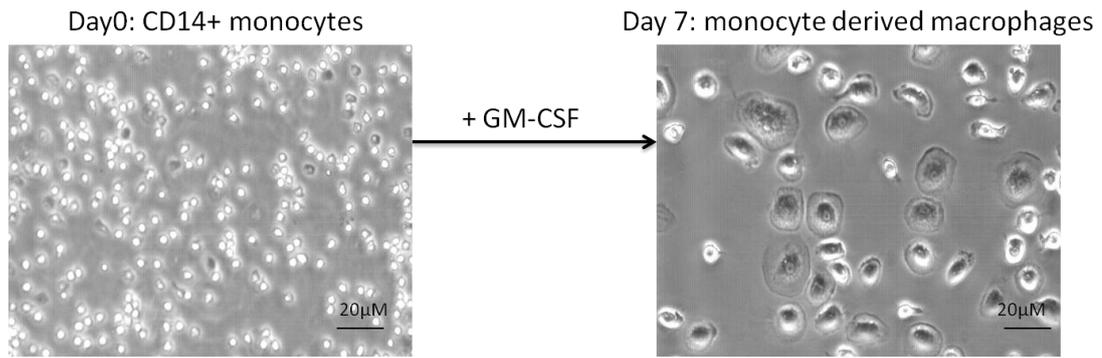
Figure 2.3   **Representative images of human CD14+ monocytes.**

hMDM cells shown at day0 and at day 7 after differentiation with GM-CSF (5ng/ml), demonstrating the morphological change.

Furthermore, flow cytometry experiments assessing the expression of CD68 were performed. CD68 is a scavenger receptor originally described as a macrophage marker, albeit CD68 is now known to be expressed in monocytes and some lymphocyte cells too. As shown in ***Figure 2.4***, there was one population of cells based on the size and granularity (as assessed by the FSC and SSC), with over 90% of which positively expressed CD68 ***(Figure 2.4)***. If remaining undifferentiated monocytes were contaminants of this culture it would be predicted that there would be two CD68+ve populations due to differential size and granularity of these two cell types (Andreesen *et al.*, 1990).
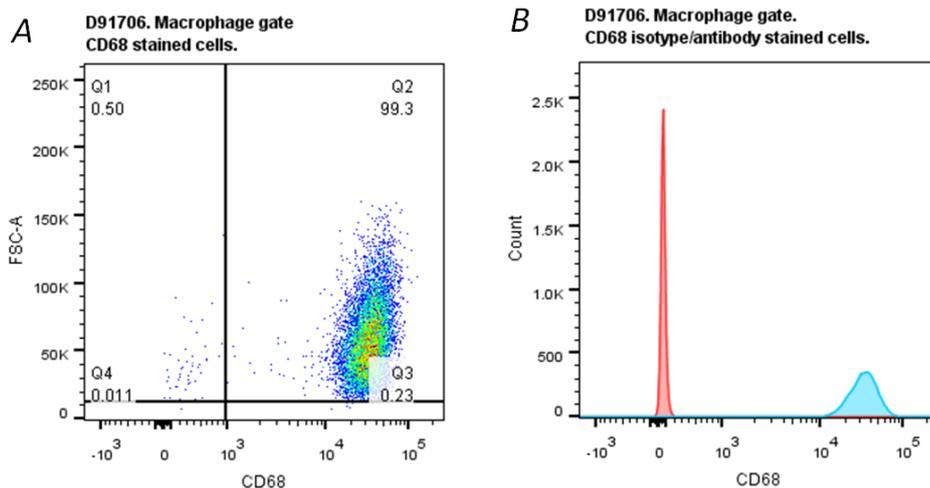
Figure 2.4   **Flow cytometric analysis CD68+ hMDMs**

*Flow cytometry was performed in hMDMs stained with CD68/isotype control **A.)** Scatter plot with CD68 stained cells over FSC-A, **B.)** Histogram to show representative MFI for isotype control and CD68+ stained cells.*

In sum, the flow cytometry data shows over 90% of CD14+ cells were obtained from the starting material; a notable morphological change occurred over a 7 day differentiation period, and a single population of CD68+ve cells was observed in flow cytometry indicated that the resulting cells had successfully differentiated into hMDMs.

2.1.6 hAM Isolation

hAM media: Roswell Park Memorial Institute medium (RPMI) 1640 (Gibco 31870-025), 10% heat inactivated FCS (Gibco 10100), 1% L-glutamine (Gibco 25030), 1% Pen/Strep (Gibco 15140).

Lung pieces were flushed with media using a needle syringe. Wash through was collected and 25ml was added to each 50ml Falcon tube, on top of 15ml of histopaque solution (Sigma 10771). Cells were spun at 350g for 25minutes with brake on low. Buffy coats were taken off and collected into a fresh 50ml tube, volume was diluted to 50ml with PBS and cells were spun at 350g for 5minutes (brake on 9). Cells were resuspended in PBS and washed/spun twice more. On the last spin, cells were counted using a haemocytometer. Cells were seeded into 96 well plates at assay-dependent density of 500,000-1million cells/ml or 50,000/100,000 cells per well (100μL volume). hAMs were left to adhere for 2 hours, and then a media wash was performed to remove non-adherent cells.

2.2 Coverslip Preparation

16mm, thickness no.1 glass coverslips (VWR) were washed in 95%ethanol, 5% acetic acid solution overnight on a rocker. The following morning, coverslips were washed with dH_2O, spread out onto filter paper and dried before autoclaving. 0.1% poly-L-lysine hydrobromide (Sigma) was used to coat the glass coverslips and aid plating of non-adherent cells (e.g. LAD2s and HLMCs). Poly-L-lysine was made to 0.1% using dH_2O and 90μL was applied per 16mm coverslips contained in a 12 well plate. Poly-L-lysine was incubated on the coverslips for 30mins at 37^oC followed by flooding the coverslips with dH_2O to wash off the poly-L-lysine. All liquid was then removed and coverslips were left to dry in the tissue culture laminar flow hood. Coverslips were kept sterile at 4^oC until use. 10-50μL of cells in suspension were applied to each coverslip and left at 37^oC for 30mins to allow adherence.

2.3 Intracellular Ca^{2+} imaging

Fluorescent Ca^{2+} indicator dyes were used to monitor changes in intracellular Ca^{2+}. Ca^{2+} selective indicator dyes are based on Ca^{2+} chelators such as EGTA developed by Roger Y. Tsien (Tsien *et al.*, 1985). The indicator dyes exhibit a spectral response following Ca^{2+} binding, this change in fluorescent signal can be quantified to measure changes in Ca^{2+}

signal. Ca^{2+} dyes can be ratiometric or single wavelength; examples of each include Fura-2 and Fluo-4/Cal-520, respectively. Membrane permeant AM ester dyes allow the dye to be loaded into the cell; following entry past the cell membrane, the ester is cleaved by esterases causing the dye to become membrane impermeable and trapped within intracellular compartments. However, indicator dyes can be actively pumped out of cells that express anion-transporter channels. In these instances, an anion-transporter inhibitor, probenecid can be included in loading and imaging solutions in order to prevent dye extrusion(Di Virgilio *et al.*, 1990).

2.3.1 Ratiometric Ca^{2+} imaging with Fura-2

Fura-2 AM is a commonly used ratiometric Ca^{2+} indicator dye. The advantage of a ratiometric dye is the reduced effects of dye leakage and photobleaching. Fura-2 AM has a dual excitation profile (at 340nm and 380nm). At 340nm Fura-2 exhibits an increase in fluorescence when Ca^{2+} concentration increases, whereas at 380nm a decrease in fluorescence signal occurs. A ratio of these two signals is then calculated in order to quantify the total change in Ca^{2+} signal. For experiments using human mast cells, cells were plated to 16mm poly-L-lysine coated coverslips (as described above) and then were loaded with fura-2 AM (1 µM) (Invitrogen Molecular Probes) in LAD2/HLMC culture media (omitting antibiotic-antimycotic) for 30 minutes at 37°C. Cells were subsequently washed in culture media without fura-2AM for 15 minutes at 37°C following by a final wash in Ca^{2+} imaging external solution for 15 minutes at room temperature. 16mm coverslips with fura-2AM loaded cells were placed into a recording chamber (Warner 24l x 13w x 4.1 H mm, volume by depth 133µl/mm – RC-25F, Warner Instruments) and superfused with external imaging solution. The flow rate was determined to be 3ml/minute. A main reservoir bottle was connected to a series of tubing and syringes which passed through a heating element before reaching the bath of the recording chamber (temperature set to 28°C). Syringes were connected to the tubing to allow addition of various different solutions. The height of these syringes was set to be the same as the main reservoir bottle to ensure a constant flow rate. Similarly, stoppers with inserted tubing were placed to seal the syringes to help maintain a constant flow following volume change. The experimental set up is detailed in *Figure 2.5*. External solution composition for use in all mast cell Ca^{2+} imaging experiments was (in mM; 120 NaCl, 10 KCl, 10 HEPES, 2 $MgCl_2$, 2 $CaCl_2$, 10 Glucose (300mOsm/litre, pH 7.3, NaOH). An inverted microscope (Axiovert S100 TV, Zeiss, Cambridge, UK) equipped with a 40x oil immersion objective (NA 1.3, Zeiss) was used to image the cells. Cells were alternately illuminated at 340 and 380 nm with a 20 ms exposure time with a monochromater (Polychrome IV, TILL Photonics, Munich, Germany). Emitted light was passed through a 510 nm band pass filter and collected by a 512B Cascade CCD camera (Photometrics, Tucson, AZ, USA) and images were acquired at 0.5 Hz.

MetaMorph® Meta imaging software (Molecular Devices, Sunnyvale, CA, USA) was used to analyse all Ca^{2+} imaging experiments. A region of interest (ROI) was placed over each cell in the field of view – the raw fluorescent values at 340 and 380nm were exported, along with background fluorescence values (taken as a region in the field of view where no cells were

present). The background-subtracted 340nm fluorescence values were then divded by the background-subtract 380nm fluorescence values to obtain the Ca^{2+} signal ratio.
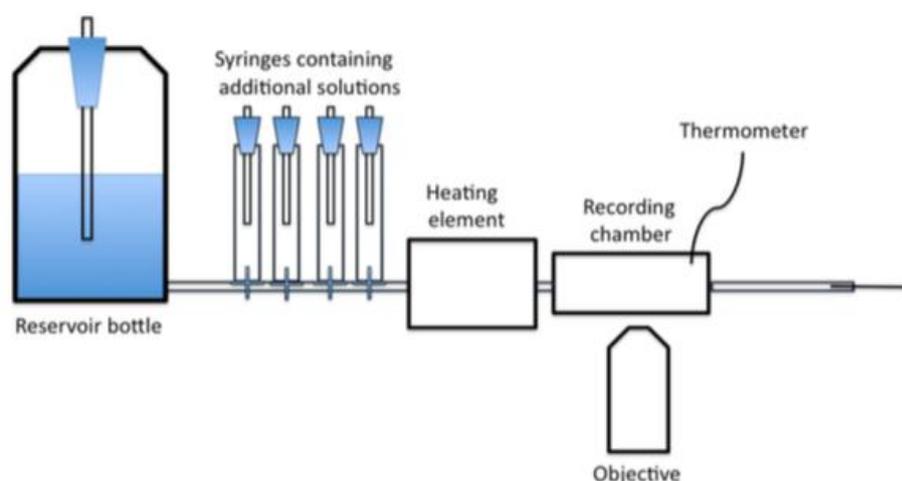
Figure 2.5   Experimental set up of Ca^{2+} imaging superfusion system.

Figure reproduced from Reuben Friend's thesis

2.3.2 Fluorometric Imaging Plate Reader (FLIPR)

Fluo-4 is an example of a single excitation wavelength Ca^{2+} indicator. Fluo-4 is excited at 488nm. Cal-520 is another single excitation Ca^{2+} indicator with improved signal to noise ratio and intracellular retention compared to dyes such as Fluo-4 (Life technologies F-14201), Cal-520 (Stratech 21130) can also be excited at 488nm. These dyes were used in FLIPR Ca^{2+} imaging assays.

FLIPR assays allow high throughput Ca^{2+} imaging assays to be carried out and are commonly used for drug screening. FLIPR assays were utilized for all experiments on macrophage cells. Here macrophages were seeded into a black-edged clear bottom 96 well plate at a density of 75,000cells/well. Culture media was replaced with FLIPR buffer containing 2µM Fluo-4AM/5µM Cal-520 and cells were loaded for 1 hour at 37°C. Loading buffer was then removed, and cells washed with FLIPR buffer. Antagonists were pre-incubated for 15minutes prior to measuring the fluorescence signal at 488nm; data acquisition was performed at a frequency 0.5Hz. FLIPR buffer contained (in mM): 1.8 $CaCl_2$, 5.6 Glucose, 2.7 KCl, 1.0 $MgCl_2$, 137.0 NaCl, 0.4 $NaHPO_4$, 20 HEPES, 11.9 $NaHCO_3$. 2.5mM probenecid was added to the FLIPR buffer for all experiments unless indicated.

An average signal test was performed before each FLIPR assay was run, to ensure the starting signal was consistent between each of the 96 wells recorded and to confirm that starting signal was within same signal window from assay to assay. To account for any

variability between starting fluorescence in each well, caused by a difference in cell number or dye loading capacity, the starting fluorescence was normalised to the mean basal values (first 10 readings). The raw data from each plate was assessed prior to normalisation to check for drug-induced changes to basal signal. Each condition was performed in triplicate to account for variability between wells. In each plate a control row of vehicle controls (DMSO or H_2O) was performed to enable any spontaneous rise in baseline fluorescence to be accounted for in further calculations, similarly a control row of agonist application was performed in each plate/for each donor to evaluate the responsiveness of each plate/donor.

Data analysis

For each donor, the mean value from the triplicate data was calculated, the data was normalised to their respective baseline values and plotted as signal over time. Data points were recorded every 2 seconds for duration of up to 30 minutes. For concentration-response graphs, data was analysed by calculating the area under the curve for each condition (values over 1 from normalised data). The % of the control response was then calculated for each donor, using the respective control data performed in parallel for each individual experiment. The mean ± SEM of the data from each donor was then plotted for the graphs presented in the present study. X axis concentration values were transformed into log values using the GraphPad Prism analysis function. Non-linear regression analysis was then performed to calculate IC50 and EC50 values. For experiments with antagonists and agonists exhibiting a sigmoid curve the following equation was used: Y=100/(1+10^((LogIC50-X)*HillSlope)) For experiments where low concentrations stimulated a response and high concentrations reduced a response a bell-shaped curve was plotted using the following equation: Span1=Plateau1-Dip, Span2=Plateau2-Dip, Section1=Span1/(1+10^((LogEC50_1-X)*nH1)), Section2=Span2/(1+10^((X-LogEC50_2)*nH2)), Y=Dip+Section1+Section2.

2.4 Determination of the appropriate concentration of Anti-IgE for activation of human mast cells.

Anti-IgE is known to initiate Ca^{2+} mobilisation in mast cells through cross-linking of the FcεRI, previous work in the Seward lab has been performed to find the optimal reagents for use in such experiments in LAD2 and HLMCs i.e. the most effective concentration and type of IgE to prime human mast cells and Anti-IgE to activate FcεRI (Kathryn Wareham and Claire Tree-Booker's theses). Ca^{2+} imaging experiments were performed as part of the present study to validate these prior findings. *Figure 2.6* shows that 1 and 3µg/ml Anti-IgE induced a significant Ca^{2+} signal and these concentrations were sufficient to initiate histamine release at a consistent and robust level. Therefore these concentrations of Anti-

IgE were considered appropriate for the initiation of Ca^{2+} signalling in human mast cells for two reasons; firstly they initiate a Ca^{2+} signal which is robust and provides a signal dynamic window from which to assess antagonist effects and secondly these concentrations were in the range needed to initiate mediator release thereby indicating the physiological relevance of Anti-IgE in this concentration range.
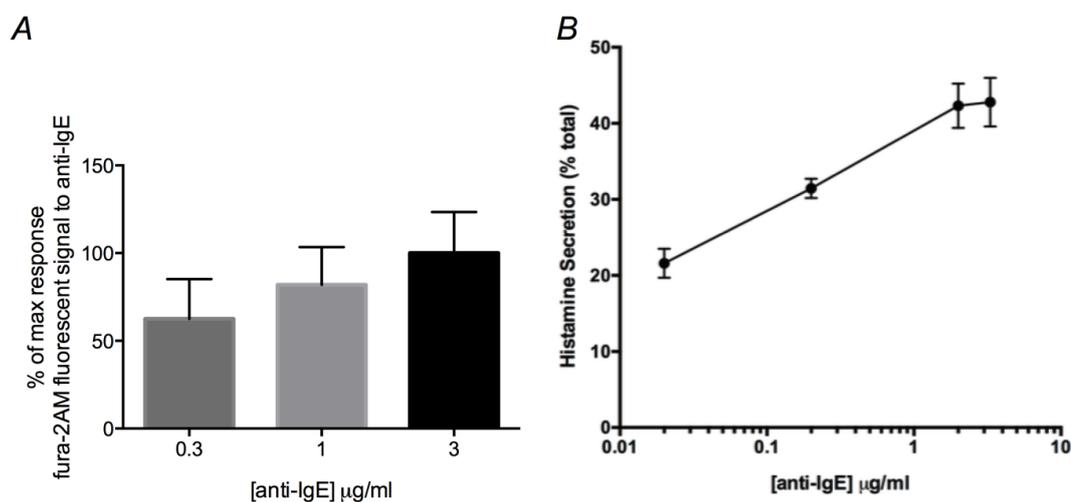
Figure 2.6 **Anti-IgE concentration validation for initiation of Ca^{2+} signalling in human mast cells.**

A.) Single cell Ca^{2+} imaging was performed as described in section 2.3.1 on fura-2AM loaded HLMCs, Anti-IgE was applied and resulting Δfluorescent signal (340/380) was analysed as Ca^{2+} signal. The bar graph shows the % of the response initiated by 3μg/ml anti-IgE as mean ± SEM from N=3 donors tested. *B.)* Histamine secretion from HLMC cells initiated by Anti-IgE, histamine release was measured as described in (Siraganian, 1975; Ennis, 1991), % of total was calculated by lysing cells with perchloric acid. N=3 donors tested. Experiments in B performed by Jasmine Farrington.

2.5 Quantitative PCR

qPCR primers were designed by PrimerDesign® melt curve specificity tests were performed by PrimerDesign as part of the primer design but were also performed in house. SYBRgreen detection chemistry was used in all qPCR experiments. SYBRgreen dye intercalates to the DNA double helix which alters its structure and leads to an increase in dye fluorescence. This means that during a PCR reaction, as more DNA is created, an increase in SYBRgreen fluorescence intensity also occurs. Because SYBRgreen dyes are non-specific, accurate results are based on good quality primer design and analysis of the primer's specificity. If a PCR reaction causes amplification of any double stranded DNA this would be reported by SYBR green, therefore in order to confirm that the signal produced is caused by amplification of the target of interest further analysis needs to be performed. This analysis is in the form of a melt curve. In all qPCR experiments in the present study, following the

PCR temperature change cycle, a melt curve cycle was performed. Here the temperature was increased above the dissociation temperature, therefore causing the double stranded DNA amplicons to be broken down and subsequently causing a decrease in fluorescent signal. The temperature at which the dsDNA dissociation occurs is known as the melting temperature. Because different sized amplicons have different melting temperatures, for each primer target sequence a specific melting temperature can be predicted. As shown in **Figure 2.7** the identity of the amplified products in a SYBRgreen PCR reaction can be predicted by performing a melt curve analysis at the end of the experiment. If only the target of interest has been amplified, there should be a single peak on the melt curve at the predicted temperature. Double peaks or misaligned peaks are indicators of primer dimer or non-specific amplification. Melt curve analysis was performed following all qPCR reactions to confirm amplification measured was specific to the primer target.
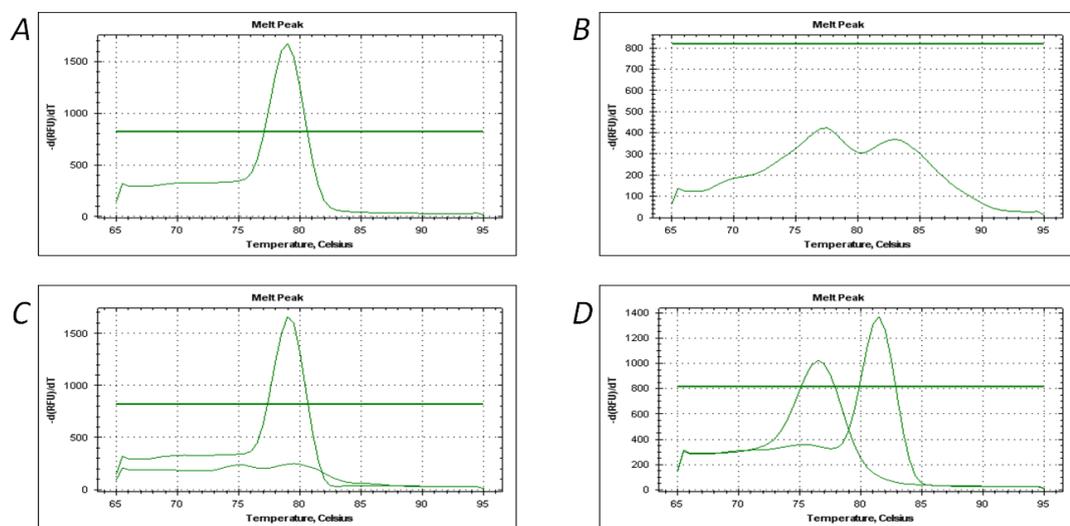
Figure 2.7   Example melt curve analysis from qPCR experiment

A.) Example of single melt curve with amplification of one target. B.) Example of melt curve with a double peak, due to primer dimer formation or non specific amplification. C.) Example of poorly dissociated dsDNA D.) Example of melt curve of with two single peaks with distinct dissociation temperatures, indicative of different target amplification

RNA was extracted from 250,000 cells/donor (RNeasy Kit. Qiagen), the optional DNase clean up step was performed. RNA concentration/purity was determined using a nanodrop (260/280 ratio ~2.0) (Thermo-scientific) and cDNA conversion was completed immediately using a high capacity RNA to cDNA kit (Applied Biosystems) according to the manufacturer's instructions. cDNA was stored at -20°C until use. QPCR was run on a BioRad thermocycler machine (for HLMC experiments) or ABI 7900 (for hMDM experiments) using 5μg of cDNA per reaction. Per reaction; 1μL of primer mix, 10μL of mastermix and 4μL of RNase/DNase free water was used. Primers were custom designed and optimised by PrimerDesign©,

'Precision mastermix for the Bio-Rad iCycler/ABI 7900 with SYBR green' was used throughout. qPCR was performed adhering to the temperature and timings as indicated in **Figure 2.8**. cDNA titration qPCR experiments were performed to evaluate the primer efficiency **(Figure 2.11 and 2.12)**, all primers tested had an efficiency of 100% ± 10 indicated by a slope in the range of 3.0-3.6.

Step	Time	Temp
Enzyme activation	2min	95°C
Denaturation	15sec	95°C
Data Collection	60sec	60°C
Melt Curve**		

Figure 2.8   qPCR protocol – temperature and timings

*** Melt curve run according to manufacturer's instructions for the ABI 7900/BioRad machine.*

Reverse transcriptase and non-template controls were used to verify that there was no genomic DNA contamination and melt curves were analysed to assess the primer specificity. geNorm analysis was performed to determine the most consistently expressed housekeeping gene in cDNA samples from numerous HLMC and hMDM donors - out of a range of 5/6 commonly used housekeeping genes. The most stably expressed housekeeping gene was 18sRNA in mast cell cDNA **(Figure 2.9)** and GADPH in macrophage cDNA **(Figure 2.10).** geNorm experiments were analysed using Qbase software to determine expression stability. In order to analyse the qPCR results, raw Ct values were normalised to the housekeeping gene (18sRNA or GAPDH) and data was expressed as 2^ΔCt.

Average expression stability of remaining reference targets
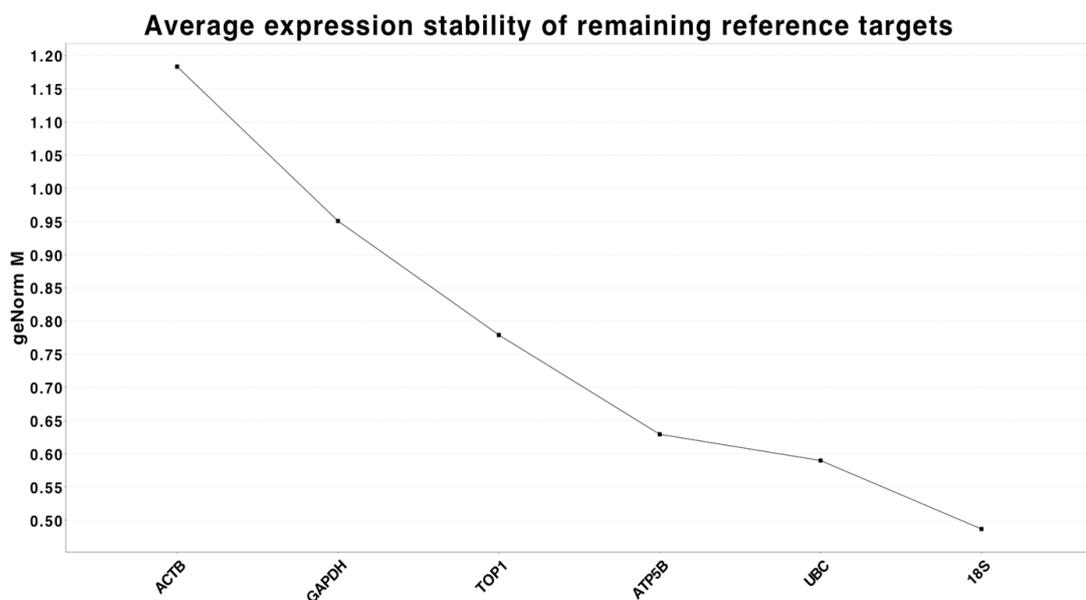
Figure 2.9   geNorm assay results from HLMC cDNA

Graph to show the average expression stability for each reference gene target. A lower geNorm M value = high expression stability. Performed with cDNA from 10 donors.

Average expression stability of remaining reference targets
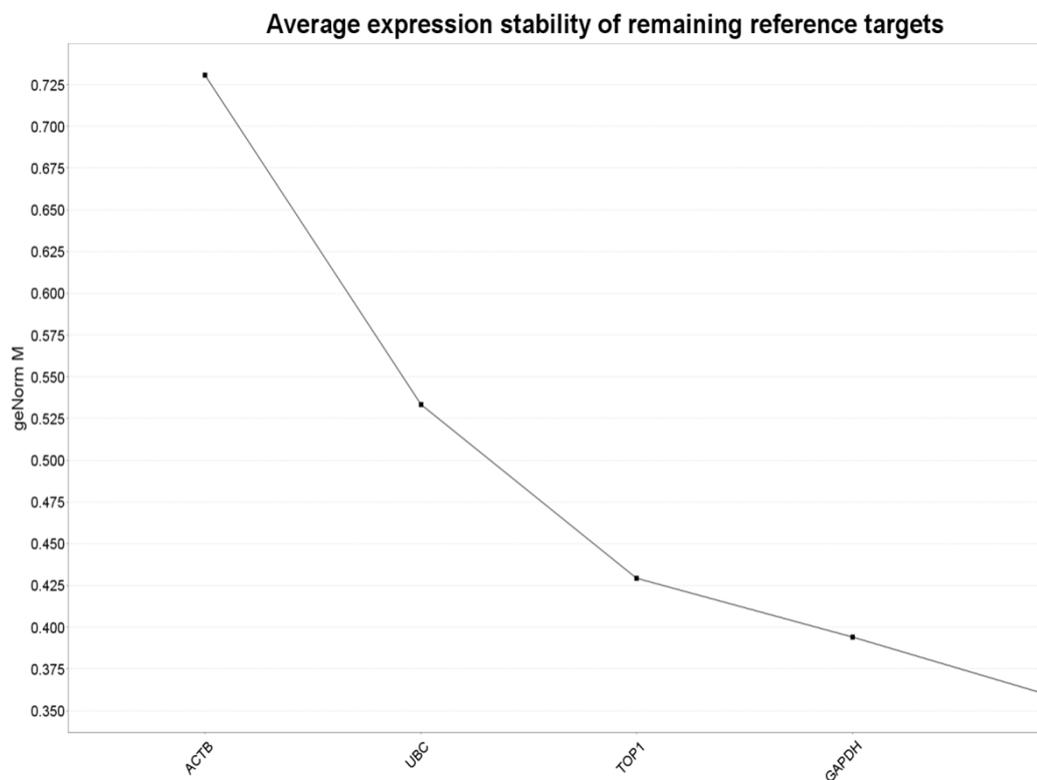
Figure 2.10   geNorm assay results from hMDM cDNA

Graph to show the average expression stability for each reference gene target. A lower geNorm M value = high expression stability. Performed with cDNA from 10 donors
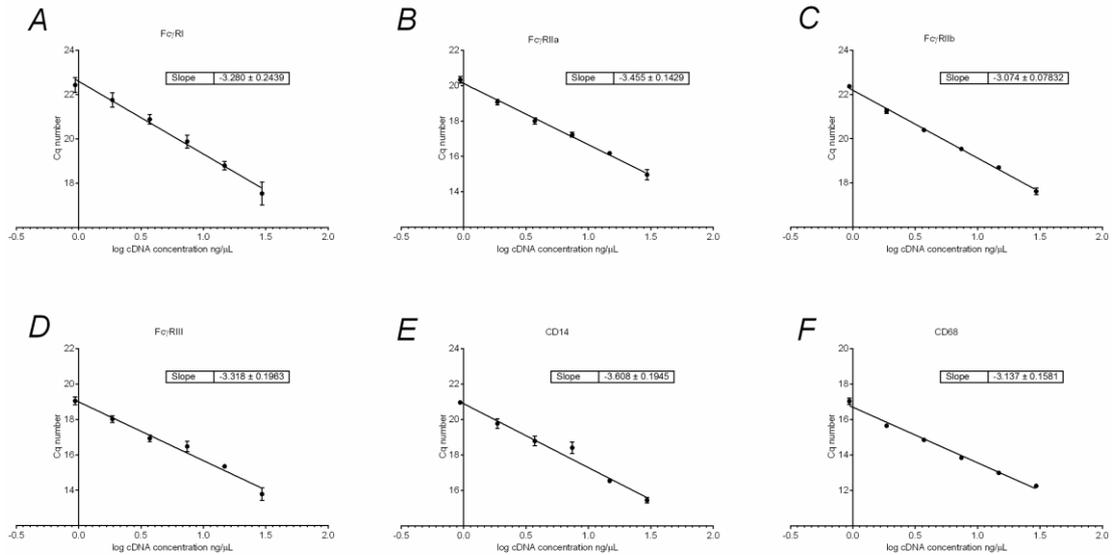
Figure 2.11   Primer efficiency standard curve – FcγR genes

qPCR experiment was performed with a titration of hMDM cDNA to calculate the primer efficiency. Efficiency calculated: 10(-1/slope-1). All primers tested had an efficiency of 100% ± 10. Slope of 3.32 = 100%, 3.6 = 90% and 3.0 = 110%. N=2
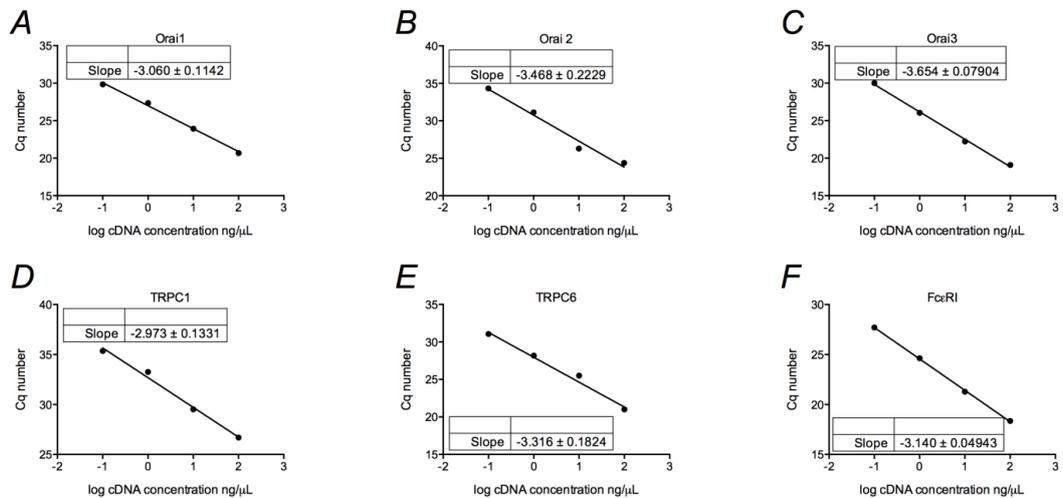
Figure 2.12   Primer efficiency standard curve – Orai and TRPC genes

qPCR experiment was performed with a titration of LAD2 cDNA to calculate the primer efficiency. Efficiency calculated: 10(-1/slope-1). All primers tested had an efficiency of 100% ± 10. Slope of 3.32 = 100%, 3.6 = 90% and 3.0 = 110%. N=2

2.6 Microarray

Microarray experiments were performed using an Agilent SurePrint G3 Gene Expression 8x60K one-colour microarray system, which enables estimation of absolute levels of gene expression between arrays. RNA was collected from 500,000 LAD2 or HLMC cells using RNeasy Kit (Qiagen) according to manufacturer's instructions. The data was normalised to the 75th percentile intensity of all non-control probes according to Agilent instructions, allowing comparison across arrays. Experiments were performed with assistance from Paul Heath at University of Sheffield.

2.7 Immunocytochemistry in mast cells

Cells were fixed with 4% paraformaldehyde + 4% sucrose (pH7.4) for 10 minutes followed by washing in PBS and permeabilisation with PBS + 0.1% Triton-X-100 (Sigma) for 15 minutes. Blocking solution of 0.02% Triton-X-100 and 0.2% fish skin gelatin (Sigma) was applied for at least 2 hours at room temperature before addition of primary antibody overnight at 4°C (TRPC1, Alomone ACC-010; TRPC6, Origene TA306349; Rabbit polyclonal IgG, Abcam ab27472 each used at 1:200). The epitope of primary antibodies were raised against intracellular amino acid residues hence the need to permeabilise the cells prior to antibody incubation. Secondary antibodies at concentrations of 1:1000 (Anti-Rabbit Alexa Fluor 488, polyclonal, Invitrogen) were incubated for 1.5 hour at room temperature before the coverslips were mounted onto glass slides using DAPI-Fluoromount G (Southern Biotech). Images were taken with an Olympus FV1000 confocal microscope with SIM-scanner on a BX61 upright microscope. Samples were illuminated at the required wavelength using 405nm and 488nm lasers and quantification was performed using Image J.

2.8 Immunocytochemistry in macrophages

Cells were fixed with 4% paraformaldehyde (pH7.4) for 10 minutes followed by washing in PBS and permeabilisation with PBS + 0.1% Saponin (Sigma) for 15 minutes. Blocking solution (0.1% Saponin, 50μg/ml Human IgG, 1% BSA (Sigma) was applied for at least 2 hours at room temperature before addition of primary antibody at 1:200 for 1 hour at room temperature (Anti-P2X7 antibody [EPR4723] ab109246 Abcam or Rabbit IgG, monoclonal – Isotype control ab172730 Abcam.). Secondary antibodies at concentrations of 1:200 (Goat F (ab') 2 Anti-Rabbit IgG – Fc (Dylight 650) pre-adsorbed. Ab98483 Abcam) were incubated for 1.5 hour at room temperature before DAPI +PBS was added and plates analysed using INCellAnalyser 2000, quantification was performed using InCell macro analysis software. The P2X7 antibody epitope was raised against an intracellular amino acid sequence hence the need to permeablise the cells prior to antibody incubation.

2.9 Western blotting

2.9.1 Western blot protocol for mast cell work

Protein lysate collection

Cells were counted using a haemocytometer. A minimum of 100,000 cells were used per protein lysate condition. The cells were washed 2x in cold PBS and resuspended in ice cold RIPA buffer (Sigma) + protease inhibitor cocktail (Fisher). 40µL of RIPA buffer was used per 100,000 cells. The cells were then freeze thawed twice, each time pipetted thoroughly between each freeze cycle. Following this, the cells were spun at 15,000rpm for 20 minutes at 4°C (the centrifuge was pre-cooled prior to spinning). The supernatent was aliquoted into 10µL volumes and stored at -80°C until further use.

Bradford Assay - determining the protein lysate concentration

BSA protein standards were made to serial dilutions ranging from 2mg/ml to 0.25mg/ml. 5µL of each protein standard was pipetted into a 96well plate in triplicate. To the blank wells add 5µL of H2O. 5µL of each protein lysate was also transferred to the 96 well plates after diluting 1 in 2. 250µL of Bradford reagent was then added to each well. The plate was incubated for 5-30 minutes and then read on a spectrophotometer to measure the absorbance at 595nm. A standard curve was created; plotting net absorbance vs. protein standard concentration to work out the concentration of the protein lysates.

Western blot protocol

SDS-PAGE running gel (10%) was made using:
2.5ml Tris (pH8.8), 200µL 10% SDS, 3.2ml Acrylamide (30%), 50µL APS 10%, 5µL TEMED, 4.10ml H$_2$O.

5% stacking gel was added on-top of running gel using:
1.25ml Tris 0.5M pH 6.8, 50µL 10% SDS, 500µL 30% Acrylamide, 5µL TEMED, 25µL APS 10%, 3.2ml H$_2$O.

Protein lysate samples were defrosted on ice and diluted in a 1:1 ratio with 2x Laemelli buffer (Sigma 38733). The samples were heated for 10 minutes at 70°C (or 90°C for non membrane proteins) and spun to remove any precipitate and kept on ice until loading to the gel. The gel was transferred to the running tank and filled with running buffer (250mM Glycine, 25mM Tris-base, 0.1% SDS – all SIgma). The wells were loaded with the protein lysates (10-20µg protein/well), with the ladder e-stained recombinant protein ladder (Fisher Cat: BP3603-500) loaded in the first well (max of 18µL volume for a 10 well comb) followed by the protein samples, the gel was run at 100V for 1-1.30 hours. The gel was removed and immersed in transfer buffer (25mM Tris-base, 192mM Glycine, 15%

methanol) and the 'transfer sandwich' was prepared. The holder was placed black side on the bench, then sponge-filter paper-gel-membrane-filter paper-sponge was stacked on top - transfer was performed at 100V for 1 hour 15 minutes. Next, the membranes were transferred into the blocking solution consisting of TBST (50mM Tris, 150mM NaCl, 0.05% Tween-20 (Sigma)) supplemented with 5% skim milk powder and placed on an orbital shaker for 1 hour 30 minutes. The primary antibodies were made up to the appropriate concentrations (initial experiments were performed to assess optimal concentration – a sample of 2/3 concentrations was tested in a range based around the manufacturer's recommendations and previous publications) with a primary antibody for a loading control such as GAPDH or α tubulin also applied. Following blocking, the membranes were transferred to plastic wallets containing the primary antibody, the wallets were sealed and the membranes incubated overnight at 4 °C on an orbital shaker.

The following day the membranes were taken out of the primary antibody solution and washed in 1xTBST 4 times for 8 minutes per wash. The secondary antibody was then prepared and incubated on the membrane in the plastic wallets for 1 hour at room temperature on an orbital rocker, followed by 4 further wash steps of 8 minute duration in 1xTBST. The membranes were transferred face up onto a flat piece of Clingfilm and the ECL reagent was added (around 1ml per membrane). At this stage the membranes were ready for developing using Amersham ECL Film, excess liquid was removed and the membrane transferred to a film cassette. Chemiluminescence film (GE healthcare cat: RPN2132) was exposed to the membrane in the dark and developed using an X-ray developer.

2.9.2 Western blot protocol for macrophage work

Reagents for western blot (NuPAGE system):
Lysis buffer

- Cell lysis buffer (cell signalling no. 9803) stock at 10x
- Protease and phosphatase inhibitor (Halt no. 78440) stock at 100x
- Solution was kept on ice at all times.

NuPAGE 10% Bis-Tris Gel NP0316
NuPAGE MOPS SDS Running Buffer NP0001 Lot 1537451
NuPAGE Transfer Buffer NP0006-1
iBlot PVDF Gel Transfer Stacks IB401002.
Odyssey LICOR Blocking Solution 92740000
Chameleon Pre-stained Ladder 928 60000 Cat 40530-03
NuPAGE LDS Sample Buffer (4X) NP0007

hMDM protein lysate preparation

Adherent cells were washed with PBS followed by addition of cell dissociation solution which was incubated in the culture flask for 5 minutes at 37°C. Cells were tapped vigorously

to unstick any cells and the cell suspension was then transferred into a 15ml Falcon tube. The suspension was centrifuged at 350g for 5 minutes, the supernatent was aspirated off and cell pellet was resuspended in cell lysis buffer + protease inhibitor (Cell signalling no. 9803 and protease and phosphatase inhibitor Halt no. 78440 -100µL per 500,000 cells). The resuspended cell solution was incubated on ice for 30minutes followed by vortexing for 5 minutes and a final centrifugation at max speed for 10minutes at 4°C. The supernatent was collected and stored at -20°C until needed.

Western Blot protocol (using NuPAGE system)

Protein lysates concentrations were determined using a Pierce BCA protein assay kit (Thermoscientific 23225 23227), following manufacturer's instructions. Desired quantities (10-20µg) were added to a loading buffer and denatured in heating block at 70°C for 10 minutes. Samples were transferred to the gel, with a pre-stained ladder added at this stage too, samples were run for 200V for 2 minutes, 60V for 15 minutes and then 170V for 50 minutes or until the ladder reached the bottom of the gel. The proteins run through the gel were then transferred to a PVDF membrane using the iBlot system, following manufacturer's instructions. The gel was placed in a sandwich: Anode – membrane – gel – filter paper – cathode, all components were wetted with transfer buffer and transfer was performed for 7 minutes (program P3). The membrane was then transferred into blocking solution for 2 hours. For blocking peptide experiments, at this stage the blocking peptide was incubated with primary antibody for at least 30minutes at room temp. The antibody and membrane were then incubated overnight at 4°C under continual rotation. The following day the membranes were washed x3 times for 5-10 minutes with TBST, the secondary antibody was then applied for 2 hours at room temperature. Another wash step for x3 times for 5-10 minutes was performed before the membrane was analysed using an infrared odyssey system.

2.10 Determining the specificity of TRPC1, TRPC6 and P2X7 antibodies

To confirm that the antibodies used in this study could be reliably used as an indicator of positive TRPC/P2X channel expression, some validation experiments were performed. Each antibody was run in a western blot experiment in order to assess the size of the band obtained. For the P2X7, TRPC1 and TRPC6 antibodies, the bands seen following antibody incubation were around the predicted size and were the only significant band seen through the protein ladder *(Figures 2.13-2.15),* giving the first piece of evidence to suggest that the antibodies used in this study are able to accurately report the expression of the peptide they are raised against. Blocking peptides raised against the TRPC1 and P2X7 peptide/epitope led to a significant reduction in the band seen at the expected channel size (*Figure 2.13 & 2.14)*, this gives further evidence to support TRPC1/P2X7 antibody selectivity. In the case of TRPC6, no blocking peptide was available, however this antibody

was assessed in cell lysates from HEK WT and HEK TRPC6 expressing cells which are expected to have a low and high TRPC6 expression level, respectively. The band at ~106kDa in the HEK-TRPC6 cells has a significantly greater intensity than that in HEK-WT-cells *(Figure 2.15),* suggesting the antibody is able to detect between low and high protein expression levels. What must be considered is that there is not conclusive proof from the validation experiments described, that TRPC1/TRPC6/P2X7 antibodies do not non specifically bind to other proteins with similar epitopes that are available in fixed cells, but not in cell lysates. However it could be argued that because under western blot conditions there is evidence for the selectivity of binding to the respective target (P2X7, TRPC1 or TRPC6) that it is unlikely that the P2X7/TRPC1/TRPC6 antibodies are reporting non-specific binding of other family members when used in immunocytochemistry experiments. Further evidence supporting the specificity of the TRPC1 antibody comes from its use in previous peer reviewed publications. For example lack of a signal induced by the TRPC1 antibody in TRPC1 blocking peptide experiments in immunocytochemistry of human astrocytoma U373 MG cells, and following TRPC1 siRNA of mouse PASMCs using western blot provides further confirmation of its specificity (Barajas *et al.*, 2008; Ng *et al.*, 2012). The TRPC6 and P2X7 antibody specificity is supported by data on the provider's website (Origene and Abcam respectively).

Taken together these experiments show that the antibodies have a high selectivity for the protein epitope they are raised against, as shown in western blot experiments. The IgG isotype control experiments performed alongside the immunocytochemistry experiments provide further evidence to suggest against non specific binding of the antibody to IgG receptors expressed in the target cells, similarly experiments incubating the secondary antibody alone provide evidence that the secondary antibody is accurately reporting signal from primary antibody targets.
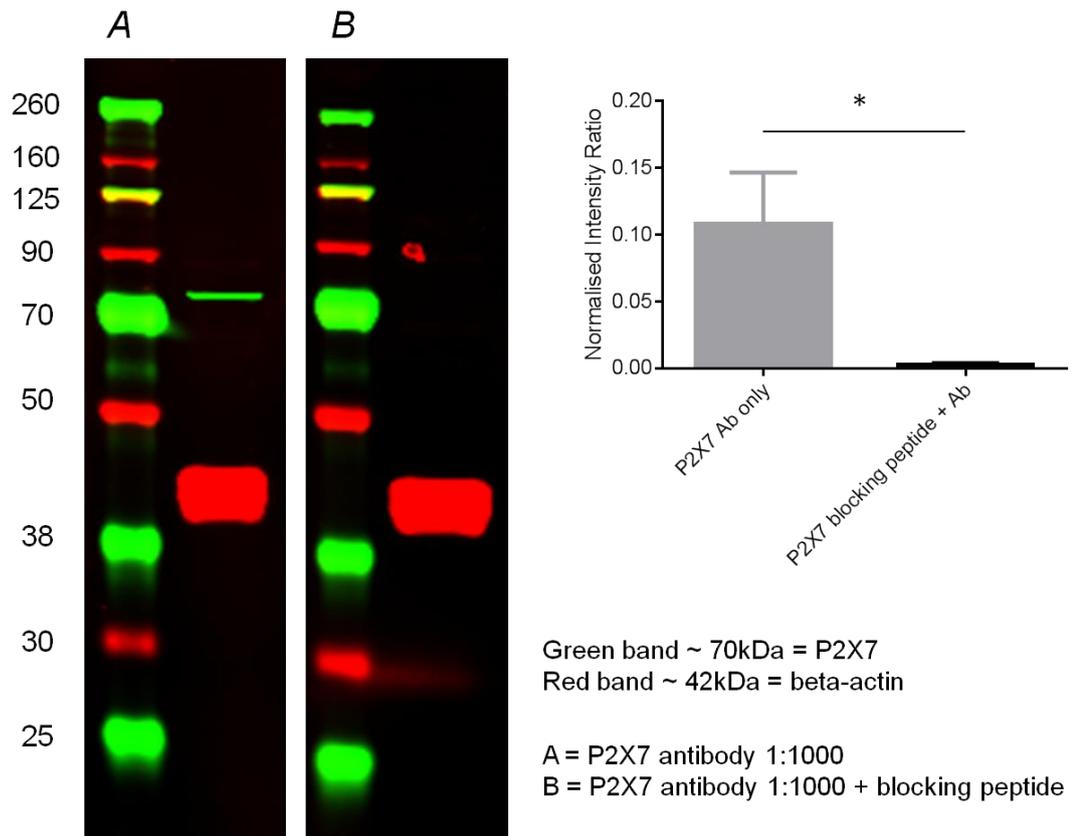
Figure 2.13   P2X7 antibody staining was significantly reduced following incubation with P2X7 blocking peptide

*Western blot experiment with protein lysates from hMDM cells. **A.)** P2X7 antibody staining **B.)** P2X7 antibody + blocking peptide. Bar graph shows mean ± SEM of normalised intensity ratio of P2X7 band in each condition. N=3. Results were analysed with students paired t-test.*
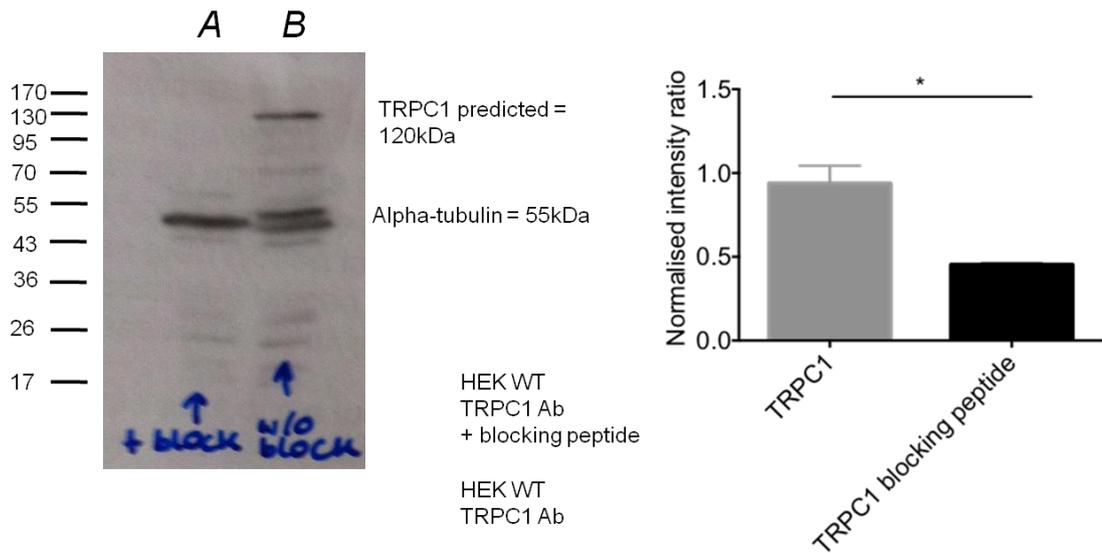
Figure 2.14   TRPC1 antibody staining was significantly reduced following incubation with TRPC1 blocking peptide

*Western blot experiment with protein lysates from WT HEK cells. **A.)** TRPC1 antibody staining with blocking peptide **B.)** TRPC1 antibody. Bar graph shows mean ± SEM of normalised intensity ratio of TRPC1 band in each condition. N=2. Results were analysed with students paired t-test.*
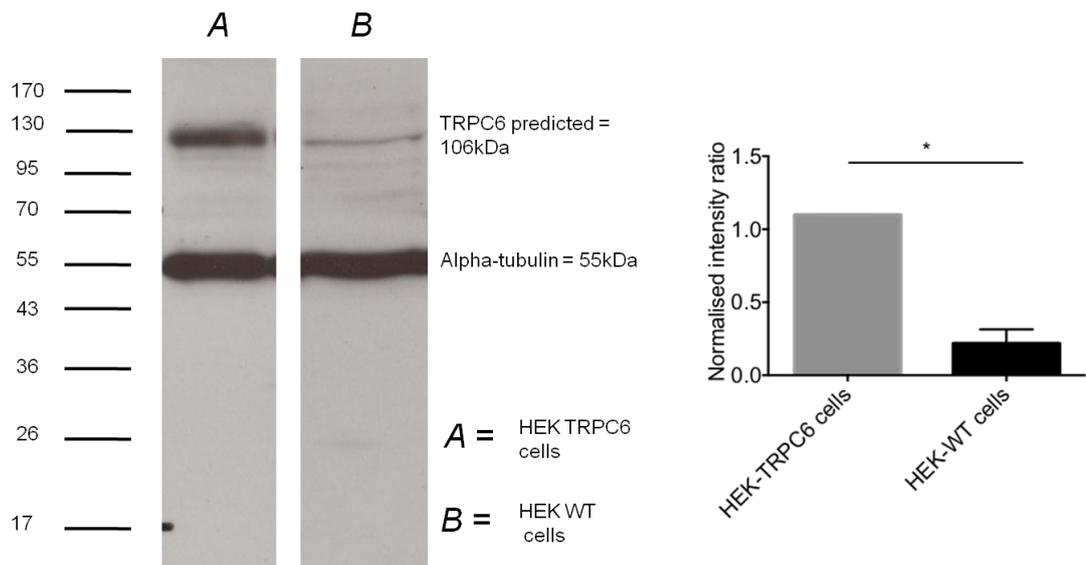
Figure 2.15   TRPC6 antibody staining was significantly reduced in HEK-WT conditions compared to HEK-TRPC6 cells

*Western blot experiment with protein lysates from WT HEK/ HEK-TRPC6 cells. **A.)** TRPC6 antibody staining in HEK-TRPC6 cells **B.)** TRPC6 antibody in HEK-WT cells. Bar graph shows mean ± SEM of normalised intensity ratio of TRPC6 band in each condition. N=2. Results were analysed with students paired t-test.*

Antibody details	Manufacturer	Catalogue number	Application used	Antibody type
Mouse monoclonal actin c-z antibody	Santa Cruz	sc8432	Western blot	Primary
Anti-P2RX7 antibody	Abcam	[EPR4723] (ab109246)	Western and immunocytochemistry	Primary
P2RX7 peptide	Abcam	(ab191248)	Western blot	Control
Rabbit IgG, monoclonal – Isotype control	Abcam	ab172730	Immunocytochemistry	Primary isotype control
(Goat F ab') secondary. Anti-Rabbit IgG – Fc (Dylight 650) pre-adsorbed.	Abcam	Ab98483	Immunocytochemistry	Secondary
TRPC6 (human anti-rabbit polyclonal)	Origene	TA306349	Immunocytochemistry and western blot	Primary
Anti-Rabbit Alexa Fluor 488, polyclonal	Invitrogen		Immunocytochemistry	Secondary
TRPC1 (human anti-rabbit polyclonal)	Alomone	ACC-010	Immunocytochemistry and western blot	Primary
Rabbit polyclonal IgG	Abcam	ab27472	Immunocytochemistry	Isotype control
Donkey anti-Mouse IRDye 680RD	LICOR	926-68072	Western blot	Secondary
Donkey anti-Rabbit IRDye 800CW	LICOR	926-32213	Western blot	Secondary

Figure 2.16   **Details of antibodies used for western blot and immunocytochemistry**

2.11 Bacterial transformation and DNA extraction

Solutions for Bacterial Transformation and DNA extraction:
Luria broth (LB): 10g Tryptone, 5g Yeast extract, 10g NaCl. (pH 7.5 NaOH). Volume made up to 1l using ddH2O

Super optimal broth with catabolite repression (SOC): 20g Tryptone, 5g Yeast extract, 10mM NaCl, 2.5mM KCL, 10mM MgCl2, 20mM Glucose in 1l dH2O.

DH5α competent cells (Sigma) were used to grow up constructs of plasmid DNA following the manufacturer's protocol. The first step was addition of 1µL of DNA to 20µL of DH5 cells incubation on ice for 30minutes; this step is to allow the DNA to stick to the cells. Next, the cells were heat shocked for 30s at 42°C – this opens up the cell membrane to allow the DNA construct to enter. Cells were then placed back on ice for 2 minutes to allow the membrane's to re-seal. 250µL of SOC media was added to cells and then were placed in a shaking incubator for 37°C for 1 hour. After this, 100µL of cell suspension was pipetted onto LB agar plates with appropriate antibiotic and left overnight at 37°C. The following day, plates were sealed with parafilm at stored upside down at 4°C.

To make a starter culture to grow up the transformed colonies, a single colony was picked by scraping off the bacteria with a pipette tip and incubating the tip in 1ml of LB broth supplemented with appropriate antibiotic for 8 hours at 37°C in a shaking incubator (225rpm). In the mean time conical flasks containing 50ml of sterile LB broth with appropriate antibiotic were prepared, ready for addition of the starter cultures. The combined mixture was incubated at 37°C in a shaking incubator (225rpm) overnight.

The next morning, the DNA constructs were extracted from the bacterial cultures using a GenElute^{TM} Plasmid midiprep kit (Sigma) as per manufacturer's instructions. If necessary, DNA was concentrated to 1µg/ml before use. Purified DNA was sequenced by the University of Sheffield Core Genomic Facility to confirm sequence integrity.

2.12 LAD2 cell transfection

A Neon® Life Technologies electroporation system was used for LAD2 transfection. LAD2 cells were counted, 100,000 cells were used per transfection condition. The appropriate number of cells was removed from the culture flask and the cell suspension was spun down at 100g for 5minutes. The pellet was resuspended in 1ml PBS and the cells were then spun again and resuspended in Buffer R (12µL per transfection). Plasmid DNA was added at a concentration of 1µg/transfection. DNA concentration was made so that the DNA volume was no more than 10% of the total volume. The cell suspension in Buffer R was taken up with the electroporation pipette, transferred to the Neon electroporation station (containing 3ml of Buffer E). Care was taken to ensure no bubbles were created in the Neon pipette tip. Following loading into the electroporation station the cells were electroporated with pulse duration of 30ms at 1600mV. Cells were transferred to a 96well plate containing LAD2 media supplemented with 100ng/ml SCF. Cells were used in experiments 48 hours

after transfection. Human STIM1-WT-YFP/MO91 with a CMV promoter was bought from Addgene, STIM1 (KK$^{684-685}$EE)/pcDNA3.1 with a CMV promoter was kindly donated by Ambudkar lab.

2.13 MSD cytokine assays

MesoScaleDiscovery (MSD®MULTI-SPOT Array System) Human Proinflammatory panel 1 V-plex with 10 cytokine detection spots, were used. MSD plate assay systems utilize an electrochemiluminutescence detection technology in order to quantify analyte. A SULFO-TAG™ label is used; this emits light upon electrochemical stimulation which can be initiated at electrode surfaces on the microplates. Each individual spot in a single well of the plate is pre-coated with a capture antibody specific for the analyte of interest. The analyte solution is then incubated with the MSD plate to allow binding of the analyte to the respective capture antibody. A SULFO-TAG™ labelled detection antibody solution is then applied which binds to the capture antibody – analyte and allows detection through application of an electrochemical signal which is passed through the electrode surface of the plate. In this case, MULTI-SPOT plates were used with a complex of 10 individual cytokine detection spots. These cytokines were: IL-1β, IL-12p70, IL-2, IL-4, IFNγ, IL-6, IL-8, IL-10, IL-13 and TNF-α.

hMDM cells were activated with LPS (0.1-1000ng/ml) with or without 10ng/ml IFNγ (as defined) for 24 hour; cells were used at day 7-10 following initial PBMC isolation and hMDM differentiation. 50,000 cells were plated in each well of a 96 well plate on the day of PBMC isolation, fresh media was added prior to agonist application and where antagonists were used these were applied for 15 minutes prior to agonist application. Supernatants were collected after the 24 hour incubation period and stored at -80°C until assay was run. MSD proinflammatory cytokine V-plex plates were used and samples were run at a dilution of 1:10 or 1:20 according to manufacturer's instructions.

2.14 Phagocytosis assay

pHrodo® labelled *E. coli* bioparticles were used to measure phagocytosis in macrophages. Phagocytotic activity was measured based on the acidification of the particles ingested - *E. coli* particles are conjugated to pHrodo® dye, a novel, fluorogenic dye that dramatically increases in fluorescence as the pH of its surroundings becomes more acidic. Therefore, upon particle ingestion into phagosomes and change in environment pH, phagocytosis activity can be measured by the increase in fluorescence.

pHrodo® red labeled *E. coli* (K-12 strain) bioparticles (Life Technologies P35361) were made up in HBSS with 20mM HEPES (Invitrogen 14025050, Sigma Aldrich 83264) to obtain a stock concentration of 1mg/ml. Macrophages were seeded into a black edged clear bottom 96

well plate (Greiner) at a density of 40,000 cells per well. Culture media was replaced with HBSS/HEPES + 1μM Cell Tracker Green CMFDA (Invitrogen - C2925) and was incubated for 30minutes at 37°C. Antagonists were then added for 15 minutes prior to media replacement with pHrodo® labeled *E. coli* (added at 20μg per well of 100μL volume) + Hoescht (0.5μg/ml). Phagocytosis was then allowed to proceed and fluorescent image from three wavelengths were acquired (DAPI (Hoescht), FITC (cell tracker green) and TexasRed (pHrodo labeled *E. coli*)) using an InCell Analyser 2000 at 1 hour time points over 4-5 hours with 4 images were acquired per well with a minimum of 5 wells used per condition for each donor. Cells were maintained at 37°C between reads. Analysis was performed using InCell analysis macro software, intact cells that were included in analysis were defined by those which positively stained with Hoescht and cell tracker green (defined as total live cells). The % of responding cells was defined as the number of cells with uptake of pHrodo out of the total number of live cells, the density in responding cells was calculated as the mean fluorescent intensity of the pHrodo red signal as calculated from each 'total live' cell from each individual well, the phagocytosis index was calculated as the fluorescent intensity of the pHrodo (TexasRed) channel per cell divided by the background signal in the TexasRed channel.

Opsonization of pHrodo® labeled *E. coli* was performed using BioParticles opsonizing reagent (Invitrogen E2870). Following reconstitution of the opsonizing reagent, 100μL was added to 100μL of pHrodo® labeled *E. coli* (20μg/μl) the solution was mixed by vortexing and then incubated for 1 hour at 37°C, the opsonized bioparticles were then washed 2 times in PBS using low speed centrifugation (800g for 10 minutes at 4°C). Resuspension of the opsonized *E. coli* was then performed following the same protocol as with non-opsonized bioparticles.

2.15 Cytotoxicity assay

Cytotoxicity of the 3 antagonist compounds used throughout the present study was tested using the Thermo Scientific™ Pierce™ LDH Cytotoxicity Assay Kit (see manufacturer's instructions for full protocol and reagent information). hMDMs cultured in a 96 well plate (75,000 cells per well) were incubated with DMSO, GSK-2160A, GSK-161A or GSK-7975A for 24 hours in a 100μL volume. Spontanous LDH activity controls, medium only controls and Maximum LDH activity control conditions were included. To obtain the maximum LDH activity 10μL of lysis buffer was used to lyse cells. 50μL of media from each condition was then transferred to a new plate and mixed with 50μL of reaction mixture. After 30 minute room temperature incubation, reactions were stopped by adding 50μL of stop solution. The absorbance at 490nm and 680nm was then measured using a plate-reading spectrophotometer to determine LDH activity. To calculate % cytotoxicity

% cytotoxicity = compound treated LDH activity – spontaneous LDH activity x 100

Maximum LDH activity – spontaneous LDH activity

Experiments were performed in triplicate with cells from 3 hMDM donors.

Cytotoxicity assay 24hr compound treatment in hMDM cells (LDH release)
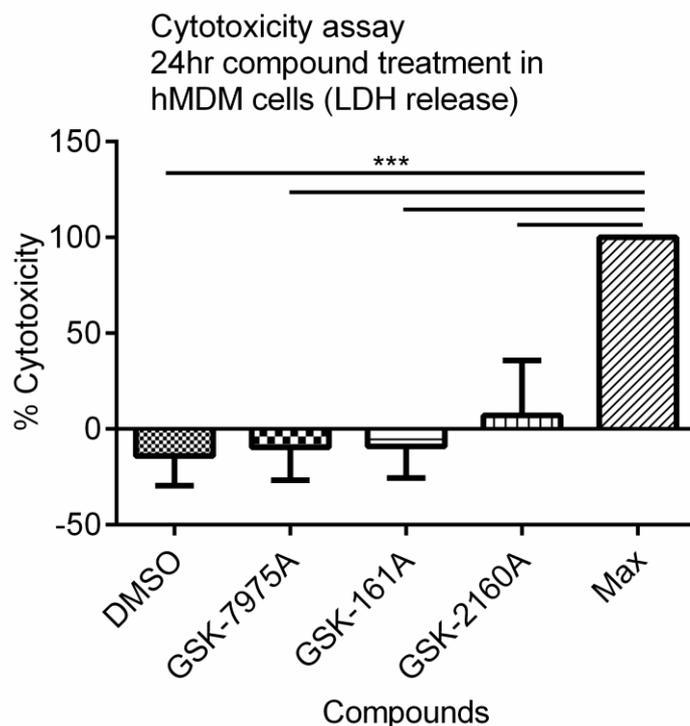
Figure 2.17   GSK-161A, GSK-2160A and GSK-7975A has no significant effect on hMDM cell viability over a 24 hour time period

Presence of the cell viability indicator enzyme LDH was quantified by colorimetric assay in hMDMs following 24 hour incubation 10µM GSK-161A, GSK-2160A or GSK-7975A or DMSO, shown in comparison to total enzyme from equivalent number of lysed cells. N=3 donors, data = mean ± SEM. Results were analysed using one-way ANOVA with Tukey's post hoc test.

2.16 Flow cytometry

Analytical flow cytometry was performed using the BD LSRFortessa machine, a FACS machine with fixed lasers. Flow cytometry is a way to analyse the relative size, internal complexity and fluorescent intensity of cells as they pass in suspension through a laser beam. The use of antibodies conjugated with fluorophores allows the expression of cell surface markers to be analysed through the fluorescent signal omitted. Flow cytometry utilizes fluidic, optic and electronic systems to give an output signal that relates to the cells size, relative complexity and fluorescent intensity as introduced above. The fluidics system controls the suction of the cells contained in suspension within a FACS tube so that they reach the 'interrogation point', which is defined as the location where the light beam is directed at an individual cell. It is the optic system which provides the excitation source i.e. a laser beam at a specific wavelength and also consists of filters and mirrors to collect the light signals. The electronic subsystem then converts the light signal into a digital electronic signal.

As a cell passes through the interrogation point where a laser beam of light is directed through the centre of the cell the light passing through the cell can be divided into: forward scatter light and side scatter light. The forward scatter light is effected by the size of the cell and its refractive index, with the larger the cell and greater the refractive index = greater FSC value. Similarly the side scatter light is affected by the internal complexity or granularity of the cell, with a more granular cell causing greater side scatter (SSC). Analysis of the FSC and SSC values can be useful in distinguishing different cell types within a mixed population. I.e. an erythrocyte and a lymphocyte would have different FSC and SSC properties. Upon set up of a flow cytometry experiment, the voltages of the FSC and SSC collection channels need to be altered so that they collect signal within the right threshold levels. By increasing the FSC and SSC voltage range this can allow debris particles to be discounted from the number of events recorded.

When assessing the expression of cell surface markers through flow cytometry the excitation and emission properties of the fluorophores used needs to be carefully considered. In the BD LSRFortessa flow cytometer there are three fixed laser beams for excitation at 355-nm UV,

450-nm violet, 488-nm blue and 640-nm red wavelengths. The use of filters that transmit or block light at specified wavelengths allows the distinction of fluorescent light from a number of different fluorophores. However the emission window of distinct fluorophores can overlap in spectral properties meaning that false signals in certain fluorophore channels can be obtained from excitation at a certain wavelength. If spectral overlap occurs in the fluorophore panel used in an experiment, compensation mechanisms can be used to prevent errors in the analysis caused by overlap in the signals. The flow cytometry experiments performed in this study were relatively simple fluorophore combinations which were chosen so that no spectral overlap occurred. Data collected was analysed in FlowJo.
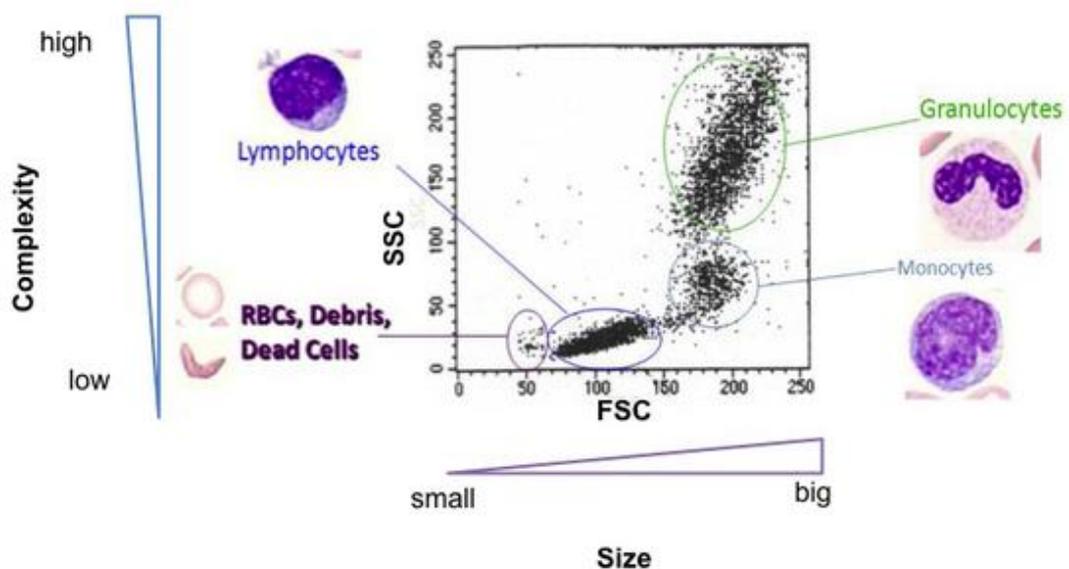
Figure 2.18   Diagram to illustrate the FSC and SSC parameters in a flow scatter plot.

From a flow cytometry experiment, showing distinct populations.
Reproduced with permission from http://www.backbonebiology.com/flow-cytometry

$5x10^5$ cells were used per condition for flow cytometry experiments. Following CD14+ cell isolation from peripheral blood mononuclear cells differentiation cells were plated into T75 nunclon tissue culture flasks and cultured with GM-CSF for 7 days to allow differentiation in hMDM cells. On the day of the experiment, cells were detached from the flask by gently using a cell scraper, no detachment agent was used. The culture flask was rinsed out with FACS buffer (PBS $^{-/-}$, 0.1% FCS) and cells were spun down at 350g for 5 minutes at room temp. Cell pellet was resuspended in 100μL/condition of FACS buffer + Human TruStain FcX™ (Fc Receptor Blocking Solution - Biolegend) (95μL of FACS buffer: 5μL of Human TruStain FcX block) and transferred into individual eppendorf tubes for different staining condition. Cells were incubated with Human TruStain FcX block solution for 5 minutes before addition of antibodies. Antibody incubation was performed for 20minutes at 4°C followed by addition of 1ml FACS buffer and a centrifugation at 350g for 5 minutes at room temp to wash off any unbound antibody. Cells were then resuspended in 300μL of FACS buffer (+ SYTOX ® Blue Nucleic Acid Stain (S11348) dead cell dye if needed) and transferred into FACS tubes ready for analysis using the BD FACS LSRFortessa.

For experiments with the CD68 antibody, with an intracellular epitope, cells were fixed and permeabilised prior to antibody incubation. This was done using a BD Cell Fix and Perm kit (BD 554714): the cells were fixed in Cytofix for 10minutes following an initial wash with PBS, cells were then scraped off the flask and the preparation process was identical to that in non-fixed cells apart from use of the Perm/Wash buffer in the place of the standard FACS buffer. Performance of the BD LSRFortessa machine was calibrated daily using cytometer set-up and tracking (CST) beads (BD biosciences). All experiments were performed with unstained controls for initial setting of voltage thresholds for the FSC/SSC gates and the fluorophore channels. Isotype controls were performed in parallel to their respective antibody conjugates.

Flow cytometry antibody details	Company	Cat number
APC anti-human CD64	Biolegend	305013
APC Mouse IgG1 isotype control	Biolegend	400121
Alexa Fluor 488 anti-human CD68	Biolegend	333811
Alexa Fluor 488 Mouse IgG2b Isotype control	Biolegend	400329
Alexa Fluor 488 anti human CD86	Biolegend	305413
Alexa Fluor 647 anti human CD14	Biolegend	325611
Alexa Fluor 647 Mouse IgG1 kappa Isotype control	Biolegend	400130

Figure 2.19   Flow cytometry antibody details

2.17 ROS assay (bacterial killing)

hMDMs were seeded into a 96 well plate at density of 50,000cells/well, cells were transferred into antibiotic free media 24hr before experiment. On the day of the experiment, culture media was replaced with HBSS with 20mM HEPES (Invitrogen 14025050, Sigma Aldrich 83264) and 20μM H2DCFDA (D-399) was added and plate incubated 30mins at 37°C. H2DCFDA was removed and cells were washed with HBSS + HEPES solution. Subsequently, antagonists were applied for 15mins, prior to addition of S. Pneumoniae (MOI 5). ROS production was then measured after 4 hrs incubation at 37°C– using a XPS Gemini plate reader to measure the signal at 485Em/535Ex nm. Heat inactived bacteria was used as a negative control and addition of 50 μM Tert-Butyl Hydrogen Peroxide was used as a positive control.

3 Chapter 3: Investigation of TRPC channel contribution to FcεRI signalling in human mast cells

3.1 Chapter 3 introduction

3.1.1 The role of Ca^{2+} in mast cell mediator release

Mast cells are key contributors to allergic disease (Metcalfe *et al.*, 1997) - inappropriate activation of the high affinity FcεRI on the mast cell surface culminates in proinflammatory mediator release and contribution to symptoms of allergic disease. FcεRI activation leads to the generation of DAG and IP_3 therefore mobilizing Ca^{2+} signalling from intracellular stores and through store/receptor operated Ca^{2+} channels. Ca^{2+} has been demonstrated to be have an important role in the control of mast cell mediator release; both degranulated mediator and newly synthesized lipid mediators and cytokines (Di Capite & Parekh, 2009).

The process of degranulation has long been recognised as being Ca^{2+}-dependent. Even before the exocytotic mechanism of degranulation was recognised, studies showed that without Ca^{2+}, degranulation of histamine was impaired (Beaven *et al.*, 1984). Following activation, mast cells can synthesise cytokines and chemokines through activation of transcription factors such as nuclear factor of activated T cells (NFAT) and nuclear factorκB (NFκB). NFAT activation and translocation occurs following dephosphorylation by the Ca^{2+}-sensitive protein calcineurin (Crabtree & Olson, 2002). However in general the level of Ca^{2+}-dependency for cytokine production mediated by transcription factors is complex. For example it has been demonstrated that NFAT and NFκB can separately regulate the production of distinct cytokines, but also that there is some overlap between transcription factor roles i.e. both NFAT and nuclear factorκB (NFκB) have been shown to be involved in TNFα production (Pelletier *et al.*, 1998; Marquardt & Walker, 2000; Klein *et al.*, 2006). Research by Dolmetsch *et al.*, (1997), shows differential dependence of transcription factor activation on the Ca^{2+} signals amplitude and duration, they demonstrate NFκB can be activated solely by intracellular Ca^{2+} signalling from store depletion (Ca^{2+} spikes), while NFAT activation is dependent on extracellular Ca^{2+} influx. These results indicate that although there are defined levels of Ca^{2+} dependency for the initiation of transcription factors involved in cytokine release, the actual Ca^{2+} dependency of each cytokine is hard to define due to the overlap in control of cytokine production between transcription factors. This should be considered in experiments where the effect of a Ca^{2+} inhibitor on release of cytokines is assessed. Although experimental inhibition of Ca^{2+} may limit the activation of one transcription factor, its activity could be compensated by another, compounding the interpretation of results. Eicosanoid production can be more simply described as Ca^{2+}-dependent due to the Ca^{2+}-dependent steps involved in their synthesis. Eicosanoids are

derived from arachidonic acid production which is regulated by the Ca^{2+}-dependent phospholipase A2 (PLA2) (Chang & Parekh, 2004). Taken together, it is clear Ca^{2+} signalling plays a crucial role in controlling human mast cell functions, therefore identification of specific Ca^{2+} channels activated downstream of specific mast cell receptors represents an important area of research. My study aims to address a gap in understanding to provide further knowledge about Ca^{2+} signalling in mast cells.

3.1.2 Evidence implicating Orai and TRPC in FcεRI-mediated mast cell signalling

In rodent and human mast cells, several studies have implicated Ca^{2+} signalling through Orai channels as crucial components of effective FcεRI-mediated mast cell mediator release. For example, in mouse foetal liver-derived mast cells, Orai1 or STIM1 knockdown causes significant attenuation in the FcεRI-mediated Ca^{2+} signalling and mediator release (Baba *et al.*, 2008; Vig *et al.*, 2008). Pharmacological inhibition of Orai channels in primary rat tracheal mast cells was shown to prevent allergen-driven contractions (Rice *et al.*, 2013). Notably Orai has also been shown to have a key role in Ca^{2+} signalling in FcεRI driven human mast cell functions. (Ashmole *et al.*, 2012) and work by the Seward lab (Wajdner *et al.,* 2015 – in press) described functional Orai/ I_{CRAC} currents and Ca^{2+} signals following FcεRI activation in HLMCs and importantly, through the use of an Orai selective antagonist, Synta66, demonstrated that inhibition of Orai channels caused a reduction in the release of proinflammatory mediators. The release of degranulated mediator, histamine was inhibited by Synta66 by 73% ± 10 demonstrating a primary role for Orai, whereas the release of IL-5, IL-8, IL-6 and CSFα was inhibited by 50-60% (Wajdner *et al.,* 2015 – in press). Notably, lipid mediator PGD_2 was not significantly inhibited by Synta66. Together these studies show the important role of Orai-mediated Ca^{2+} signalling in FcεRI-mediated human mast cell activation; however it also suggests that Orai is not the only Ca^{2+} channel required for the release of cytokine and lipid derived mediators.

In addition to Orai, the involvement of TRPC channels in FcεRI-mediated mast cell activation and mediator release has been reported in numerous studies using rodent mast cell models. Similarly, *in vivo* studies of allergic disease have implicated TRPC channels as key contributors. However unlike research into Orai signalling in mast cells, until now, no work has addressed the contribution of TRPC channels to FcεRI-mediated signalling in human mast cells. In mast cells there are several examples where aspects of cell signalling or receptor expression are not replicated in a human model therefore studies designed to address the translation of findings from rodent models into primary human cells are crucial (Bischoff, 2007).

The first report of TRPC having a role in mast cell biology was work performed by (Ma et al., 2008). This study using the RBL-2H3 rat mast cell line, described that RBL cells express TRPC1, 2, 3, 5 and 7 but not TRPC6. Interestingly this study showed that shRNA knockdown of TRPC5 substantially impaired the Sr^{2+} and Ca^{2+} entry following both thapsigargin or

antigen stimulation. Interestingly here TRPC5 activity was shown to be dependent on Orai1/STIM1, as Orai1/STIM1 knockdown impaired store operated Sr^{2+} influx. Subsequent work, also in RBL-2H3 cells emphasised an alternate role for TRPC; (Cohen et al., 2009) demonstrate shRNA mediated knockdown of TRPC1 causes a decrease in responsiveness to antigen and a decrease in the frequency of Ca^{2+} waves located at the extended protrusions of the RBL cells. Therefore Cohen's study indicates TRPC channels have a role in localised Ca^{2+} signalling within microdomains rather than controlling global Ca^{2+} signalling. The importance of TRPC channels in rodent mast cell FcεRI signal transduction is corroborated by two more studies; examination of the phenotype of Fyn-/- BMMCs (Sanchez-Miranda *et al.*, 2010) showed that TRPC channels regulate FcεRI/Fyn-dependent FcεRI-mediated signalling and degranulation. A more detailed investigation by (Suzuki *et al.*) supports this, they showed Fyn-/- BMMCs have attenuated degranulation, reduced antigen induced Ca^{2+} signals and impaired inward and outward currents in patch clamp assays. This led to a hypothesis that the Fyn phenotype is caused by loss of a non-selective Ca^{2+} current. Examination of TRPC channel protein expression in the Fyn-/- BMMCs showed that TRPC1 levels were reduced in Fyn deficient mice, and convincingly TRPC1 current was restored when Fyn kinase was reconstituted and TRPC1 over-expression could rescue the FcεRI-mediated degranulation and Ca^{2+} entry (Suzuki *et al.*). In summary, this study indicates TRPC1 has a role in global Ca^{2+} signalling and is critical for degranulation in BMMCs.

Literature on TRPC function in rodent mast cell signalling is inconsistent; in contrast to the studies described above, (Medic et al., 2013) examined BMMCs from TRPC1 knockout mice, finding a seemingly opposite phenotype to that seen in the Fyn$^{-/-}$ mice. Although these BMMCs displayed low TRPC1 expression, they had an enhanced FcεRI induced Ca^{2+} entry and subsequent enhanced transcription of Ca^{2+}-dependent transcription factors (NFAT and JUN). The discrepancy between this study and others could be due to differences in methodology; (Medic et al.) permanently delete TRPC1 from development which could lead to permanent phenotypic alterations, whereas (Cohen et al.) and (Suzuki et al.) used transient knockdown techniques. An *in vivo* model of TRPC1$^{-/-}$ mice reported by (Yildirim et al., 2012) found a reduction in Th2 cytokines and chemokines in the lungs of ovalbumin sensitized mice. The methodology of TRPC1$^{-/-}$ knockdown by (Yildirim et al.) is consistent with (Medic et al.), yet there is a direct contrast in expected results, however, the cell types mediating the phenotype of the *in vivo* model are unknown. A study by (Sel et al., 2008) shows similar results to the TRPC1$^{-/-}$ *in vivo* mouse (Yildirim et al.) but with a TRPC6$^{-/-}$ knockout mouse, here in addition to reduced Ca^{2+} signalling there was also a decrease in ovalbumin induced Th2 cytokines compared to the WT controls.

Taken together these studies suggest that the TRPC channels have important roles in FcεRI-mediated rodent mast cell biology. However the specific role of TRPC channels is highly variable in each different study described, the reasons for these differences could be due to a combination of factors. It is important to note both the differences in methodologies, and the differences incurred by the complex regulation of TRPC activity based on the level of expression of other family members/interacting partners. Several of the studies described above, delineating the function of TRPC, were performed using mouse knockout models or siRNA knockdown. Use of these methods has been a necessity due to the lack of

selective pharmacological tools to distinguish between receptor subtypes, but the possibility of compensatory mechanisms complicating the results must be taken into account.

In combination the results from the studies described show that there is a clear role for Orai channels in FcεRI-mediated rodent and human mast cell biology, similarly there is clear evidence for some role of TRPC channels to FcεRI regulated rodent mast cells however there is a clear lack of studies assessing TRPC contribution to human mast cell biology. The aim of my study was to address this novel and important area of research with the hypothesis that TRPC channels would contribute to FcεRI Ca^{2+} signalling in human mast cells, based on the supporting evidence described.

3.2 Results

3.2.1 Assessment of TRP, Orai and STIM family mRNA expression in LAD2 and HLMCs through microarray

A microarray study was performed to assess the expression of TRP, Orai and STIM families in both LAD2 and HLMC cells. The results of these experiments confirm previously published work that Orai and STIM family genes are expressed in HLMCs at mRNA level and also show the expression of Orai and STIM into LAD2 mast cells. The microarray data presented in *Figure 3.1* shows positive expression of Orai1, 2 and 3; Orai 1 and 2 expression was greatest with relative expression levels of 3-4 whereas Orai2 was expressed at more than half these levels, at <1 relative expression. Similarly, STIM1 was expressed at greater levels compared to STIM2.
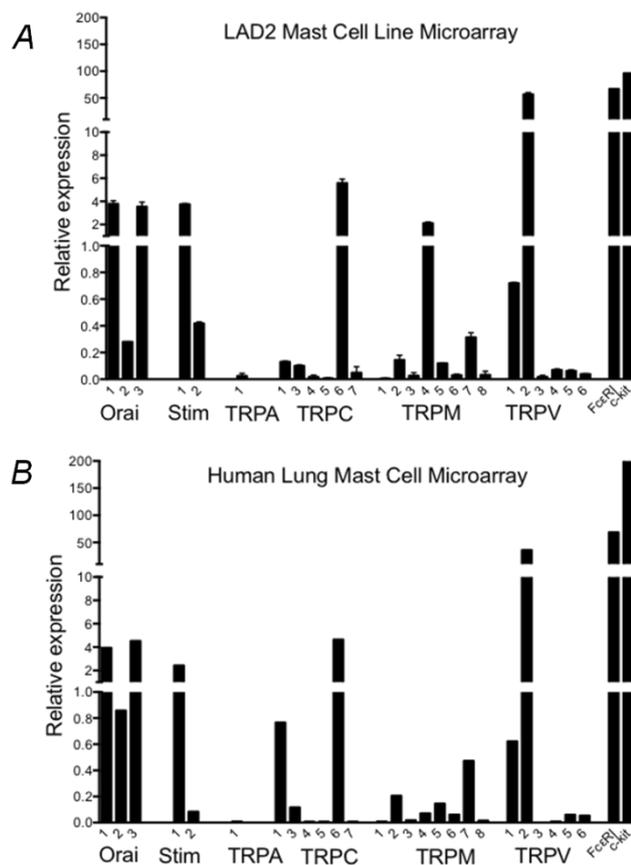
Figure 3.1   Orai, STIM and TRP family mRNA expression as assessed by microarray

*Microarray data was normalised to the 75th percentile of all non-control probes, according to Agilent instructions. **A.)** LAD2 mRNA expression from three independent RNA extractions ± SEM **B.)** HLMC mRNA expression from one HLMC donor.*

The microarray experiments also revealed novel information about the expression levels of members of the TRP channel family. There are several classes of the TRP family, including the ankyrin, canonical, vaniloid, and melanostatin transient receptor potential families *(Section 1.5)*. Although this study focuses on the function of the TRPC channel family, the expression of other TRP families was also assessed to provide preliminary data to direct future research in the field. Of more direct relevance, the commonly reported promiscuity of TRP channels in terms of channel heteromerisation and interaction *(Section 1.5.9)* means that identifying potential partners for TRPC in mast cells is important. Microarray data demonstrates that members of the TRPC, TRPM and TRPV family are expressed in both LAD2 and HLMC cells. TRPV2 was most highly expressed with relative expression levels around 50 in both cell types. TRPV1 was also expressed in LAD2 and HLMCs, however the expression levels were much lower at ~0.6-0.7. Of the TRPM family, TRPM2 and M7 were expressed in both cell types at similar levels. TRPM4 was also expressed in HLMC and LAD2s, but its expression is far greater in LAD2s than in HLMCs, with more than a 10-fold difference in expression *(Figure 3.1)*. TRPM7 has previously been functionally characterised in human mast cells (Wykes *et al.*, 2007), demonstrating that this level of mRNA expression

is sufficient to provide a functional contribution to cell physiology. Finally, the results presented in *Figure 3.1* also show novel evidence that TRPC1, TRPC3 and TRPC6 are expressed in LAD2 and HLMCs, with TRPC6 expressed at the highest levels in both cell types (~5), TRPC1 was expressed at around 0.2 in LAD2s and 0.8 in HLMCs, and TRPC3 around 0.1 in both cell types. Together these results show Orai, STIM and a range of TRP channel families are expressed at mRNA level with high correlation in levels of expression between LAD2 and HLMC cells.

3.2.2 Confirmation of mRNA expression of the Orai, STIM and TRPC family in other HLMC donors by qPCR

Quantitative PCR was used to verify the consistency of expression of TRPC subtypes in HLMCs between different lung donors. geNorm assays were initially performed to verify the most stably expressed housekeeping gene from which to normalise, 18SrRNA *(Figure 2.9)* was demonstrated to have an M value of less than 0.55 and was the most stably expressed out of the 5 other genes assessed in HLMC cDNA. SYBR green primer probe technology was used in these experiments, therefore primer specific amplification of the target gene was assessed for each experiment using a melt curve analysis *(Figure 2.7)*. Similarly cDNA concentration titration experiments were performed to ascertain the primer efficiency *(Figure 2.12)*. Together these data provide validation that the qPCR results can be interpreted to assess relative quantitative gene expression.

qPCR was performed in HLMC cells from 4 additional lung donors which allowed an assessment into any variation in expression between donors. Whereas the microarray data showed no expression of TRPC5 and TRPC7, qPCR showed low expression of TRPC5 and TRPC7 in donors P294 and P315 but not in donors P312 and P319. There was a significantly higher expression of Orai2 in Donor P312 compared to the other three donors. However, all other gene expression values were largely consistent between donors. Notably, all donors showed high expression levels for FcεRI, which has a key role in mast cell function.
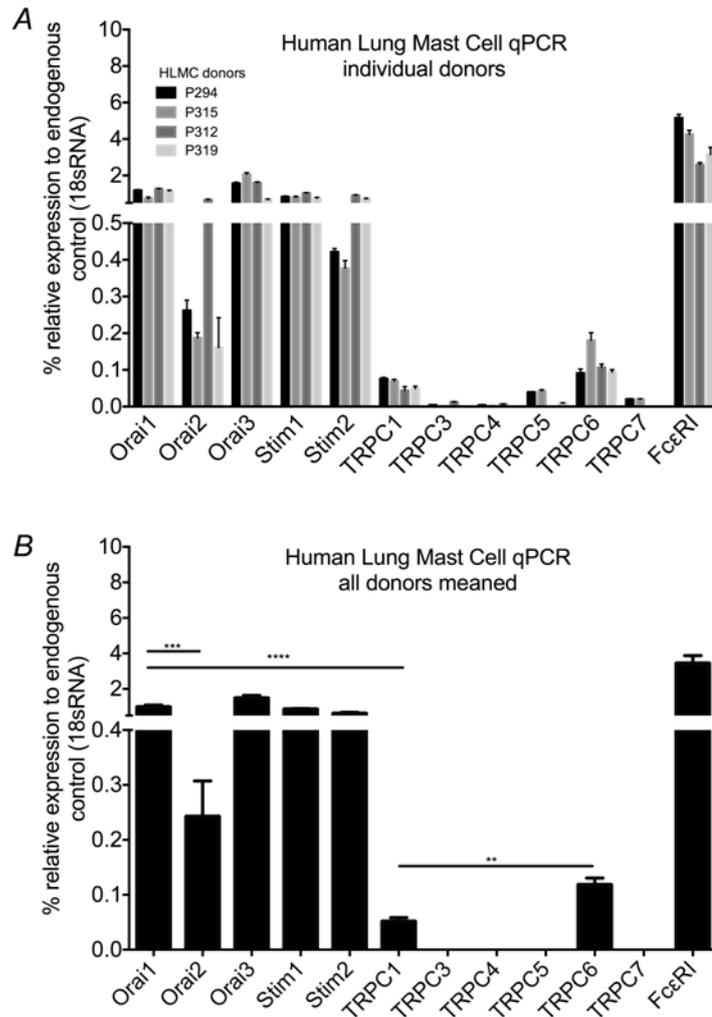
Figure 3.2   Orai, STIM and TRPC mRNA expression as assessed by qPCR in further HLMC donors

Quantitative PCR to assess the expression of Orai, STIM and TRPC mRNA in HLMCs. Expression was normalised to 18S endogenous control and expressed as % relative to 18S. −RT and NTC controls were performed to show no genomic contamination was present. SYBR green probes were used and melt curves plotted to assess primer specificity. ***A.)*** *mRNA expression with data from individual donors presented.* ***B.)*** *mRNA expression with data from all donors meaned. Results were analysed using one-way ANOVA with Tukey's multiple comparison test. * p <0.01, **** p<0.0001*

In general the qPCR results presented in ***Figure 3.2*** confirmed that Orai and STIM expression follows a similar expression profile as observed in the microarray experiments; however only expression of TRPC1 and TRPC6 was observed by qPCR, TRPC3 was not seen at significant levels. As in the microarray results TRPC6 expression was higher compared to TRPC1, however the levels of TRPC6 were not in line with the expression of Orai and STIM genes as shown in microarray. The reasons for these discrepancies could be explained due to differences in the specificity of the individual gene amplification between the two techniques. In summary, the experimental results presented in ***Figures 3.2*** confirm the

previously published data that Orai and STIM families are expressed in human mast cells. The results also show novel evidence that there are numerous members of the TRP channel family expressed in LAD2s and HLMCs at mRNA level and in general the expression is consistent between the two cell types. Identification of the expression of certain members of the TRP family provides useful information from which to direct future ion channel mast cell research. Of particular interest in respect to the present study; TRPC1 and C6 are shown to be expressed in both LAD2 and HLMC cells at mRNA level. This result provided identification of the TRPC family members to focus upon for the rest of this study.

3.2.3 TRPC1 and TRPC6 expression was observed in HLMCs and LAD2s at protein level.

Based on the evidence from the microarray and qPCR experiments, follow up studies to verify the protein expression of TRPC1 and TRPC6 were performed by immunocytochemistry *(Figure 3.3-3.5).* As described in *Section 2.10 (Figure 2.14 and 2.15)*, the selectivity of the TRPC1 and TRPC6 antibodies were supported by a western blot experiments. Data presented in *Figure 3.3 and 3.4* shows that TRPC1 and TRPC6 are expressed in HLMCs with a MFI significantly greater than the MFI seen in IgG isotype control conditions (TRPC1 MFI – background = 36.8 ± 4.8 n=31, TRPC6 MFI – background = 31.6 ± 1.1 n=41, IgG isotype control MFI-background = 16.7 ± 0.7 n=69). Fluorescent intensity profiles shown in *Figure 3.3E and 3.4E* indicate that the intensity profile is evenly distributed through the cell diameter rather than being brighter at the edges of the cell as would be seen if the expression was localised to the plasma membrane. TRPC1 protein expression was also found in LAD2 cells *(Figure 3.5)*, giving confidence to translatability of TRPC channel expression between LAD2 and HLMC mast cells. (TRPC1 MFI-background = 142.7 ± 1.1 n=41, IgG isotype control MFI – background = 45.7 ± 1.4 n=35). Together these results show evidence to support the expression of TRPC1 and TRPC6 in human mast cells at protein level.
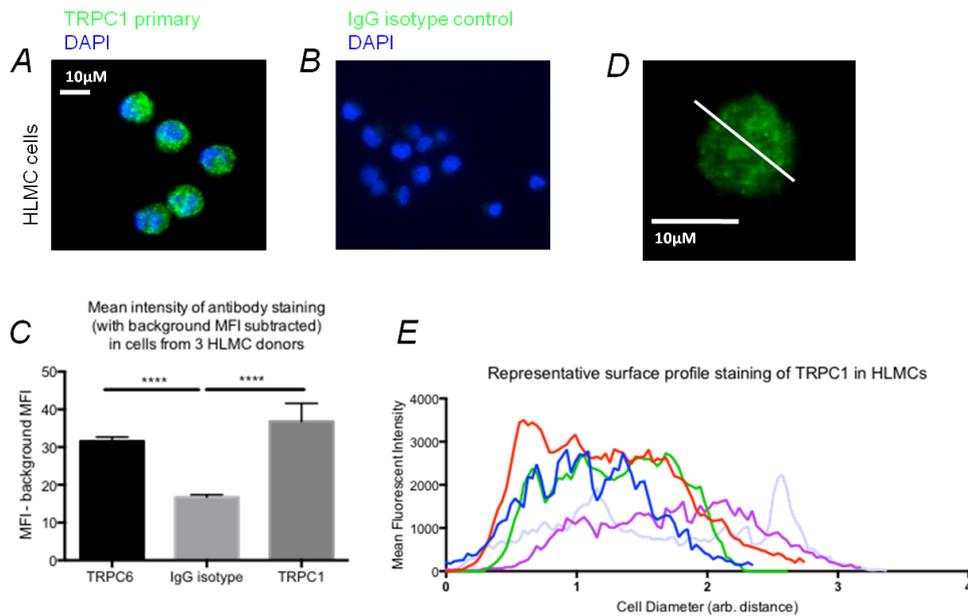
Figure 3.3   TRPC1 expression in HLMCs at protein level

Immunocytochemistry to assess TRPC1 channels in HLMCs, cells were stained with:
A.) *anti-TRPC1* ***B.)*** *IgG isotype control, and all cells were fixed with DAPI fluoromount. Cells were imaged using a fluorescent confocal microscope, images taken at 488 and 405nm.* ***C.)*** *Bar graph shows quantification of mean fluorescent intensity of cells in each conditions mean ± SEM,* ***D.)*** *Example cell for surface profile analysis* ***E.)*** *TRPC1 surface profile fluorescent intensity. N=3 donors. Results were analysed using one-way ANOVA with Tukey's multiple comparison test. * p <0.01 **** p<0.0001*
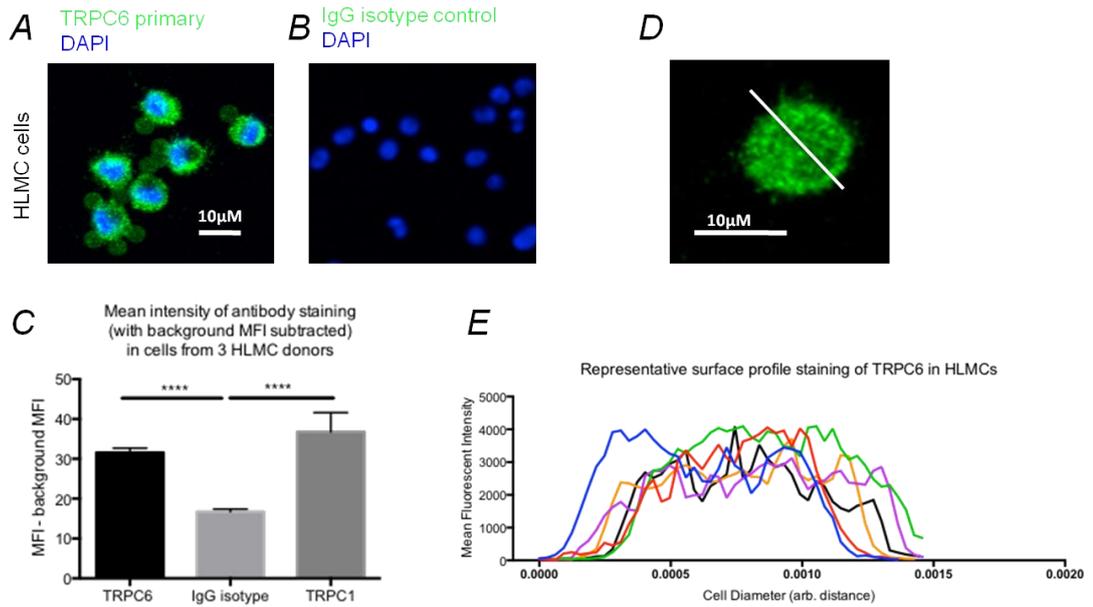
Figure 3.4   TRPC6 expression in HLMCs at protein level

*Immunocytochemistry to assess TRPC6 channels in HLMCs, cells were stained with: **A.)** anti-TRPC6 **B.)** IgG isotype control, and all cells were fixed with DAPI fluoromount. Cells were imaged using a fluorescent confocal microscope, images taken at 488 and 405nm **C.)** Bar graph shows quantification of mean fluorescent intensity of cells in each conditions mean ± SEM, **D.)** Example cell for surface profile analysis **E.)** TRPC6 surface profile fluorescent intensity. N=3 donors. Results were analysed using one-way ANOVA with Tukey's multiple comparison test. * p <0.01 **** p<0.0001*
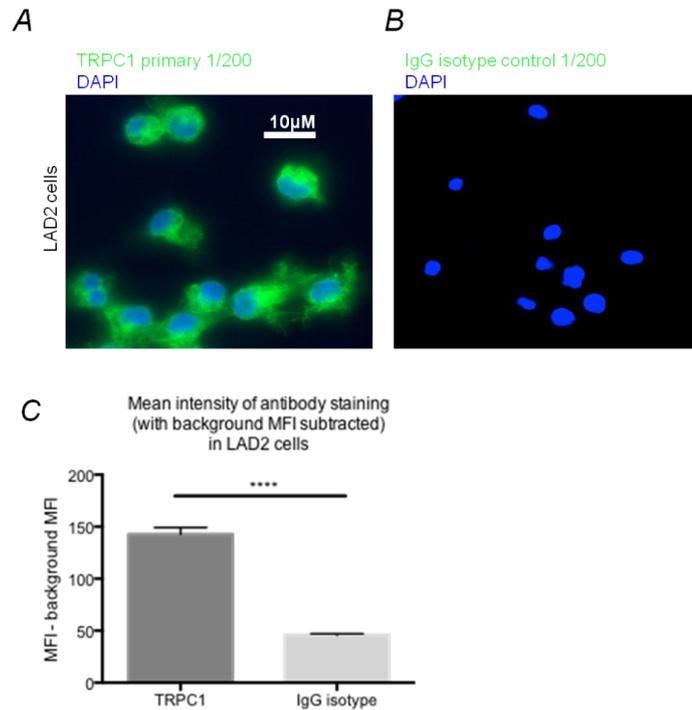
Figure 3.5   TRPC1 expression in LAD2s at protein level

*Immunocytochemistry to assess TRPC1 channels in LAD2s, cells were stained with: **A.)** anti-TRPC1 **B.)** IgG isotype control, and all cells were fixed with DAPI fluoromount. Cells were imaged using a fluorescent microscope, images taken at 488 and 405nmm**C.)** Bar graph shows quantification of mean fluorescent intensity of cells in each conditions mean ± SEM, **D.)** TRPC1 surface profile fluorescent intensity. Results were analysed using one-way ANOVA with Tukey's multiple comparison test. * p <0.01 **** p<0.0001*

3.2.4 Orai/Orai-regulated Ca^{2+} entry contributes to FcεRI Ca^{2+} signalling in LAD2 and HLMCs

To investigate the contributors to FcεRI-mediated Ca^{2+} entry, Synta66, an Orai selective inhibitor was used to show the contribution of Orai and Orai regulated channels.

A concentration of 10μM concentration Synta66 has been shown to have a high selectivity for Orai channels and a comprehensive list of ion channels and receptors were shown to be insensitive to 10μM Synta66 treatment (Di Sabatino *et al.*, 2009). The compound structure of Synta66 and its comparison to other Orai selective antagonists was shown in (Derler *et al.*, 2013). Similarly data obtained by the Seward laboratory (Claire Tree-Booker thesis) has demonstrated that 10μM Synta66 was insensitive against OAG induced signals in HEK-

TRPC6 cells and in S1P induced signals in HEK-TRPC5 cells. Further work by the Seward lab has shown that 10µM was the IMAX concentration for inhibition of store-operated currents in HEK Orai1/STIM1 expressing cells. In combination these pieces of data provide robust evidence that 10µM Synta66 causes maximal inhibition of Orai-mediated currents and that it is selective for Orai channels.
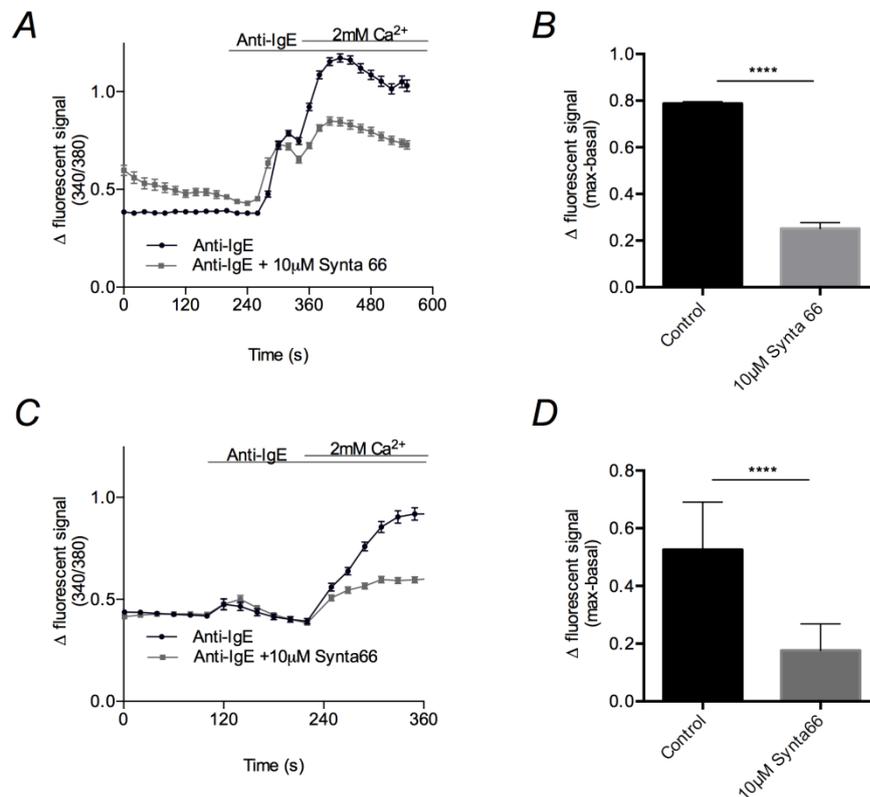
Figure 3.6 **FcεRI activated Ca^{2+} influx in HLMCs and LAD2s is partly inhibited by Orai inhibitor, Synta66**

*Single cell Ca^{2+} Imaging of fura 2-AM loaded HLMCs/LAD2s. HLMCs and LAD2s were incubated overnight with 300ng/ml IgE **A.)** Ca^{2+} signal over time, 3µg/ml Anti-IgE and external solution containing 2mM Ca^{2+} were bath applied as indicated by the horizontal bars. 10µM Synta66 was preapplied for 15mins prior to experiment and kept constant throughout. A&C shows mean of cells per donor ± SEM **B.)** Bar graph showing mean fluorescence change in Ca^{2+} signal (t300sec - t0sec) for conditions with and without Synta66. n>40 cells from each donor N=3 donors. **C&D.)** = same as A&B but for LAD2 cells. Results were analysed using unpaired students t-test ***p<0.001, ****p<0.0001. Experiments performed by Jasmine Farrington and Claire Tree-Booker.*

In order to separate the Ca^{2+} signal induced by ER store release and from the Ca^{2+} influx through plasma membrane channels, Ca^{2+} 'add back' protocol was performed. Here the Anti-IgE stimulus was initially applied in the absence of extracellular Ca^{2+} to reveal any Ca^{2+}

signal initiated by store release alone, and then extracellular Ca^{2+} was reapplied to monitor the resulting influx through plasma membrane channels. As shown in **Figure 3.6** the kinetics of the FcεRI induced Ca^{2+} signal exhibited an initial fast increase in signal (store max – basal = 40/60sec for LAD2/HLMC) followed by a more sustained signal rise (max-basal = 130/100 second for LAD2/HLMC). In HLMCs pre-application of 10µM Synta66 reduced the Anti-IgE induced Ca^{2+} influx by 69%, and in LAD2s Synta66 caused a 67% inhibition. Interestingly, Synta66 had no effect on the store component of the signal in either cell type, although the amplitude of the store signal was shown to be consistently higher in HLMCs vs. LAD2 cells (~0.3 vs. 0.1 Δsignal). This data gives clear evidence of the contribution of Orai and Orai regulated channels to FcεRI-mediated Ca^{2+} signalling in HLMC and LAD2 cells. The translation in the effect of Synta66 between HLMC and LAD2 cells provides evidence to indicate that Anti-IgE mediated signalling is mediated by the same mechanism in HLMC and LAD2 cells.

Although 10µM of Synta66 was shown to completely ablate the Orai-mediated current in a HEK O/S over-expression system **(Jasmine Farrington's thesis)** the results here show the EMAX concentration of Synta66 causes a less than 70% inhibition in the signal, therefore suggesting that there are other contributory signals to the FcεRI-mediated Ca^{2+} entry. This evidence contributes to that already illustrated in **Setion 3.1** in support of the hypothesis of TRPC contribution to FcεRI signalling.

3.2.5 STIM1-regulated TRPC does not contribute to FcεRI or SOCE in LAD2 cells

At present, there is a deficit of selective pharmacological tools to inhibit TRPC channels, particularly in the differentiation between TRPC and Orai channel activity. We sought another approach to test the functional contribution of TRPC channels to FcεRI signalling in human mast cells. As described in **Section 1.5.8** STIM1 has been shown to electrostatically interact with TRPC channels to control their activation. (Zeng *et al.*, 2008) reported that the Lys [684-685] region of STIM1 electrostatically interacts with TRPC1 aspartate residues to control gating of TRPC1, but notably not Orai channels. Therefore mutating this Lys region of STIM1 to glutamate reverses the charge so that STIM1 is no longer able to activate TRPC1, i.e. creating a TRPC1 inactivating mutant. (Cheng *et al.*, 2011a) use this STIM1-KK[684-685]EE mutant to identify the contribution of STIM1 regulated TRPC1 signalling in HSG cells, without interfering with Orai functionality. Further studies have demonstrated that STIM1 gates all TRPC channels with the Lys [684-685] region (Lee *et al.*, 2010). This significant finding has provided a way to independently assess the contribution of TRPC to Ca^{2+} signalling. The YFP tagged - STIM1-KK[684-685]EE construct as used and validated by (Zeng *et al.*, 2008) and (Cheng *et al.*, 2011a) was kindly donated to the Seward lab for use in the present study. The construct sequence integrity was confirmed by sequencing before it was used in further experiments. YFP tagged - STIM1-KK[684-685]EE or STIM1-WT constructs were transfected into LAD2 human mast cells by electroporation. Successfully transfected cells were monitored by visualisation of the cells expressing the YFP tag. Initial validation

experiments as presented in ***Figure 3.7*** show live time lapse imaging experiments of LAD2 cells transfected with the YFP tagged constructs. The results of these experiments display that the normalised YFP intensity was significantly greater at the plasma membrane following thapsigargin activation (WT=1.00 to 1.18 ± 0.06 N=3 and STIM1-KK$^{684-685}$EE = 1.00 to 1.13 ± 0.07 N=3), indicating that the STIM1 constructs are able to translocate to the plasma membrane upon store depletion. These results confirm that the YFP tagged STIM1 constructs functioned as expected based on the known role of the STIM1 protein and provide validation of the constructs activity.

Ca^{2+} imaging experiments were performed with cells successfully transfected with the STIM1 constructs aiming to determine whether STIM1-regulated TRPC was contributing to the Ca^{2+} signalling in LAD2 cells. First LAD2 cells were stimulated with thapsigargin to monitor whether STIM1 regulated TRPC1 was a contributor to the resulting signal from this generic store depletion protocol. However, the results presented in ***Figure 3.8*** show there was no change in the Ca^{2+} signalling between the STIM1-WT and STIM1-KK$^{684-685}$EE expressing cells; in either the max-basal Ca^{2+} signal or the 1st derivative (mean change of Ca^{2+} signal of 0.41 ± 0.06 n=23 and 0.35 ± 0.06 n=25 was seen in STIM1-KK$^{684-685}$EE and STIM1-WT cells respectively). Similar results were shown when the transfected cells were activated with Anti-IgE ***(Figure 3.9)***, a mean change in Ca^{2+} signal of 0.6 ± 0.1 (n=20) was seen in both STIM1-WT and STIM1-KK$^{684-685}$EE expressing cells. In order to assess the amount of construct expression was not different between the STIM1-WT and STIM1-KK$^{684-685}$EE constructs, the standard deviation of the YFP intensity in cells from each condition was measured. This analysis revealed that there was no significant difference in the YFP intensity between the two conditions (STIM1-WT SD of YFP intensity=212.0 ± 50 n=20, STIM1-KK$^{684-685}$EE cells =167.1 ± 20.4 n=30), so a differential level of transfected protein expressed per cell was unlikely to explain the lack of attenuation of the Ca^{2+} signalling in STIM1-KK$^{684-685}$EE expressing cells. Unfortunately, as transfection of cells is required to express the TRPC1 inactivated mutant (STIM1-KK$^{684-685}$EE), it was not possible to perform the same experiments in HLMCs, due to technical limitations in the transfection of a primary cell type. Neon electroporation was attempted in HLMCs but sufficient numbers of viable cells were not recovered from this methodology. Taken together, these results provide evidence that STIM1-regulated TRPC channels do not contribute to thapsigargin or FcϵRI induced Ca^{2+} signalling in LAD2 cells. These results are contrary to the original hypothesis described.

A

Before TG | After TG

STIM1-WT

2μM

STIM1 KK684-685EE

B

STIM1 WT

*

Normalised YFP intensity

Before TG | After activation 2μM TG

C

STIM1 KK684-685EE

**

Normalised YFP intensity

Before TG | After activation 2μM TG
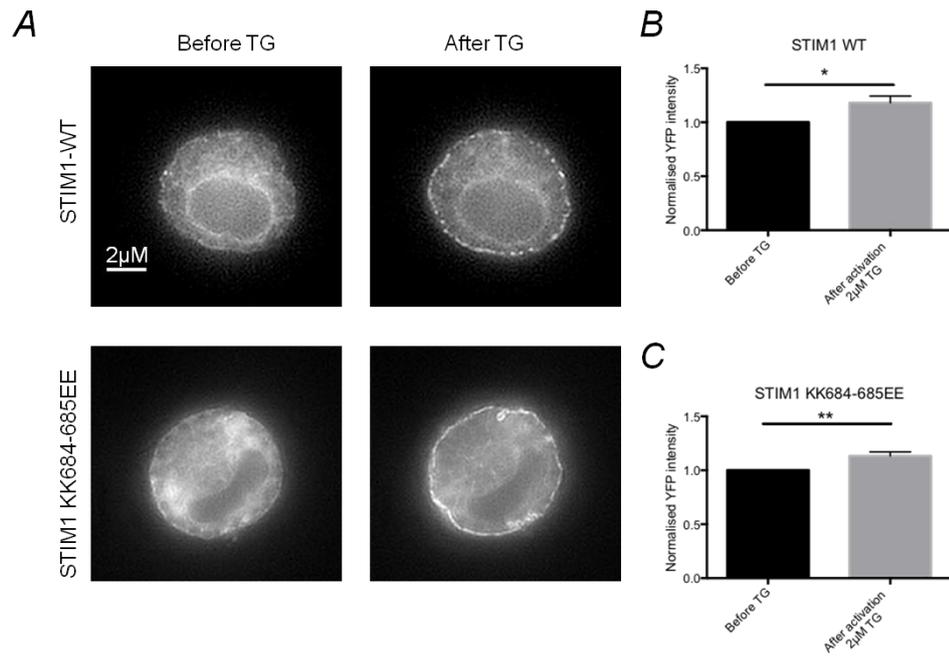
Figure 3.7   YFP tagged STIM1-WT and STIM1 KK$^{684-685}$EE constructs translocate to plasma membrane following store-depletion

Live time lapse imaging of LAD2 cells transfected with YFP tagged - STIM1 WT or STIM1 KK$^{684-685}$EE constructs. 2μM Thapsigargin (TG) was applied to visualise translocation of STIM1 to the plasma membrane. Images were normalised for bleaching and are representative cells from 3 experiments, n=6 cells. B&C.) YFP intensity at the plasma membrane before and after TG treatment, values were normalised to fluorescence at beginning of time lapse. Results were analysed using an unpaired t-test. **p<0.01, **p<0.001.
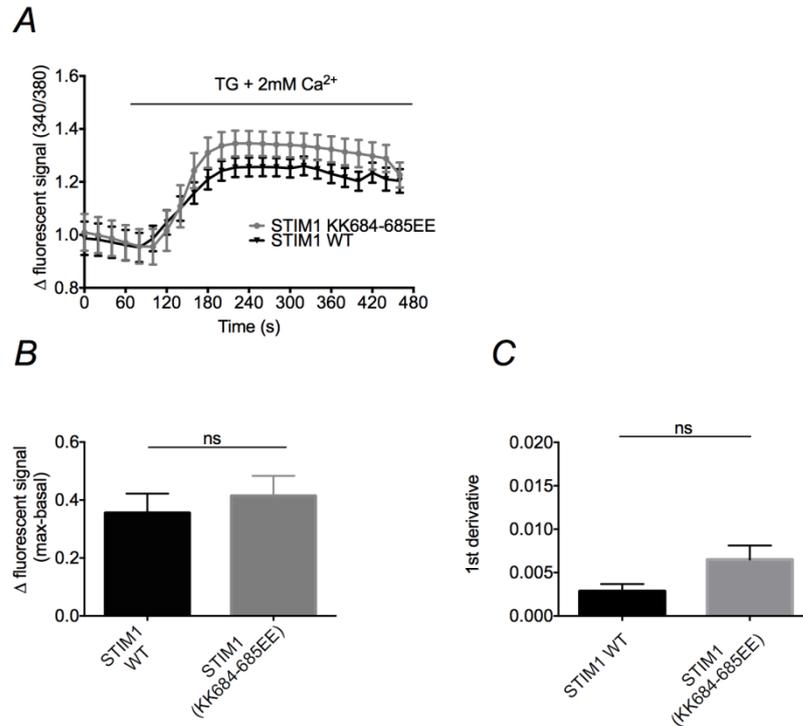
Figure 3.8   STIM1-regulated TRPC does not contribute to thapsigargin mediated Ca^{2+} entry in LAD2 mast cells

*Single cell Ca^{2+} imaging of fura 2-AM loaded LAD2 cells transfected with YFP-STIM1-WT or YFP-STIM1 KK$^{684-685}$EE. Experiments were performed 48hr after transfection. **A.)** Ca^{2+} signal over time, 2μM thapsigargin was applied as indicated by horizontal bars, mean ± SEM. **B.)** Bar graph showing mean fluorescent change in Ca^{2+} signal (max-basal) **C.)** Bar graph showing the 1st derivative of the Ca^{2+} signal at t=400s. All data is shown as mean ± SEM. n > 20 cells N=3 experiments. Only YFP+ cells were included for analysis. Results were analysed using unpaired students t-test, ns p>0.05*
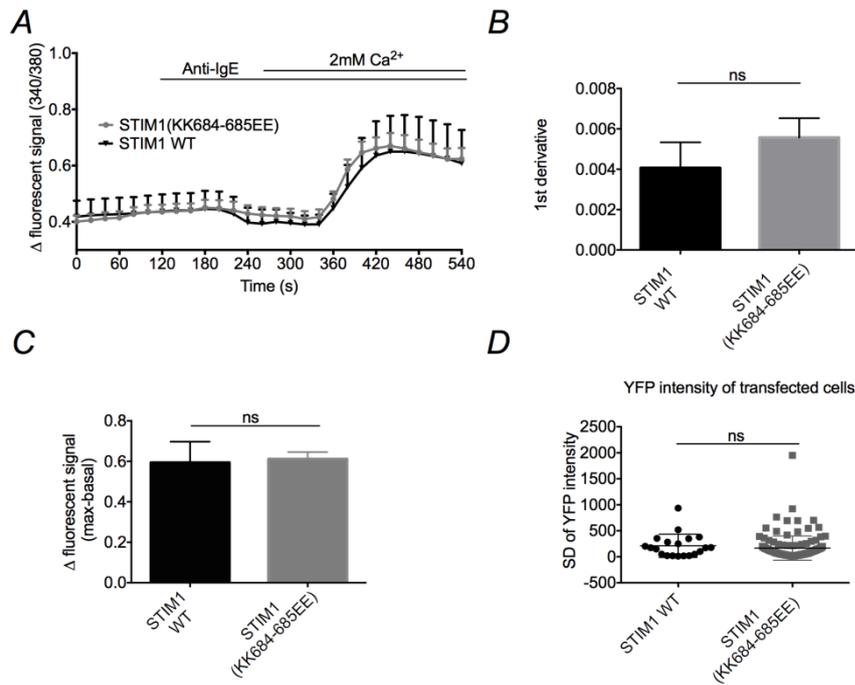
Figure 3.9   STIM1 regulated TRPC does not contribute to FcεRI mediated Ca²⁺ entry in LAD2 mast cells

*Single cell Ca²⁺ imaging of fura 2-AM loaded LAD2 cells transfected with YFP-STIM1-WT or YFP-STIM1 KK⁶⁸⁴⁻⁶⁸⁵EE. Experiments were performed 48hr after transfection. LAD2s were incubated overnight with 300ng/ml IgE prior to experiment. **A.)** Ca²⁺ signal over time, 1μg/ml Anti-IgE applied as indicated by horizontal bars, mean ± SEM. **B.)** Bar graph showing the 1ˢᵗ derivative of Ca²⁺ signal at t=400s. All data is shown as mean ± SEM. **C.)** Bar graph showing mean fluorescent change in Ca²⁺ signal (max-basal) **D.)** Bar graph showing standard deviation of YFP intensity in transfected cells. n > 10 cells N=3. Only YFP+ cells included for analysis. Results were analysed using unpaired students t-test, ns p>0.05.*

3.2.6 TRPC6 channels are not contributors to Ca²⁺ signalling in HLMCs

Results presented thus far have demonstrated a role for Orai but not STIM1 regulated TRPC contributing to FcεRI induced Ca²⁺ entry. In order to selectively identify the contribution of TRPC6 to Ca²⁺ signalling in human mast cells, recently discovered TRPC3/6 agonists and antagonists from GSK were used. These compounds were shown to be potent and selective for TRPC3/6, demonstrated in previous publications (Washburn *et al.*, 2013; Seo *et al.*, 2014b). The TRPC3/6 antagonist, GSK2833503A (GSK-3503A) is a selective inhibitor of TRPC3 and TRPC6 with at least 100-fold selectivity over other Ca²⁺-permeable channels (example 19 in Washburn *et al.*, 2013). GSK1702934A (GSK-2934A) is a potent TRPC3/6

agonist and did not stimulate TRPV4, TRPA1, M1, M4, CaV1.2, hERG, NaV1.5, or CXCR5 receptors at concentrations <10µM (supplementary data in Wajdner *et al.,* 2015 – in press)

In order to find the EC80 and EMAX for the agonist and antagonist, respectively, Ca^{2+} imaging experiments were performed in HEK 293 cells over-expressing TRPC6. A concentration-response curve as presented in ***Figure 3.10*** shows that GSK-2934A induces Ca^{2+} signals with a pEC50= 6.3 ± 0.04 N=3, whilst the antagonist GSK-3503A inhibits TRPC3/6 mediated Ca^{2+} signals pIC50=7.8 ± 0.03 N=3. These results allowed appropriate concentrations of the compounds to be used in further experiments in HLMCs. The potency for each of these compounds found from the data in ***Figure 3.10*** is in accordance with the reported potency in experiments performed during compound validation at GlaxoSmithKline. Interestingly, these compounds were shown to have similar activity in rat TRPC3/6 models (supplementary data in Wajdner *et al.,* 2015 – in press).
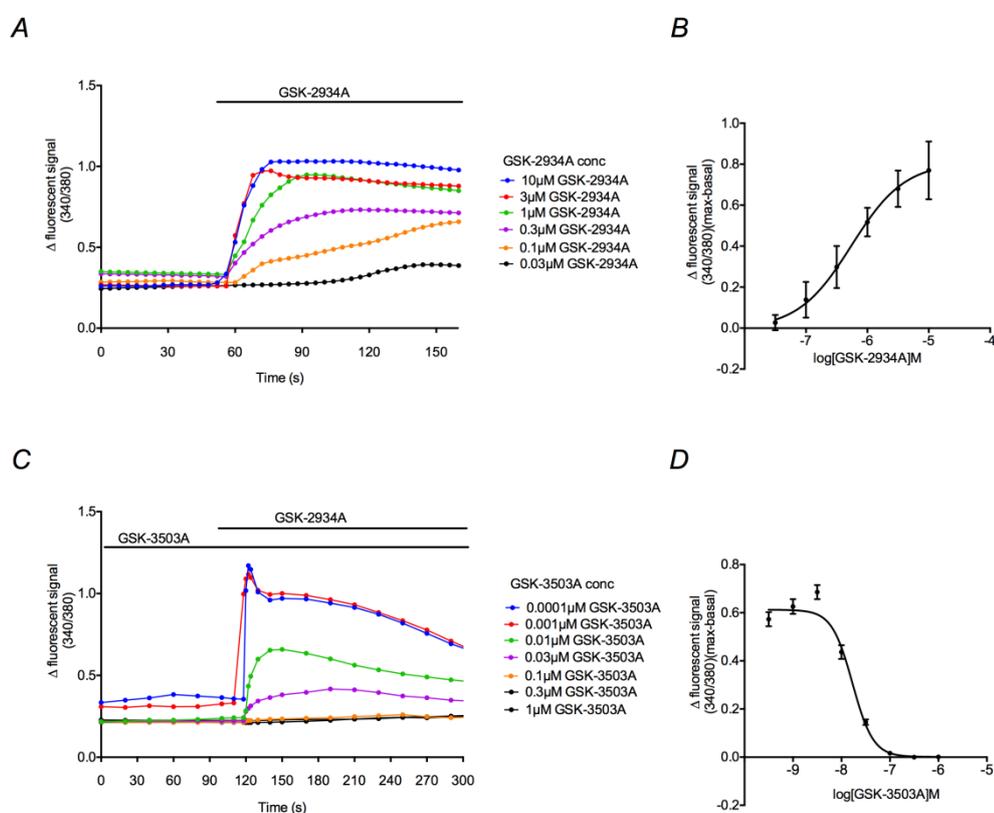
Figure 3.10   TRPC3/6 agonist and antagonist concentration-response validation in HEK-TRPC6 cells

*Single cell Ca^{2+} imaging of fura 2-AM loaded HEK-TRPC6 cells. **A.)** Ca^{2+} signal over time response to GSK-2934A agonist; GSK-2934A applied at varying concentrations as indicated by the horizontal bars. Graph shows mean signal from all cells tested. **B.)** Concentration-response curve in HEK-TRPC6 cells – summarising change in Ca^{2+} signal to varying concentrations of GSK-2934A agonist **C.)** Ca^{2+} signal over time – effect pre-incubation of varying concentrations of antagonist GSK-3503A to 3µM GSK-2934A induced Ca^{2+} signal. Graph shows mean signal from all cells tested **D.)***

Concentration-response curve summarising change in Ca^{2+} signal to varying concentrations of GSK-2934A agonist. n>20 cells N=3 independent experiments. Data is shown as mean ± SEM.

Following these initial validation experiments, Ca^{2+} imaging in HLMCs was performed. 3µM of the GSK-2934A TRPC3/6 agonist was applied to fura-2AM loaded HLMCs (***Figure 3.11)***, however the TRPC3/6 agonist was shown not to induce a significant increase in Ca^{2+} signal above the baseline (0.01 ± 0.001, n=126 cells N=5 donors). The same cells did respond to a stimulus of Anti-IgE applied at the end of the experiment as an experimental control, with the response in the range of magnitude typically observed in the Seward lab (Δ0.6) therefore confirming that the cell viability and experimental set-up were not to blame for the lack of signal induced by GSK-2934A.

There has been previous work showing that TRPC6 channels are not located at the plasma membrane until translocation is initiated by signalling proteins (Cayouette *et al.*, 2004; Monet *et al.*, 2012), therefore further experiments were performed taking this into consideration. In order to test whether TRPC6 activity is coupled to FcεRI mast cell signalling, the effect of the TRPC3/6 antagonist (2µM GSK-3503A) on FcεRI-induced Ca^{2+} influx was investigated. The results presented in ***Figure 3.12*** show that FcεRI activation induced a mean max-basal change of 0.6 ± 0.02 (n=49 cells N=3 donors) in control HLMC, which was the same as the 0.6 ± 0.02 (n=45 cells N=3 donors) response seen in GSK-3503A pre-treated cells. In combination, these data demonstrate that when using selective pharmacological tools, there is no evidence for a contribution from TRPC3/6 to FcεRI-initiated Ca^{2+} signalling in HLMCs.
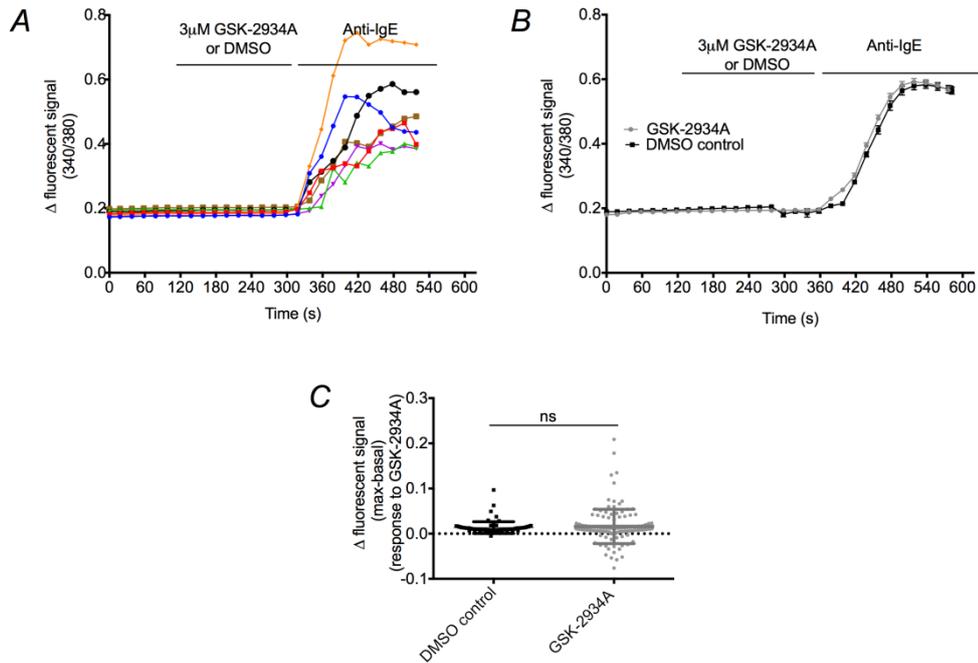
Figure 3.11   TRPC3/6 agonist has no effect on Ca²⁺ signalling in HLMCs

*Single cell Ca^{2+} imaging of fura 2-AM loaded HLMCs. HLMCs were incubated overnight with 300ng/ml IgE **A-C.)** Ca^{2+} signal over time; DMSO vehicle control/ 3μM GSK-2934A was applied as indicated by the horizontal bars, followed by Anti-IgE at 1μg/ml. **A.)** Single cell example traces, **B.)** All cells meaned. **C.)** Scatter graph showing Ca^{2+} signal in response to TRPC3/6 agonist (t=240sec-t=60sec) - before Anti-IgE application, line in bar graphs shows mean ± SEM. n>80 cells for each condition, N=3 donors. Results were analysed using unpaired students t-test, ns p>0.05.*
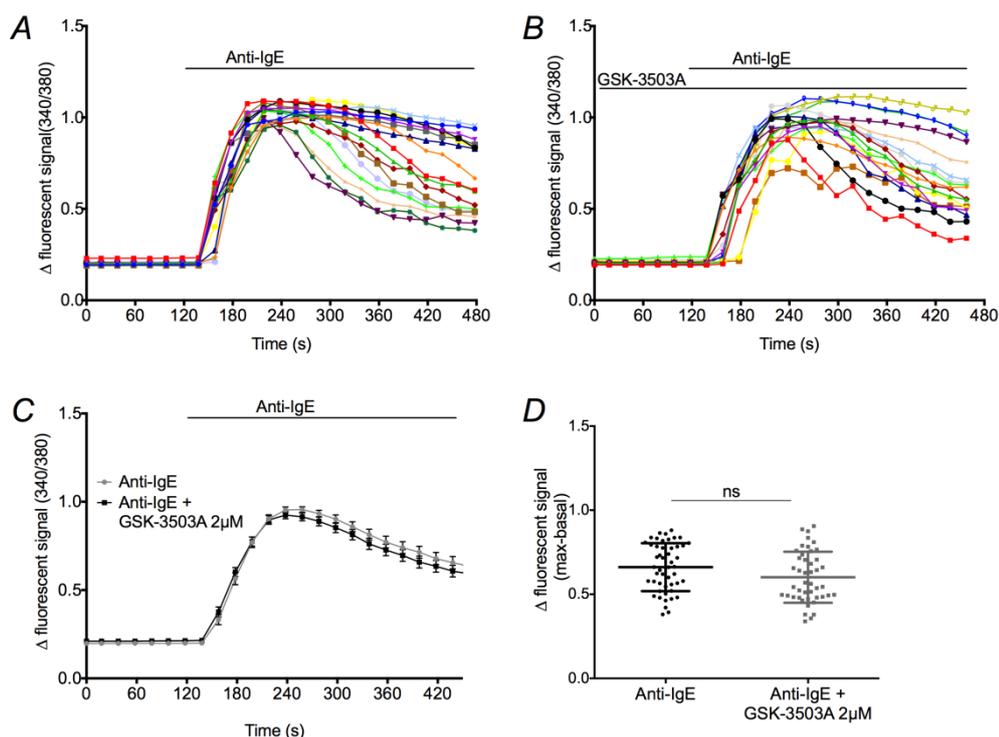
Figure 3.12   TRPC3/6 antagonist has no effect on FcεRI mediated Ca²⁺ signalling

*Single cell Ca²⁺ imaging of fura 2-AM loaded HLMCs. HLMCs were incubated overnight with 300ng/ml IgE. **A-C.)** Ca²⁺ signal over time. 2µM of GSK-3503A antagonist was pre-applied for 15 minutes before bath application of 1µg/ml Anti-IgE, as indicated by the horizontal bars. A&B show example single cell traces, **C.)** shows mean signal from all cells tested **D.)** Scatter graph showing change in Ca²⁺ signal (max-basal) to Anti-IgE in each cell from all experiments. n>50 cells for each condition N=3 or 4 donors. Results were analysed using students unpaired t-test, ns p>0.05*

Translocation of TRPC6 has been reported to occur through several different mechanisms. Gq-protein mediated receptor activation; ER store depletion and PI3K activation have all been shown to cause an increase in TRPC6 receptor expression at the plasma membrane (Cayouette *et al.*, 2004; Monet *et al.*, 2012). While it is clear that FcεRI is initiating ER store depletion, the involvement of PI3K in FcεRI signalling could be dependent on whether the classical or alternative FcεRI signalling cascade is initiated (Gilfillan & Tkaczyk, 2006), similarly the Gq mediated translocation is not addressed through FcεRI activation. To account for this TRPC6 mediated Ca²⁺ signalling in HLMCs was studied following c-kit receptor activation (SCF ligand) and P2Y (ADP ligand) receptor activation. c-kit signalling cascade is similar to that in the alternative FcεRI cascade and utilises PI3K whereas P2Y activates a Gq protein mediated receptor activation. Application of the c-kit agonist, SCF, to HLMCs was shown to induce oscillatory Ca²⁺ signals *(Figure 3.13).* When the TRPC3/6 antagonist was pre-applied before application of SCF, there was no significant change in

the area under the curve (62.73 ± 30.36 n>50, N=3 in SCF control and 95.74 ± 15.23 n> 50, N=3 in SCF + GSK-3503A) or the normalised max of the Ca^{2+} signal (1.67 ± 0.07 n>50, N=3 in SCF control and 2.18 ± 0.24 n>50, N=3 in SCF + GSK-3503A) compared to control conditions, providing no evidence for TRPC3/6 contribution to SCF mediated Ca^{2+} signalling. Similarly, *Figure 3.13* shows that application of the P2Y agonist, ADP, to HLMCs induced a fast transient Ca^{2+} signal, however there was no significant change in the ADP induced Ca^{2+} signal when the TRPC3/6 antagonist was pre-applied (mean Ca^{2+} signal 0.04 ± 0.005 n>50, N=4 in ADP + GSK-3503A and 0.07 ± 0.004 n>50, N=4 in ADP control). In summary, use of the TRPC3/6 selective compounds indicated there is no activity of TRPC6 as plasma membrane localised Ca^{2+} influx channels in human mast cells.
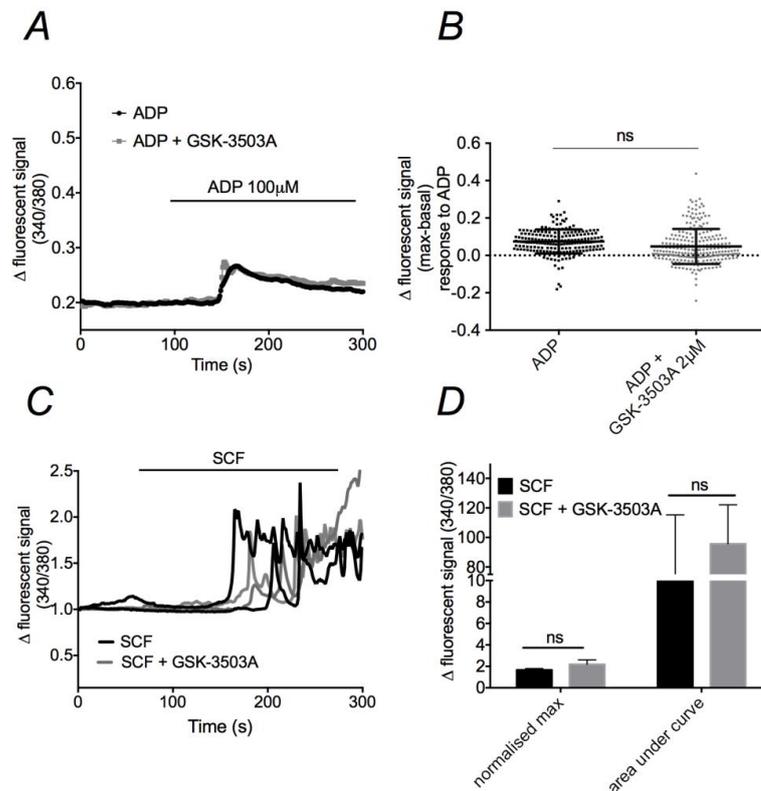
Figure 3.13 TRPC3/6 antagonist has no effect on P2Y or c-kit receptor mediated Ca^{2+} signalling

*Single cell Ca^{2+} Imaging of fura 2-AM loaded HLMCs. **A.)** Mean Ca^{2+} signal over time. 2μM of GSK-3503A antagonist was pre-applied for 15 minutes before bath application of 100μM ADP, as indicated by the horizontal bars. **B.)** Scatter graph showing change in Ca^{2+} signal (max-basal) to ADP in each cell from all experiments, **C.)** shows representative Ca^{2+} signal traces from individual cells, 100μg/ml SCF applied as indicated by horizontal bars and 2μM GSK-3503A was pre-applied for 15minutes prior to agonist application. **D.)** shows a bar graph summarising the normalised max (max calculated from signal after normalisation to baseline fluorescence) and the area under the curve change in Ca^{2+} signal to SCF. n>50 cells for each condition over N=3 or 4 donors. Results were analysed using student's unpaired t-test/Two-way ANOVA with Bonferroni post test, as appropriate. ns p>0.05*

3.3 Discussion

The results from this chapter shows novel evidence in support of a model for human FcεRI-induced mast cell activation with involvement of Orai but not TRPC-mediated Ca^{2+} entry. Microarray and qPCR experiments demonstrate that Orai1, 2, 3; STIM1 and 2; TRPC 1 and 6 are expressed in LAD2 and HLMC cells at the level of mRNA. Notably immunocytochemistry data provided evidence for the expression of TRPC1 and 6 at protein level. In corroboration with previous publications, my data shows Orai-mediated Ca^{2+} signalling as a component of FcεRI Ca^{2+} signalling in HLMCs and also in LAD2 cells. In contrast to previous studies, this work shows no contribution of TRPC1 or TRPC3/6 to FcεRI-mediated Ca^{2+} signalling in LAD2s/HLMCs, respectively. These results provide important novel contributions regarding TRPC biology in human mast cells.

Orai and TRP channel expression via microarray in LAD2 and HLMC

TRP channels are known for their ability to form heteromeric channel complexes with other family members (Hofmann *et al.*, 2002; Tsiokas, 2009; Ma *et al.*, 2011b; Cioffi *et al.*, 2012b; Storch *et al.*, 2012), with numerous combinations reported. Similarly TRPC channels have been shown to functionally interact with SOCE channel components, Orai and STIM proteins (Huang *et al.*, 2006; Jardin *et al.*, 2008; Zeng *et al.*, 2008; Cheng *et al.*, 2011c; Hong *et al.*, 2011). To ascertain the expression profile of TRP channel genes and other known interacting Ca^{2+} channels, in LAD2s and HLMCs, a microarray study was performed. Assessing the mRNA expression of these genes in LAD2 and HLMC mast cells in parallel has provided useful indications into the channels with functional significance in human mast cell biology. Our results showed expression of Orai and STIM family members, with the expression profile of family members consistent with previously published findings in HLMCs (Ashmole *et al.*, 2012) and as reported in human macrophage cells *(Chapter 5)*. Orai2 and STIM2 expression was shown to be lower than other Orai and STIM family members in LAD2s and HLMCs. My study shows novel evidence for the expression of TRPC1 and TRPC6 in LAD2 and HLMC cells. A gene chip affymetrix expression array performed in 2003 did not reveal any expression of TRPC1-7 in HLMC cells, the reasons for the differences are not known. However, (Bradding *et al.*, 2003) also reported no expression of P2X4 or P2X7 in HLMCs which was subsequently contradicted in a study by the Seward and Bradding labs (Wareham *et al.*, 2009) where RT-PCR experiments showed positive expression of the P2X1, 4 and 7 in HLMC cells and electophysiology experiments determined functional activity. This demonstrates that perhaps a difference in sensitivity between methodologies is responsible for the discrepancies seen.

Notably, my data reveals the expression profile of other TRP family members in mast cells. For example TRPM2, 4, 5 and 7 and TRPV1 and V2 members was reported, whereas TRPA channel mRNA expression was not. Importantly, TRPM7 has previously been shown to have a crucial role in regulating human mast cell survival (Wykes *et al.*, 2007). This provides

evidence to support that gene expression at this level is sufficient for a contributory role in human mast cells. Emerging evidence has suggested that TRP channels have important roles in respiratory disease, with many TRPA, V and M channel activators (e.g. eicosanoids, low pH, osmolarity changes, temperature alteration factors) found to be increased in airway disease (Grace *et al.*, 2014). With mast cells as crucial effector cells in the pathogenesis of asthma, understanding TRP channel expression is key for delineating the potential contribution of TRP mediated mast cell activation in lung disease.

Of all the genes studied in the microarray experiments, TRPV2 expression was found to be the highest expressed of all the TRP channels present, by over 10fold. TRPV2 is a temperature regulated ion channel, with activation by temperatures ~52°C. TRPV2 expression has also been shown in RBL-2H3 and HMC-1 mast cells and similarly the indication of TRPV2 activity has been demonstrated in these studies either by 52°C heat induced Ca^{2+} signalling in Ca^{2+} imaging assays (Stokes *et al.*, 2004), or through observation of TRPV2 like currents that are ruthenium red sensitive (Zhang *et al.*, 2012). The high expression of TRPV2 in both LAD2 and HLMC cells and previous indications of activity in other mast cell types indicates that investigation into the functional role of TRPV2 in mast cells is a worthwhile area for further research.

Orai and TRPC expression in HLMCs from a number of donors – investigating donor to donor expression variability

Results of the qPCR experiments confirm that Orai and STIM families are expressed in HLMCs at mRNA level and shows that TRPC1 and TRPC6 are expressed albeit with TRPC6 expression lower than in the microarray. Slight differences seen in the data from the qPCR to the microarray experiments are possibly a result of the differences in the methodology between these two techniques. Some donor variability in the expression of TRPC channel subtypes was observed through the qPCR experiments, for example TRPC3 and TRPC5 were shown to be expressed at low levels in half of the donors assessed. Recent publications have demonstrated that TRPC6 expression is variable, depending on the hypoxic status of the tissue and the exposure to cigarette smoke. Cigarette smoke (3-6month exposure) and 10nM nicotine were shown to cause an increase in TRPC1 and TRPC6 mRNA & protein in rat pulmonary arterial smooth muscle cells and similarly potentiate the Ca^{2+} signal induced by CPA. Similarly chronic hypoxia induction into PASMCs and pulmonary venous smooth muscle cells also showed an increase in TRPC1 and TRPC6 mRNA (Wang *et al.*, 2014a; Xu *et al.*, 2014). Although these studies have been performed in rat pulmonary arterial smooth muscle tissue/cells, it is possible that the variability existing in my study is a result of donor hypoxia/cigarette exposure. An important area for further research would be to investigate the effect of cigarette exposure and hypoxia on the function of Ca^{2+} signalling in mast cells.

TRPC1 and TRPC6 expression at protein level

Evidence supporting the expression of TRPC1 and TRPC6 at protein level was demonstrated through immunocytochemistry experiments. Reassuringly, the expression of TRPC1 and TRPC6 as observed at mRNA level was also observed at protein level, with positive expression of TRPC1 and TRPC6 seen in the over 90% of cells imaged. Notably the surface expression profile observed for TRPC1 and TRPC6 revealed a diffuse localization rather than within distinct plasma membrane regions, this could be due to the intracellular location prior their translocation initiation by signalling proteins (Cayouette *et al.*, 2004; Monet *et al.*, 2012). Of all the TRPC channel family members assessed at mRNA and protein level, my study has revealed a combination of TRPC 1 and TRPC6 expression in LAD2 and HLMC cells. Original work by (Hofmann *et al.*, 2002) described that TRPC channels were only capable of forming heteromeric channel complexes with other members of their subfamily (i.e. TRPC1/4/5 and TRPC3/6/7), however further work has established that TRPC channels have wider heteromultimerization capability (Storch *et al.*, 2012). For example, a TRPC1-TRPV4-TRPP2 channel assembly with a flow-induced Ca^{2+} signal was described in vascular endothelial cells (Du *et al.*, 2014).

Based on the evidence for TRPC1 and TRPC6 expression in human mast cells it would be interesting to use biochemical or structural experiments to determine if TRPC1 and TRPC6 directly interact with each other or with other TRP channel members in human mast cells.

Synta66 inhibits FcεRI-mediated Ca^{2+} entry in HLMCs and LAD2 cells

Aside from the demonstration of expression of TRPC1 and TRPC6, the second aim of my study was to assess what contribution TRPC channels made to FcεRI signalling. As discussed in **Section 3.1**, there have been numerous reports demonstrating that TRPC channels are functionally active as FcεRI contributors in rodent mast cells, although the details of these studies indicate a complex activity (Ma *et al.*, 2008; Sel *et al.*, 2008; Cohen *et al.*, 2009; Suzuki *et al.*, 2010b; Freichel *et al.*, 2012; Yildirim *et al.*, 2012; Medic *et al.*, 2013).

In respect to FcεRI signalling, my study confirms the contribution of Orai-mediated Ca^{2+} entry to FcεRI activation in LAD2 and HLMC cells, through the use of the Orai selective antagonist Synta66. Orai contribution to FcεRI signalling in human mast cells has previously been demonstrated by Ashmole *et al.*, where they similarly use Synta66 in HLMC cells. To my knowledge we are the first to specifically show the translation of Orai activity in FcεRI signalling in LAD2 cells. Although Synta66 caused a significant inhibition of the FcεRI-mediated Ca^{2+} signal, there was ~30% signal remaining. The signalling cascade downstream of FcεRI leads to production of known activators of the TRPC family; PLC and DAG. It was therefore considered whether this Synta66 insensitive component of the FcεRI Ca^{2+} signal was evidence of TRPC channel activity. Furthermore, Synta66 does not cause inhibition of directly activated TRPC channels (**Section 3.2.4**) - evidence that this compound is selectively inhibiting Orai-mediated Ca^{2+} signalling. However, if the model of TRPC1 activation as Orai-dependent, proposed by Ambudkar's group (Cheng *et al.*, 2011a) – described in **Section 1.5.8**), is applicable in human mast cells, then inhibition of Orai activity would ablate TRPC activity too, albeit indirectly. This line of thinking does not discount the involvement of

TRPC to FcεRI signalling but suggests that TRPC Ca^{2+} entry could be also Synta66 sensitive as it is an Orai-dependent Ca^{2+} signal.

The findings of this study, utilising tools to specifically ablate TRPC function, provide convincing evidence that TRPC channels are not composing the remaining Synta66-insensitive Ca^{2+} signal, and neither are they a component of the Synta66 sensitive Ca^{2+} signal. This result leads to the question; what other Ca^{2+} channel is conducting the Synta66 insensitive Ca^{2+} signal? Interestingly, as shown in (Wajdner et al 2015 – in press) and Ashmole et al 2012, FcεRI regulated Ca^{2+}-dependent mediator release is also not fully inhibited by 10μM Synta66, further evidence suggestive of another Ca^{2+} channel being activated downstream of FcεRI. It could be reasoned that although 10μM Synta66 has been demonstrated to cause 100% inhibition of Orai-mediated currents in HEK Orai/STIM cells, the compound may not cause complete endogenous channel inhibition. Evidence for this hypothesis is provided in work by Ashmole et al 2013. Here Ashmole et al. describe a Synta66 insensitive component of their FcεRI-mediated signal and FcεRI-mediated degranulation. However, following over-expression of a dominant negative Orai1 using a lentiviral method a full inhibition of degranulation was seen. This illustrates a potential underestimation of channel involvement when using the pharmacological tools available. However, the variability in the level of inhibition by Synta66 in our work suggests that this is not a complete explanation of the Synta66 insensitive Ca^{2+}/mediator release. Interestingly, the L-type voltage-gated Ca^{2+} channel (Cav1.2) was shown to be expressed in RBL-2H3 and BMMC cells and importantly was demonstrated to have a role in FcεRI-mediated IL-13 and TNFα release (Yoshimaru et al 2009). Microarray data from the Seward lab confirms the mRNA expression of Cav1.2 in human mast cells; further investigation is required to determine if Cav1.2 also contributes to FcεRI-mediated signalling in HLMCs and LAD2s.

Translation between LAD2 and HLMC biology observed in this study and differences between rodent and human mast cell biology

To my knowledge, we are the first to show experimental evidence of Orai-mediated Ca^{2+} entry in LAD2 cells in parallel to HLMCs. Similarly the expression analysis data shows a high degree of translation in the expression of Orai, STIM and TRP channel families in LAD2s and HLMCs. This data is important for the comparison of experiments examining Orai activity between primary HLMCs and the model human mast cell, LAD2s. Given the reported differences between mast cell biology in human and rodent models there is a possibility for disparity between experiments performed in human and rodent models. An example of this is demonstrated by IL-3 receptor activity; in murine mast cell populations there is a physiological response to IL-3, whereas in human mast cells very low IL-3 receptor expression is detected and no observable response (Bischoff, 2007). This emphasises the need for caution in translating data from mouse models into humans. The present study has provided a degree of confidence in the functional translatability between primary human mast cells and the LAD2 human mast cell model – showing that LAD2s represent a

useful mast cell model for the study of Ca^{2+} signalling where primary human cells are not available.

As described above a number of studies have shown TRPC involvement in FcεRI or allergen- induced signalling in rodents (Ma *et al.*, 2008; Sel *et al.*, 2008; Cohen *et al.*, 2009; Suzuki *et al.*, 2010b; Freichel *et al.*, 2012; Yildirim *et al.*, 2012; Medic *et al.*, 2013). Although the differences in the methodology used in the rodent studies and in my human study must be considered. The results of my study imply there is a discord between the functionality of TRPC channels in rodent mast cells compared to human mast cells, thus emphasizing the importance of caution in the translation between animal and human models.

TRPC channels do not contribute to FcεRI-mediated signalling in human mast cells

In contrast to the original hypothesis formed from data in the literature *(Section 3.1.2)*, the results shown in this study do not provide any evidence for contribution of STIM regulated TRPC to FcεRI or thapsigargin mediated Ca^{2+} entry in LAD2 mast cells. The kinetics, magnitude and store release component of the signals in both thapsigargin and FcεRI activating conditions were not significantly different in the STIM1 KK$^{684-685}$EE expressing cells compared to that seen in the STIM1 WT expressing control cells. Furthermore, despite an increased likelihood of TRPC contributing to FcεRI-mediated signalling due to the range of downstream signalling activated, no effect was observed with the STIM1 TRPC inactivating mutant in response to either stimulus.

Initially the question was posed as to whether the lack of effect of the STIM1 mutant was due to technical problems; however a number of pieces of evidence show this is an unlikely explanation.
The STIM1 KK$^{684-685}$EE mutant used in this study was obtained from the Ambudkar lab, who had previously demonstrated its functionality as a way to ablate the function of STIM regulated TRPC1 – STIM1 regulated TRPC inactivating mutant. Upon receipt of the STIM1 constructs from the Ambudkar group, STIM1 KK$^{684-685}$EE (and WT control) were sequenced after bacterial transformation to confirm construct sequence integrity. In the present study further validation experiments confirmed the functional activity of the transfected STIM constructs in LAD2 cells. Live time lapse imaging experiments showed that both the STIM WT- YFP and STIM1 KK$^{684-685}$EE -YFP constructs translocated to the plasma membrane following a store depletion protocol using thapsigargin – indicating the STIM constructs were able to function according to their endogenous role. As the nature of these experiments compared the Ca^{2+} signalling seen in the STIM1-WT and STIM1 KK$^{684-685}$EE mutant conditions, the possibility of differential expression levels of STIM1-WT and STIM1 KK$^{684-685}$EE was considered as an explanation for the lack of inhibition by STIM1 KK$^{684-685}$EE mutant. To address this, quantification of the intensity of the YFP constructs per cell was performed. The results show that there was no significant difference in the YFP intensity, between the cells expressing the STIM-WT versus STIM1 KK$^{684-685}$EE constructs, suggesting no difference in expression levels of the constructs. Taken together these data provides

evidence supporting the functionality of the STIM1 KK$^{684-685}$EE mutant and STIM1-WT constructs.

To my knowledge, no studies have distinguished a role of STIM2 in the electrostatic interaction and gating of TRPC channels. However it cannot be discounted that STIM2 could be activating TRPC mediated Ca^{2+} entry in compensation for the presence of the inactive STIM1 construct. This possibility cannot be explored without further investigation into the interaction between STIM2 and TRPC channels. It was also considered whether if endogenous STIM1 expression was enhanced in STIM1 KK$^{684-685}$EE mutant cells to compensate for the expression of the mutated version. However if this were the case it would be expected that there was an enhanced Ca^{2+} signal in the STIM1 KK$^{684-685}$EE mutant conditions compared to the STIM-WT conditions because any enhanced endogenous STIM1 expression would be additive to the STIM1 KK$^{684-685}$EE in respect to the STIM protein available to activate the Orai channels. These experiments were designed to investigate the function of TRPC as STIM regulated channels, therefore in a store-operated manner, it is arguably more likely that a compensation of enhanced Orai signalling could be occurring to keep the levels of Ca^{2+} signalling constant, however based on the dependence of TRPC on Orai for store-operated activation, tools were not available to test this possibility.

The results from my study provide evidence to show that there is no contribution of TRPC channels to Ca^{2+} signalling following thapsigargin and FcεRI-mediated activation in human mast cells. Although my results are in contrary to the majority of studies reported in rodent models (Ma *et al.*, 2008; Sel *et al.*, 2008; Cohen *et al.*, 2009; Suzuki *et al.*, 2010b; Freichel *et al.*, 2012; Yildirim *et al.*, 2012; Medic *et al.*, 2013) one of these studies, Medic *et al.*, 2013, saw an opposite phenotype, where an enhancement in the FcεRI-mediated Ca^{2+} entry and an enhancement in the transcription of the Ca^{2+}-dependent transcription factors, NFAT and JUN was observed following TRPC1 deletion. Similarly the work by Yildirim and Sel cannot be conclusively taken as evidence of TRPC contribution to mast cell activity but rather in allergic mediated inflammation. For example in (Sel *et al.*, 2008), the reduction in Th2 cytokines seen in response to allergic stimulation in TRPC6$^{-/-}$ mice could be mediated by other immune cells such as eosinophils rather than mast cells. Lastly the method investigation of TRPC1 activity by Suzuki and colleagues (linking TRPC1 activity as the explanation for the Fyn$^{-/-}$ phenotype) could be resulting in indirect disruption to TRPC1 activity and thus inferring a sole dependence on TRPC1 is misleading. This further examination of the literature and highlight of discrepancies seen in previous studies illustrate the complexity in the role of TRPC function in mast cells and suggest that further knowledge of the role of TRPC proteins will aid the understanding and interpretation of these studies.

TRPC3/6 selective compounds have no effect on Ca^{2+} signalling in HLMCs

In addition to FcεRI signalling, the contribution of TRPC6 to Ca^{2+}-induced by other mast cell receptors activation was considered. C-kit and P2Y receptor signalling pathways were chosen as components of signalling proteins downstream of these receptors can be coupled to TRPC6 plasma membrane translocation. C-kit signalling has largely been studied as a receptor which acts in cooperation with the FcεRI - SCF+ Anti-IgE activation has been shown to potentiate FcεRI mediated Ca^{2+} signalling and mediator release when compared to Anti-IgE signalling alone (Hundley *et al.*, 2004; Lewis *et al.*, 2013a; Smrž *et al.*, 2013). SCF has also been shown to initiate Ca^{2+} signalling when individually applied (Hundley *et al.*, 2004; Smrž *et al.*, 2013), however in contrast to my results, the kinetics of the SCF induced signal in other studies did not display an oscillatory signal nor did prior work seek to identify the Ca^{2+} channel involved in mediating the c-kit regulated Ca^{2+} signal. (Lewis *et al.*, 2013b) show that SCF is capable of mediating mediator release without the involvement of FcεRI activation, showing there was a donor variability in the response seen, which correlated to the expression level of the c-kit receptor. Signalling downstream of the c-kit receptor follows a cascade similar to the alternative activatory pathway of the FcεRI receptor – it is reasonable to hypothesise the potentiation caused by SCF addition is due to this signalling cascade being switched on. The signalling factors that are part of the alternative cascade are dependent on PI3K, demonstrated by the inhibitory activity of wortmannin. Interestingly there are studies implicating TRPC channels are dependent on PI3K activation however my study results suggest that TRPC6 channels at least are not contributing here (Monet *et al.*, 2012). Notably, SCF is found at increased levels in asthmatic patients providing a good reason to investigate Ca^{2+} channel characterisation as part of c-kit receptor signalling (Da Silva & Frossard, 2005).

Purinergic receptors expressed on mast cells are known to have important roles in degranulation (Gao *et al.*, 2010; Gao *et al.*, 2013) and therefore identification of an ion channel responsible for the Ca^{2+} signal induced by the GPCR P2Y family would also be useful. ADP initiated a transient signal which was relatively small in magnitude compared to that induced by FcεRI and thapsigargin, this signal is in line with that observed in macrophages in response to bzATP, a P2X agonist *(Section 4)*. Nonetheless no inhibition of the ADP response by TRPC3/6 antagonist was seen in my study. Expression of P2Y channels has been described in RBL-2H3 and LAD2 mast cells (Gao *et al.*, 2010; Gao *et al.*, 2013). Similarly ADP mediated Ca^{2+} mobilisation has been recorded in cord blood derived human mast cells and in RBL-2H3 cells (Feng *et al.*, 2004; Gao *et al.*, 2010). However to my knowledge little work has focused on characterisation of the Ca^{2+} channels involved in P2Y receptor Ca^{2+} mobilisation. Whilst the experiments investigating c-kit and P2Y signalling provide further evidence that TRPC6 channels are not functionally active in global Ca^{2+} signalling in human mast cells, it is clear that there are gaps in the knowledge of the specific regulation of the Ca^{2+} signal mediated by these two receptors.

The complexity of TRPC channel activity

Despite no contribution of TRPC channels to FcεRI-mediated Ca^{2+} signalling in human mast cells or of TRPC6 in P2Y and c-kit HLMC signalling, as already suggested, further consideration of the complexity of TRPC channels is necessary to aid interpretation of these results. The issue of TRPC6 translocation was addressed, using previously identified activators of TRPC6 translocation. However, (Albarran *et al.*, 2014) showed another route of controlling TRPC6 localisation and functionality whereby STIM1 over-expression led to the translocation of TRPC6 from the plasma membrane to the ER. Without further investigation, it is not clear whether the levels of STIM1 expression human mast cells are at a level necessary to affect TRPC6 localisation. Nonetheless, Albarran's study illustrates that other factors may be influencing TRPC activity that must be considered in the data interpretation.

Finally, evidence that TRPC channels can have functions not directly linked to their function as a Ca^{2+} influx channel is described by (Py *et al.*, 2014). Instead Py and colleagues show that TRPC1 acts a substrate for caspase-11 which is needed for the degradation in the production of IL-1β in mouse peritoneal macrophages. This highlights that although this study has focused on the role of TRPC as contributors to Ca^{2+} signalling in human mast cells, the methods used in this study would not reveal other roles TRPC may have. In relation to this, it has been suggested that rather than having important roles in driving Ca^{2+} signalling, TRP channels have predominant roles in regulating the driving force for Ca^{2+} entry via other channels. TRP channels can conduct Na^{+} entry which causes plasma membrane depolarisation which could act to reduce the driving force for Ca^{2+} (Vennekens & Nilius, 2007). Further experiments would be necessary to explore these speculations.

3.4 Conclusion and future directions

Throughout the discussion of the results of this thesis a number of areas with potential for further investigation have been suggested to increase the understanding of the role of Ca^{2+} signalling in human mast cells. In sum, my data has shown evidence supporting no role for TRPC1 or 6 in FcεRI-mediated global Ca^{2+} signalling in human mast cells. However it is possible that the positive expression of these channels is indicative of other yet undiscovered roles. Nevertheless, my data has provided an important contribution to the literature demonstrating that TRPC Ca^{2+} signalling is not significantly contributing to FcεRI-mediated signalling, contrary to suggestions from rodent models. Furthermore, this study supports the model whereby Orai Ca^{2+} influx is the primary conducer of FcεRI signalling in human mast cells. This provides key information which will guide the development of potential therapeutics aiming to attenuate FcεRI-mediated allergic disease.

4 Chapter 4: Investigation of P2X7 contribution to Ca^{2+} signalling and bacterial handling in human macrophages

4.1 Chapter 4 Introduction

P2X7 is expressed in a range of immune cells and has been specifically implicated with functions in macrophage cells. For example; P2X7 activation in LPS primed macrophages is important for directing the production and release of mature of IL-1 regulated cytokines, IL-1β (Ferrari *et al.*, 1997b; Solle *et al.*, 2001). P2X7 activation has also been associated with the control of nitric oxide (NO) release and cytokine production via NF-κB (Ferrari *et al.*, 1997a; Sperlágh *et al.*, 1998). Another well known function of mediated by P2X7 activation is apoptosis (Mackenzie *et al.*, 2005). Significantly, emerging data has implicated P2X7 with a role in the pathogenesis of COPD this suggesting that P2X7 could be a therapeutic target for COPD treatment. ***Section 4.1*** summarises key studies which have led to the generation of this hypothesis and contrarily the evidence for P2X7 involvement in bacterial handling is also discussed.

4.1.1 Evidence implicating P2X7 as a novel target for COPD treatment

A number of studies describe a correlation between ATP, P2X7 and COPD pathogenesis. Under normal physiological conditions, the endogenous agonist for P2X7, ATP, is present at low concentrations extracellularly and is tightly regulated through the action of ectonucleotideases to break down excess ATP. However during an event which leads to hypoxia, infection or inflammation extracellular ATP levels can rise significantly, through the release from inflammatory or epithelial cells or through a downregulation of ectonucleotideases (Lucattelli 2010). (Lommatzsch *et al.*, 2010) reported increased levels of ATP in BALF from COPD sufferers vs. non smokers, and showed that P2X7 expression was greater on macrophages from COPD patients. Similarly, ATP mediated release of pro-inflammatory mediators; matrix metalloproteinase-9 (MMP-9) and IL-1β was enhanced in macrophages isolated from the BALF of COPD patients. Substantiating work by Cicko *et al.*, 2010 showed that P2Y$_2$R deficient mice had less smoke induced lung inflammation vs. controls. Whilst, Mortaz *et al.*, 2009 showed that cigarette smoke activated purinergic signalling in mouse neutrophils which led to downstream CXCL8 & elastase release. In relation to this, P2X7 attenuation was shown to lead to a reduction in acute cigarette smoke induced lung inflammation in mice. In BALF collected from mice following cigarette smoke exposure, in P2X7 antagonist or P2X7 knockout conditions there was a reduction in IL-6, IL-1β, keratinocyte-derived chemokine (KC), IFNγ and macrophage inflammatory

protein-2 (MIP-2) and the number of macrophages was reduced compared to control BALF (Lucattelli *et al.*, 2011). (Eltom *et al.*, 2011) describe supporting results from a P2X7$^{-/-}$ mice, a reduction in the release of inflammatory cytokines in response to cigarette smoke exposure was seen in BALF from P2X7$^{-/-}$ animals compared to controls. Together, these studies demonstrate the protective effect of P2X7 inhibition to reduce the cigarette smoke induced inflammation and provide evidence to support the inhibition of P2X7 as a target to treat COPD.

P2X7 has also been implicated in regulating inflammatory responses during viral infection. The P2X7 inhibitor, oATP caused a reduction in the inflammatory response in macrophage and epithelial co-cultures following adenovirus infection. The reduction in the inflammatory response in these experiments was determined by an inhibition in NO generation, a reduction in the number of ROS positive cells and a decrease induction of IL-6 and KC. Similarly in P2X7 deficient J774.A1 mouse macrophage cell line and primary mouse peritoneal macrophage it was shown that there was less IL-1β and IL-18 following adenoviral infection, compared to controls. Importantly, intranasal adenoviral infection in mice deficient in P2X7 or caspase-1 led to an enhanced survival rate compared to WT animals most likely due to the reduced inflammatory response demonstrated in P2X7 inhibition/deletion settings (Lee *et al.*, 2012). This result provides evidence that supports the involvement of P2X7 in a viral exacerbation condition, as is seen in COPD and asthma. This hypothesis is supported by the research of Birrell and Belvisi. A publication from their group (Eltom *et al.*, 2014) hypothesises that the exacerbations of asthma and COPD are caused by enhanced ATP levels. Excess ATP could activate the P2X7/caspase-1 axis within extracellular vesicles, leading to IL-1β and IL-18 release and subsequently causing proinflammatory symptoms. Their paper showed that LPS, H. influenzae and viral mimetic, poly:IC caused the release of extracellular vesicles which when followed by ATP stimulation led to increased levels of IL-1β and IL-18 release. Together these results emphasise the contributory role of P2X7 to the excessive proinflammatory response seen in COPD patients.

P2X7 has also been implicated with a role in acute lung injury, a major cause of hypoxemia respiratory failure initiated by trauma, infection and sepsis. (Wang *et al.*, 2015) recently showed that blockage of P2X7 attenuated acute lung injury through reduction of NLRP3 inflammasome pathway activation. NLRP3 is crucial for the activation of caspase-1 and therefore IL-1β maturation. This shows another example of how dysregulation of IL-1β through P2X7 activity causes lung disease.

In sum, this data gives compelling evidence that P2X7 receptors would make an effective drug target to treat diseases such as COPD, where exacerbations following a bacterial or viral infection are commonplace. Similarly, the data also implies that P2X7 activity could be involved in the pathogenesis of cigarette smoke induced inflammation and acute lung injury.

4.1.2 The role of P2X7 in macrophage bacterial handling

Despite the compelling evidence in favour of targeting P2X7 as a treatment for COPD, evidence suggests that P2X7 also has a role in the control of bacterial phagocytosis and intracellular bacterial killing. The key role macrophages have in immune defence against bacterial infection means that understanding if P2X7 inhibition would hamper these innate immune roles is important. A summary of the central studies providing this evidence are described here. In hMDMs infected with M.bovis BCG, ATP application was shown to induce apoptosis of infected cells and reduced the bacterial viability by 50-70%. Inhibition of P2X7 by o-ATP caused ATP treatment to be ineffective in initiating bacterial killing (Lammas *et al.*, 1997). Similarly, macrophages from P2X7$^{-/-}$ mice had impaired ability in ATP-induced mycobacterium killing. The mechanism involved in the ATP-P2X7 driven bacterial killing was shown to be due to a fusion of the phagosome-lysosome - this was absent in non-ATP stimulated macrophages (Fairbairn *et al.*, 2001). Likewise, (Fernando *et al.*, 2007) showed that a loss of function polymorphism in human P2X7 led to increased susceptibility to *M. tuberculosis*, illustrating the importance of P2X7 in the regulation of *M. tuberculosis* infection. In relation to this, several P2X7 receptor polymorphisms were shown to reduce macrophage apoptosis and mycobacterium killing (Saunders *et al.*, 2003; Fernando *et al.*, 2005).Together these studies implicate P2X7 with an important role in mediating ATP-induced mycobacterium killing.

In addition to the mycobacterium species, P2X7 has also been shown to direct the killing of the intracellular bacteria of the Chlamydia genus. ATP treatment of Chlamydia infected macrophages was shown to cause a 70-90% death of intracellular bacteria (Coutinho-Silva *et al.*, 2001). Conversely, in some cells types there was a reported resistance to P2X7 mediated Chlamydia killing, thus illustrating the potential diversity in the mechanisms of bacterial killing between cells and also between bacteria. The P2X7 receptor was shown to mediate the killing of an intracellular parasite, Toxoplasma gondii. Macrophages isolated from patients with a P2X7 1513C loss of function polymorphism had impaired ability to kill intracellular, Toxoplasma gondii after exposure to ATP (Lees *et al.*, 2010). Although these examples suggest a role for P2X7 in the killing of two bacteria types and intracellular parasite, the role of P2X7 receptor signalling in the killing of all types of bacteria is yet to be determined. Similarly, this work was largely performed in mouse macrophage models or in human macrophage cell lines; therefore it remains to be conclusively shown whether the same involvement occurs in primary human macrophage cells.

P2X7 signalling was shown to be important in regulating phagocytosis by macrophages. Phagocytosis is accompanied by the re-arrangement in the actin-myosin cytoskeleton and initial studies implicated P2X7 with a role in controlling cytoskeleton reorganisation (Gu *et al.*, 2009). Subsequent work showed that P2X7 has a dual role in phagocytosis; as the level of ATP regulated whether P2X7 enhanced or limited phagocytosis. In the absence of extracellular ATP, P2X7 expression on HEK-293 cells conferred phagocytic ability to this cell type, inhibitors of P2X7 or non-muscle myosin heavy chain IIA (NMMHC-IIA) inhibited phagocytosis of beads and live *S. aureus*. Conversely, the application of the ATP caused an

inhibition of the phagocytosis of beads and *S. aureus*. The involvement of P2X7 receptor in this ATP mediated inhibition was confirmed by the lack of effect of ATP on phagocytosis in macrophages from P2X7$^{-/-}$ mice. The reason for the varying role of P2X7 to macrophage phagocytosis is not clear (Gu *et al.*, 2010). Further investigations suggested that P2X7 receptor acts as a scavenger receptor due to similarities in the cytoskeletal arrangement, topology and tissue distribution, suggesting ligands on the surface of foreign particles bind to P2X7 and initiate phagocytosis similarly to other phagocytic receptors such as scavenger, FcγR and CRs (Gu *et al.*, 2011). Together the work by Gu and colleagues suggested a role for P2X7 phagocytosis performed by macrophage cells, indicating another risk associated with P2X7 inhibition as a therapeutic.

In sum, the work described throughout **Section 4.1** has provided compelling evidence to suggest that P2X7 represents a novel target to treat COPD, due to the contributory role P2X7 has in mediating cigarette smoke and viral induced inflammation. However, macrophages also have crucial roles in the innate immune defence and these roles must be kept intact for proper immune system homeostasis. P2X7 signalling has also been implicated with a regulatory role in the handling of bacterial infection. Due to differences described throughout this thesis regarding the pharmacology and characteristics of P2X7 between species it is key to assess the effect of the P2X7 antagonists on bacterial handling and ion channel function using the same human macrophage model throughout. Similarly Ca^{2+} influx is a key function mediated by P2X7 channels, as discussed in **Section 5.1** and **Section 4.1.2** there is evidence to support the involvement of Ca^{2+} in the control of the production of proinflammatory cytokines, in phagocytosis and bacterial killing. Further understanding the effect of P2X7 inhibition on Ca^{2+} signalling constitutes a worthwhile area of investigation to complete the knowledge of the role of P2X7 in human macrophage biology. The aim of my study was to address whether P2X7 had a significant contribution to purinergic Ca^{2+} signalling in human macrophages and whether P2X7 pharmacological inhibition significantly affected the phagocytosis of bacteria and killing of bacteria by human macrophages.

4.2 Results

4.2.1 P2X7 is expressed in hMDM and hAMs

In order to confirm the expression of P2X7 in hMDMs and hAMs, immunocytochemistry experiments were performed. A monoclonal P2X7 selective antibody was validated using a blocking peptide in a western blot experiment, results of which are described in **Section 2.10**. Using the P2X7 antibody immunocytochemistry experiments reveal that hMDM and hAM cells both show positive expression of P2X7, the mean fluorescent intensity (MFI) in P2X7 stained hMDMs was 22.93 ± 5.32 versus 4.23 ± 0.96 in the isotype control (mean ± SEM N=4) **(Figure 4.1)**. Similar values were obtained in hAMs; P2X7 stained hAMs showed a MFI of 26.21 ± 2.18 versus 4.23 ± 0.96 in the isotpye control (mean ± SEM N=4). These results give strong evidence that P2X7 is expressed at protein level in both hMDM and hAM cells. Interestingly, the staining profile of P2X7 in hMDMs vs. hAMs was noticeably

different, in MDMs the surface profile shows a distribution suggestive of increased staining at the plasma membrane location *(Figure 4.2)* whereas in the AMs the surface profile shows a more diffuse staining pattern. Although the images were not acquired using confocal microscopy, it would be expected that if diffuse staining was caused by a light refractive artifact that this would be the same in both cases. On the whole, the data presented here give confirmation of the expression of P2X7 at a protein level, which is in line with previously published literature in mouse and human macrophage models.
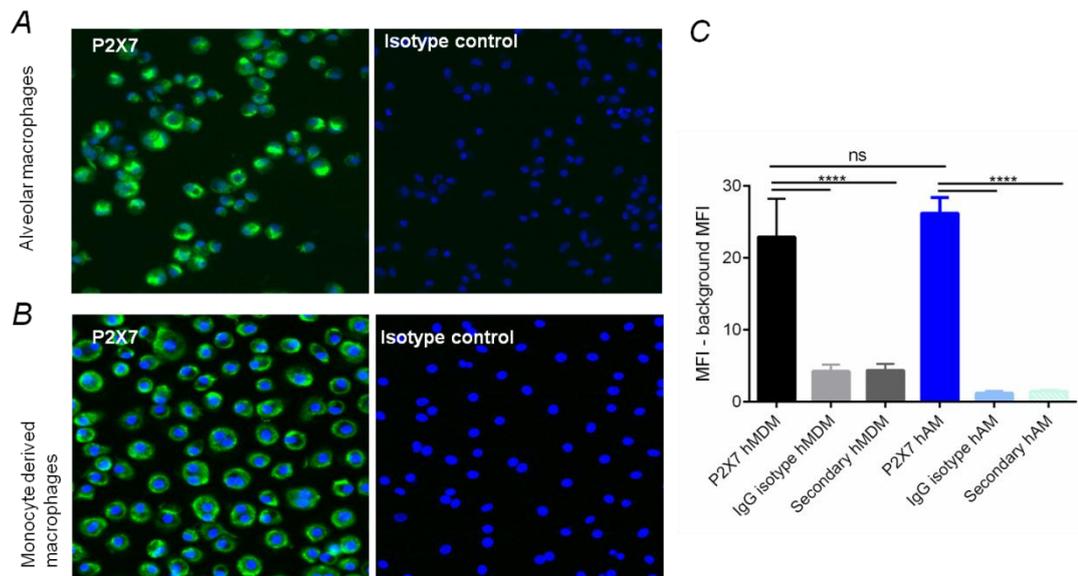
Figure 4.1   P2X7 expression in hMDMs and hAMs.

Immunocytochemistry to assess P2X7 expression in macrophage cells, - hMDMs and hAMs were stained with anti-P2X7 antibody and Hoescht/*IgG isotype control antibody and* Hoescht *(1:200 concentration), fluorescent images were taken at 650 and 405nm using an INCell Analyser **A.)** hAMs, **B.)** hMDMs.   **C.)** Bar graph shows quantification of mean fluorescent intensity of cells in each conditions mean ± SEM. N=4 donors (hMDMs), N=2 donors (hAMs). Results were analysed using one-way ANOVA with Tukey's multiple comparison test. * p <0.01 ** p <0.001*
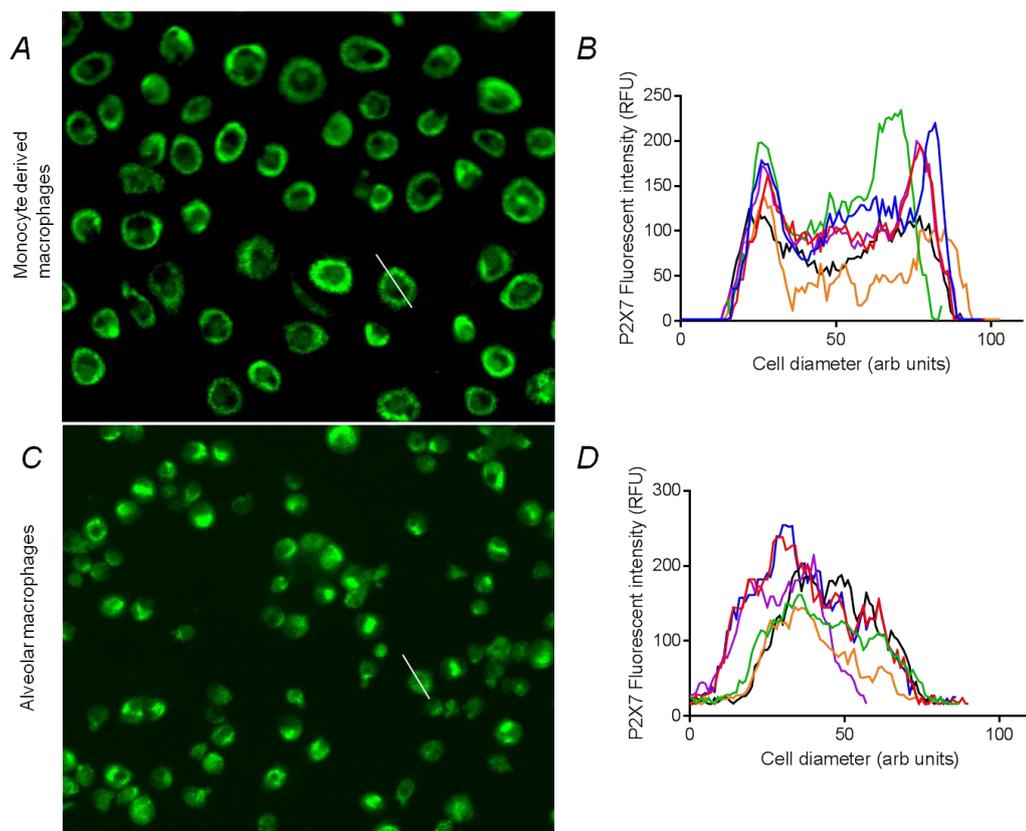
Figure 4.2   **P2X7 antibody staining surface profile**

*Immunocytochemistry to assess P2X7 channels in macrophage cells, hMDMs and hAMs were stained with anti-P2X7 antibody (1:200 concentration), fluorescent images were taken at 650nm using an INCell Analyser **A&C.)** Representative images to demonstrate the staining profile of P2X7 in the macrophage cells. **B&D.)** surface plot profile of P2X7 expression. Representative of cells from N=4 donors (hMDMs), N=2 donors (hAMs).*

4.2.2 ATP and bzATP initiate a concentration-dependent increase in Ca^{2+} signal in hMDMs

To investigate the functional contribution of P2X7 channels to Ca^{2+} signalling in hMDMs a series of Ca^{2+} imaging experiments were devised. These experiments were performed using a FLIPR machine as described in **Section 2.3.2.** The Ca^{2+} signalling was measured in response to purinergic ligands, bzATP and ATP, applied at a range of concentrations. ATP induced a concentration-dependent Ca^{2+} signal, a transient signal was produced which reached maximum signal intensity by 1 minute and returned to baseline levels within 3-4 minutes of ATP application **(Figure 4.3)**. The normalised average signal change in response to 33μM of ATP was 1.23. The concentration-response to ATP **(Figure 4.4)** showed a bell-shaped relationship with the EC_{50} ~9.6 ± 4μM/pEC50 = 4.9 ± 0.3 n=5, the concentration-response was plotted as the percentage of the max from Ca^{2+} signal area under the curve

values. Concentration-response experiments were also performed with bzATP *(Figure 4.3),* bzATP initiated a Ca^{2+} signal with similar kinetics to that induced by ATP. The signal maximum was also reached by 1 minute with a return to baseline levels by 2-3 minutes. However the magnitude of the normalised average signal change to 33µM of this bzATP was ~0.33 which is almost 10 fold lower than the response induced by ATP *(Figure 4.3)*. bzATP had an EC_{50} of 9µM ± 0.2/pEC50 = 5.0 ± 0.2 N=5 *(Figure 4.4)* Control experiments shown in *Figures 4.3C&D* show there was a significant difference in the Ca^{2+} signal induced by bzATP and ATP between 0external Ca^{2+} and normal Ca^{2+} conditions, the mean Ca^{2+} signal induced by ATP in Ca^{2+} versus 0external Ca^{2+} conditions was (34.16 ± 1.49 with Ca^{2+} and 2.84 ± 1.30 in 0externalCa^{2+}, N=2 mean ± SEM, normalised AUC values) and in the two conditions in response to bzATP the Ca^{2+} signal was (26.03 ± 5.61 with Ca^{2+} and 5.63 ± 1.31 in 0external Ca^{2+}, mean ± SEM, N=4, normalised AUC values). These results demonstrate that ATP and bzATP agonists are initiating a significant Ca^{2+} influx from plasma membrane localised Ca^{2+} channels but that a Ca^{2+} signal from intracellular stores is also a component.
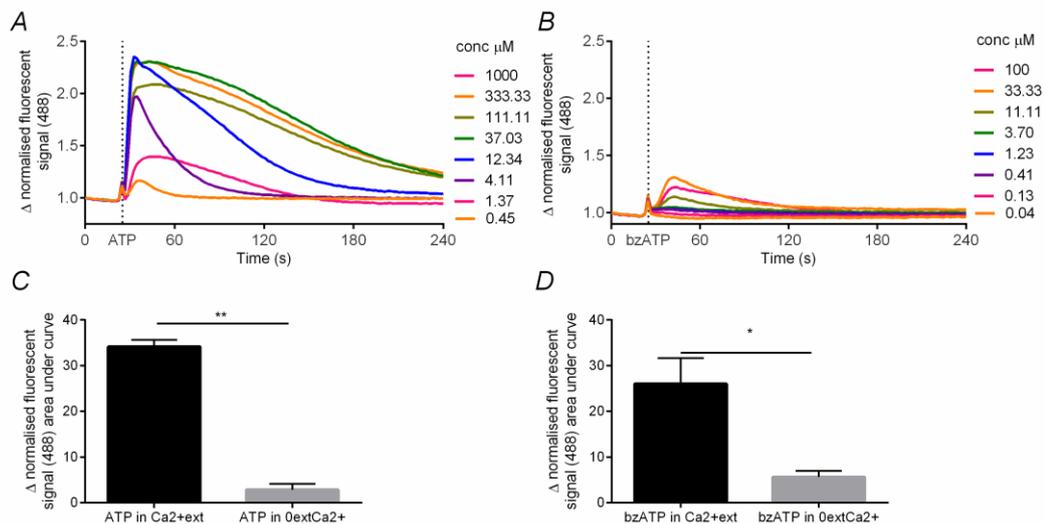
Figure 4.3   **ATP and bzATP initiates a concentration-dependent Ca^{2+} signal in hMDMs.**

*Ca^{2+} imaging of fluo-4 AM loaded hMDMs using FLIPR. **A&B.)** Ca^{2+} signal over time, bzATP/ATP was applied at t=20s and was present throughout experiment duration. These are representative traces from an N>5 donors, signal was normalised to baseline fluorescent values. **C&D.)** Comparison of the Ca^{2+} signal induced by 30µM ATP/bzATP with and without Ca^{2+} present in the external solution, values taken from area under curve analysis. Bar graph shows mean ± SEM. Results were analysed using a paired student's t-test. N=4. * p <0.01 **** p<0.0001*
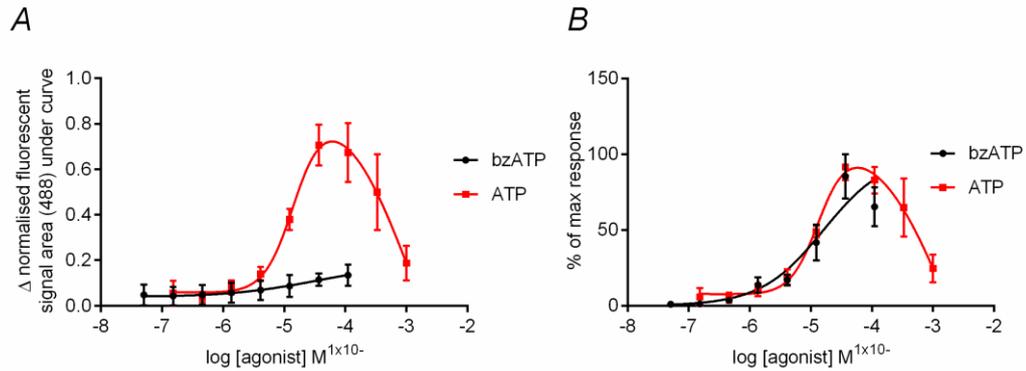
Figure 4.4 **ATP and bzATP concentration-response curve in hMDMs**

*Ca^{2+} imaging of fluo-4 AM loaded hMDMs using FLIPR – analysis of signal/time data shown in Figure 4.3. **A.)** Concentration-response curve showing area under curve values from normalised signal/time (signal was normalised to baseline fluorescent values). **B.)** Concentration-response curve showing percentage of max Ca^{2+} response as calculated from area under curve values. N=5 donors.*

These experiments show evidence for the activity of ATP and bzATP sensitive Ca^{2+} influx receptors in hMDMs. The EC50 of ATP and bzATP found in the present study are not in the range predicted for a cell that expresses P2X7 alone and instead are suggestive of the expression of a range of P2X or P2Y channels. Further comparison of the results in my study to those reported from heterologous expression systems is discussed in ***Section 4.3***.

4.2.3 Effect of non-selective purinergic antagonists on ATP mediated Ca^{2+} signalling

To investigate the overall purinergic receptor contribution to Ca^{2+} mobilisation following ATP and bzATP stimulation FLIPR experiments were performed with non-selective purinergic antagonists, suramin and PPADs. As widely reported classical purinergic antagonists these compounds would be expected to inhibit the Ca^{2+} signal induced by P2X and P2Y channels. Notably it was seen that PPADs but not suramin ***(Figure 4.5)*** caused a concentration-dependent inhibition in the ATP/bzATP induced Ca^{2+} signal. PPADs inhibited the Ca^{2+} signal induced by 30µM ATP/bzATP with a pIC50 of 5.6 ± 0.3 and 5.6 ± 0.5 N=4, respectively. Suramin had no effect on the Ca^{2+} signal induced by 30µM bzATP and ATP measured in 4 donors. The potential explanation for the pharmacological profile obtained with suramin and PPADs is discussed in ***Section 4.3***. Importantly, from this data it can be taken that the present assay conditions are sensitive enough to detect an inhibition of the 30µM bzATP and ATP mediated Ca^{2+} signals in hMDMs.
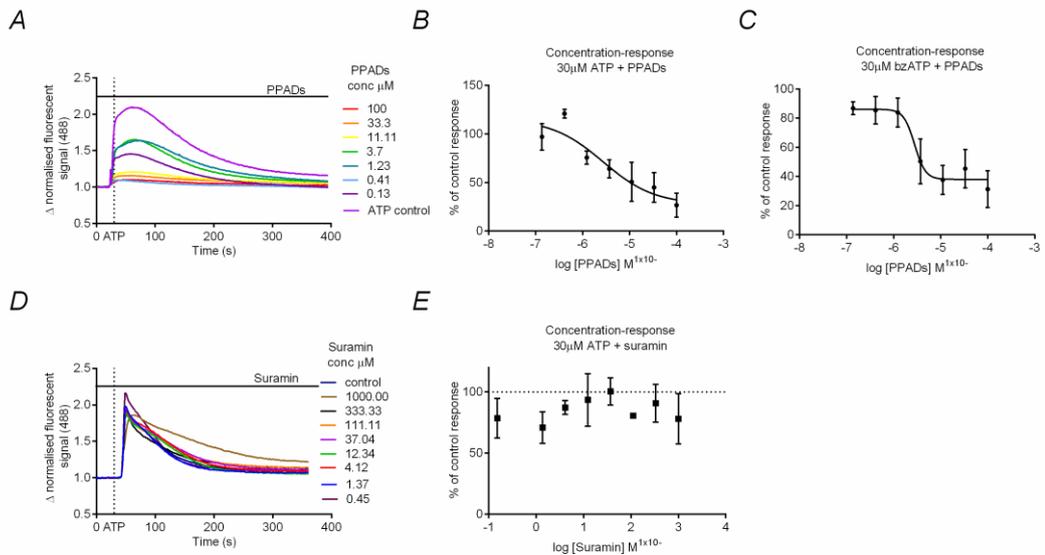
Figure 4.5   ATP activated Ca^{2+} influx in hMDMs is inhibited by PPADs but not by suramin in a concentration-dependent manner

> *Ca^{2+} imaging of fluo-4 AM loaded hMDMs using FLIPR, agonists were applied at t=20s and remained throughout, antagonists were pre-applied 15mins prior to agonist application and remained for experiment duration. **A.)** Representative Ca^{2+} trace in response to 30µM ATP in the presence of PPADs signal was normalised to baseline fluorescent values.   **B&C.)** Concentration-response curve showing percentage of control response to 30µM ATP/bzATP, N=3. **D.)** Representative Ca^{2+} trace in response to 30µM ATP in the presence of suramin **E.)** Concentration-response curve showing percentage of control response to ATP, N=3. All concentration-response data was calculated using area under curve values. Results were analysed using one-way ANOVA with Tukey's multiple comparison test. ns p>0.05*

4.2.4 P2X7 antagonists do not inhibit the bzATP/ATP mediated Ca^{2+} signalling in hMDMs

The results from **Figures 4.3-4.4** show evidence of ATP/bzATP stimulated purinergic Ca^{2+} channels in hMDMs. Based on the EC50s in response to bzATP and ATP, the evidence is supportive of a range of purinergic channels that are active in hMDMs and suggest against P2X7 having a predominant contribution to the Ca^{2+} signalling induced by ATP/bzATP. However taken on its own, although this data suggests that other purinergic channels have a greater contribution to Ca^{2+} signalling in hMDMs, it does not prove against a P2X7 contribution. The distinct contribution of P2X7 to the ATP and bzATP induced Ca^{2+} signals was investigated using selective P2X7 antagonists. The P2X7 antagonists used in the present study have been well validated as potent and selective P2X7 inhibitors. GSK-2160A and GSK-3583A have been robustly tested in FLIPR and electrophysiology assays to demonstrate their effectiveness at inhibition of P2X7 *(Section 1.6.7)*. In HEK-hP2X7 cells

141

GSK-2160A was reported to have a pIC50 of 8.5 and was shown to have no significant activity at 50 targets in a radio-ligand binding assay (CEREP), 32 targets (tested at GSK), 31 Kinases and no effect at hERG. Secondly, (Ali *et al.*, 2013) assess the pharmacokinetic and pharmacodynamic activity of GSK-2160A in man. (Ali *et al.*, 2013) showed that GSK-2160A was effective in the inhibition of IL-1β production from human whole blood. Although it cannot be confirmed that this was driven through inhibition of IL-1β production from macrophage cells, it is likely that macrophage inhibition was contributory to these results. Importantly, this data showed that GSK-2160A is effective in the inhibition of endogenous receptors as well as in over-expression systems. Together these data provide confidence that the GSK P2X7 antagonists are robust tools to measure P2X7 contribution from.

In my study, neither of the P2X7 selective antagonists caused a significant inhibition of ATP nor bzATP induced Ca^{2+} signals *(Figure 4.6)*. No significant reduction in the ATP or bzATP induced Ca^{2+} signal was seen to GSK-2160A or GSK-3583A at a range of concentrations following stimulation with 30µM ATP/bzATP. These agonist concentrations were chosen as they were closest to the EC80 values (as revealed through the experiments in *Figure 4.4*) and provided a stable maximum response with the greatest dynamic window from which to measure the effect of the antagonist from. The results plotted in *Figure 4.6* show the % control values from the area under the curve Ca^{2+} signal at each antagonist concentration, similarly no inhibition was seen when the concentration-response curve was plotted using max-basal values. When the results from *Figures 4.3-4.6* are taken together, these results are supportive of no contribution of homomeric P2X7 to Ca^{2+} signalling in hMDMs.
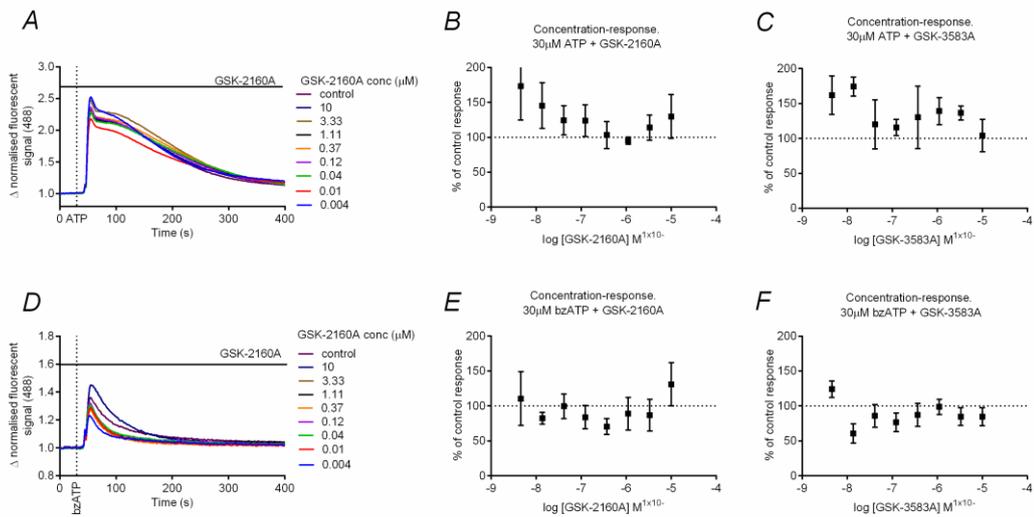
Figure 4.6   bzATP/ATP mediated Ca^{2+} influx in hMDMs is not significantly inhibited by P2X7 antagonists; GSK-2160A and GSK-3583A

*Ca^{2+} imaging of fluo-4 AM loaded hMDMs using FLIPR. **A&D.)** Representative graphs showing Ca^{2+} signal induced by 30μM ATP/bzATP in the presence of GSK-2160A. Agonists were applied at t=20s, antagonists were pre-incubated for 15min prior to agonist addition, both kept constant throughout duration. Signal was normalised to baseline fluorescent values. **B&C.)** Concentration-response for P2X7 antagonists showing % of control response (30μM ATP), mean ± SEM N=5 donors. **E&F.)** Concentration-response for P2X7 antagonists showing % of control response (30μM bzATP) mean ± SEM N=5 donors. Concentration-response data calculated from area under curve values. Results were analysed using one-way ANOVA with Tukey's multiple comparison test. ns p>0.05*

4.2.5 Investigation into experimental influencers of P2X7 signalling

Consideration was made as to whether the experimental conditions of this study were influencing the activity of P2X7 mediated Ca^{2+} signalling, by masking its contribution or limiting its activation capacity. Based on evidence from the literature, two factors with potential influencing capacity on P2X7 activity were investigated.
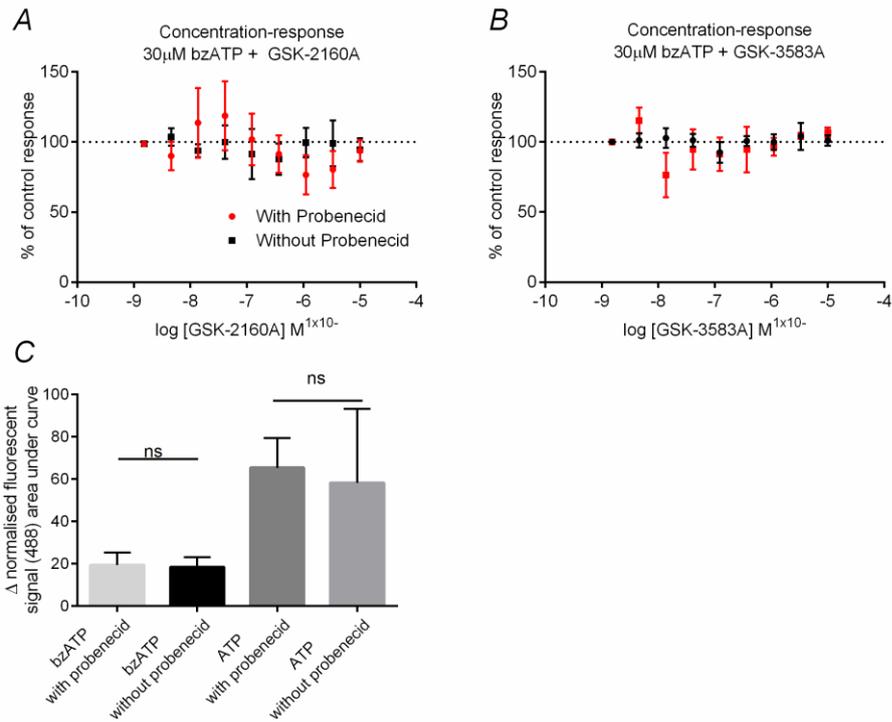
Figure 4.7   Removal of probenecid from FLIPR buffer had no significant effect on P2X7 antagonist activity or bzATP/ATP mediated Ca^{2+} signal in hMDMs

*Ca^{2+} imaging of fluo-4 AM loaded hMDMs using FLIPR, antagonists were pre-incubated for 15mins prior to agonist application at t=20s, Ca^{2+} signal was measured for a duration of 400s agonist and antagonist kept constant throughout. **A&B.)** Concentration-response of Ca^{2+} signal induced by 30µM bzATP, with and without probenecid included in FLIPR buffer with a range of concentrations of GSK-2160A (A) or GSK-3583A (B). Graphs are showing % of control response calculated from area under curve values. **C.)** Comparison of the control Ca^{2+} response to 30µM bzATP/ATP with and without probenecid included in FLIPR buffer, bar graph is shown as normalised area under curve values mean ± SEM. Area under curve values were taken from fluorescent signal over time following normalisation to baseline fluorescence. Results were analysed using one-way ANOVA with Tukey's multiple comparison test. ns p>0.05,* p <0.01 ****, p<0.0001. N=5.*

Probenecid has been shown to cause inhibition of P2X7 mediated currents and Ca^{2+} signalling in HEK-P2X7 cells (Bhaskaracharya *et al.*, 2014). Probenecid is an organic anion transporter inhibitor and is commonly added to FLIPR buffer to prevent the Ca^{2+} indicator dye being extruded from the cell after initial loading. A concentration of 1mM was demonstrated to be effective in P2X7 inhibition by (Bhaskaracharya *et al.*, 2014), whereas 2.5mM probenecid was used in the FLIPR buffer in the experiments described in ***Figure 4.6***. The possibility of probenecid limiting the activation of P2X7 in hMDMs was tested by performing further FLIPR imaging, excluding probenecid present in the FLIPR loading buffer. The inhibition capacity of P2X7 antagonists, GSK-2160A and GSK-3583A to the Ca^{2+} signal

144

induced by bzATP in conditions with and without probenecid was assessed in parallel. The results in **Figure 4.7** demonstrate that there was no significant effect of the P2X7 antagonists on the Ca^{2+} signal induced by bzATP or ATP in conditions with or without probenecid present. Notably, neither was there any significant change in the Ca^{2+} signalling response to 30μM ATP or bzATP when probenecid was excluded. Whilst a Ca^{2+} signal of 19.37 ± 5.90 was observed in response to bzATP with probenecid present, a Ca^{2+} signal of 18.36 ± 4.64 was seen without probenecid, a value that was not significantly different (normalised mean area under curve values ± SEM N=6). Similarly the ATP normalised signal was 65.26 ± 14.08 and 58.23 ± 34.88 N=4, with and without probenecid respectively again values that were not significantly different (normalised mean area under curve values ± SEM N=4). Together these results suggest that probenecid had no effect on the bzATP/ATP induced Ca^{2+} signal in hMDMs and provide further evidence to support against an involvement of homomeric P2X7 to bzATP/ATP Ca^{2+} signalling in hMDMs.
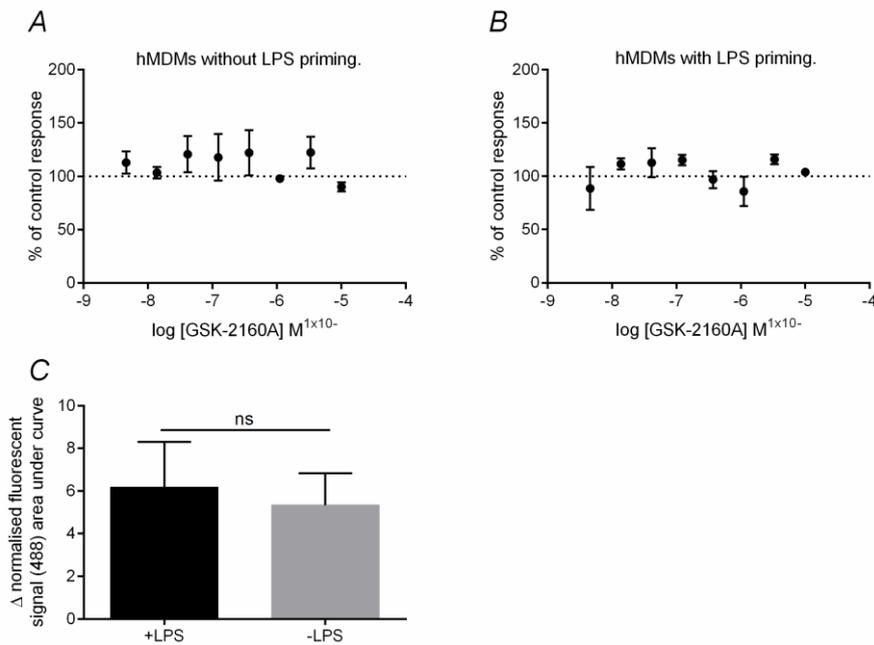
Figure 4.8 **24hr priming of hMDMs with LPS had no significant effect on the Ca^{2+} signal induced by 30μM bzATP nor did it alter the activity of P2X7 antagonist (GSK-2160A)**

*Ca^{2+} imaging of fluo-4 AM loaded hMDMs using FLIPR; hMDMs were primed for 24hr with 100ng/ml LPS prior to experiment. Antagonists were pre-incubated for 15mins prior to agonist application at t=20s both kept constant throughout experiment duration, Ca^{2+} signal was measured for duration of 400s. **A&B.)** Concentration-response curve of signal induced by 30μM bzATP in the presence of GSK-2160A - without LPS priming (A) - with LPS priming (B). Data showing percentage of control response calculated from area under curve values. **C.)** Comparison of the control Ca^{2+} signal induced by 30μM bzATP in cells with and without LPS priming, bar graph shows normalised area under curve Ca^{2+} signal, mean ± SEM. Area under curve values were taken from fluorescent signal over time following normalisation to baseline fluorescence. Results were analysed using unpaired students t-test. ns p<0.05, * p <0.01, **** p<0.0001. N=3.*

(Humphreys & Dubyak, 1996) describe how P2X7 expression and function can be modulated by the treatment with pro-inflammatory cytokines and bacterial products in the THP-1 monocytic cell line. For example; LPS and IFNy treatment was shown to increase the bzATP induced changes in cytosolic Ca^{2+} and ethidium uptake with a corresponding increase in the P2X7 mRNA levels. Therefore further FLIPR experiments were performed to test whether LPS priming would affect P2X7 mediated Ca^{2+} entry in hMDMs. No change in the responsiveness of the P2X7 antagonists was seen following 24 hour LPS priming, no significant inhibition of the bzATP induced Ca^{2+} signal seen in LPS primed hMDMs *(Figure 4.8)*. Similarly, there was no difference in the control Ca^{2+} signal initiated by bzATP in LPS primed vs. unprimed cells, the mean signal induced by bzATP was 6.18 ± 2.10 N=3 in LPS primed hMDMs vs. 5.34 ± 1.50 N=3 in unprimed cells (normalised area under curve values, mean ± SEM) *Figure 4.8*. These results suggest that LPS priming has no effect on the activity of P2X7 in hMDMs.

In sum, the results in *Figure 4.1 & 4.2* show evidence to support that hMDMs express P2X7 channels at protein level; however the FLIPR assay results *(Figures 4.3-4.8)* do not show evidence to suggest that P2X7 is functionally active as a homomeric Ca^{2+} influx channel under these conditions. Nevertheless, these results do support the activity of other purinergic receptors the possible identity of which is discussed in *Section 4.3*.

4.2.6 Investigating the contribution of P2X7 to purinergic mediated Ca^{2+} signalling in hAMs

Although hMDMs represent a more physiologically relevant macrophage model than an immortalised cell line or a mouse model, due to the known heterogeneity of macrophages (see *Section 1.3.4*) we also wanted to study the effects of the GSK P2X7 antagonists on Ca^{2+} signalling in hAMs. This cell type is more physiologically relevant to the end target this study is aiming to investigate, i.e. in a COPD patient, macrophages resident in the lung would be amongst the population of cells to be targeted by a P2X7 therapeutic. Therefore it is important to find out whether the results obtained in hMDMs are translatable to the tissue resident macrophages.

Unfortunately due to the limitations in human tissue availability through the duration of the P2X7 study only 2 donors of hAM cells were obtained for experiments. However the results of these experiments provided interesting preliminary results which indicate key differences between the results seen using MDMs, follow-up studies would be critical to complete target validation work.
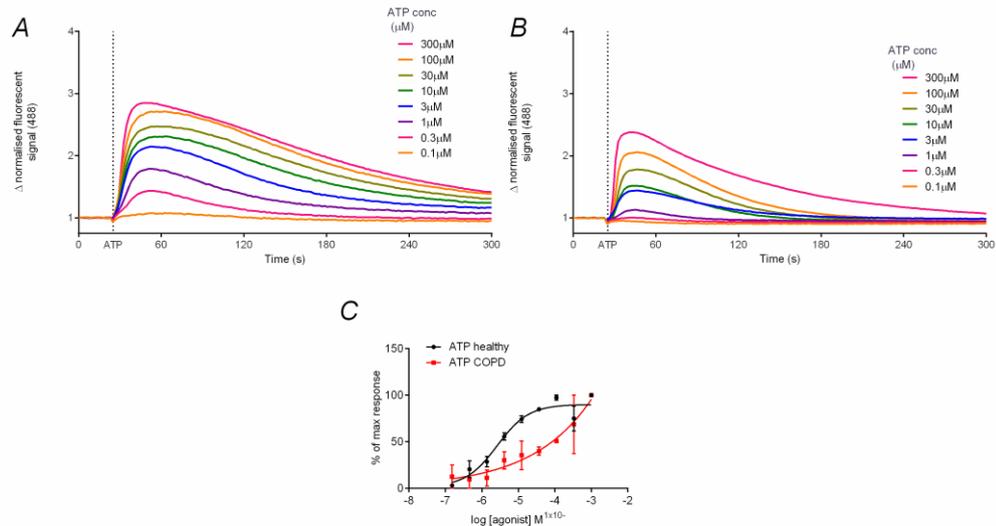
Figure 4.9   **ATP activated Ca^{2+} influx in hAMs from healthy and COPD donors**

*Ca^{2+} imaging of fluo-4 AM loaded healthy and COPD hAMs using FLIPR. **A&B.)** Representative Ca^{2+} trace, response to varying concentrations of ATP, agonist application at t=20s and kept constant throughout - in healthy hAM (A) and COPD hAMs (B). Signal normalised to baseline fluorescent value. **C.)** concentration-response curve showing percentage of max response, using area under curve values, mean ± SEM. N=2 donors for each group.*

Results in **Figure 4.9** show the Ca^{2+} signal initiated by ATP in healthy and COPD cells - there are similarities in the kinetic signature obtained following ATP stimulation to that seen by ATP in the hMDM cells, with a return to baseline signal within 4-5 minutes in both hMDM and hAM cells. Similarly, the maximum signal increase had occurred within 1 minute in hAM and hMDM cells. The concentration-response relationship displayed a sigmoidal/linear relationship in response to increasing ATP concentrations **(Figure 4.9C)**, in contrast to the bell-shaped response seen to ATP in hMDMs. The pEC50 of ATP in healthy hAM cells was 5.6 ± 0.2 N=2 and around 4.8 in COPD hAMs N=1, this was in contrast to the 4.8 ± 0.3 pEC50 shown in hMDM cells. This pharmacological profile is indicative of a significant contribution of purinergic receptors with a lower potency for ATP in hAM cells than those seen in hMDM and COPD hAM cells.

Interestingly the ATP response in the COPD hAMs resulted in a Ca^{2+} signal with a lesser magnitude and with a lower potency than the hAM cells, (signal change to 100µM ATP is 1.50 in healthy hAMs and 1.00 in COPD hAMs), although these results must be interpreted with caution due to the low N numbers, finding differences in the Ca^{2+} signalling in COPD vs. healthy hAMs could provide indicators into changes that have occurred in COPD macrophages to cause aberrant activity.
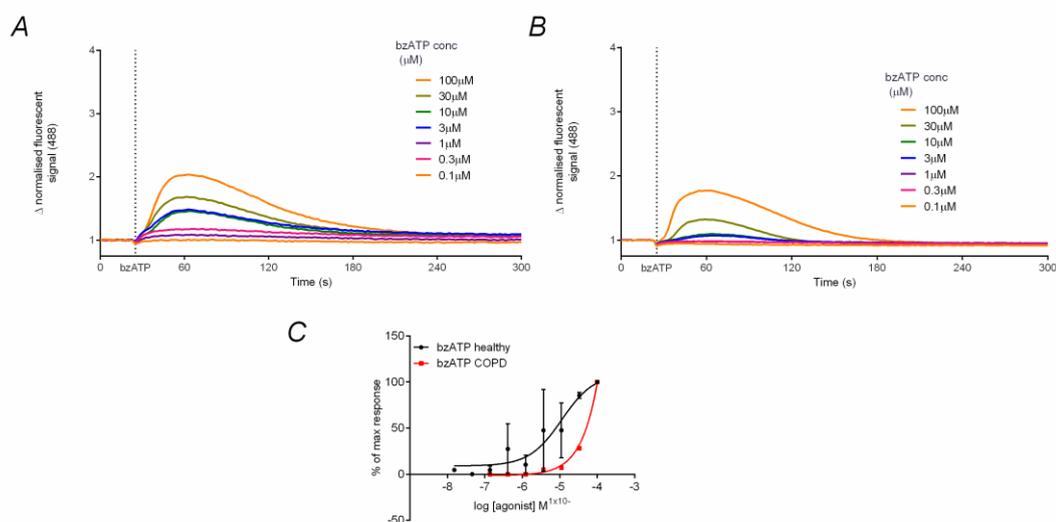
Figure 4.10   bzATP activated Ca²⁺ influx in hAMs from healthy and COPD donors

*Ca²⁺ imaging of fluo-4 AM loaded AMs using FLIPR. **A&B.)** Representative Ca²⁺ trace, response to varying concentrations of bzATP, agonist application at t=20s and kept constant throughout - in healthy hAM (A) and COPD hAMs (B). Signal normalised to baseline fluorescent value. **C.)** concentration-response curve showing percentage of max response using area under curve values, mean ± SEM. N=2 donors for each*

Results displayed in **Figure 4.10** show the concentration-response to bzATP in healthy and COPD hAM cells from 2 donors. The kinetics of the Ca²⁺ mobilisation initiated by bzATP are similar to those observed in the hMDM cells, with a return to baseline signal within 4 minutes. The pEC50 of bzATP in healthy hAMs was 4.9 ± 0.4 N=2, this is compared to 5.0 ± 0.2 N=5 in hMDMs. An accurate pEC50 for bzATP in COPD hAMs cannot be accurately derived from the current data in one donor, however it is clear that bzATP has a lower potency in COPD hAMs compared to healthy hAMs and hMDMs.

Notably, in contrast to the work shown in **Figures 4.6-4.8**, the GSK-2160A P2X7 inhibitor was shown to inhibit the Ca²⁺ signal induced by bzATP in healthy hAMs and ATP in healthy and COPD hAMs, in a concentration-dependent manner **(Figure 4.11).** The pIC50 for GSK-2160A to ATP mediated Ca²⁺ signals was 6.3 ± 0.5 N=1, in healthy hAMs and 6.4 ± 0.9 N=1 in COPD hAMs, however the pIC50 to bzATP was ambiguous and estimated to be around 10.9. The raw Ca²⁺ signal traces showed a drop in the baseline fluorescence upon agonist application, subsequently there is not an obvious inhibitory pattern when looking at the Ca²⁺ signal over time trace; however the concentration-response curve demonstrates a concentration-dependent inhibition. This data has been plotted as the percentage of control response as calculated from area under the curve values. It must be emphasised that these results must be taken as preliminary finding, as experiments have only been performed in one hAM donor, but they indicate that there may be important differences in the functional contribution of P2X7 to Ca²⁺ signalling in hMDM and hAM cells.
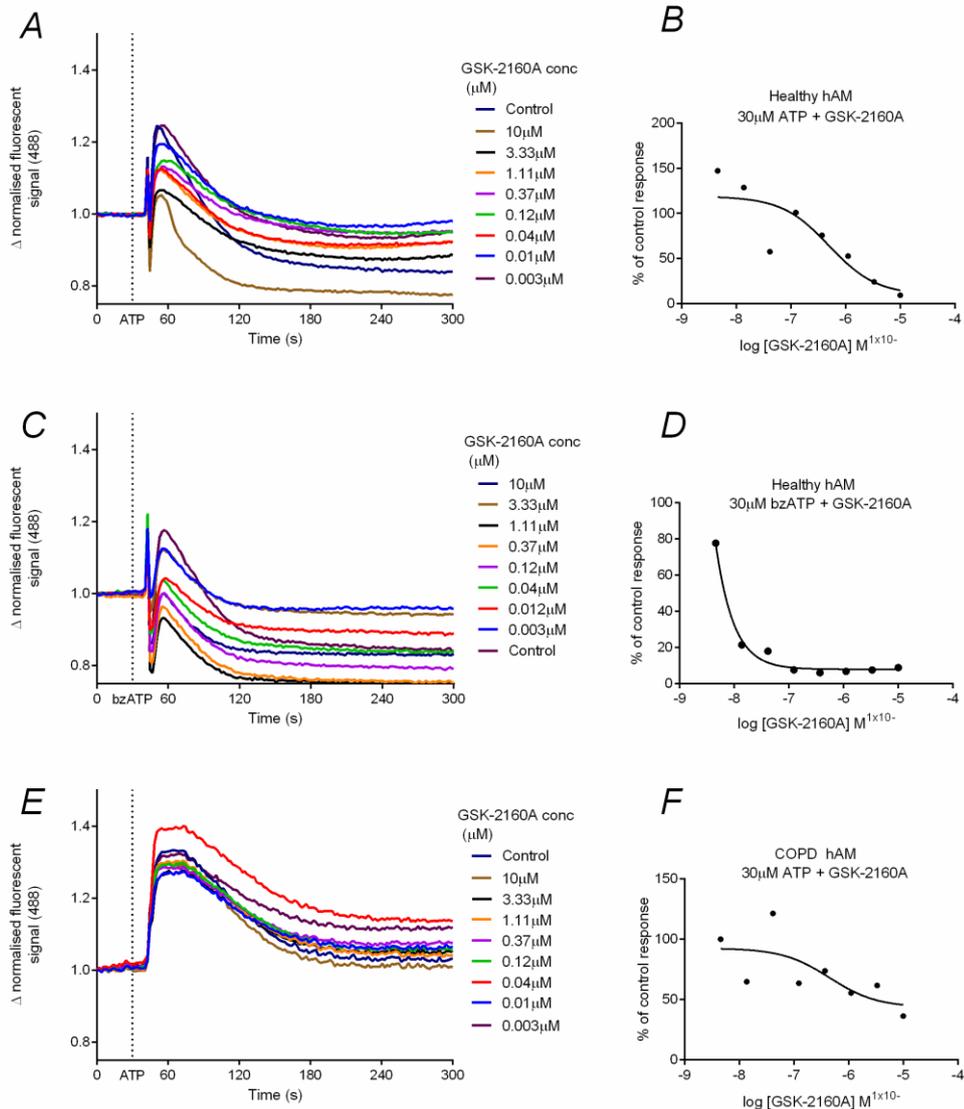
Figure 4.11   Effects of the P2X7 antagonist GSK-2160A on bzATP and ATP induced Ca^{2+} signal in hAMs, preliminary data from one donor

*Ca^{2+} imaging of fluo-4 AM loaded hAMs using FLIPR. **A, C, E.)** Representative Ca^{2+} trace, response to varying concentrations of bzATP/ATP in the presence of GSK-2160A, agonist application at t=20s, antagonist pre-incubated for 15min prior to agonist, both kept constant throughout experiment. Signal normalised to baseline fluorescent value. **B, D, F.)** Concentration-response curve showing effect of GSK-2160A on 30µM bzATP/ATP induced signal, data represented as % of control response calculated from area under curve values. N=1, 1 healthy and 1 COPD.*

4.2.7 P2X7 contribution to macrophage bacterial handling

Despite the lack of evidence shown for P2X7 contribution to bzATP/ATP mediated Ca^{2+} influx in hMDMs, further experiments were performed to discharge the risk of P2X7 inhibition in bacterial handling. There have been numerous examples where P2X7 has been described as controlling downstream functions independently of cation influx (Surprenant *et al.*, 1996; Brough *et al.*, 2003; Qu *et al.*, 2007) therefore investigating the activity of P2X7 antagonists on macrophage bacterial handling is equally important.

The effect of the P2X7 antagonists on hMDM bacterial handling was assessed through the evaluation of phagocytosis assays using pHrodo labelled *E. coli*. 10μM of GSK-2160A was kept constant throughout the phagocytosis assay; the intensity of the pHrodo labelled particles found in acidic intracellular compartments was used as readout of phagocytosis. The phagocytosis of pHrodo labelled *E. coli* was assessed through the phagocytosis index, density in responding cells and the % of responding cells. The inhibitor of F-actin polymerisation, Cytochalasin-D was shown to significantly inhibit phagocytosis under all parameters measured. The phagocytosis index in control conditions was 1.31 ± 0.03 N =3, this was not significantly different in the presence of GSK-2160A at 1.31 ± 0.04 N=3, however Cytochalasin-D significantly reduced the phagocytosis index by 0.99 ± 0.007, the % of responding cells was 73% ± 3.4 in control and 70% ± 2.9 with GSK-2160A however there was only 0.55% responding cells in Cytochalasin-D conditions. The density in responding cells was 1581 ± 102.6 in control, 1559 ± 171.3 in the presence of GSK-2160A and 384 ± 13.5 in Cytochalasin-D conditions (all numbers = mean ± SEM). The significant reduction by Cytochalasin-D in all experiment read-outs provides confidence in the assay methodology, however the data also shows no supportive evidence for P2X7 contribution to pHrodo labelled phagocytosis *(Figure 4.12).*
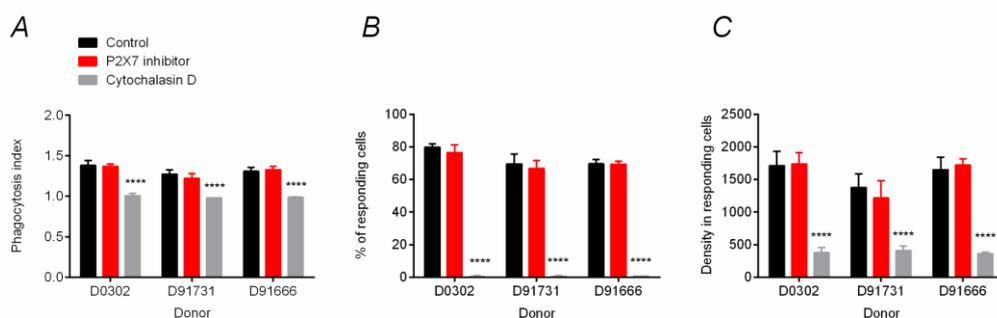
Figure 4.12   P2X7 antagonist (GSK-2160A) caused no significant inhibition to the phagocytosis of pHrodo labelled *E. coli* by hMDM cells

*hMDMs were pre-incubated with; vehicle, 10μM Cytochalasin-D or 10μM GSK-2160A before uptake of opsonised pHrodo labelled E. coli was assessed at 3hr post infection, 20μg of E. coli was added to each well of 40,000 hMDMs. hMDMs were stained with cell tracker green (1μM) and Hoescht (0.05μg/well) to enable quantification of intact cells. Bar graphs show the mean ± SEM for each donor tested **A.)** phagocytotic index. **B.)** percentage of responding cells. **C.)** density in responding cells. Results were analysed using two-way ANOVA with Tukey's multiple comparison test. N=3 donors.*

Experiments to assess the effect of P2X7 antagonists in macrophage bacterial killing were also performed (data obtained by Simon Hall and Katie Anders at GSK). Bacterial killing assays were performed by using the measurement of ROS (as an indirect readout) following infection of the macrophages with S. pneumoniae bacteria. These experiments demonstrated that there was no significant effect of bzATP as an agonist to enhance ROS mediated bacterial killing, or of the P2X7 antagonists (GSK-2160A and GSK-3583A) in the inhibition of bacterial killing (data not shown).

Together these results provide no evidence for the contribution of P2X7 to macrophage bacterial handling and when the results obtained in hMDM cells are considered alone, the results from this study provide evidence to suggest a discharge of the risk involved in impairing macrophage ability to handle bacterial infection by attenuating P2X7 activity. However it is clear that experiments to validate the effects of the P2X7 inhibitor in ATP induced Ca^{2+} signalling and bacteria handling in hAMs need to be performed before a final conclusion can be made.

4.3 Discussion

In sum, the results presented in **Chapter 4** indicate expression of P2X7 in hMDM cells and hAM cells but the pharmacological profile observed from the FLIPR assay results suggest that the P2X7 receptor is not functionally active as a Ca^{2+} influx channel in hMDMs under these conditions.

Expression of P2X7 in hMDMs

The results from my study have provided evidence for P2X7 protein expression in hMDMs, however my results have shown no evidence for P2X7 contribution to Ca^{2+} signalling. This apparent contradiction in results warrants the question of whether the P2X7 antibody staining as shown in the present study is selective for P2X7 or whether it is reporting nonspecific protein binding. As discussed in **Section 2.10** antibody validation experiments show that the P2X7 antibody effectively and solely binds to the antigen it was raised against, there was only 1 band observed in the protein ladder following P2X7 antibody incubation and this was removed following blocking peptide preincubation. The IgG isotype control experiments illustrate that there is no non specific binding of the antibody to native IgG receptors on the cell of interest, however what cannot be conclusively proven is whether the P2X7 antibody binds to other receptors when a potentially different repertoire of epitopes are available in a fixed hMDM cells as opposed to cell lysates from hMDM cells. Although this latter possibility is unlikely based on the expected larger repertoire of epitopes in a western blot experiment compared to protein expression in their native state, i.e. in immunocytochemistry. The results demonstrated a significant level of expression in comparison to the IgG isotype controls and the staining pattern observed is consistent with an active ion channel protein location Therefore it can be taken with relative confidence that the P2X7 staining observed is reflective of P2X7 expression.

Pharmacology of ATP and bzATP responses in hMDMs

A robust Ca^{2+} signal was induced by ATP which had a relatively large magnitude, however the EC50 of ATP in hMDMs obtained in my study, 9.6 ± 4µM reflects potency in the range associated with the activation of P2X family members other than P2X7. As summarised by North 2002, the EC50 for ATP at hP2X7 is 1000µM which is 100 fold greater than the value obtained in my study, whereas the EC50 for ATP EC50 at P2X2, P2X4 and P2X5 is closer to 10µM, suggesting a major contribution to the ATP-mediated Ca^{2+} signal from these other P2X family members. Therefore taken alone, the pharmacology of the ATP-mediated Ca^{2+} signal in hMDMs does not support a model of predominant homomeric P2X7 channel activity. The activity of bzATP gives an EC50 closer to what would be expected from P2X7 activation although the signal induced by bzATP was significantly smaller in magnitude compared to that induced by ATP. The inhibition of ATP and bzATP induced Ca^{2+} signal by PPADs but not suramin is suggestive of a contribution of P2X4. Whilst PPADs and suramin are pan purinergic receptor antagonists, suramin is a weak antagonist of P2X4 with a reported IC50 at hP2X4 of 178.1µM ± 46.9 (Garcia-Guzman *et al.*, 1997). PPADs is shown to be largely ineffective at rP2X4R inhibition (Jacobson *et al.*, 2002), however it has been demonstrated to have an IC50 of 27.5µM ± 3.4 to hP2X4R. Although the IC50 for PPADs obtained in my study (~2.7µM) is closer to that reported for P2X1, 2, 3 and 5 (EC50 ~1-5µM) (North & Surprenant, 2000) the insensitivity to suramin provides compelling evidence for some contribution of P2X4, although it could be that P2X4 contributes as part of a heteromeric channel complex. (Chessell *et al.*, 1998) report the IC50 for PPADs and suramin in hP2X7 as 1 and 70µM respectively therefore indicating the possibility of P2X4/P2X7 interaction too, this is discussed further in *Section 4.3.* The distinct contribution of P2X7 channel activity was evaluated by the use of P2X7 antagonists (GSK-2160A and GSK-3583A), however no significant inhibition was observed to either the Ca^{2+} signal induced by bzATP or ATP thereby providing compelling evidence that P2X7 was not contributing to the ATP/bzATP mediated Ca^{2+} signal in hMDM cells in my study. As described in *Section 1.6.4* there are numerous reports of P2X7 activity in human and mouse monocyte and macrophage cells, therefore the results obtained in the present study were contrary to my original hypothesis. The initial characterisation of hP2X7, (Rassendren *et al.*, 1997) performed a comparison of hP2X7 activity in HEK-293 cells expressing hP2X7 and hMDMs with endogenous P2X7 expression. Rassendren reported the activity of P2X7 in hMDMs to be similar to P2X7 in HEK-293 cells and proposed that due to the similar pharmacological profile between the two cell types, hMDMs predominantly express homomeric P2X7 channels. However, Rassendren used hMDMs taken from only one donor, whereas in my study the experiments were performed using hMDMs from numerous blood donors. It is possible that variable expression of P2X7 splice variants and or P2X7 SNPs in the hMDMs used in my study vs. Rassendren could be an explanation of the different results seen. Alternatively, the interaction of P2X4 and P2X7 channels in my study could be resulting in an altered pharmacological profile which is a combination of these two channel types; this is discussed further in *Section 4.3*.

Consideration was made as to whether the culture conditions used in my study was responsible for the lack of P2X7 activity observed. As discussed in **Section 4.2.5** previous work in the literature has shown that priming hMDMs with bacterial products can enhance P2X7 activity. In this regard I tested the effect of 24 hour LPS priming on the ATP/bzATP induced Ca^{2+} signal and the effect of the P2X7 antagonists, but found no significant difference. Although investigating LPS priming was a valid line of investigation, there are differences in the experiments performed by Humphreys and Dubyak that could explain the lack of change seen in my study. Humphreys and Dubyak performed experiments in the THP-1 monocytic cell line which has relatively low P2X7 expression levels, therefore it is possible that the change seen following LPS/IFNγ priming was due to very low level of P2X7 in control cells to begin with, and suggests that the main cause of LPS induced P2X7 potentiation was due to an increase in expression. Although direct comparisons cannot be made, the convincing protein expression of P2X7 channels in resting hMDMs shown in my study suggest that a lack P2X7 channel expression is not responsible for the lack of functional contribution seen.

Based on the literature, another possible influencing factor to P2X7 activity was the presence of probenecid in the FLIPR buffer. A recent publication demonstrated that probenecid, was an inhibitor of P2X7 channels. Therefore experiments were performed without probenecid to see whether this revealed a P2X7 contribution, however no significant change in the effect of the P2X7 antagonist on bzATP induced Ca^{2+} entry was seen thereby discounting this as an explanation for the lack of P2X7 activity.

Confirmation of the FLIPR methodology having an appropriate dynamic range to detect signal inhibition was demonstrated through the experiments monitoring the inhibitory action of PPADS on signal induced by ATP and bzATP. If excessive gain set up and threshold of signal, or conversely a signal with a small dynamic range was to blame for the lack of inhibition seen by the P2X7 antagonists, it would be expected that no inhibition would be observed for any signal induced by bzATP and ATP. However PPADs was demonstrated to inhibit the bzATP and ATP induced Ca^{2+} signal, in a concentration-dependent manner, demonstrating the sensitivity of the FLIPR assay as it was able to resolve Ca^{2+} signal changes in the dynamic range exerted by bzATP and ATP stimulation.

The distinction of P2X7 activity in the present study is reliant upon the activity of P2X7 selective antagonists, however as discussed in **Section 4.2.4** there are numerous pieces of evidence which provide confirmation that these antagonists are effective in P2X7 inhibition. Firstly initial validation of the compounds in FLIPR and patch clamp electrophysiology experiments using HEK cells over-expressing human and rat P2X7 confirm compound activity and IC50. As part of these validation experiments the inhibitors were shown to be inactive at 50 receptors and ion channels (CEREP) and 31 Kinases and had no effect at hERG. Secondly, the compound, GSK-2160A, was used in a publication to assess its pharmacokinetic and pharmacodynamic properties in man (Ali *et al.*, 2013). GSK-2160A caused inhibition of IL-1β production from human whole blood. Although it cannot be confirmed that this was driven through inhibition of IL-1β production from macrophage cells, given the predominant contribution of macrophages in IL-1β production, it is likely that macrophage inhibition was contributory to these results. Importantly, this data shows

that the compound is effective in the inhibition of endogenous receptors as well as in over-expression systems. Thirdly, the positive inhibition of the bzATP/ATP mediated Ca^{2+} signal in one donor of healthy and COPD hAMs demonstrates that the compounds are active under the assay conditions used in this study. Lastly, a chemical QC experiment was performed to validate the chemical properties of the batch of P2X7 antagonists used in the present study. Taken together, this data gives compelling evidence that the compound is active and effective in the blockage of P2X7 receptors in a number of assay types.

There is evidence that P2X7 activation can be inhibited by extracellular divalents such as Ca^{2+} and Mg^{2+} (Surprenant *et al.*, 1996; Rassendren *et al.*, 1997). The possibility of this being an explanation for the results presented here was not directly investigated, so cannot be ruled out, however there are a number of pieces of evidence which suggest this explanation is unlikely. Where the effect of Ca^{2+}/Mg^{2+} concentration on P2X7 activity has been studied previously, the action of the divalents was shown to decrease the magnitude of the Ca^{2+} signal/current seen but not to alter the potency of the agonist for the receptor (Surprenant *et al.*, 1996). As significant Ca^{2+} signals were observed for ATP/bzATP activation it would be expected that even if the signal was attenuated by the Ca^{2+}/Mg^{2+} concentration that would be sufficient signal remaining to observe the effects of a P2X7 antagonist. Similarly, the preliminary results indicating P2X7 mediated Ca^{2+} entry in hAM cells were performed under the same experimental conditions as in hMDMs therefore showing that the concentrations used in this study are not hindering P2X7 activation completely. Likewise, other studies have been able to successfully measure P2X7 mediated Ca^{2+} entry using a Ca^{2+} indicator dye and Ca^{2+}/Mg^{2+} concentrations in the external solution at comparable levels, suggesting that this is not a likely explanation for my results (Cabrini *et al.*, 2005). Taken from a different perspective, the focus of this study was to observe the effects of the P2X7 antagonists on human macrophages under physiological conditions, i.e. to understand how inhibition of P2X7 would affect human macrophage biology under conditions as close to those occurring *in vivo* as possible. This means that understanding whether P2X7 was active in low divalent conditions would be interesting from a mechanistic point of view, but would not help in the understanding of how P2X7 antagonists might act to alter Ca^{2+} signalling in human macrophages in 'physiological' conditions. The ultimate aim of the present study was to understand and elucidate the effects of the P2X7 antagonists, GSK-2160A and GSK-3583A on human macrophage Ca^{2+} mobilisation and bacterial killing and was not designed as an in depth characterisation of P2X7 pharmacology. In sum, the points discussed above provide evidence to confirm that the lack of inhibition of Ca^{2+} signalling by the P2X7 antagonists is reflective of a lack of P2X7 Ca^{2+} influx activity in hMDMs under the present assay conditions.

Potential for P2X7 activity in hMDMs independent of Ca^{2+} signalling

P2X7 mediated K^+ efflux has been convincingly demonstrated to be the signalling modality specific to P2X7 receptors which leads downstream maturation of IL-1β in LPS primed macrophages. Notably there is some evidence to suggest that P2X7 mediated K^+ efflux is required independently from Ca^{2+}, suggesting two independent roles for the P2X7 receptor

(Brough *et al.*, 2003; Franchi *et al.*, 2007; Qu *et al.*, 2007; Piccini *et al.*, 2008; Katsnelson *et al.*, 2015). The results obtained from the FLIPR assay do not allow investigation of the K^+ signalling component and therefore we cannot rule out that K^+ efflux is occurring following P2X7 agonist application. It may be that a small amount of Ca^{2+} entry does occur through the P2X7 channel in the experiments demonstrated here, but if the primary function P2X7 activation is K^+ efflux (and non selective Na^+ influx), this could explain why a significant inhibition is not seen with the P2X7 antagonists in Ca^{2+} imaging experiments, yet there is evidence to support P2X7 protein expression. The details of further experiments that could be performed to address this possibility are discussed in ***Section 4.4***.

Could P2X7 channels be forming heteromers with P2X4 in hMDMs?

Another possible explanation for the lack of effect of the P2X7 antagonists and other pharmacological evidence suggesting lack of P2X7 activity could be due to expression of P2X4/P2X7 heteromers. P2X4 and P2X7 channels have a high sequence homology and are the most similar of all the P2X family members, they have often been found to be expressed in the same tissues/cell types. Of particular note to my study, P2X4 and P2X7 are the most commonly expressed P2X channels in immune cells (Bowler *et al.*, 2003; Xiang & Burnstock, 2005). Functional interaction of P2X4 and P2X7 channels have been shown in airway ciliated cells, where the expression of an ATP gated P2X receptor was demonstrated with biophysical and pharmacological properties of both P2X4 and P2X7 (Ma *et al.*, 2006). Similarly, (Casas-Pruneda *et al.*, 2009) describe receptors in secretory epithelia with ATP activated currents that have distinct functional and pharmacological characteristics to homomeric P2X4 and P2X7 HEK-293 expression cells. As described in ***Section 1.6.6***, the data in the literature is supportive of a homotrimeric interaction of P2X4 and P2X7 rather than a direct heterotrimeric interaction (Nicke, 2008); (Antonio *et al.*, 2011); (Guo *et al.*, 2007). Through the study of a variety of P2X heteromeric channel assemblies it has been observed that in general the properties of a heteromer are a combination of the properties of the subunits it is formed from (Jiang *et al.*, 2003). Therefore the pharmacological profile of the Ca^{2+} signal initiated by bzATP and ATP from this study could be explained by of a functional interaction between P2X4 and P2X7; the insensitivity of the ATP induced Ca^{2+} signal to suramin could indicate suggestive of a P2X4 contribution (Jacobson *et al.*, 2002) and the EC50 for ATP is in line with that previously demonstrated by a P2X4 channel (North, 2002). A close functional interaction between these two P2X subtypes could cause a conformational change or even a close interaction between subunit structures could block the P2X7 antagonist binding site and explain the lack of inhibition by the antagonists. Further experiments would be required in order to confirm whether the results seen here are due to P2X7 and P2X4 homotrimeric channels or whether the data described above is simply indicative of a homomeric P2X4 contribution or P2X4 heteromeric interaction with another purinergic family member.

P2X7 in phagocytosis and bacterial killing in hMDMs

Importantly, the results demonstrated through this study showed that the P2X7 antagonists do not cause a significant inhibition of the phagocytosis of pHrodo labelled *E. coli* and also had no effect on the production of ROS, as a readout of bacterial killing. Previous studies investigating the role of P2X7 in phagocytosis have been performed in mouse peritoneal macrophage cells, human PBMCs and in HEK-293 cells transfected with P2X7, flow cytometry was used to assess the phagocytosis uptake of fluoresbrite yellow-green carboxylate microspheres (YG beads), *S. aureus*, *E. coli* or apoptotic cells (Gu *et al.*, 2010; Gu *et al.*, 2011). Work in Gu's 2011 study demonstrates that anti-P2X7 mAb and recombinant P2X7 extracellular domain (ED) inhibited the phagocytosis of YG beads, *E. coli* and *S. aureus* by human PBMCs, showing contrast in the data presented in my study. The reasons for these differences could be due to the difference in expression/functionality of P2X family members in PBMCs vs. hMDMs or differences in the methodology. Notably, the evidence for other P2 receptors to Ca^{2+} signalling in hMDMs in my study suggests it is possible that these other P2X receptors may compensate for P2X7 when its functionality is hindered.

Secondly, whilst prior investigations have demonstrated a role for P2X7 in regulating the killing of *Mycobacterium* and *Chlamydia*, to my knowledge, this study was the first to assess the contribution of P2X7 to the killing of *S. pneumoniae*. *Chlamydia* and *Mycobacterium* are both classified as obligate or facultative intracellular parasites which utilise the intracellular machinery of the cell to replicate (Baron 1996 medical microbiology 4th edition; Sherris Medical Microbiology, 5th Edition), whereas *S. pneumoniae* is an extracellular bacteria and is capable of replicating independently. It could be that the intracellular killing pathways utilised are different dependent on the bacteria type and differentially involve P2X7 signalling. A differential Ca^{2+} involvement in phagocytosis has been shown to occur dependent on particle type (Nunes & Demaurex, 2010).

When the lack of effect of P2X7 antagonists on bacterial phagocytosis and killing are taken in combination with the evidence that P2X7 does not contribute to ATP/bzATP mediated Ca^{2+} signalling in hMDMs, these pieces of data from hMDMs suggest that there is little risk associated with P2X7 inhibition. There is no evidence to suggest that P2X7 inhibition would have an effect on the critical function of macrophages in bacterial handling, a role that is particularly needed to remain intact in COPD patients. However, due to the preliminary findings in hAMs which are suggestive of P2X7 contribution to Ca^{2+} signalling, contrary to that seen in hMDMs, further experiments in hAM cells are required to ensure no differences are seen between hMDM/hAM bacterial handling functions as well.

Differences in hMDM and hAM Ca^{2+} handling responses

In contrast to the Ca^{2+} imaging results obtained in hMDM cells, the preliminary data obtained in hAM cells suggests a contribution of P2X7 to the bzATP and ATP mediated Ca^{2+} signalling. The concentration-response relationship initiated by ATP in hAMs demonstrated a classical sigmoidal/linear relationship with the EC50 around 2.63µM however the concentration-response to ATP in hMDMs exhibited a bell-shaped response with a

decrease in the response to ATP at concentrations over 100µM. As it is known that concentrations of around 100-1000µM are required to maximally activate P2X7 the concentration-response data from these two cell types indicate that there is a greater contribution of P2X7 channels to the hAMs than hMDMs. Further evidence for P2X7 activity was shown as the P2X7 antagonists inhibited the ATP and bzATP induced Ca^{2+} signal, in a concentration-dependent manner. However the pIC50 for GSK-2160A in the healthy hAMs and COPD hAMs was 6.3 which show a lower potency than was reported for hP2X7 homomeric channels expressed in HEK-293 cells (pIC50 of 8.5). Similar variability was observed in the activity of Synta66 between different cell types, for example in Jurkat T cells Synta66 was shown to have an IC50 of 1µM whereas in VSMCs it was shown to be 26/43nM (Di Sabatino *et al.*, 2009; Li *et al.*, 2011). This apparent observed lower potency of the GSK-2160A compound to ATP induced Ca^{2+} signals in hAMs compared to that reported in HEK-293 P2X7 expressing cells could be explained by differences in the level of P2X7 protein expressed in these difference assays thus affecting protein binding.

Due to the wide accessibility of blood donations and easy isolation of CD14+ peripheral blood mononuclear cells, a large number of groups now utilise blood derived hMDMs for *in vitro* experiments. A pub med search of 'human blood derived monocyte derived macrophages' yields over 8000 results indicating the vast use of this cell type. Since the recent findings that tissue resident macrophages are not derived from blood mononuclear cells but are instead foetal derived and maintained *in situ* during steady state conditions (Dey *et al.*, 2014), this has brought to question the translatability of this macrophage model as a mature macrophage cell type. However, due to the difficulties in obtaining primary human tissue from which to isolate tissue resident macrophages, blood MDMs is arguably a more representative macrophage model than immortalised macrophage cell lines and similarly has a key role in translation from mouse models.

Reports of functional differences between murine and human biology in mast cells have been described above *(Section 3.3)*, similar differences have also been shown in monocyte and macrophage cells. A 2010 study transcriptionally analysed the differences between murine and human monocyte subsets. A high level of similarity was seen between murine and human monocyte subsets; however key differences were also reported. Interestingly, the largest difference in expression profile reported between the two species was in classical scavenger and apoptotic cell recognition molecules (Ingersoll *et al.*, 2010). Further differences between mononuclear phagocytic cells from two species were summarised by (Reynolds & Haniffa, 2015).

Although current macrophage model systems may have flaws in the translation to human tissue resident cell, determination of components found in the extracellular milieu in macrophage tissue resident locations could be a novel way to create a monocyte derived tissue specific mature macrophage, albeit a challenging feat. (Guth *et al.*, 2009) described an adoptive transfer of GFP+ve BMDMs to the mouse airway that led to a change in the cell differentiation characteristics that were in line with the hAM phenotype. The high expression of CD11c in hAMs but not in other tissue-resident macrophages was used as the predominant indicator of adoption of the hAM phenotype in this study. Through GM-CSF

knockdown studies it was found that locally produced GM-CSF was required for directing the CD11+ve phenotype to BMDMs where it was shown that blood monocytes adopted the phenotypic characteristics of hAM cells when transferred to the lung tissue environment provides evidence that this methodology is theoretically possible. A worthwhile area of future investigation would be to comprehensively identify the components in the local environment that confer the tissue specific phenotype. Successful validation of such methods could be performed by comparison of the artificially created 'mature' tissue specific macrophage with cells isolated from this area.

The specific reasons for differences seen between hAM and hMDM purinergic Ca^{2+} signalling in my study could be due to a number of possibilities. Considering the medical history of the hAM donors, it is known both the donors of the healthy and COPD hAM cells were smokers (Healthy donor, L282, was a 57year old male smoker, COPD donor, 53year old male smoker who had been diagnosed with COPD for 5-6 years). In could be that the *in vivo* lung environment and constant exposure to cigarette smoke may have had a significant effect on the P2X7 expression and functionality and that this may account for the active involvement in Ca^{2+} signalling seen here in comparison to the hMDM cells, indeed (Lucattelli *et al.*, 2011) describe a significant upregulation of P2X7 mRNA in neutrophils and macrophages isolated from the BALF of mice exposed to cigarette smoke of 5 cigarettes for 3 consecutive days, providing support to this hypothesis.

It has been demonstrated that the activity of P2X7 exhibits variation dependent on the species but also between individual donors due to polymorphisms. There have are over 1500 SNPs of P2X7 as reported by NCBI SNP database, although the majority of these are intronic it has been shown that gain of function mutations such as the A348T mutation leads to a protection against infection, however gain of function mutations are associated with an increased risk of developing certain inflammatory diseases (Bartlett *et al.*, 2014). It would be worthwhile to evaluate the sequence of the P2X7 gene found in the hAM versus the hMDM donor cells to investigate whether polymorphic exceptions in the hAM cells were an explanation of the findings in my study. P2X7 is also known to form 7 naturally occurring splice variants (Cheewatrakoolpong *et al.*, 2005) with P2X7A the member first described in (Rassendren *et al.*, 1997). Each P2X7 splice variant can vary in its distribution, its functional characteristics but also in the associated cellular functions it controls (Adinolfi *et al.*, 2010), again it would be important to identify the splice variant distribution seen in the hMDM and hAM cells as differentiated/isolated in this study to see whether this shed any light on the functional differences suggested.

In conclusion, the results of this study using hMDMs indicate that inhibition of P2X7 does not represent a risk in the interference of macrophage Ca^{2+} signalling or bacterial handling. Nevertheless the preliminary data suggesting a difference in the Ca^{2+} signalling in hAM cells shows that translation experiments are required to confirm the activity of P2X7 in hAMs and whether the interpretations made from the hMDM experiments are physiologically valid. These results highlight the importance of translating biological studies into the most

physiologically relevant system available, to confirm that the conclusions obtained are accurate.

4.4 Future directions

In order to provide definite conclusions to answer the original research objectives set, further experiments in a larger number of hAM donors are required. Both FLIPR experiments and bacterial handling assays are required to validate or discharge the preliminary results obtained in hAM cells. These experiments would be the priority to complete this work for publication.

Although outside the scope of my study aims, from a basic science point perspective there are number of avenues of investigation which could be explored in order to better understand P2X7 in hMDMs under these assay conditions. Whilst a number of these experiments have been published in other macrophage cell types, they would help to fully understand the biology of P2X7 in hMDM cells under the present assay conditions and to confirm why differences are seen in my experimental conditions compared to others. Although the Ca^{2+} signalling experiments have revealed no activity of P2X7 in hMDMs, to understand fully the components of ion flow following P2X receptor activation, patch clamp electrophysiology could be performed, for example this would allow discernment of the potential for K^+ efflux occurring in response ATP/bzATP. It has been demonstrated that P2X7 contribution to IL-1β maturation is mediated by K^+ efflux and is independent to Ca^{2+} signalling (Brough *et al.*, 2003; Franchi *et al.*, 2007; Qu *et al.*, 2007; Piccini *et al.*, 2008; Katsnelson *et al.*, 2015). Therefore it may be that K^+ efflux mediated by P2X7 is a distinct function of P2X7 channels and important for regulating downstream cellular functions. In relation to this, to directly elucidate P2X7 regulated downstream functions in hMDMs, YO-PRO or ethidium dye uptake assays could be performed to find whether bzATP/ATP activation lead to P2X7 mediated pore formation. Similarly mature IL-1β production assays could be performed following ATP stimulation in the presence and absence of P2X7 antagonists; this would allow confirmation regarding P2X7 activity independently to Ca^{2+} signalling. A recent study by (Liang *et al.*, 2015) investigated the effect of extracellular Ca^{2+} on the allosteric interaction with P2X7. To further understand the effect of extracellular Ca^{2+} on P2X7 activation in my assay conditions, dye overload patch clamp electrophysiology experiments could be performed, as described in Liang's work. Similarly, further Ca^{2+} imaging experiments could be performed in the presence of low divalent concentrations to elucidate the potential effect on P2X7 activity. As discussed earlier in *Section 4.3*, although the activity of P2X7 activity in low divalent conditions is not relevant for the purpose of the present study from a mechanistic perspective it would be an interesting comparison study to understand the activity of P2X7 in hMDMs in 'physiological' conditions (normal divalent external solution) vs. 'P2X7 tuned conditions' (low divalent external solution).

One of the discussed possibilities for the lack of inhibition seen by P2X7 inhibitors in the present study was the potential for P2X4/P2X7 heteromeric/functional interaction. Co-IP

and FRET experiments could be performed to assess the interaction of the two proteins. Whereas, electrophysiology could be used to measure the desensitisation properties of the ATP induced current, utilising the distinct densensitisation characteristics reported in homomeric P2X4 and P2X7 channels. Potentiation induced by Ivermectin was traditionally used as a way to distinguish P2X4 from other P2X channels, however (Nörenberg *et al.*, 2012) recently demonstrated that human P2X7 was also sensitive to ivermectin therefore invalidating this as an approach.

Finally, a direction for further study would be to ascertain how the P2X7 antagonist used in the present study altered in activity between different SNPs and splice variants of hP2X7. Parallel genetic analysis of the P2X7 expression from hMDM and hAM donors would be an interesting way to understand further about the variability in the results between hMDM/hAM/donors.

Together, it can be seen that there are a number of avenues for further investigation that the results from the present study have revealed. Most importantly, the present study has identified preliminary differences between hMDM and hAM purinergic signalling which represents a significant area of interest to follow up upon.

5 Chapter 5: Investigation of Orai contribution to Ca^{2+} signalling and function in human macrophages

5.1 Chapter 5 introduction

Ca^{2+} has been specifically linked to macrophage functions explored in this study e.g. inflammatory mediator production, phagocytic ingestion and phagosomal maturation – however there are a number of gaps in knowledge which show there is scope for further work in this field. This chapter summarises what is already known about Ca^{2+} signalling in macrophage biology and describes the experiments performed as part of this PhD project to investigate the role of Orai in human macrophage signalling.

5.1.1 The role of Ca^{2+} in production of inflammatory mediators from macrophages

The activation of transcription factors, NFAT and NF-κB requires Ca^{2+} signalling (Dolmetsch *et al.*, 1997) as discussed in more depth in ***Section 3.1.1.*** NF-κB and NFAT have both been shown to have a role in innate immune responses and activation of endogenous macrophage receptors including TLR, Dectin and CD14 are known to lead to NFAT and NF-κB activation (Vallabhapurapu & Karin, 2009; Buxadé *et al.*, 2012; Zanoni & Granucci, 2012). We therefore hypothesized that Ca^{2+} signalling is a crucial factor in the control of macrophage transcriptionally activated cytokines.

Recent characterisation of a selenoprotein (SelK) has aided the identification of certain Ca^{2+} regulated functions in macrophage cells. Selenium is an essential micronutrient which has important roles in the regulation of immune cell responses. Selenium is incorporated into selenoproteins as the amino acid selenocysteine which provides it with active properties. (Verma *et al.*, 2011) described for the first time that SelK is an ER localised membrane protein expressed in immune cells. Ca^{2+} signalling assays revealed that the Ca^{2+} signal induced by the TCR, chemokine receptor (CCR) and FcγR respectively was impaired in SelK$^{-/-}$ T cells, neutrophils and BMDMs. Importantly the SelK deletion did not affect signalling induced by thapsigargin, therefore providing evidence that SelK does not change the amount of Ca^{2+} in the ER store, or the SOCE through plasma membrane channels. Later work by the Hoffman group identified that SelK acts to interfere with Ca^{2+} mobilisation through regulating IP$_3$R expression via IP$_3$R palmitoylation (Fredericks *et al.*, 2014). This implicates SelK with a role in the regulation of receptor signalling where involvement of IP$_3$R occurs, FcγR, TCR and CRR all being examples of such receptor signalling cascades.

SelK$^{-/-}$ has been used as a tool by which to impair receptor mediated Ca^{2+} signalling, in a study designed to investigate into FcγR regulated mediator production in BMDM cells (Huang *et al.*, 2012). The authors showed that FcγR stimulation with immune complex caused the release of IL-6, TNFα, monocyte chemoattractant protein-1 (MCP-1), macrophage inflammatory protein-3α (MIP3α) and PGE2 at detectable levels and that in SelK$^{-/-}$ BMDMs there was a reduction in the level of release of TNFα, PGE2, IL-6 up to 50%. As SelK$^{-/-}$ is known to disrupt FcγR mediated Ca^{2+} signalling it is likely that the reduction seen in the release of certain mediators is due to their dependence on Ca^{2+} for their production/secretion. Similarly, FcγR activation of MAPK regulated ERK phosphorylation and resulting proinflammatory cytokine production was impaired in SelK$^{-/-}$ mice, to a similar degree as observed with Ca^{2+} chelation by BAPTA pre-treatment. Two other MAPKs; p38 and c-Jun N terminal kinase (JNK) were not significantly affected by SelK depletion indicating they do not require FcγR mediated Ca^{2+} signalling in the same way. SelK has been demonstrated to have a role in control of IP$_3$ regulated Ca^{2+} mobilization therefore these results suggest that FcγR- regulated mediator release in BMDMs is regulated by Ca^{2+}. In sum, the known Ca^{2+} dependency of NFAT and NF-κB transcriptional activation and evidence supporting Ca^{2+} dependency of FcγR mediated macrophage functions exemplify the importance of Ca^{2+} in macrophage biology.

5.1.2 The role of Ca^{2+} in macrophage phagocytosis

The Ca^{2+} dependency of phagocytosis is controversial. Initial studies linked a rise in intracellular Ca^{2+} with phagocytic ingestion, for example (Young *et al.*, 1984) demonstrated that an increase in intracellular free Ca^{2+} occurred following FcγR receptor activation, with initiation of Ca^{2+} signal seen in seconds and the signal lasting around 5-10 minutes. In the absence of extracellular Ca^{2+}, the FcγR induced Ca^{2+} response was reduced by 70%, concurrently the phagocytic index in J774 and peritoneal mouse macrophages was reduced by 60% and 95%, respectively. Work on mouse peritoneal macrophage cells by (Hishikawa *et al.*, 1991) showed that intracellular Ca^{2+} store depletion is sufficient for one or two phagocytic events of IgG coated beads however extracellular Ca^{2+} influx appear necessary for multiple phagocytic events. Conversely, a study by (McNeil *et al.*, 1986) showed no increase in Ca^{2+} signal during FcγR mediated phagocytosis in mouse peritoneal macrophages. An explanation for the discrepancy seen between these studies could be explained by differences in methodology – with (McNeil *et al.*, 1986) recording the average Ca^{2+} signal in a population of cells rather than Ca^{2+} signal from individual cells, as in (Hishikawa *et al.*, 1991). (Kruskal & Maxfield, 1987) postulated that as phagocytosis is an asynchronous event in different cells, the Ca^{2+} increase occurs in different cells at different times. This could mean that when an average Ca^{2+} signal measurement was made from a cell population any Ca^{2+} changes seen might average out to below the sensitivity of the assay method. (Di Virgilio *et al.*, 1988) compared the Ca^{2+} signal primary macrophages from mouse peritoneum and in the J774 macrophage cell line using quin2 and fura-2 Ca^{2+} indicator dyes and different acquisition methods. Although Di Virgilio and colleagues corroborate that an increase in Ca^{2+} occurs following FcγR activation and subsequent

phagocytotic particle ingestion, in their study no effect on phagocytosis was seen in the absence of extracellular Ca^{2+}, following intracellular Ca^{2+} store depletion. Possibly the simplest interpretation for the conflicting results in the literature is due to numerous receptors simultaneously involved in the control of phagocytosis, with differential Ca^{2+} dependency. Whilst some receptors might signal via an elevation in cytosolic Ca^{2+}, other receptors might not involve Ca^{2+} and therefore the requirement for Ca^{2+} in phagocytosis can be circumvented. This hypothesis is supported by (Lew & Stossel, 1980) – in their study they report that phagocytosis is differentially Ca^{2+}-mediated dependent on the receptor initiating the phagocytic process. For example a change in intracellular Ca^{2+} concentrations reduced FcγR mediated phagocytosis in human neutrophils; whereas C3bR mediated phagocytosis was unaffected. Which step in the ingestion of particles may be regulated by Ca^{2+} is unclear. Moreover, whether differences exist in dependency of phagocytosis on Ca^{2+} in different populations of macrophages *(Section 1.3.4)* is also unclear. These unknown factors highlight gaps in knowledge in this area.

As described in **Section 1.3.3**, phagocytosis is a complex process with many distinct phases involved. Upon particle internalisation into a phagosome, phagosome maturation must occur for the phagocytic cell to destroy the foreign particle. Phagosomal maturation encompasses steps of phago-lysosome fusion and also phagosomal acidification. Interestingly, (Nunes & Demaurex, 2010) suggest that there is more evidence for the phagosome maturation process versus particle ingestion to be dependent on Ca^{2+} signalling. Evidence suggesting a role for Ca^{2+} in phagosomal maturation has been shown in numerous studies. (Downey *et al.*, 1999) perform a study in COS-1/CHO cells transfected with FcγRIIA to infer phagocytic properties to this cell type. Here they found that phagosomal acidification was reduced but not abolished by chelation of intracellular Ca^{2+}. Conversely, (Zimmerli *et al.*, 1996), found that phago-lysosome fusion in hMDMs, as assessed by lysosomal-associated membrane protein 1 (LAMP) markers, was resistant to reduction in intracellular Ca^{2+} concentration. These experiments were performed for phagosomes containing: zymosan, staphylococci and mycobacterium bovis bacillus calmette–guérin (*M. bovis* BCG). However, Zimmerli and colleagues did not assess the intracellular killing mechanisms of the phagocytosed particles and therefore direct comparisons between these two studies cannot be made. (Malik *et al.*, 2000) show evidence for the involvement of Ca^{2+} signalling in phagosome-lysosome maturation and phagosome acidification in hMDMs. Here the Ca^{2+} ionophore ionomycin was shown to increase the rate phagosome-lysosome fusion and phagosome acidification, as assessed by cathepsin D, LAMP-1, CD63 markers and LysoTracker Red to assess phagosomal pH, following *Mycobacterium tuberculosis* (*M. tuberculosis*) infection. Opposite results were seen when Ca^{2+} chelator MAPTAM and EGTA were added in addition to *M. tuberculosis* - supporting the specific role of Ca^{2+} in mediating the phagosome maturation parameters measured. Interestingly the phagosome acidification was not reduced to the same level as phagosome-lysosome fusion in EGTA conditions, suggesting only a small increase in intracellular Ca^{2+} is required for normal acidification. Notably, other experiments performed by (Malik *et al.*, 2000) showed that the involvement of Ca^{2+} in phagosome maturation was dependent on the receptor involved in particle detection. In predominantly complement mediated *M. tuberculosis* phagocytosis, there was no increase in Ca^{2+} and

subsequently *M. tuberculosis* had significantly improved rates of intracellular survival. Alternatively, when *M. tuberculosis* was opsonized to enable FcγR mediated phagocytosis, Ca^{2+} signalling was observed and the intracellular *M. tuberculosis* viability was reduced. Further investigation is required to ascertain whether the role of Ca^{2+} in the phagosome maturation and bacterial killing of *M. tuberculosis* is required for other bioparticle types. However, the apparent coupling of the receptor initiating phagocytosis and Ca^{2+} dependency highlights again that there is distinct variability in the Ca^{2+} dependency of phagocytosis dependent on particle type. In sum, the variability of results from the studies discussed above show the importance of Ca^{2+} in phagocytosis but also indicate the gaps of knowledge in this area.

5.1.3 Evidence implicating Orai in macrophage biology

Evidence supporting a role for Orai & SOCE in macrophage cytokine release and phagocytosis has been described in a small number of studies in rodent macrophages. In mouse peritoneal macrophages SK&F96365, a non-selective SOCC antagonist, caused significant inhibition to LPS + IFNγ mediated Ca^{2+} signals as well as IL-10, TNFα, IL-6 and MCP-1, NO and ROS release. Similarly, phagocytosis of pHrodo® labelled *E. coli* was reduced (~25%) by SK&F96365 pre-treatment. It has been assumed that appropriate vehicle controls have been performed in parallel for these experiments, but no obvious statement of their use was indicated in the text, so interpretations must be made with caution (Ye *et al.*, 2012a; Ye *et al.*, 2012b). In another study in peritoneal macrophages taken from STIM1$^{-/-}$ mice, it was shown that there was an attenuation in FcγR mediated Ca^{2+} signalling and impaired Fcγ-mediated phagocytosis. Following immune complex induced pneumonitis there was a reduction in levels of secreted TNFα and MIP-2 in BALF compared to control mice. *In vivo* studies revealed that STIM1$^{-/-}$ mice were protected against IgG mediated anemia, IgG mediated thrombocytopenia and anti-GPIIb/IIIa induced anaphylaxis. Similarly BALF collected and lung tissue examined following IgG IC-mediated pneumonitis/alveolitis in STIM1$^{-/-}$ mice revealed that C5a mediated neutrophil migration was impaired compared to WT mice. However, it could be argued that *in vivo* work showing involvement of STIM1 in IgG mediated autoimmune disease is not direct evidence of STIM1 involvement in macrophage biology but in any cell where FcγRs are expressed. Nevertheless the *in vitro* work showed attenuation of FcγR Ca^{2+} signalling and FcγR-mediated phagocytosis in STIM1$^{-/-}$ macrophages therefore showing convincing evidence for a role of SOCE signalling in macrophage biology (Braun *et al.*, 2009). In the J774A.1 macrophage cell line CD38 internalisation following FcγR mediated phagocytosis of IgG opsonized particles was shown to be crucial for Ca^{2+} mobilization. The non-selective Ca^{2+} antagonist, SK&F96365 was shown to inhibit FcγR mediated Ca^{2+} signal and IgG bead internalisation, the latter by 38% providing evidence that SOCE – regulated through CD38 is important for FcγR mediated phagocytosis in J774A.1 macrophages (Kang *et al.*, 2012).

Whilst these three studies support a role of SOCE in TLR and FcγR signalling and function, contradictory results were observed by (Vaeth *et al.*, 2015). Inducible ablation of STIM1 and STIM2 in BMDMs caused a significant inhibition to the thapsigargin induced Ca^{2+}

signalling, indicating the functional activity of SOCE in BMDMs, however no alteration in response to STIM1 or STIM2 ablation was found in any macrophage functions tested. Contrary to the study by Braun, Vaeth described no attenuation in the phagocytosis of IgG coated fluorescent beads and *S. aureus* in STIM1 STIM2 ablated BMDMs. Interestingly chelation of intracellular Ca^{2+} with BAPTA did cause a reduction to phagocytosis of IgG coated beads – suggesting some general requirement for Ca^{2+}, however an alternative explanation for the effect of BAPTA could be an alteration to the BMDMs metabolic activity. Assessment of the contribution of STIM regulated Orai to phagosome maturation was also performed, using LAMP markers to assess phago-lysosome fusion no difference was seen in BMDMs from WT and STIM ablated cells. Similarly, PRR ligand mediated cytokine production and activation of NLRP3/NLRP4 inflammasomes was also shown not be affected by STIM ablation. Likewise, T cell responses initiated by BMDMs were not changed in STIM ablated mice. Work by Vaeth and colleagues (2015) suggest that Orai Ca^{2+} signalling is active in macrophages but is not critical for mediating innate functions of the macrophage. The reasons for the differences in the results reported by Vaeth versus Braun could be explained by heterogeneity in the macrophage cells used – peritoneal macrophages were used in Braun et al, whilst BMDMs were used by Vaeth. Nevertheless, together these studies have shown evidence supporting a role for SOCE in rodent macrophage signalling.

To my knowledge there have not been any studies into the contribution of Orai to Ca^{2+} signalling or function in human macrophages, indicating that this is a significant gap in the current picture of macrophage biology. Taken together, the work from mouse models has provided preliminary data suggesting the importance of SOCE in macrophages. Given the potential significance of the findings and the lack of work currently performed in human macrophages the aim of this investigation was to investigate the activity and function of Orai signalling in human macrophages, with the hypothesis that Orai-mediated Ca^{2+} signalling was active and contributing to TLR and FcγR signalling cascades.

5.2 Results

5.2.1 Orai and STIM are expressed in hMDMs at mRNA level

The expression of members of the Orai and STIM families at mRNA level in hMDMs was assessed using quantitative PCR. It is increasingly accepted that the characteristic housekeeping genes such as β- actin are not stably expressed in each cell type (Bustin, 2002). To control for this, as described in Methods *Section 2.5* geNorm experiments were performed find the most stably expressing housekeeping gene in my cell of interest, hMDMs. The results indicate that GAPDH is expressed at consistent levels between the 10 donors tested and has a geNorm stability value of less than 0.40; therefore this gene was used for normalisation in further hMDM qPCR experiments *(Figure 2.10)*. SYBR green primer probe sets were used, validation of primer specificity and efficiency was performed

by performing a melt curve analysis *(Figure 2.7)* and cDNA concentration titration experiments, respectively *(Figure 2.11)*. Together, these validation experiments allow the qPCR data to be interpreted as a relative quantitative assessment of mRNA expression. As shown in *Figure 5.1,* qPCR results demonstrated that all Orai and STIM family members were expressed at mRNA level, with Orai1 and STIM1 ($6.2 \times 10^{-4} \pm 1.2 \times 10^{-4}$ and $7.1 \times 10^{-4} \pm 1.5 \times 10^{-4}$) expressed at significantly higher levels than Orai2 and STIM2 ($1.5 \times 10^{-4} \pm 2.47 \times 10^{-5}$ and $2.4 \times 10^{-4} \pm 4.41 \times 10^{-5}$), respectively. As shown in *Figure 5.1A* there is variability in the expression between hMDM donors, in particular D91232 showed a lower expression of STIM1 and STIM2 than the other four donors evaluated. Nevertheless, expression of each Orai and STIM family member was seen in all donors assessed.
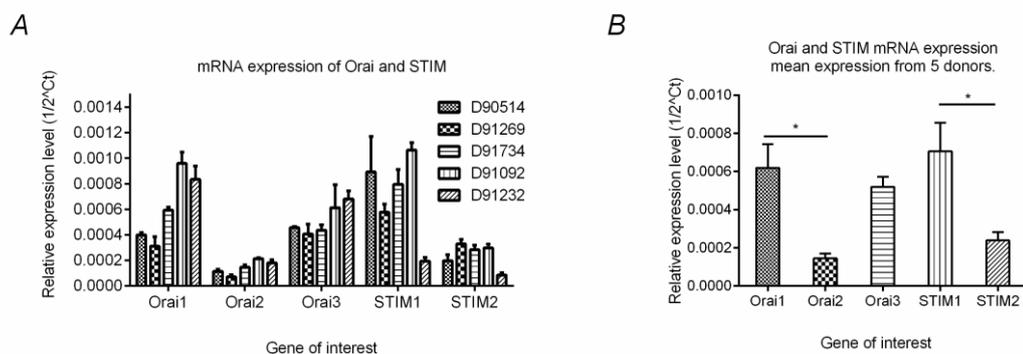
Figure 5.1   Orai and STIM are expressed in hMDMs at mRNA level

*Quantitative PCR was performed using cDNA isolated from hMDM cells; SYBR green primer/probe technology was used to assess mRNA expression. Data is presented as relative expression 1/2^Ct levels and was normalised to GAPDH. **A.)** mRNA expression from each individual hMDM donor, mean ± SEM from donor triplicates **B.)** mean ± SEM expression of all donors tested. Results were analysed using one-way ANOVA with Tukey's multiple comparison test. N=5 donors. * p <0.01, **** p<0.0001*

5.2.2 Thapsigargin initiates a concentration-dependent Ca²⁺ influx in hMDMs

Having obtained evidence of the presence of Orai and STIM mRNA these results warranted further investigation to assess whether the store-operated Orai/STIM channels are functionally active in hMDM cells. Ca^{2+} signalling assays following passive store depletion using thapsigargin and FLIPR were used as described in *Section 2.3.2*. Results show that thapsigargin initiated a concentration-dependent Ca^{2+} signal in hMDMs, with two kinetically distinguishable phases at concentrations of 0.12µM and above *(Figure 5.2)*.

Based on zero external Ca^{2+} controls (mean area under curve 803.4 ± 289 N=6) *(Figure 5.2B&E)* the data suggests that the initial faster and smaller increase in the Ca^{2+} signal, with maximum signal reached by 3 minutes is caused by Ca^{2+} release from the intracellular stores, whilst the larger more sustained Ca^{2+} signal rise (mean area under curve 1863 ± 243 N=6, with maximum signal reached by 15minutes) is formed by Ca^{2+} influx across the plasma membrane. The concentration-response relationship exhibited by thapsigargin in hMDMs showed a bell shaped curve, concentrations of thapsigargin higher than 3.3μM exhibited a less than maximal response. The pEC50 for thapsigargin in this cell type was 7.2 ± 0.2 N=6, as calculated from the whole concentration range. These data indicate that there are SOCCs present in hMDMs, with a potential contribution from Orai/STIM channels.

5.2.3 GSK-7975A significantly inhibits the Ca^{2+} signal initiated by thapsigargin

To confirm the contribution of Orai channels to the Ca^{2+} influx mediated by thapsigargin, an Orai selective antagonist was utilized. GSK-7975A is a well validated compound that has been shown to have a high selectivity for Orai channels over a number of other ion channels and receptors (Derler *et al.*, 2013). Importantly it is insensitive to TRPC channel proteins (at concentrations 10μM and lower) unlike the majority of the SOCE inhibitors used *(Section 1.4.10)*. Preincubation of hMDMs for 15 minutes with GSK-7975A inhibited the thapsigargin mediated Ca^{2+} entry in a concentration-dependent manner *(Figure 5.2B&D)*. The IC50 of GSK-7975A from these experiments was 1.9μM or pIC50 6.0 N=4. This is in line with previously published values for this inhibitor in heterologously expressed channels in RBL (pIC50 6.1 ± 0.1) and Jurkat T cells (pIC50 6.3 ± 0.03) (Derler *et al.*, 2013; Rice *et al.*, 2013). The initial Ca^{2+} signal (6.86% of max ± 4.37 N=4) observed in the presence of 10μM of GSK-7975A is likely to represent Ca^{2+} release from intracellular stores, based on the data obtained with thapsigargin applied in zero external Ca^{2+}, showing a signal in the same order of magnitude. Taken together the qPCR data and Ca^{2+} signalling studies provides compelling evidence for the expression of functional Orai channels in hMDMs.
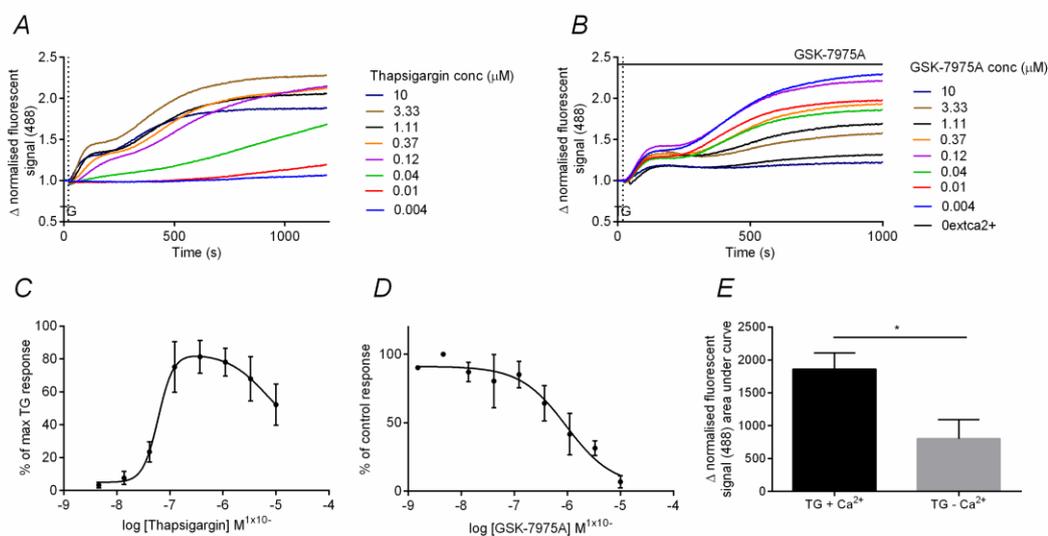
Figure 5.2 **Thapsigargin (TG) activates concentration-dependent Ca²⁺ influx in hMDMs that is sensitive to inhibition by the Orai selective antagonist, GSK-7975A**

Ca²⁺ imaging of hMDMs loaded with fluo-4, using FLIPR. **A.)** *Ca²⁺ signal over time, 1µM TG was applied at t=30s and kept constant throughout. Signal was normalised to baseline fluorescent value. This is a representative trace from N=5 donors tested* **B.)** *Ca²⁺ signal over time, 1µM TG added at t=30s to varying concentrations of GSK-7975A which was pre-incubated for 15mins prior to agonist application and kept constant throughout. Signal was normalised to baseline fluorescent value.* **C.)** *Concentration-response curve to TG, showing percentage of max Ca²⁺ response N=5 donors.* **D.)** *Concentration-response curve – response to 1µM TG in the presence of varying concentrations of GSK-7975A, graph showing percentage of control response. N=5 donors. Concentration-response graphs calculated using area under curve values from normalised signal/time.* **E.)** *Bar graph representing the Ca²⁺ signal induced by 1µM TG in hMDM cells incubated with and without Ca²⁺ as a component of the external solution, mean ± SEM. Results were analysed using an unpaired t-test. N=5 donors. * p <0.01, **** p<0.0001*

5.2.4 TRPC3/6 agonist GSK-2934A has no effect on Ca²⁺ signalling in hMDMs

TRPC channels have often been shown to act in concert with Orai channels (Ambudkar *et al.*, 2007; Liao *et al.*, 2007; Liao *et al.*, 2009; Smyth *et al.*, 2010) with some subtypes shown to have a store-operated mode of activation. For these reasons, it was investigated whether TRPC channels were also active in hMDMs. For most TRPC subtypes, selective pharmacological tools are not available to allow discernment of individual channel contribution, however recently validated selective TRPC3/6 agonists and antagonists are currently the exception (Seo *et al.*, 2014b). Therefore the effect of the selective TRPC3/6 agonist – GSK-2934A was tested in hMDMs. Previously, it was shown that the EC50 for TRPC3/6 agonist in a TRPC6 HEK cell line was 0.5µM **(Figure 3.10)**, however experiments in

168

hMDMs showed that concentrations in the range of 0.03-10µM did not induce any Ca^{2+} signal (data not shown); therefore suggesting that TRPC3/6 is not functionally active in hMDMs.

Taken together the data presented in *Figures 5.1&5.2* provides novel evidence for the functional activity of Orai-mediated Ca^{2+} signalling in hMDM cells. This is an exciting finding that leads to the question; what is the role of Orai-mediated Ca^{2+} entry in hMDMs. As discussed in *Section 1.1.3*, the discernment of the role of Orai in other immune cells has shown the SOCC to have crucial roles in immunology. Further work in my study addresses Orai-mediated Ca^{2+} signalling in control of human macrophage functions.

Macrophages express a number of endogenous surface receptors which can initiate a range of signalling cascades. Although thapsigargin is a useful tool to assess SOCCs, it is not a physiological agonist and is a relatively crude tool for studying Orai channel activity. Consequently, experiments were performed to investigate whether Orai-mediated Ca^{2+} entry contributed to signalling downstream of an endogenous macrophage receptor. Receptors which have been implicated in the initiation of signalling cascades with a potential for SOCC activation were considered; FcγR, TLR, Dectin and chemokine receptors are all examples of such receptors. As described in *Section 5.1* there are a number of studies which show evidence to support the involvement of Orai in TLR and FcγR signalling, based on this preliminary evidence the contribution of Orai to FcγR and TLR signalling was focused upon in my study.

5.2.5 LPS (+IFNγ) mediated cytokine release was not sensitive to GSK-7975A inhibition

Investigation into the contribution of Orai signalling to LPS mediated Ca^{2+} entry was performed in experiments presented in *Figures 5.3 & 5.4.* As summarised in *Section 5.1*, a number of studies have shown that inhibition of SOCE can lead to impairment in the LPS mediated cytokine release, in particular that of IL-6 and TNF-α. Cytokine assays using MSD ELISA plates were performed to ascertain the importance of Orai-mediated Ca^{2+} signalling in LPS mediated cytokine release from hMDM cells. 100ng/ml of LPS was applied to hMDMs for 24 hours and supernatants collected after this stimulation period. 100ng/ml concentration of LPS was chosen based on the concentration-response of TNF-α release to a titration of LPS. Results presented in *Figure 5.3* shows that LPS induced the release of a number of cytokines, including; TNFα, IL-6, IL-1β, IL-12p70, IL-13, and IL-10 were detected within the upper and lower limits of detection. IL-8 was detected but above the higher limits of detection. IL-12p70 and IL-1β were released in the range of 62-80 in LPS stimulation conditions, IL-13 at 475.2 ± 21.32, IL-6 at 6006 ± 617 whereas IL-10 and TNFα were released at 15599 ± 3807 and 65248 ± 3294 respectively (all ng/ml mean ± SEM N=4). To compare the results of this present study with the work reported in peritoneal macrophages (Ye *et al.*, 2012a) stimulation of hMDMs with LPS + IFNγ was also performed. Interestingly, in comparison to LPS treatment alone, the release of IL-12p70 and TNFα was

significantly higher, with an increase in release from 79.61 ± 9.73 to 461 ± 108.0 and 65248 ± 3291 to 118848 ± 8852 (ng/ml, mean ± SEM N=4) whereas release of IL-10 was significantly reduced to 4295 ± 1478 from 15599 ± 3807 (ng/ml, mean ± SEM N=4). Other cytokines were not significantly affected by addition of IFNγ. Notably, there was no significant reduction in cytokine release in conditions where 10µM GSK-7975A has been pre-applied. This data suggests that Orai-mediated Ca^{2+} entry is not required for TLR4 mediated cytokine release.
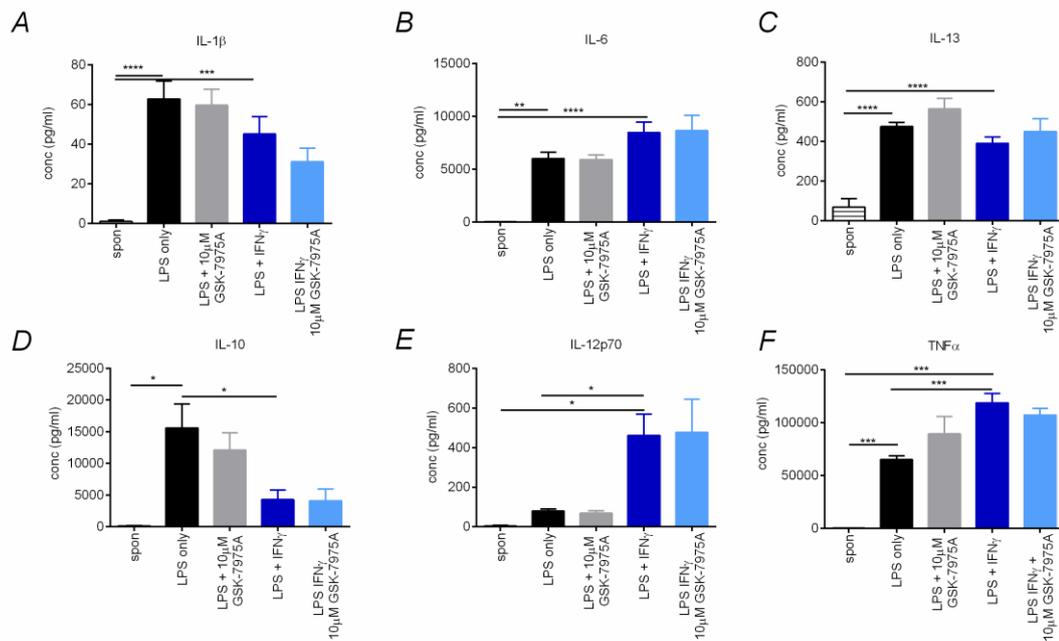
Figure 5.3 **Effect of 10µM GSK-7975A on LPS (+IFNγ) stimulated cytokine release from hMDMs**

hMDMs were activated with 100ng/ml LPS or 100ng/ml LPS + 10ng/ml IFNγ for 24hrs with 10µM GSK-7975A pre-applied for 15 minute before stimulus and kept constant throughout. After 24hr incubation, supernatants were collected, diluted 1:10 and run on pro-inflammatory V-plex MSD plate. Of the 10 cytokines present in the blot: IL-6, IL-8, TNFα, IL-10, IL-12p70, IL-13 and IL-1β were detectable at levels well above the lower limit of detection. Graphs show the concentration in pg/ml, mean ± SEM. Results were analysed using one-way ANOVA with Tukey's multiple comparison test. N=3 donors. * p <0.01, **** p<0.0001

5.2.6 LPS did not induce a significant increase in Ca^{2+} signal, over a time course of 20 minutes, in hMDMs

Although, the cytokine assays revealed no role for Orai-mediated Ca^{2+} signalling in LPS mediated cytokine production, there is evidence to suggest that LPS initiates Ca^{2+} entry **(Section 5.1)**, FLIPR experiments were undertaken to investigate the Ca^{2+} signalling

occurring downstream of TLR4. No Ca^{2+} signal increase was observed following application of 0.1-1000ng/ml LPS, over a time course of 20 minutes **(Figure 5.4)**. However a small increase in Ca^{2+} signal was seen at 80 minutes following LPS addition at concentration of 37.03μM and below. The change in the Ca^{2+} signal seen at 80 minutes to 37.03μM was significant compared to the vehicle control wells (mean normalised Ca^{2+} signal 1.53 ± 0.03 in 37.03μM LPS and 1.28 ± 0.01 in spontaneous control, N=3) , however no concentration-dependency to the response was seen (response to LPS at 80minutes showed a normalised Ca^{2+} signal in the range of 1.51-1.56 at 37.03μM concentration), posing the question as to whether it was a direct LPS-TLR4 mediated Ca^{2+} signal or whether an indirect mechanism was causing the activation. These experiments were also performed in IFNγ primed hMDMs with the same effect on LPS reported (data not shown). Due to the lack of concentration-dependency seen and the very small dynamic window seen in the response, no further experiments into the Ca^{2+} signalling downstream of LPS were performed.
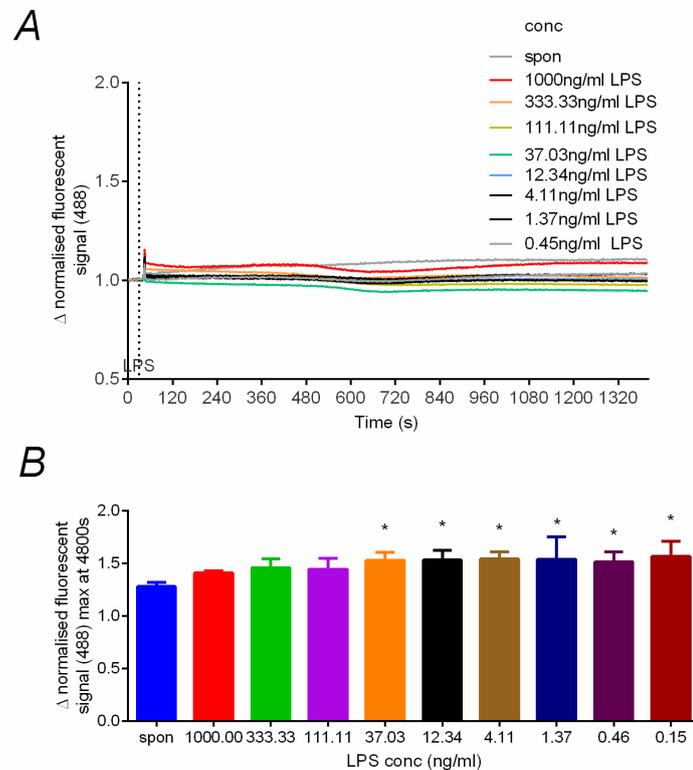
Figure 5.4   LPS application to hMDMs results in no concentration-dependent change to the Ca^{2+} signalling

*Ca^{2+} imaging of hMDMs loaded with cal-520 using FLIPR. **A.)** Ca^{2+} signal over time, LPS at a range of concentrations was applied at t=30s and kept constant throughout, signal was normalised to baseline fluorescent value. This is a representative trace from N=3 donors tested **B.)** Bar graph showing the normalised Ca^{2+} signal at t=4800s, following LPS application, mean ± SEM of all donors tested. Results were analysed using one-way ANOVA with Tukey's multiple comparison test. N= 3 donors. * p <0.01, **** p<0.0001*

5.2.7 Anti-IgG causes a concentration-dependent increase in Ca²⁺ signal in hMDMs

In the FcγR signalling cascade; following ITAM phosphorylation, Syk and LYN pathways are initiated leading to activation of PLCγ (Crowley *et al.*, 1997; Wen *et al.*, 2002), generation of IP_3, store emptying and SOCE. It is therefore possible that signalling downstream of FcγR activation initiates Ca^{2+} influx that is mediated by STIM and Orai, in a similar manner to FcεRI and T cell receptor activation. Experiments were performed to address the contribution of Orai-mediated Ca^{2+} signalling to FcγR signalling.

FLIPR experiments revealed that Anti-IgG initiated a concentration-dependent Ca^{2+} signal with kinetics markedly different from those induced by thapsigargin. In response to Anti-IgG the Ca^{2+} signal reached its maximum by 4 minutes following agonist application and then gradually decreases back to baseline levels *(Figure 5.5)*. Whereas following thapsigargin activation the signal was sustained throughout the 20 minute experiment duration *(Figure 5.2).* The continual presence of thapsigargin throughout the experiment duration would be causing permanent store depletion (SERCA ATPase inhibitor), subsequently a continual Orai activity and sustained signal is possible. However the activation of FcγR may not lead to full store depletion and the signal is also dependent on the receptor-PLC coupling and the inhibitory activity of FcγRIIb to restrict activation; therefore differences in kinetics are not unexpected. The initial rise in the Ca^{2+} signal induced by Anti-IgG was not composed of two kinetically distinct phases, however Anti-IgG induced Ca^{2+} signal in 0 $extca^{2+}$ conditions was of a significantly smaller magnitude and duration compared to the signal induced in the presence of Ca^{2+}. The mean Ca^{2+} signal induced by 1/100 Anti-IgG in external Ca^{2+} was 519 ± 161, whereas the Ca^{2+} signal caused by Anti-IgG application in zero external Ca^{2+} numbers was 88.16 ± 28.64 (area under curve values, mean ± SEM, N=6) *(Figure 5.7B).* This demonstrates that the Anti-IgG Ca^{2+} signal is composed of an intracellular store release component in addition to Ca^{2+} influx occurring through plasma membrane Ca^{2+} channels. Although the concentration-response curve data *(Figure 5.5B)* does not indicate that the maximum response has been reached with 1/30 concentration, due to the volume of Anti-IgG required even for 1/30 dilutions it was deemed uneconomical to use higher concentrations. Instead it was considered whether the conditions for measuring Ca^{2+} signalling downstream of the FcγR could be optimised to obtain a response with a greater magnitude.
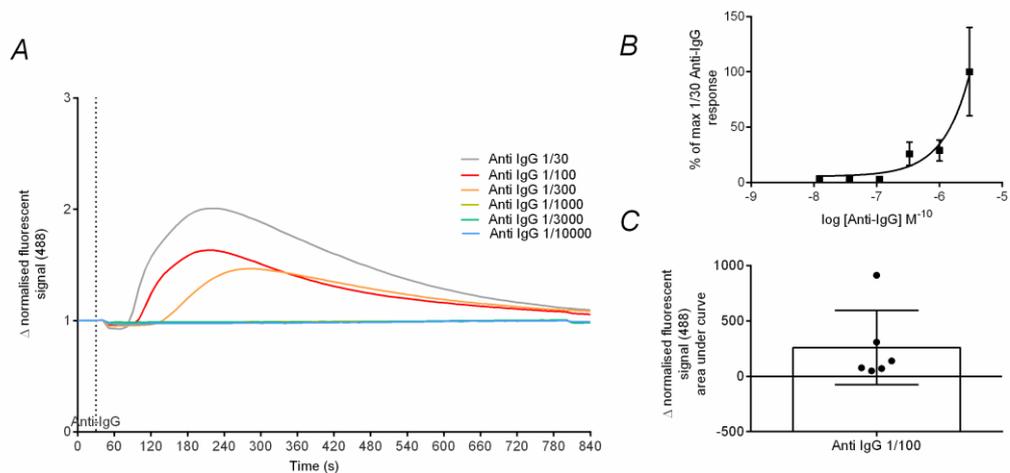
Figure 5.5   **Anti-IgG induces a concentration-dependent Ca^{2+} signal in hMDMs**

*Ca^{2+} imaging of Cal-520 loaded hMDMs using FLIPR. **A.)** Ca^{2+} signal over time, Anti-IgG was applied at t=30s at a range of concentrations, and kept constant throughout. Signal was normalised to baseline fluorescence value. This is a representative trace from N=6 donors. **B.)** Concentration-response curve, mean ± SEM values from all donors plotted as % of signal mean signal induced by 3µg/ml response (max concentration used), response calculated from area under curve values. **C.)** Signal in response to 1/100 Anti-IgG, area under curve value for each donor tested, mean ± SEM. N=6*

5.2.8 FcγRI/CD64 mRNA and protein expression was enhanced by IFNγ priming

As there are both inhibitory and activatory FcγR *(Section 1.3.5)* that may be co-activated, the ratio of activatory and inhibitory receptor expression is likely to dictate whether an ITAM or ITIM signalling cascade predominates (Nimmerjahn & Ravetch, 2008b). Importantly, ITAM directed signalling is expected to lead to Ca^{2+} entry, whereas ITIM turns off Ca^{2+} signalling by inactivation through SHIP. Expression analysis of the FcγR subtypes was performed to investigate the ratio of inhibitory and activatory subtypes in hMDMs. qPCR data shows that the high affinity activatory subtype, FcγRI, was expressed at relatively low mRNA levels in unprimed hMDMs ($8.9 \times 10^{-4} \pm 2.2 \times 10^{-4}$, relative expression mean ± SEM, N=5), with no significant difference between the level of FcγRI and FcγRIIb ($1.3 \times 10^{-3} \pm 2.5 \times 10^{-4}$, relative expression mean ± SEM, N=5) *(Figure 5.6)*. It is likely that a consequence of relatively low FcγRI mRNA expression was translated in the results of Ca^{2+} imaging FLIPR experiments. Anti-IgG was shown to initiate a Ca^{2+} signal however the magnitude of this signal was relatively small and variable between donors *(Figure 5.5C)*. It is well established in the literature that FcγRI expression, the high affinity FcγR subtype, can be enhanced via priming with IFNγ (Kårehed *et al.*, 2007; Sellge *et al.*, 2014), studies have also indirectly shown that other agents such as LPS and TNFα can initiate an increase in FcγR expression (Rubel *et al.*, 1999; Wijngaarden *et al.*, 2008). The effect of IFNγ/LPS/TNFα

priming on FcγR expression was investigated here, concentrations of these priming agents used in my study was based from the literature; however a range of concentrations were tested in preliminary experiments to find the EC80. Ca^{2+} imaging FLIPR experiments showed that IFNγ but not LPS or TNFα cause a significant increase in the Anti-IgG mediated Ca^{2+} influx, following 24 hour IFNγ priming this was an average signal change from 306.1 ± 78.8 to 972.3 ± 283.2 (area under curve mean ± SEM, N=4) *(Figure 5.7)*. Following 24hour IFNγ priming of hMDM cells, qPCR data confirmed a significant up regulation in the FcγRI mRNA levels, with an approximate 10 fold increase in mRNA levels in primed cells (from $8.9X10^{-4}$ ± $2.2x10^{-4}$ to $1.03X10^{-2}$ ± $7.6x10^{-4}$, relative expression mean ± SEM, N=5). FcγRIIb was found to be down regulated, however the decrease of FcγRIIb expression was not statistically significant ($1.34x10^{-3}$ ± $2.5x10^{-4}$ down to $5.95x10^{-4}$ ± $1.0x10^{-4}$, relative expression mean ± SEM, N=5). Flow cytometry experiments indicated that FcγRI protein expression was also increased following IFNγ priming, with the MFI in unprimed cells was 4162 ± 1034 whilst in IFNγ primed cells it was more than 5 fold higher at 23900 ± 2579 (mean ± SEM, N=4) *(Figure 5.8).* These results show that priming of hMDMs with IFNγ for 24hour increases high affinity activatory FcγRI subtype expression. Moreover is also enhanced the Anti-IgG mediated Ca^{2+} signal, providing a signal with a larger dynamic window.
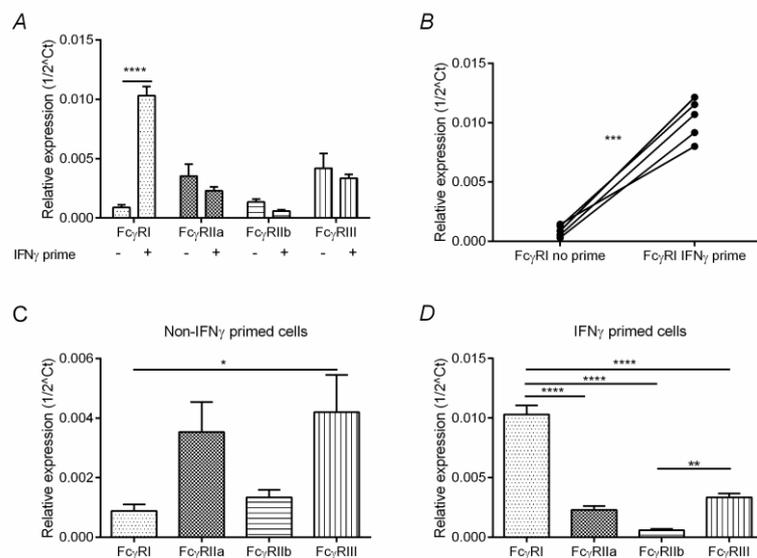
Figure 5.6   FcγR subtypes expressed in hMDMs at mRNA level, FcγRI mRNA expression is enhanced following 24hr priming with IFNγ

*Quantitative PCR was performed using cDNA isolated from hMDM cells; SYBR green primer/probe technology was used to assess mRNA expression. Where stated hMDMs were primed for 24hr with IFNγ at 10ng/ml. Data is presented as relative expression 1/2^Ct levels and was normalised to housekeeping gene levels. **A.)** mean ± SEM expression of all donors tested. **B.)** each data point represents the FcγRI mRNA expression level of each donor tested, before and after IFNγ priming. **C.)** Mean mRNA expression of all FcγR subtypes before IFNγ priming. **D.)** Mean mRNA expression of all FcγR subtypes after IFNγ priming. Results were analysed using one-way ANOVA with Tukey's multiple comparison test... N=5 donors. * p <0.01, **** p<0.000*
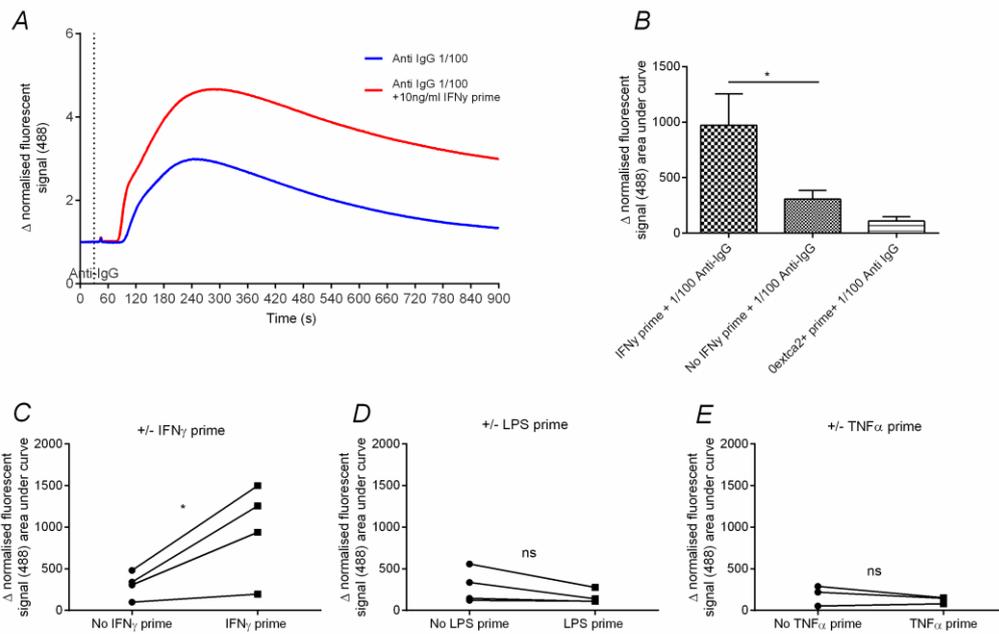
Figure 5.7   Anti-IgG induced Ca^{2+} signalling is enhanced by IFNγ priming but unaffected by TNFα and LPS treatment

*Ca^{2+} imaging of hMDMs using FLIPR. **A.)** Ca^{2+} signal over time, 1/100 Anti-IgG was applied at t=30s to hMDMs with and without IFNγ priming (10ng/ml for 24hr). This is a representative trace from N=4 donors. **B.)** bar graph showing mean Ca^{2+} signal ± SEM in response to 1/100 Anti-IgG with and without prior IFNγ priming + 0extca^{2+} control **C-E.)** Scatter plot showing values of the Ca^{2+} signal in response to 1/100 Anti-IgG (area under curve) from all donors –C.) With and without prior IFNγ priming **D.)** With and without LPS priming for 24hr (111ng/ml). **E.)** With and without prior TNFα priming for 24hr (11ng/ml). Results were analysed using students paired t-test. N=4. * p <0.01, **** p<0.0001*
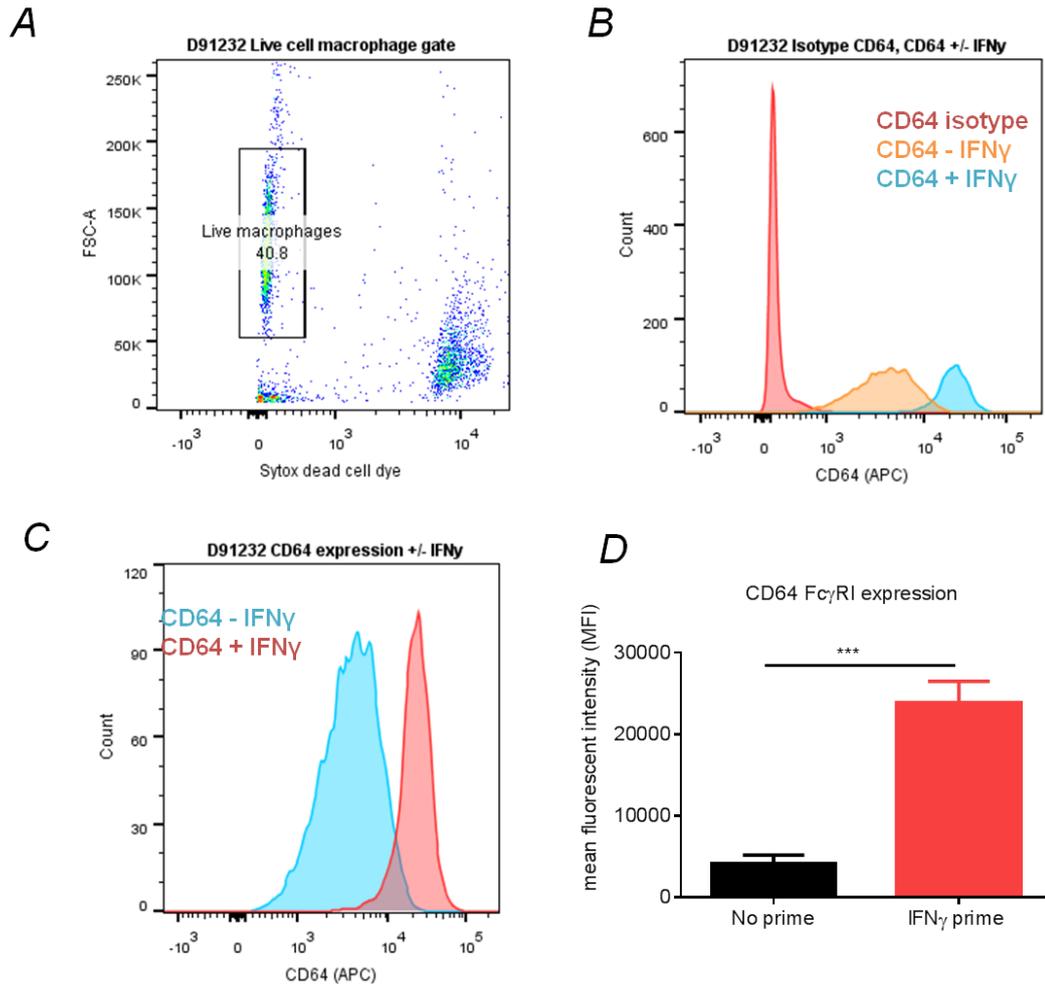
Figure 5.8   FcγRI protein expression is enhanced following 24hr priming with IFNγ

*The expression of FcγRI in hMDMs at protein level was quantified using flow cytometry. Where stated hMDMs were primed for 24hr with IFNγ 10ng/ml. A single population of hMDM cells were used in the experiments, cells were blocked with FcX solution to prevent nonspecific binding prior to incubation with a conjugated CD64/FcγRI antibody (5μL/1mil cells). **A.)** Scatter plot of the events recorded in a typical experiment, Sytox dead cell dye and FSC were used to create a gate for live hMDM cells. **B.)** Representative histogram from one donor to show the mean fluorescent intensity of cells stained with FcγRI antibody +/- IFNγ priming or the FcγRI isotype control. **C.)** Representative histogram from one donor, showing the MFI of cells stained with FcγRI antibody +/- IFNγ priming. **D.)** Bar graph summarising the MFI values in +/- IFNγ priming conditions from all donors tested, mean ± SEM. Results were analysed using paired students t-test. N=5. * p <0.01, **** p<0.0001*
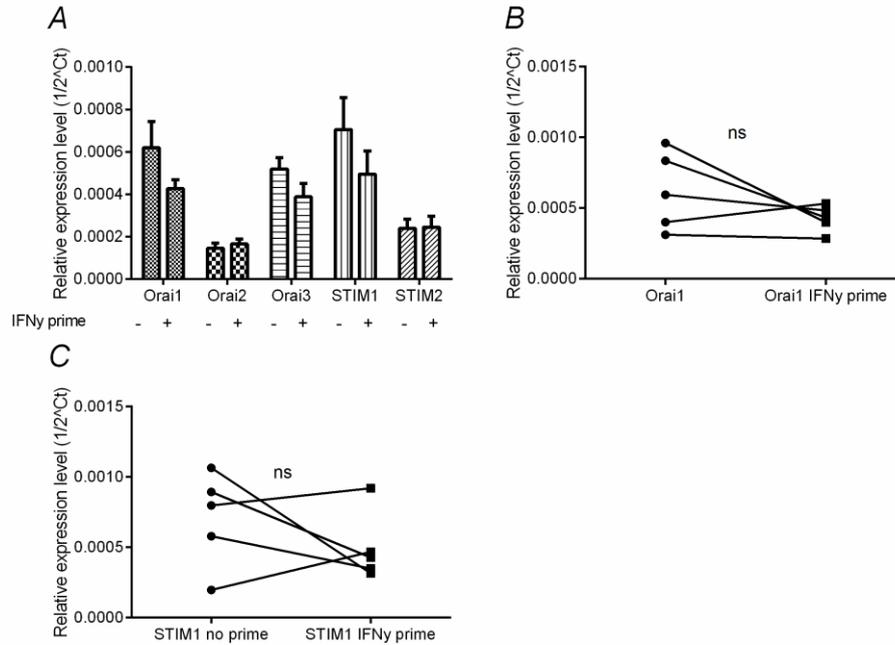
Figure 5.9   Orai and STIM mRNA expression   is not significantly altered by IFNγ priming

*Quantitative PCR was performed using cDNA isolated from hMDM cells; SYBR green primer/probe technology was used to assess mRNA expression. Data is presented as relative expression 1/2^Ct levels and was normalised to housekeeping gene levels. **A.)** mRNA expression as mean of data from all donors before and after IFN priming. **B&C.)** Graph showing data points from each individual donor, mRNA expression before and after IFN priming **B.)** Orai1, **C.)** STIM1. From each individual hMDM donor. Results were analysed using paired students t-test. N=5. * p <0.01, **** p<0.0001*

To investigate whether the enhanced Ca^{2+} signal in IFNγ primed cells was caused by an increase in Orai/STIM mRNA level, qPCR experiments were performed to assess the mRNA in IFNγ primed cells. As shown in **Figure 5.9**   there was no significant effect on the expression of Orai and STIM mRNA levels following IFNγ priming (Orai1 expression = 6.20×10^{-4} ± 1.2×10^{-4} in unprimed conditions and $4.26 \times 10^{-4} \pm 4.2 \times 10^{-5}$ in IFNγ prime conditions, STIM1 expression = $7.05 \times 10^{-4} \pm 1.50 \times 10^{-4}$ in unprimed conditions and $4.95 \times 10^{-4} \pm 1.09 \times 10^{-4}$ in IFNγ prime conditions, relative expression mean ± SEM, N=5). To assess whether the functional activity of SOCCs were enhanced independent of receptor; Ca^{2+} imaging experiments were performed to compare the Ca^{2+} influx initiated by thapsigargin in IFNγ primed cells vs. unprimed cells. No difference in thapsigargin mediated Ca^{2+} signalling was seen (Ca^{2+} signal, area under curve was 598.1 ± 97.9 in non primed cells and 609.3 ± 61.1 in IFNγ primed cells, mean ± SEM, N=4) **(Figure 5.10).** These data strongly suggest that there was no change to the Orai expression or functional activity in IFNγ primed cells and that the priming activity occurs at the level of the FcγRI receptor. Based on these results further experiments investigating Ca^{2+} signalling via FcγR were performed in IFNγ primed cells.
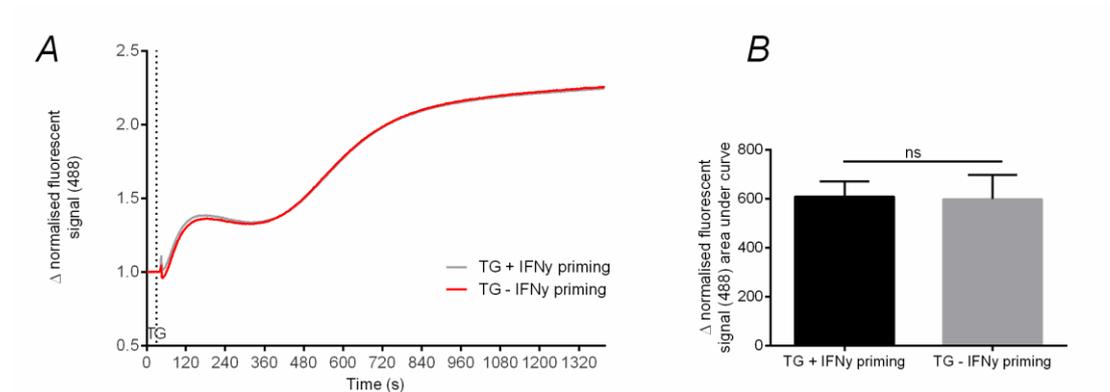
Figure 5.10 **Thapsigargin induced Ca^{2+} signalling in hMDMs is not altered by IFNγ priming**

*Ca^{2+} imaging of hMDMs loaded with Cal-520 using FLIPR. Overlaid data from control unprimed (grey trace) and hMDMs primed for 24hr with IFNγ 10ng/ml (red trace). **A.)** Ca^{2+} signal over time, 1µM TG was applied at t=30s and kept constant throughout. Signal was normalised to baseline fluorescent value. These are representative traces from N=3 donors tested showing TG induced Ca^{2+} signal with and without IFNγ priming. **B.)** Bar graph quantifying the TG mediated Ca^{2+} signal, calculated using area under the curve values from signal/time data, in +/- IFNγ conditions, mean ± SEM. Results were analysed using an unpaired students t-test. N=3.* p <0.01, **** p<0.0001*

5.2.9 Anti-IgG Ca^{2+} signalling is abolished following inhibition of Syk, with GSK-161A

To confirm that Anti-IgG application was initiating the signal transduction downstream of FcγRI, experiments were performed to disrupt the FcγR signalling cascade, through inhibition of Syk with GSK-161A (otherwise known as NVP-QAB-205). Syk is well defined as a critical step in the FcγR pathway (Crowley *et al.*, 1997). GSK-161A is a well validated Syk inhibitor and was shown to inhibit Anti-IgE mediated tryptase release in cord blood derived monocytic cells (CBDMCs) with a pIC50 of 7.2 and 7.1 in screening experiments (Kaur *et al.*, 2013). In my study, Ca^{2+} imaging experiments showed that GSK-161A caused a concentration-dependent inhibition of the Anti-IgG mediated Ca^{2+} signal in IFNγ primed hMDMs *(Figure 5.11)* with a pIC50 of 7.3 ± 0.05, (mean ± SEM, N=3). Following stimulation with 1/100 Anti-IgG in the presence of 1µM of GSK-161A, there was a Ca^{2+} signal that was 1.3% ± 0.5 of the max, indicating Syk inhibition ablated Ca^{2+} store depletion, as would be expected based on its position in the signalling cascade. This data gives convincing evidence that Anti-IgG initiated a Syk-dependent FcγR signalling cascade.
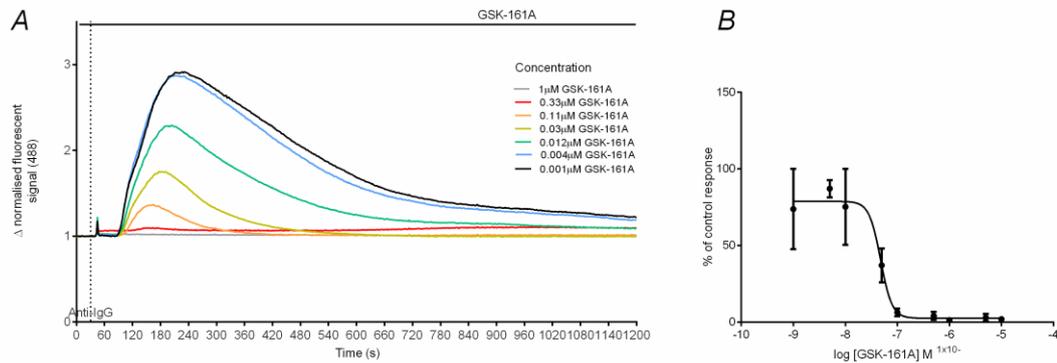
Figure 5.11 **Anti-IgG induced Ca^{2+} signalling in IFNγ primed hMDMs is inhibited by Syk antagonist GSK-161A in a concentration-dependent manner**

*Ca^{2+} imaging of hMDMs loaded with Cal-520 using FLIPR, hMDMs were primed for 24hr with IFNγ 10ng/ml. **A.)** Representative trace of Ca^{2+} signal over time, 1/100 Anti-IgG was applied at t=30s to hMDMs after cells were pre-incubated with GSK-161A for 15minutes, solutions kept constant throughout. Signal was normalised to baseline fluorescent value. **B.)** Concentration-response curve to varying concentrations of GSK-161A followed by 1/100 Anti-IgG challenge, showing percentage of control response, calculated from area under curve values of signal/time data. N=3 donors.*

5.2.10 GSK-7975A inhibits Anti-IgG mediated Ca^{2+} signalling in IFNγ primed hMDMs in a concentration-dependent manner

Thus far the data presented shows that in IFNγ primed hMDMs, Anti-IgG application initiates a robust Syk-dependent Ca^{2+} signal with an intracellular store release component and Ca^{2+} influx through plasma membrane channels. To ascertain whether Orai channels are mediating part or all of the Anti-IgG mediated Ca^{2+} signal, the Orai selective antagonist, GSK-7975A was used. FLIPR experiments showed that GSK-7975A caused a concentration-dependent reduction in the Anti-IgG induced Ca^{2+} signal in IFNγ primed hMDMs **(Figure 5.12)**. The IC50 of GSK-7975A on the Anti-IgG mediated Ca^{2+} signal was 1.55x10^{-6}M/pIC50 = 5.8 ± 0.3, mean ± SEM, N=9 and 10μM GSK-7975A inhibited 84.75% of the Ca^{2+} signal. The IC50 was in line with that in thapsigargin activating conditions (1.93x10^{-6}M). As seen in the thapsigargin experiments, 10μM GSK-7975A did not cause a full inhibition of Ca^{2+} signal, however the zero external Ca^{2+} controls showed a remaining Ca^{2+} signal of the same order of magnitude and with the same kinetics, indicating any remaining signal is composed of Ca^{2+} release from internal store depletion. This gives convincing evidence of the contribution of Orai channels to FcγR mediated Ca^{2+} entry in IFNγ primed hMDMs, a novel and significant finding. Having linked FcγR Ca^{2+} signalling with a dependence on Orai – further experiments were performed to address the functional application of these findings.
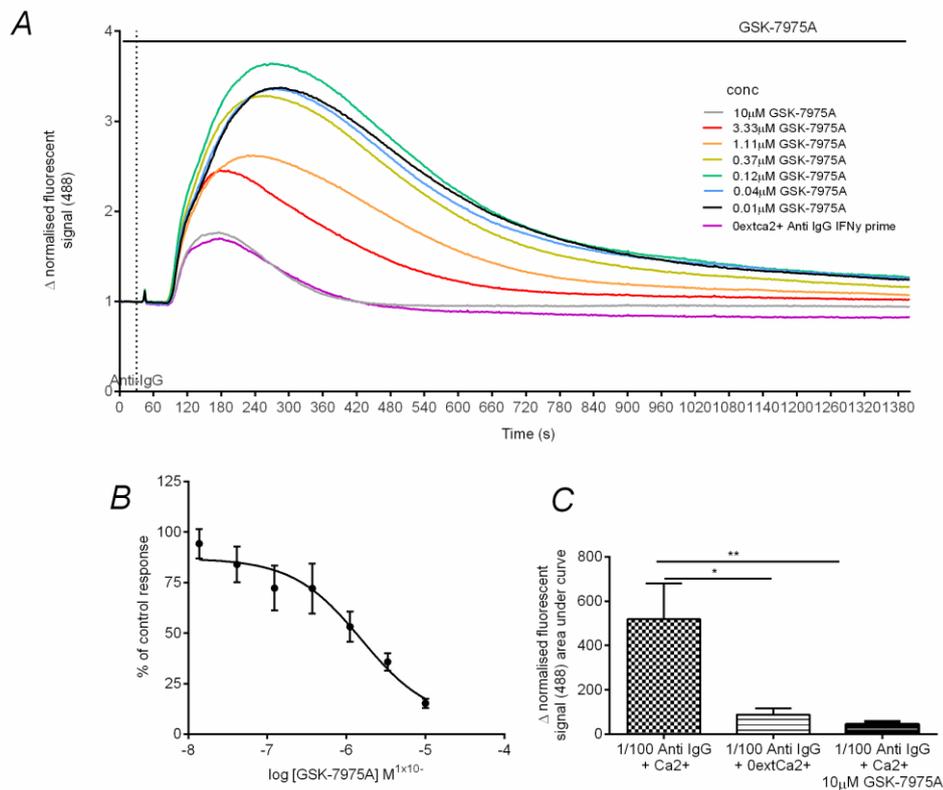
Figure 5.12 **Anti-IgG induced Ca^{2+} signalling in IFNγ primed hMDMs is inhibited by Orai antagonist GSK-7975A in a concentration-dependent manner**

*Ca^{2+} imaging of hMDMs loaded with Cal-520 using FLIPR, hMDMs were primed for 24hr with IFNγ 10ng/ml **A.)** Representative Ca^{2+} signal over time trace, 1/100 Anti-IgG was applied at t=30s to hMDMs that were pre-incubated with GSK-7975A for 15minutes – both kept constant throughout. Signal was normalised to baseline fluorescent value. **B.)** Concentration-response curve to varying concentrations of GSK-7975A followed by 1/100 Anti-IgG challenge, showing percentage of control response. N=9 donors. **C.)** Bar graph summarising the mean Ca^{2+} signal induced by 1/100 Anti-IgG in cells bathed in external solution with and without Ca^{2+}. B&C calculated using area under curve values from normalised signal/time data. Results were analysed using student's unpaired t-test. N=3 donors. * p <0.01, **** p<0.0001*

5.2.11 Anti-IgG (+LPS) activation of IFNγ primed hMDMs did not lead to a significant release of proinflammatory cytokines

As discussed in **Section 1.3.3**, the release of cytokines from macrophages is another key role in which they carry out their immune function. Data in **Figure 5.4** showed that Orai was not a contributor to LPS mediated cytokine release in hMDMs. Emerging data is

highlighting the importance of FcγR in regulating cytokine release in co-ordination with PRR activation, although FcγR activation alone is not sufficient to induce cytokine production (Vogelpoel *et al.*, 2015). Due to the novel findings in the present study of Orai contribution to FcγR signalling the involvement of Orai to FcγR-mediated cytokine release in human macrophages was investigated.

Cytokine assays were performed in IFNγ primed hMDM cells, supernatants were collected 24hour after agonist application and the LPS + Anti-IgG stimulus was kept constant throughout. The release of IL-1β, IL-12p70, IL-2, IL-4, IL-6, IL-8, IL-10, IL-13, and TNF-α was measured, the release of IL-13, IL-8, IL-6, IL-10 and TNFα was detected within the upper and lower limits of detection, however no significant decrease was seen through the application of 10μM GSK-7975A. Also, no significant difference was seen in the cytokine release between the LPS and the LPS with supplemented Anti-IgG stimuli, except for IL-13 which was significantly enhanced by a dual stimulus of LPS + Anti-IgG *(Figure 5.13).* These results demonstrate that there was no significant involvement of GSK-7975A sensitive Ca^{2+} channels in the production of cytokines initiated by TLR4 and FcγR activation in IFNγ primed hMDMs.
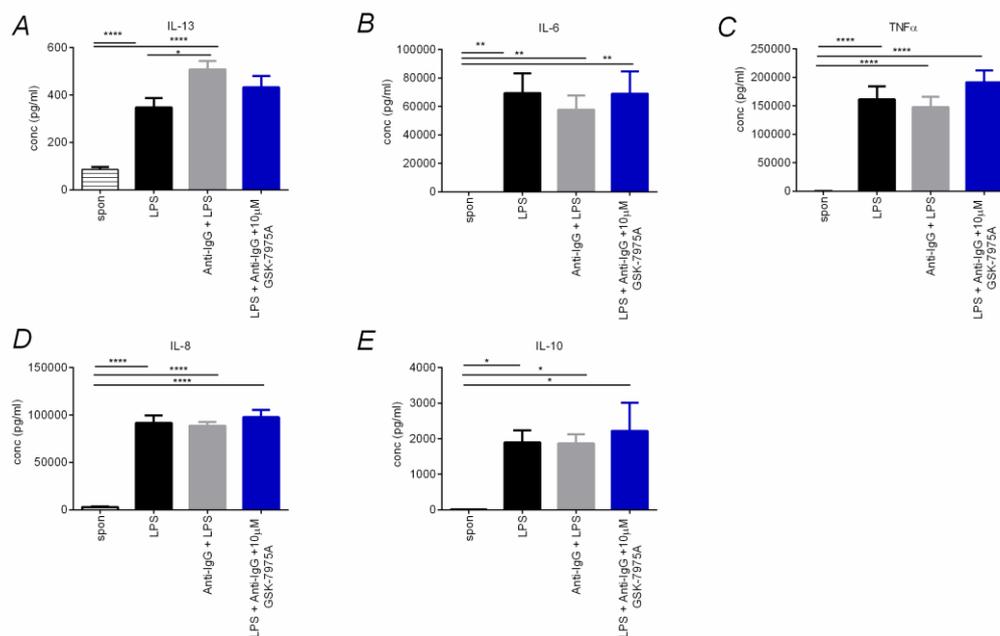
Figure 5.13   **Effect of 10μM GSK-7975A on LPS (+/-IFNγ) + Anti IgG stimulated cytokine release from hMDMs**

hMDMs primed for 24hr with IFNγ 10ng/ml prior to activation with 100ng/ml LPS or 100ng/ml LPS + 1/100 Anti-IgG for 24hrs with 10μM GSK-7975A pre-applied for 15 minute before stimulus and kept constant throughout. After 24hr incubation, supernatants were collected, diluted 1:10 and run on pro-inflammatory V-plex MSD plate. Of the 10 cytokines present in the blot: IL-13, IL-8, IL-6, IL-10 and TNFα were detectable at levels above the

lower limit of detection. Graphs show the concentration in pg/ml, mean ± SEM. Results were analysed using one-way ANOVA with Tukey's multiple comparison test. N=3 donors. * p <0.01, **** p<0.0001

5.2.12 Phagocytosis of pHrodo® labelled *E. coli* is insensitive to GSK-7975A in unprimed hMDMs

Phagocytosis is an important function performed by macrophages as a key response to a bacterial attack. There are reports in the literature indicating involvement of Ca^{2+} in the phagocytosis process (Nunes & Demaurex, 2010), as is discussed in depth in **Section 5.1**. Similarly there are numerous receptors shown to be involved in initiating phagocytosis, including; scavenger, lectin, Fcγ and CRs (Taylor *et al.*, 2005). The involvement of each of these receptors is dependent on the type of particle detected by the macrophage for ingestion, although there is overlap in the presence of ligands for these receptors on certain particle types, e.g. an IgG opsonized bacterial particle will also express ligands for scavenger receptors. Similarly it has been shown that unopsonized *E. coli* can activate FcγR independently of IgG coating through mannose like adhesions on their surface (Salmon *et al.*, 1987).

Phagocytosis experiments were performed using a pHrodo® labeled *E. coli*, either opsonized or unopsonized. Due to the pHrodo® tag, this enabled an accurate quantification of successful particle phagocytosis – through fluorescent microscopy and subsequent quantification of the intensity of the associated pHrodo® fluorophore. Upon ingestion into the acidic phagosome, the fluorescently tagged *E. coli* is excited to emit fluorescent light. Unlike traditional approaches this method means that the bacteria can remain present throughout the experiment and no wash steps are required. This assay has the advantage that any damage/activation of the cell initiated by washing or labelling to assess binding/internalisation is prevented and moreover the assay allows a time-course experiment to be performed by real-time monitoring of the pHrodo® *E. coli* uptake. However, as the experimental read out for this assay is dependent on pH of the phagosomal compartment, it is possible that a decrease in signal could be caused either by a decrease in the number of particles ingested or by a decrease in the acidification of the phagosome. As both of these processes are classified as mechanisms involved in phagocytosis the assay can be used to study modulators of phagocytosis generally but cannot be specifically linked to ingestion or phagosomal maturation. The phagocytosis experiments were quantified to give three read outs of successful phagocytosis; density in responding cells, phagocytosis index and % of responding cells.

Phagocytosis experiments were first performed with unopsonized *E. coli* in the presence of the Orai antagonist GSK-7975A. Although, as described above, there is some evidence to suggest that unopsonized *E. coli* can activate FcγR, it is more commonly reported that *E. coli* phagocytosis is mediated by the MARCO scavenger receptor and other scavenger receptors (van der Laan *et al.*, 1999) which to my knowledge based on the signalling cascade, is unlikely to activate Orai channels. The results shown in **Figure 5.14** demonstrate

that the Orai antagonist had no significant effect on the phagocytosis of unopsonized *E. coli* (phagocytosis index was 1.56 ± 0.31 in control conditions and 1.13 ± 0.45 in GSK-7975A, density in responding cells was 1134 ± 339 in control conditions and 995 ± 298 in GSK-7975A treated conditions, signal at 3hour time point, mean ± SEM, N=6). However, Cytochalasin-D, an inhibitor of actin polymerization and well reported phagocytosis inhibitor was shown to significantly inhibit phagocytosis of pHrodo® labeled *E. coli* in this assay therefore verifying the assay conditions.
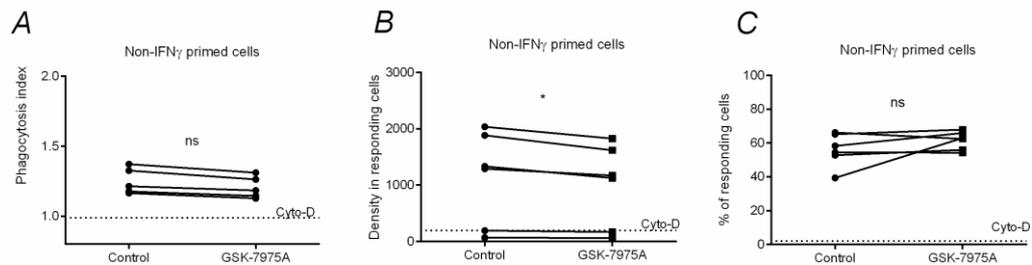
Figure 5.14   GSK-7975A had no significant effect on the phagocytosis of pHrodo labelled *E. coli* in non-primed hMDM cells

hMDMs were pre-incubated with; vehicle, 10µM Cytochalasin-D or 10µM GSK-7975A before uptake of pHrodo labelled E. coli was assessed at 3 hours post infection by fluorescent microscopy using an INCell Analyser, 20µg of E. coli was added to each well of 40,000 hMDMs. hMDMs were stained with cell tracker green (1µM) and Hoescht (0.05µg/well) to enable quantification of intact cells. Graphs show the individual data points for each donor tested in control and GSK-7975A conditions, the level of inhibition by Cytochalasin-D is inhibited by the hashed line on each graph. ***A.)*** *phagocytotic index.* ***B.)*** *density in responding cells.* ***C.)*** *percentage of responding cells. Results were analysed using students paired t-test N=6 donors. * p <0.01, **** p<0.0001*

5.2.13   Phagocytosis of opsonized pHrodo® labelled *E. coli* in IFNγ primed hMDMs is attenuated by GSK-7975A

To investigate FcγR mediated phagocytosis more directly, pHrodo® labeled *E. coli* were opsonized by coating the particles with polyclonal IgG. Orai antagonist (10µM GSK-7975A) caused a significant reduction in the phagocytosis of opsonized *E. coli* in IFNγ primed hMDMs. The phagocytosis index was significantly reduced from 1.74 ± 0.11 in control to 1.38 ± 0.15 N=6 in GSK-7975A conditions (mean ± SEM), similarly the density of responding cells was significantly reduced from 3641 ± 1139 in control, to 2889 ± 1077 N=4 in GSK-7975A conditions (mean ± SEM). Notably, the % of responding cells was not affected by the Orai antagonist, indicating again that Orai-mediated Ca^{2+} signalling has a role in controlling the magnitude or efficiency of phagocytosis ***(Figure 5.15)***. These results provide novel

evidence for the involvement of Orai signalling in opsonized bacterial phagocytosis in IFNγ primed hMDMs.
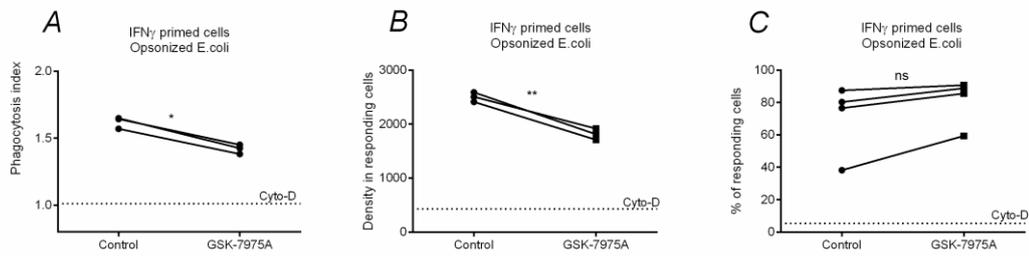
Figure 5.15   GSK-7975A causes significant inhibition to the phagocytosis of opsonized pHrodo labelled *E. coli* by IFNγ primed hMDM cells

*IFNγ (24hr prime at 10ng/ml) hMDMs were pre-incubated with; vehicle, 10μM Cytochalasin-D or 10μM GSK-7975A before uptake of opsonized pHrodo labelled E. coli was assessed at 3 hours post infection by fluorescent microscopy using an INCell Analyser, 20μg of E. coli was added to each well of 40,000 hMDMs. hMDMs were stained with cell tracker green (1μM) and Hoescht (0.05μg/well) to enable quantification of intact cells. Graphs show the individual data points for each donor tested in control and GSK-7975A conditions, the level of inhibition by Cytochalasin-D is inhibited by the hashed line on each graph. A.) phagocytotic index. B.) density in responding cells. C.) percentage of responding cells. Results were analysed using students paired t-test N=4 donors. * p <0.01, **** p<0.0001*

5.2.14   Phagocytosis of non-opsonized pHrodo® labelled *E. coli* in IFNγ primed hMDMs is attenuated by GSK-7975A

Phagocytosis experiments of unopsonized *E. coli* in IFNγ primed MDMs were also shown to be significantly attenuated by pre-treatment with the Orai antagonist. The density in responding cells was significantly reduced (1935 ± 190 in control and 1224 ± 160 in GSK-7975A conditions, mean ± SEM, N=7) as was the phagocytosis index (1.36 ± 0.05 in control and 1.17 ± 0.03 in GSK-7975A conditions, mean ± SEM, N=7), however the % of responding cells was not affected by GSK-7975A *(Figure 5.16)*. Taken together the results from these experiments suggest that Orai-mediated Ca^{2+} signalling has a role in the phagocytosis of pHrodo® labelled *E. coli* in IFNγ primed hMDMs but not in unprimed cells.
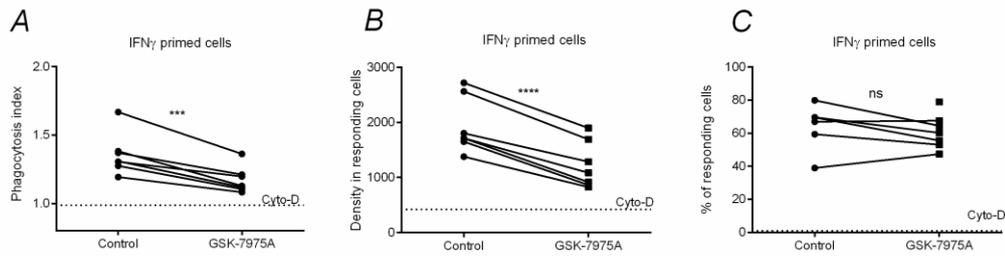
Figure 5.16   GSK-7975A causes significant inhibition to the phagocytosis of pHrodo labelled _E. coli_ by IFNγ primed hMDM cells

*IFNγ (24hr prime at 10ng/ml) hMDMs were pre-incubated with; vehicle, 10µM Cytochalasin-D or 10µM GSK-7975A before uptake of pHrodo labelled E. coli was assessed at 3 hours post infection by fluorescent microscopy using an INCell Analyser, 20µg of E. coli was added to each well of 40,000 hMDMs. hMDMs were stained with cell tracker green (1µM) and Hoescht (0.05µg/well) to enable quantification of intact cells. Graphs show the individual data points for each donor tested in control and GSK-7975A conditions, the level of inhibition by Cytochalasin-D is inhibited by the hashed line on each graph. **A.)** phagocytotic index. **B.)** density in responding cells. **C.)** percentage of responding cells. Results were analysed using students paired t-test N=7 donors. * p <0.01, **** p<0.0001*

5.2.15   GSK-7975A decreases pHrodo® labelled _E. coli_ phagocytosis at the same rate over 1-5hour time course

Figures 5.14-5.16 display phagocytosis data from the 3 hour time point, however the experiment was performed over a 4-5 hour time course and this is presented in **_Figure 5.17_**. The kinetic profile of the phagocytosis experiment show a parallel change in the phagocytosis parameters over time in the control and GSK-7975A conditions. In the IFNγ primed cells, the level of inhibition caused by GSK-7975A was shown to be relatively consistent at each time point. For example there is a difference between control and GSK-7975A treated conditions of 0.27, 0.28 and 0.27 in the phagocytosis index of opsonized _E. coli_ by IFNγ primed cells at 1.5, 3 and 4 hour post infection, respectively. In non IFNγ primed cells, the phagocytosis index and density in responding cell signals were lower in GSK-7975A conditions, but as indicated by the overlap in the standard error of the mean, no significant difference in the two conditions was seen at any time point. Although the % of responding cells was not affected by GSK-7975A in any condition, the amount of % of responding cells varied between conditions. The lowest amount of % responding cells was seen in the non IFNγ primed hMDMs (42-59.2%), whereas the highest level of responding cells was seen in the IFNγ primed hMDMs infected with opsonized pHrodo® labelled _E. coli_ (55-81%) **_(Figure 5.17)_**. In sum these results show that the involvement of Orai in phagocytosis of pHrodo® labelled _E. coli_ in IFNγ primed cells occurs to the same degree over a 4 hour time course.
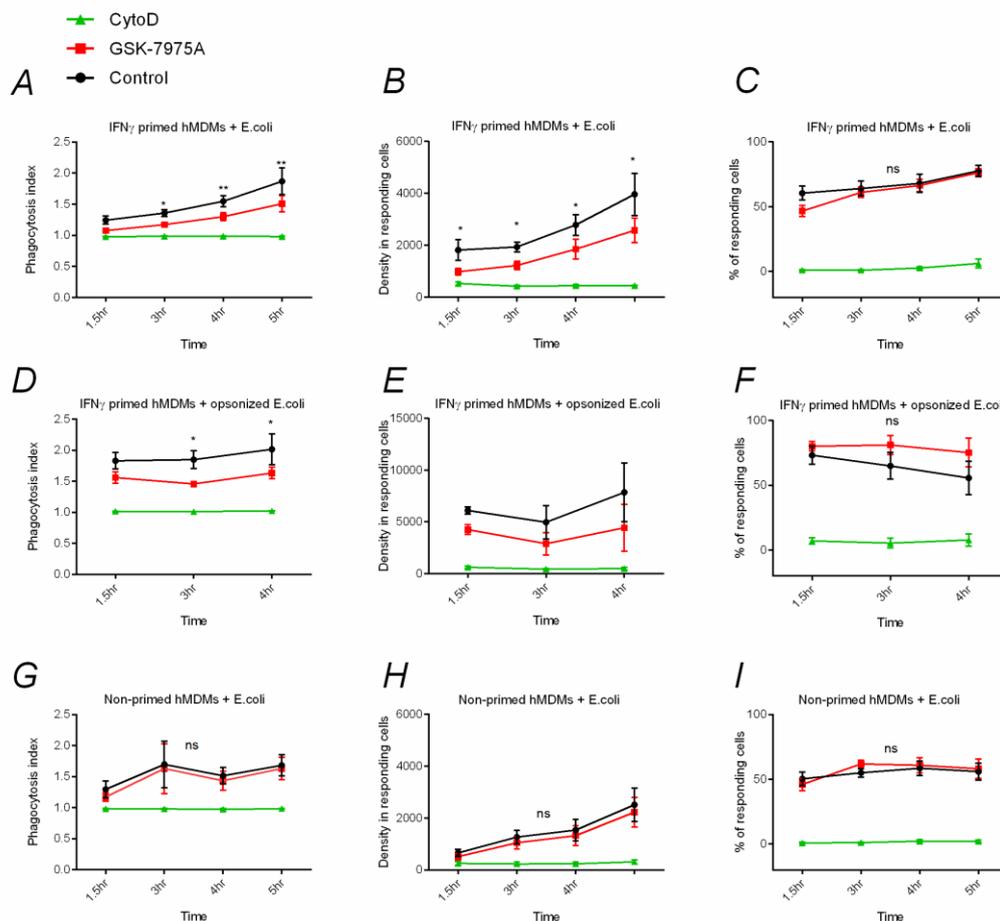
Figure 5.17 **Phagocytosis of opsonised/non opsonized pHrodo labelled *E. coli* in primed hMDM cells over a 4/5 hour duration**

*IFNγ primed/unprimed hMDMs (24hr prime at 10ng/ml) were pre-incubated with; vehicle, 10µM Cytochalasin-D or 10µM GSK-7975A before uptake of opsonised pHrodo labelled E. coli assessed at 3 hours post infection by fluorescent microscopy, 20µg of E. coli was added to each well of 40,000 hMDMs. hMDMs were stained with cell tracker green (1µM) and Hoescht (0.05µg/well) to enable quantification of intact cells. Graphs show the individual data points for each donor tested in control and GSK-7975A conditions and Cytochalasin-D over the 4/5 hour time course. **A, D, G.)** Phagocytotic index. **B, E, H.)** Density in responding cells. **C, F, I.)** Percentage of responding cells. N=4-7 donors. Results were analysed using Two-way ANOVA with Sidak's post hoc test, stars denoted on the graph indicate significant difference between GSK-7975A and control conditions* p <0.01, **** p<0.0001*

5.2.16 GSK-7975A inhibits thapsigargin induced Ca²⁺ entry in hAM cells in a concentration-dependent manner.

When lung tissue was available, translation of these experiments to investigate Orai function in hAMs was performed. Unfortunately throughout the duration of these

experiments there were only lung resident cells available to allow one experiment type to be translated. ***Figure 5.18*** shows FLIPR data from hAMs. hAMs were also found to have a concentration-dependent Ca^{2+} signal in response to thapsigargin; this was inhibited by GSK-7975A. Although this data is from one lung donor, it provides indication that Orai-mediated Ca^{2+} signalling is active in this cell type also.
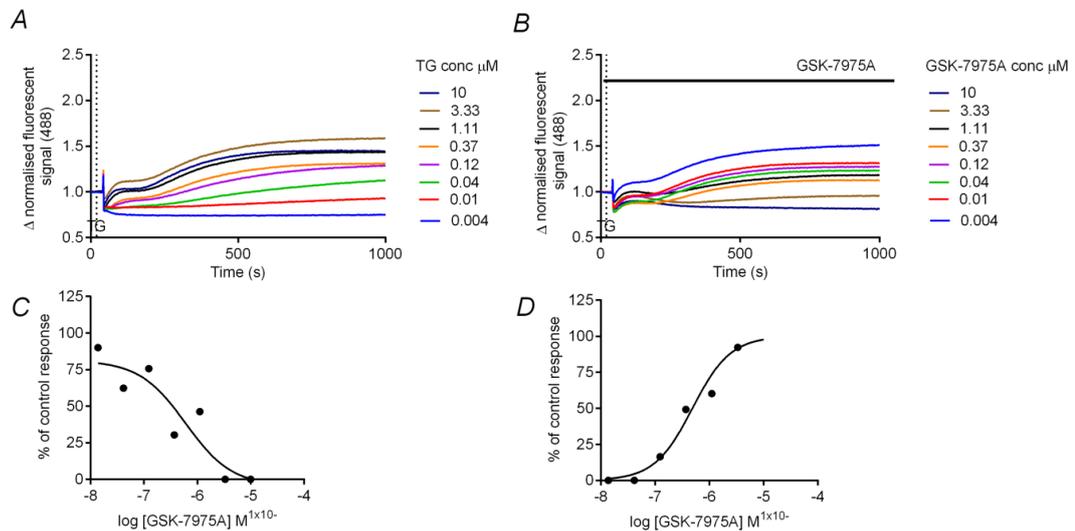
Figure 5.18   Thapsigargin activates concentration-dependent Ca^{2+} influx in hAMs that is sensitive to inhibition GSK-7975A

*Ca^{2+} imaging of hAMs using FLIPR. **A.)** Ca^{2+} signal over time, 1µM TG was applied at t=30s. This is a representative trace from N=5 donors tested **C.)** Concentration-response curve to TG, showing percentage of max Ca^{2+} response (calculated from area under curve N=5 donors. **B.)** Ca^{2+} signal over time, 1µM TG added at t=30s to varying concentrations of pre-applied GSK-7975A. **D.)** Concentration-response curve to varying concentrations of GSK-7975A, showing percentage of control response. N=1 donor.*

5.3 Discussion

Taken together the results from this chapter show novel evidence for the functional activity of Orai-mediated Ca^{2+} entry in hMDMs. Through the use of an Orai selective antagonist it was demonstrated that Orai-mediated Ca^{2+} signalling is a critical component of hMDM SOCE and notably Orai-mediated Ca^{2+} entry is the predominant contributor of Ca^{2+} signalling induced following Anti-IgG activation. Inhibition of Orai-mediated Ca^{2+} signalling led to a significant reduction in the phagocytosis of pHrodo® labelled *E. coli* by IFNγ primed hMDMs but not in unprimed hMDMs. The data presented in this chapter shows evidence for Orai-mediated activity in human macrophages for the first time and provides interesting findings which will help in the direction of future work.

Orai and STIM family expression in hMDM cells

The quantitative PCR experimental results shown in this chapter demonstrate that all members of the Orai and STIM family are expressed at mRNA level. Orai1 and 3 and STIM1 were expressed at levels significantly greater than Orai 2 and STIM2. This mRNA expression profile is in line with that seen in HLMCs (see **Section 3** and (Ashmole *et al.*, 2012). All three Orai family members have been demonstrated to mediate functional I_{CRAC} Ca^{2+} currents (Lis *et al.*, 2007), although the majority of past work in the literature has focused on elucidating the function of Orai1. Nonetheless, Orai2 has been shown to have a very similar expression profile to Orai1 but data in the literature is unclear about the functional role of Orai2 (Hoth and Niemeyer 2013). Orai3 has been shown to have a wider range of functions, with heteromeric interaction with Orai1 forming a non-store-operated channel, the arachidonic acid activated channel. Interestingly Orai3 has been particularly implicated in cancer, with increased Orai3 expression found in MCF-7 breast cancer cells and breast cancer tissue (Faouzi *et al.*, 2011). GSK-7975A, the Orai inhibitor used in my study, is known to inhibit Orai1 and Orai3 with similar potency (Derler *et al.*, 2013), however whether the compound would inhibit Orai1/3 heteromeric channels has not been directly assessed. To further understand the individual contribution of Orai subtypes to the Ca^{2+} signalling in hMDMs further experiments are necessary. Investigation of Orai1/3 arachidonic acid sensitive channels could be performed by using arachadonic acid as a ligand to activate hMDMs. Arachidonic acid is a pre-cursor produced in the process of PG synthesis. Although PG is produced by a wide range of cells, PGD is produced by HLMCs (Ricciotti & FitzGerald, 2011). This link to the availability of arachidonic acid in the lung immune cell environment gives evidence for physiological relevance in this investigative approach. To further evaluate the distinct roles of the different Orai channels as homomeric assemblies in macrophage biology would require utilisation of genetic manipulation to knockdown each Orai subtype.

This thesis also reports mRNA expression of STIM1 and STIM2 in hMDMs. Similarly to the Orai family, the majority of past work has focused on the role of STIM1; however, as discussed in detail in **Section 1.4.5** further investigations have revealed that STIM2 is involved in the activation of SOCE following a relatively small depletion in ER Ca^{2+} levels. Therefore, STIM2 is a more sensitive Ca^{2+} sensing protein, and importantly is coupled with a moderate activation of Orai channels, arguably with the purpose to re-fill the stores and maintain homeostasis (Ong *et al.*, 2015). Investigation into whether STIM1 and 2 expression profile was maintained at protein level would be required before further work was performed to assess the functional consequence of a predominant STIM1 or STIM2 expression. It is possible that a lower STIM2 protein expression may occur to regulate the inappropriate SOCE activation initiated by the more sensitive subtype, again further investigation utilizing genetic knockdown techniques would allow further evaluation of the specific STIM1 or STIM2 contribution.

Orai contribution to Ca^{2+} signalling in human macrophages

The results reported in this thesis show evidence supporting the functional activity of Orai-mediated Ca^{2+} entry as a critical contributor to SOCE in hMDMs. Notably this thesis also provides convincing novel evidence that Orai-mediated Ca^{2+} entry is the primary contributor to the Ca^{2+} signalling observed following Anti-IgG activation in IFNγ primed hMDM cells. Based on the ablation of the Anti-IgG induced signal by the Syk inhibitor and the increase in Ca^{2+} signal following an increase in FcγRI expression this gives convincing evidence that the Anti-IgG Ca^{2+} entry is mediated through FcγR activation, however further experiments to block FcγRI would be required to validate if the increase in Ca^{2+} signal by Anti-IgG is caused by FcγRI specifically. The activity of SOCC in macrophage signalling is in line with previously published work in mouse macrophage models, as summarised in **Section 5.1.3**. In (Braun *et al.*, 2009; Vaeth *et al.*, 2015) STIM1$^{-/-}$ mice and STIM1 and STIM2 inducible ablation in BMDMs have been used to delineate a contributory role of SOCC to FcγR signalling. Similarly in (Ye *et al.*, 2012b) and (Kang *et al.*, 2012) non-selective Orai antagonists were utilised to indicate SOCE activity in mouse macrophage cells. However, although the work by Braun, Vaeth, Kang, Ye and I use a variety of experimental approaches to infer SOCE activity in macrophage cells, the tools used do not provide direct proof of reduction in current through Orai channels as explanation for the results seen. Although the attenuation of Ca^{2+} in the absence of STIM is suggestive of Orai involvement in peritoneal macrophages and BMDMs (Braun *et al.*, 2009; Vaeth *et al.*, 2015), STIM1 is also capable of activating TRPC channels, which can act as SOCCs too (Zeng *et al.*, 2008; Lee *et al.*, 2010) (refer to **Section 1.5.8** for details). Therefore studies to genetically ablate STIM cannot be taken as confirmation of Orai involvement, but show STIM regulated SOCE. In my study, although a number of experiments have validated GSK-7975A as an Orai selective pharmacological tool (Ashmole *et al.*, 2012; Derler *et al.*, 2013); it could be argued that GSK-7975A does not exclude the involvement of TRPC channels, indirectly. In HSG cells, TRPC1 channel activation was shown to be dependent on Ca^{2+} influx through Orai channels (Cheng *et al.*, 2011a; Cheng *et al.*, 2011b), it is therefore possible that TRPC channels are also composing a component of the GSK-7975A sensitive Ca^{2+} signal seen in the my hMDM experiments, albeit indirectly. However based on the model proposed by Cheng *et al.*, 2011, any tool whereby Orai activity was inhibited would also interfere with TRPC activity. To further evaluate the direct activity of Orai as a Ca^{2+} influx channel in human macrophages, patch clamp electrophysiology experiments together with knockdown strategies could be performed to characterise the biophysical properties of the store-operated currents.

Possibility of TRPC contribution

As discussed in depth throughout **Section 1.5** the mechanism of TRPC channel activation is complex, with TRPC family members exhibiting store-operated modes of activation under certain conditions. In this respect, the contribution of TRPC channels to the store-operated/Orai regulated Ca^{2+} signalling seen in hMDMs cannot be ruled out. My experiments with TRPC3/6 agonist (GSK-234A) indicate at least that these TRPC subtypes

are not functionally active in hMDMs. Previous studies have indicated the potential activity for TRPC6 in hAMs, mRNA and protein expression analysis indicated TRPC6 expression in hAMs that was enhanced in hAMs from COPD patients (Finney-Hayward *et al.*, 2010). Some evidence of TRPC6 activity was further demonstrated through patch clamp experiments – platelet activating factor (PAF), was used to activate TRPC6 - with 50-60% of macrophages tested displaying current-voltage relationships consistent with activation of a non-selective cation current which moreover was inhibited by non-selective TRPC antagonist SK&F96365. While indications of TRPC6 activity in human macrophages were provided by Finney-Hayward's work, without the use of a selective TRPC6 antagonist or TRPC6 knockdown, it is possible that the results observed are mediated by other TRPC family members or non-selective cation channels (Finney-Hayward *et al.*, 2010). Although outside the scope of the present study, further elucidating the role of TRPC channels in macrophage biology could represent a novel area of study. TRPC6 in particular has been demonstrated to have a key role in the direction of neutrophil chemotaxis (Lindemann *et al.*, 2013). Similarly, as described in **Section 3.1.2** *in vivo* mouse models indicate that TRPC6 is important for the control of symptoms of allergic disease (Sel *et al.*, 2008), confirmation of TRPC expression in hMDMs would be required to direct further experiments.

LPS mediated Ca^{2+} signalling

The data described in this thesis shows no increase in Ca^{2+} in response to LPS stimulation over duration of 20 minutes, a small rise in Ca^{2+} signal was observed by 80 minutes but this was not concentration-dependent. In murine microglia LPS is also observed to increase basal Ca^{2+} concentration but caused no significant transient response (Hoffmann *et al.*, 2003), conversely, (Ye *et al.*, 2012b) show LPS + IFNγ to initiate a Ca^{2+} signal rise over time in mouse peritoneal macrophages, with an trending increase in signal from 30 minutes and measurements taken over a total of 3hours. In my study the Ca^{2+} signal was quantified by taking an average reading from a well containing 75,000 cells rather than imaging the Ca^{2+} signal in individual cells. It is possible that if there is differential LPS response by macrophages within the population, in terms of kinetics and magnitude, that the average Ca^{2+} signal measured would not reflect an increase in Ca^{2+} signal in a small population of cells. Indeed in (Ye *et al.*, 2012b), single cell Ca^{2+} measurements were performed.

Orai contribution to hMDM cytokine release

As described in **Section 5.1** there are mixed reports regarding the role of SOCE in the control of LPS mediated cytokine production. The aforementioned (Ye *et al.*, 2012b) show a reduction in the LPS and IFNγ mediated release of IL-10, TNF-α, IL-6 and MCP-1 following pre-treatment with SK&F96365. In murine microglia, SOC inhibitors and Orai1/STIM1 siRNA attenuated LPS induced TNFα and IL-6 production (Michaelis *et al.*, 2015). In contrast (Vaeth *et al.*, 2015) show that in BMDMs PRR ligand mediated cytokine release was not affected by STIM1/STIM2 ablation . My results demonstrated no effect of the Orai antagonist on LPS or LPS + IFNγ mediated cytokine production. This is in line with the work by Vaeth and colleagues. The reasons for differences between the works of Ye compared to

Michaelis and Vaeth could be a combination of heterogeneity between macrophage types used in each study, and the different tools used to define SOCE contribution. The confirmation of Orai inhibition having no impact on the LPS induced cytokine release has a positive implication in respect to unwanted effects of Orai inhibition. LPS induced cytokine release occurs in order to tackle a bacterial infection, therefore impairing this response would limit the ability of the macrophage to handle the bacterial infection. As described in **Section 5.1**, Orai-mediated signalling is a potential target for the treatment of allergic disease, as Orai is a key contributor to FcεRI-mediated signalling. Therefore assessing any risks in the inhibition of Orai in other immune functions is important.

The key role of FcγR in directing cytokine release is emerging. Sole activation of FcγR is not sufficient to drive cytokine release, and interaction with other stimuli, generally PRRs is required (Vogelpoel *et al.*, 2015). (Braun *et al.*, 2009) measured the release of TNFα and MIP-2 in the BALF from mice following immune complex induced pneumonitis. Interestingly they observed attenuation in release in STIM1$^{-/-}$ animals. My results assessing cytokine release from Anti-IgG and LPS stimulated hMDMs did not reveal any Orai contribution. Vogelpoel's work reported that FcγRIIa is the predominant receptor involved in mediating cytokine production. FcγRIIa mRNA expression is relatively low in the hMDMs used in my study; speculatively it is possible that this is the explanation for no obvious modulation of cytokine release by Anti-IgG application, irrespective to Orai. Similarly, it may be that a difference in methodology to assess the cytokine release from macrophages following infection with opsonized bacteria could give different results. It is also possible that the complex interaction between the stimulation of inhibitory ITIM and activatory ITAM FcγR may be an explanation for the lack of change seen with Anti-IgG as a co-stimulus to LPS - ITIM could prevent activation of ITAM over a time frame required to initiate cytokine transcription. Lastly, the results reported by (Braun *et al.*, 2009) are using an *in vivo* mouse model, where the interplay and communication between the immune cells activated following pneumonitis are likely to have a major impact on the cytokine production reported.

Orai involvement in the phagocytosis of pHrodo® labelled *E. coli*

In the present study, phagocytosis was assessed using a pHrodo® labelled *E. coli* assay system. In this methodology, the pH tag on the *E. coli* bioparticles dictates that the fluorescent signal only occurs upon internalisation into an intracellular acidic compartment. The assay methodology provides evidence that particle of interest has been successfully ingested into the phagocytic cell, as opposed to merely binding to the phagocyte cell surface. In phagocytosis assays where fluorescent bioparticle uptake is measured by confocal microscopy, further staining and washing steps are required to differentiate between particle binding to the cell surface and internalisation. The results described in **Section 5.2.13-14** of this thesis, show an inhibitory effect of the Orai antagonist on the phagocytosis of pHrodo® labelled *E. coli* into IFNγ hMDMs. The weaker signal reported in GSK-7975A conditions could be a result of either; a direct decrease in the amount of pHrodo® labelled *E. coli* internalised, or alternatively an impairment in the acidification that

occurs in the phago-lysosome as part of phagosome maturation. To identify which particular aspect of the phagocytosis process is affected by antagonist activity, further experiments should be performed. For example flow cytometry experiments with fluorescently tagged bioparticles could be performed to assess the internalisation process. A bacterial killing, ROS assay or measurement of phagolysosomal pH reporter could be performed to measure the effect of compounds on phagosome maturation. Whilst the specific mechanism of action of the Orai antagonist on phagocytosis was not assessed in my study, as both internalisation and phagosome maturation constitute crucial components of the phagocytosis process, the results of this assay provide useful information to identify a general phagocytosis modulator.

It is theoretically possible that in the presence of the Orai inhibitor, the *E. coli* particles were instead directed down an endocytic pathway, with acidification a component of this mechanism too, the pHrodo® signal would still be produced. Although endocytosis of pathogens has been reported, largely these instances have been in non-phagocytic cells where the pathogen is utilising the ingestion process to evade immune detection (Bonazzi & Cossart, 2006). The differential level of phagocytosis of opsonized *E. coli* vs. unopsonized and in IFNγ primed cells suggests engagement of the phagocytotic receptors. If endocytotic pathways were being utilised to mediate bacterial entry into the cell it would be expected that factors to enhance the microbicidal properties of the cell (IFNγ) (Schroder *et al.*, 2004) and factors to engage FcγR phagocytic receptors (IgG opsonization) would have no significant effect on the level of phagocytosis. It can therefore be taken as unlikely for pHrodo® labelled *E. coli* to be endocytosed rather than phagocytosed in my study.

Markedly, significant involvement of Orai-mediated Ca^{2+} signalling in regulating the phagocytosis of *E. coli* by hMDMs was only seen in cells that had been primed with IFNγ. The phagocytic index and the density of opsonized and non-opsonized *E. coli* uptake in the responding cells were significantly attenuated by Orai inhibition, in IFNγ primed cells. The original hypothesis was that Orai Ca^{2+} signalling would contribute to the phagocytosis of opsonized *E. coli* but not non-opsonized *E. coli* because of the previously established involvement of Orai in FcγR mediated Ca^{2+} signalling. It would be expected that a greater sensitivity to GSK-7975A was seen in the IFNγ primed hMDMs ingesting opsonized *E. coli* vs. non opsonized *E. coli*, if IgG opsonization was dictating Orai involvement. Instead the results suggest that the IFNγ priming is causing a modulatory effect on the mechanism by which hMDM are ingesting phagocytic particles possibly through induction of a differential phagocytic receptor expression profile. From the results of my study it has been shown that IFNγ leads to a significant increase in the expression of the FcγRI subtype, the high affinity activatory subtype – at mRNA and protein level. Concurrently an increased Ca^{2+} signal is seen following Anti-IgG activation in IFNγ primed cells, therefore indirectly showing that this increase in signal is likely to be due to an increase in activation of FcγRI.

It was considered whether an alternative explanation for the enhanced Ca^{2+} signal in IFNγ primed cells, and perhaps an explanation for the Orai-dependent phagocytosis in IFNγ cells was that IFNγ priming also led to an increase in Orai/STIM expression; however the results from qPCR experiments indicate this did not occur. Importantly, the thapsigargin mediated

Ca^{2+} signal – a readout of the active Orai Ca^{2+} signal – was unaffected by IFNγ priming, consistent with the view that IFNγ priming does not have an effect on the Orai channel expression or function, per se. IFNγ is a ligand for the IFNγ receptor which initiates a JAK-STAT signalling pathway and is well known as an activator of macrophages directing them down an 'M1' phenotype - increasing their receptor mediated phagocytosis and microbial killing activity (Schroder *et al.*, 2004). IFNγ priming is known to enhance macrophage and neutrophil phagocytosis (Maródi *et al.*, 1993; Marchi *et al.*, 2014). Interestingly (Boehm *et al.*, 1997) describe that IFNγ priming of monocytes and macrophages leads to several changes in the gene expression of some surface receptors. For example; the macrophage mannose receptor, CD14, scavenger receptor and CR-type 1 are down regulated by IFNγ treatment. In contrast, FcγRI, C3 and β-1γ1 integrin receptors are up regulated by IFNγ treatment. With the majority of these receptors having been implicated in phagocytosis – a change in expression of phagocytic receptors could be dictating how IFNγ priming is changing Orai involvement. (van der Laan *et al.*, 1999) demonstrate that *E. coli* is phagocytosed by the MARCO scavenger receptor. Alternatively, an early paper looking into the mechanisms of macrophage phagocytosis of *E. coli* shows that FcγR on human PMN cells can facilitate the opsonin-independent phagocytosis of *E. coli* through lectin-carbohydrate interactions between the bacteria and FcγR receptor. The binding and phagocytosis of *E. coli* by PMNs was inhibited by D-mannose and α methylmannoside, showing evidence for the dependency on mannose for successful phagocytosis. However, blocking FcγR with an antibody, also caused a similar attenuation of the phagocytosis of *E. coli* by PMNs, implicating FcγRs as an alternative phagocytic regulator of *E. coli* (Salmon *et al.*, 1987). Speculatively, a change in expression of phagocytic receptors induced by IFNγ and a subsequent switch in phagocytosis of *E. coli* mediated by FcγR could be an explanation for my results, however further experiments to evaluate this hypothesis, these are described in *Section 5.4*.

Investigation into Ca^{2+} dependency of phagocytosis in neutrophil cells has also revealed some possible alternate explanations for the results seen in the present study. In HL-60 neutrophil like cells, it was observed that intracellular Ca^{2+} store depletion was sufficient for the ingestion of IgG opsonized zymosan particles but that Orai1/STIM1 induced Ca^{2+} entry was required for ROS production, thus indicating a role for Orai1/STIM1 in the steps of phagosomal maturation (Steinckwich *et al.*, 2011). In bone marrow derived neutrophils further delineation of how Orai1/STIM1 contributed to phagocytosis was described. STIM1 was reported to recruit the ER to the phagosome where it mediates localised Ca^{2+} elevations through Orai1 channels which lead to actin shedding, an early event of phagosomal maturation. Interestingly this study showed for the first time the activity of STIM1/Orai1 at the phagosomal membrane. Notably, knockout of STIM1 attenuated phagocytosis of opsonized RBC/zymosan particles, but only when there was a high particle: cell ratio, i.e. implying that STIM1 has a particular role in sustaining high levels of phagocytotic ingestion. In my experiments, although the ratio of *E. coli*: hMDMs was consistent throughout experiments, the effect of IFNγ priming on the cells may have been the factor which switched the hMDMs to phagocytosing particles at a higher rate. A higher density of *E. coli* was measured in responding cells in IFNγ primed conditions compared to non IFNγ primed conditions (mean density = 1935 in IFNγ primed vs. 1134 in unprimed),

this is in line with the predicted action of IFNγ – to enhance the microbicidal properties of macrophages. Replication of some of the experiments performed by Steinckwich would allow evaluation of whether the results obtained in neutrophils translated into human macrophages.

(Vaeth *et al.*, 2015) report no attenuation in the phagocytosis of IgG coated fluorescent beads or *S. aureus* in BMDM cells following STIM1 and STIM2 ablation, but the use of Ca^{2+} chelator BAPTA did impair the uptake of IgG coated beads, indicating some role for Ca^{2+} signalling. In contrast another study of phagocytosis in STIM1$^{-/-}$ mice, this time investigating peritoneal macrophages showed a significant impairment FcγR mediated phagocytosis (Braun *et al.*, 2009). The difference in these two studies could be explained by the difference in macrophage cell type used, or could reflect minor differences in methodology; for example the type of particle used to assess phagocytic ingestion or the ratio of bioparticles: macrophage cells.

In summary, the results presented in this chapter show that Orai-mediated Ca^{2+} signalling is a key contributor downstream of Syk-dependent Anti-IgG activation and show Orai has a contributory role in *E. coli* phagocytosis by hMDMs in IFNγ primed cells. Evidence for Orai in mediating phagocytosis in hMDMs provides preliminary evidence to direct further research to expound these findings.

5.4 Future directions

Based on the results obtained in this chapter there are numerous directions of further research that should be pursued.

A primary area of interest is to further delineate the role of Orai-mediated Ca^{2+} signalling in macrophage phagocytosis. Initially it would be useful to utilise a wider range of techniques to define which aspect of phagocytosis the Orai signalling is contributing to. This could be done by performing separate bacterial ingestion assays using fluorescently tagged bioparticles and flow cytometry. Similarly the phagosomal maturation could be evaluated through bacterial killing or indirectly through a ROS assay. The results of this thesis indicate that IFNγ priming may be modulating the signalling processes utilized to mediate *E. coli* phagocytosis – to involve Orai signalling. However this preliminary evidence requires follow up work to fully understand what effect IFNγ is having on hMDMs. Experiments to confirm if IFNγ priming is directly leading to Orai involvement in phagocytosis or whether the results could be explained by an indirect effect on hMDMs caused by IFNγ priming are needed. In particular, experiments could be performed to confirm or discount whether IFNγ acts to decrease mannose and scavenger receptor expression, resulting in the phagocytosis of *E. coli* being mediated by interaction with the FcγR through mannose specific adhesions on the surface, as is seen in (Salmon *et al.*, 1987). To evaluate the hypothesis proposed by Salmon and colleagues, experiments could be performed to

directly assess the effect of FcγR inhibition of *E. coli* phagocytosis and to evaluate the expression profile of phagocytic receptors before and after IFNγ priming. To test whether Orai contribution only occurs in phagocytosis of higher volumes of particle, as seen in neutrophils (Steinckwich *et al.*, 2011) experiments could be performed to directly alter the ratio of macrophages to bacteria and investigate Orai-dependence. In relation to the disease application of my study, macrophages have crucial roles in the phagocytosis of bacteria which enter the lungs, for example: *Streptococcus pneumoniae, Haemophilus influenzae, Staphylococcus aureus* and *Mycobacterium tuberculosis*. Experiments should therefore be performed to investigate whether Orai signalling had a similar role in the control of phagocytosis of bacteria encountered in the lung, and similarly to compare the difference in Orai involvement before and after IFNγ priming and in opsonized and non-opsonized bacteria. Based on the known PLC-coupled signalling cascade initiated downstream of the Dectin-1 receptor (Xu *et al.*, 2009), investigating the contribution of Orai-mediated Ca^{2+} entry to the phagocytosis of Dectin regulated particles and Dectin-1 mediated cytokine production represents an attractive research avenue. (Xu *et al.*, 2009) show that signalling downstream of Dectin-1 is associated with PLCγ2 and that this is critical for the mediation of Ca^{2+} influx and cytokine production downstream of Dectin-1 activation in DCs.

My study has primarily utilised hMDM cells, due to the limited availability of tissue resident cells. As discussed in **Section 1.3.4**, it is well known that there is a wide heterogeneity of macrophages between tissue resident locations and blood derived cells. Particularly for the application of lung disease, investigation into the contribution of Orai-mediated Ca^{2+} entry to the phagocytic capacity of hAMs should be investigated. Similarly as the phagocytic ability of macrophages from COPD cells is known to be impaired, investigating whether there are any changes in the involvement of Orai in the phagocytosis process could provide useful information. Efferocytosis, the uptake of apoptosed cells is a process with mechanisms similar to phagocytosis. Orai/Ca^{2+} signalling involvement has not yet been delineated for this process either.

Whilst work in this thesis showed no involvement of Orai in the cytokine release following TLR4 and Anti-IgG stimulation, investigation into the Orai involvement in cytokine production following stimulation with opsonized bacteria commonly encountered in the lung was not performed. Such experiments would provide a more physiological approach from which to confirm whether Orai was redundant in FcγR/PRR mediated cytokine release.

Although more commonly known for their role in phagocytosis and in inflammatory mediator release, macrophages are also contributors to antibody-dependent cell cytotoxicity (ADCC). ADCC of B cell lymphoma was shown to be regulated via the PI3K/protein kinase B (Akt) pathway in IFNγ primed murine macrophages (Joshi *et al.*, 2009). Importantly, FcγR are known to be critical for effective ADCC (Nimmerjahn & Ravetch, 2008a). Based on the indication of Orai involvement in FcγR signalling, performing experiments to investigate its contribution would be worthwhile. Understanding the biology of ADCC has key therapeutic applications, as ADCC is the mechanism that is

manipulated by immuno-oncotherapy therapies such as herceptin that are designed to target and eliminate tumour cells (Mellor *et al.*, 2013).

In conclusion, whilst work in this thesis has showed that Orai is functionally active in hMDMs there are a number of further avenues of research which could be undertaken based on the initial findings of my study. In particular, to fully understand the translational impact of the findings, further work needs to be performed in lung derived cells in combination with disease causing pathogens.

6 Chapter 6: Conclusion

This thesis has provided novel findings which increase the understanding of the role of Ca^{2+} signalling in mast cell and macrophage biology. Significantly, important gaps in the current knowledge have been addressed, in addition new experimental evidence to guide and direct further research to complete understanding in the area has been generated. In particular it was shown that Orai but not TRPC channels have an important role in FcεRI mediated Ca^{2+} signalling in human mast cells, which provides vital information regarding the contributors to allergic signalling pathways. Secondly it was demonstrated that P2X7 does not significantly contribute to ATP and bzATP Ca^{2+} signalling in hMDMs under these assay conditions and similarly P2X7 inhibition has no effect on the phagocytosis of pHrodo labelled *E. coli* or in ROS-mediated bacterial killing of *S. pneumoniae*. Preliminary data showed that P2X7 Ca^{2+} signalling activity was different between hMDM and hAM cells highlighting the importance of translating macrophage biology into the relevant tissue resident cells. Lastly, novel evidence is described for the activity of Orai-mediated Ca^{2+} signalling in human macrophages. Orai-mediated Ca^{2+} signalling was shown to be a crucial component of FcγRI signalling- a central signalling pathway for bridging innate and adaptive macrophage functions. Orai inhibition had no effect on the production of LPS or LPS and Anti-IgG mediated cytokine release however Orai inhibition significantly impaired the phagocytosis of *E. coli* by IFNγ primed hMDMs. In summary, the results of my research provides important insight in the knowledge of how Ca^{2+} signalling pathways could be contributing or preventing mast and macrophage related disease.

7 References

Aderem A & Underhill DM. (1999). Mechanisms of phagocytosis in macrophages. *Annu Rev Immunol* **17,** 593-623.

Adinolfi E, Cirillo M, Woltersdorf R, Falzoni S, Chiozzi P, Pellegatti P, Callegari MG, Sandonà D, Markwardt F, Schmalzing G & Di Virgilio F. (2010). Trophic activity of a naturally occurring truncated isoform of the P2X7 receptor. *FASEB J* **24,** 3393-3404.

Al-Afif A, Alyazidi R, Oldford SA, Huang YY, King CA, Haidl ID, Anderson R & Marshall JS. (2015). Respiratory syncytial virus infection of primary human mast cells induces the selective production of type I interferons, CXCL10, and CCL4. *J Allergy Clin Immunol*.

Albarran L, Dionisio N, Lopez E, Salido GM, Redondo PC & Rosado JA. (2014). STIM1 regulates TRPC6 heteromultimerization and subcellular location. *The Biochemical journal* **463,** 373-381.

Alberto AV, Faria RX, Couto CG, Ferreira LG, Souza CA, Teixeira PC, Fróes MM & Alves LA. (2013). Is pannexin the pore associated with the P2X7 receptor? *Naunyn Schmiedebergs Arch Pharmacol* **386,** 775-787.

Ali Z, Laurijssens B, Ostenfeld T, McHugh S, Stylianou A, Scott-Stevens P, Hosking L, Dewit O, Richardson JC & Chen C. (2013). Pharmacokinetic and pharmacodynamic profiling of a P2X7 receptor allosteric modulator GSK1482160 in healthy human subjects. *Br J Clin Pharmacol* **75,** 197-207.

Alicia S, Angélica Z, Carlos S, Alfonso S & Vaca L. (2008). STIM1 converts TRPC1 from a receptor-operated to a store-operated channel: moving TRPC1 in and out of lipid rafts. *Cell Calcium* **44,** 479-491.

Ambudkar IS, Ong HL, Liu XB, Bandyopadhyay B & Cheng KT. (2007). TRPC1: The link between functionally distinct store-operated calcium channels. *Cell Calcium* **42,** 213-223.

Amcheslavsky A, Wood ML, Yeromin AV, Parker I, Freites JA, Tobias DJ & Cahalan MD. (2015). Molecular biophysics of Orai store-operated Ca2+ channels. *Biophys J* **108,** 237-246.

Andreesen R, Brugger W, Scheibenbogen C, Kreutz M, Leser HG, Rehm A & Löhr GW. (1990). Surface phenotype analysis of human monocyte to macrophage maturation. *J Leukoc Biol* **47,** 490-497.

Antonio LS, Stewart AP, Xu XJ, Varanda WA, Murrell-Lagnado RD & Edwardson JM. (2011). P2X4 receptors interact with both P2X2 and P2X7 receptors in the form of homotrimers. *Br J Pharmacol* **163,** 1069-1077.

Arango Duque G & Descoteaux A. (2014). Macrophage cytokines: involvement in immunity and infectious diseases. *Front Immunol* **5,** 491.

Ashmole I, Duffy SM, Leyland ML, Morrison VS, Begg M & Bradding P. (2012). CRACM/Orai ion channel expression and function in human lung mast cells. *J Allergy Clin Immunol* **129**.

Barajas M, Andrade A, Hernandez-Hernandez O, Felix R & Arias-Montaño JA. (2008). Histamine-induced Ca2+ entry in human astrocytoma U373 MG cells: evidence for involvement of store-operated channels. *J Neurosci Res* **86**, 3456-3468.

Barjaktarevic IZ, Arredondo AF & Cooper CB. (2015). Positioning new pharmacotherapies for COPD. *Int J Chron Obstruct Pulmon Dis* **10**, 1427-1442.

Barnes PJ. (2008). Immunology of asthma and chronic obstructive pulmonary disease. *Nat Rev Immunol* **8**, 183-192.

Barnes PJ. (2010). New therapies for asthma: is there any progress? *Trends in Pharmacological Sciences* **31**, 335-343.

Barnes PJ. (2011). Glucocorticosteroids: current and future directions. *Br J Pharmacol* **163**, 29-43.

Barnes PJ. (2014). Chronic obstructive pulmonary disease. *Clin Chest Med* **35**, xiii.

Barsumian EL, Isersky C, Petrino MG & Siraganian RP. (1981). IgE-induced histamine release from rat basophilic leukemia cell lines: isolation of releasing and nonreleasing clones. *Eur J Immunol* **11**, 317-323.

Bartlett R, Stokes L & Sluyter R. (2014). The P2X7 Receptor Channel: Recent Developments and the Use of P2X7 Antagonists in Models of Disease. *Pharmacological Reviews* **66**, 638-675.

Beaven MA. (2009). Our perception of the mast cell from Paul Ehrlich to now. *Eur J Immunol* **39**, 11-25.

Beaven MA, Rogers J, Moore JP, Hesketh TR, Smith GA & Metcalfe JC. (1984). The mechanism of the calcium signal and correlation with histamine release in 2H3 cells. *J Biol Chem* **259**, 7129-7136.

Beigi RD, Kertesy SB, Aquilina G & Dubyak GR. (2003). Oxidized ATP (oATP) attenuates proinflammatory signaling via P2 receptor-independent mechanisms. *Br J Pharmacol* **140**, 507-519.

Bennich HH, Ishizaka K, Johansson SG, Rowe DS, Stanworth DR & Terry WD. (1968). Immunoglobulin E: a new class of human immunoglobulin. *Immunology* **15**, 323-324.

Bhaskaracharya A, Phuong D-U, Jalilian I, Spildrejorde M, Skarratt KK, Fuller SJ, Sluyter R & Stokes L. (2014). Probenecid Blocks Human P2X7 Receptor-Induced Dye Uptake via a Pannexin-1 Independent Mechanism. *Plos One* **9**.

Birnbaumer L. (2009). The TRPC class of ion channels: a critical review of their roles in slow, sustained increases in intracellular Ca(2+) concentrations. *Annu Rev Pharmacol Toxicol* **49,** 395-426.

Bischoff SC. (2007). Role of mast cells in allergic and non-allergic immune responses: comparison of human and murine data. *Nature Reviews Immunology* **7,** 93-104.

Blair NT, Kaczmarek JS & Clapham DE. (2009). Intracellular calcium strongly potentiates agonist-activated TRPC5 channels. *J Gen Physiol* **133,** 525-546.

Boehm U, Klamp T, Groot M & Howard JC. (1997). Cellular responses to interferon-gamma. *Annu Rev Immunol* **15,** 749-795.

Bonazzi M & Cossart P. (2006). Bacterial entry into cells: a role for the endocytic machinery. *FEBS Lett* **580,** 2962-2967.

Boulay G, Zhu X, Peyton M, Jiang M, Hurst R, Stefani E & Birnbaumer L. (1997). Cloning and expression of a novel mammalian homolog of Drosophila transient receptor potential (Trp) involved in calcium entry secondary to activation of receptors coupled by the Gq class of G protein. *J Biol Chem* **272,** 29672-29680.

Boumechache M, Masin M, Edwardson JM, Górecki DC & Murrell-Lagnado R. (2009). Analysis of assembly and trafficking of native P2X4 and P2X7 receptor complexes in rodent immune cells. *J Biol Chem* **284,** 13446-13454.

Bousquet SM, Monet M & Boulay G. (2010). Protein kinase C-dependent phosphorylation of transient receptor potential canonical 6 (TRPC6) on serine 448 causes channel inhibition. *J Biol Chem* **285,** 40534-40543.

Bowler JW, Bailey RJ, North RA & Surprenant A. (2003). P2X4, P2Y1 and P2Y2 receptors on rat alveolar macrophages. *Br J Pharmacol* **140,** 567-575.

Boyce JA. (2007). Mast cells and eicosanoid mediators: a system of reciprocal paracrine and autocrine regulation. *Immunol Rev* **217,** 168-185.

Bradding P, Okayama Y, Kambe N & Saito H. (2003). Ion channel gene expression in human lung, skin, and cord blood-derived mast cells. *J Leukoc Biol* **73,** 614-620.

Brake AJ, Wagenbach MJ & Julius D. (1994). New structural motif for ligand-gated ion channels defined by an ionotropic ATP receptor. *Nature* **371,** 519-523.

Brandman O, Liou J, Park WS & Meyer T. (2007). STIM2 is a feedback regulator that stabilizes basal cytosolic and endoplasmic reticulum Ca2+ levels. *Cell* **131,** 1327-1339.

Braun A, Gessner JE, Varga-Szabo D, Syed SN, Konrad S, Stegner D, Vogtle T, Schmidt RE & Nieswandt B. (2009). STIM1 is essential for Fc gamma receptor activation and autoimmune inflammation. *Blood* **113,** 1097-1104.

Brazer SC, Singh BB, Liu X, Swaim W & Ambudkar IS. (2003). Caveolin-1 contributes to assembly of store-operated Ca2+ influx channels by regulating plasma membrane localization of TRPC1. *J Biol Chem* **278,** 27208-27215.

Broom DC, Matson DJ, Bradshaw E, Buck ME, Meade R, Coombs S, Matchett M, Ford KK, Yu W, Yuan J, Sun SH, Ochoa R, Krause JE, Wustrow DJ & Cortright DN. (2008). Characterization of N-(adamantan-1-ylmethyl)-5-[(3R-amino-pyrrolidin-1-yl)methyl]-2-chloro-benzamide, a P2X7 antagonist in animal models of pain and inflammation. *J Pharmacol Exp Ther* **327,** 620-633.

Brough D, Le Feuvre RA, Wheeler RD, Solovyova N, Hilfiker S, Rothwell NJ & Verkhratsky A. (2003). Ca2+ stores and Ca2+ entry differentially contribute to the release of IL-1 beta and IL-1 alpha from murine macrophages. *J Immunol* **170,** 3029-3036.

Brownlie RJ, Lawlor KE, Niederer HA, Cutler AJ, Xiang Z, Clatworthy MR, Floto RA, Greaves DR, Lyons PA & Smith KG. (2008). Distinct cell-specific control of autoimmunity and infection by FcgammaRIIb. *J Exp Med* **205,** 883-895.

Brugger W, Kreutz M & Andreesen R. (1991). Macrophage colony-stimulating factor is required for human monocyte survival and acts as a cofactor for their terminal differentiation to macrophages *in vitro*. *J Leukoc Biol* **49,** 483-488.

Burnstock G & Kennedy C. (1985). Is there a basis for distinguishing two types of P2-purinoceptor? *Gen Pharmacol* **16,** 433-440.

Bustin SA. (2002). Quantification of mRNA using real-time reverse transcription PCR (RT-PCR): trends and problems. *J Mol Endocrinol* **29,** 23-39.

Butterfield JH, Weiler D, Dewald G & Gleich GJ. (1988). Establishment of an immature mast cell line from a patient with mast cell leukemia. *Leuk Res* **12,** 345-355.

Buxadé M, Lunazzi G, Minguillón J, Iborra S, Berga-Bolaños R, Del Val M, Aramburu J & López-Rodríguez C. (2012). Gene expression induced by Toll-like receptors in macrophages requires the transcription factor NFAT5. *J Exp Med* **209,** 379-393.

Cabrini G, Falzoni S, Forchap SL, Pellegatti P, Balboni A, Agostini P, Cuneo A, Castoldi G, Baricordi OR & Di Virgilio F. (2005). A His-155 to Tyr polymorphism confers gain-of-function to the human P2X7 receptor of human leukemic lymphocytes. *J Immunol* **175,** 82-89.

Carreras-Sureda A, Cantero-Recasens G, Rubio-Moscardo F, Kiefer K, Peinelt C, Niemeyer BA, Valverde MA & Vicente R. (2013). ORMDL3 modulates store-operated calcium entry and lymphocyte activation. *Hum Mol Genet* **22,** 519-530.

Casas-Pruneda G, Reyes JP, Pérez-Flores G, Pérez-Cornejo P & Arreola J. (2009). Functional interactions between P2X4 and P2X7 receptors from mouse salivary epithelia. *J Physiol* **587,** 2887-2901.

Cayouette S, Lussier MP, Mathieu EL, Bousquet SM & Boulay G. (2004). Exocytotic insertion of TRPC6 channel into the plasma membrane upon Gq protein-coupled receptor activation. *J Biol Chem* **279,** 7241-7246.

Chang WC & Parekh AB. (2004). Close functional coupling between Ca2+ release-activated Ca2+ channels, arachidonic acid release, and leukotriene C-4 secretion. *J Biol Chem* **279,** 29994-29999.

Cheewatrakoolpong B, Gilchrest H, Anthes JC & Greenfeder S. (2005). Identification and characterization of splice variants of the human P2X7 ATP channel. *Biochem Biophys Res Commun* **332,** 17-27.

Chen W, Thielmann I, Gupta S, Subramanian H, Stegner D, van Kruchten R, Dietrich A, Gambaryan S, Heemskerk JW, Hermanns HM, Nieswandt B & Braun A. (2014). Orai1-induced store-operated Ca(2+) entry enhances phospholipase activity and modulates canonical transient receptor potential channel 6 function in murine platelets. *J Thromb Haemost* **12,** 528-539.

Cheng KT, Liu X, Ong HL, Swaim W & Ambudkar IS. (2011a). Local Ca(2)+ entry via Orai1 regulates plasma membrane recruitment of TRPC1 and controls cytosolic Ca(2)+ signals required for specific cell functions. *PLoS Biol* **9,** e1001025.

Cheng KT, Ong HL, Liu X & Ambudkar IS. (2011b). Contribution of TRPC1 and Orai1 to Ca(2+) entry activated by store depletion. *Adv Exp Med Biol* **704,** 435-449.

Cheng KT, Ong HL, Liu X & Ambudkar IS. (2011c). Contribution of TRPC1 and Orai1 to Ca(2+) entry activated by store depletion. *Adv Exp Med Biol* **704,** 435-449.

Cheng KT, Ong HL, Liu X & Ambudkar IS. (2013). Contribution and regulation of TRPC channels in store-operated Ca2+ entry. *Curr Top Membr* **71,** 149-179.

Chessell IP, Michel AD & Humphrey PP. (1998). Effects of antagonists at the human recombinant P2X7 receptor. *Br J Pharmacol* **124,** 1314-1320.

Choi S, Maleth J, Jha A, Lee KP, Kim MS, So I, Ahuja M & Muallem S. (2014). The TRPCs-STIM1-Orai interaction. *Handb Exp Pharmacol* **223,** 1035-1054.

Cicko S, Lucattelli M, Mueller T, Lommatzsch M, De Cunto G, Cardini S, Sundas W, Grimm M, Zeiser R, Duerk T, Zissel G, Boeynaems J-M, Sorichter S, Ferrari D, Di Virgilio F, Virchow JC, Lungarella G & Idzko M. (2010). Purinergic Receptor Inhibition Prevents the Development of Smoke-Induced Lung Injury and Emphysema. *Journal of Immunology* **185,** 688-697.

Cioffi DL, Wu S, Chen H, Alexeyev M, St Croix CM, Pitt BR, Uhlig S & Stevens T. (2012a). Orai1 Determines Calcium Selectivity of an Endogenous TRPC Heterotetramer Channel. *Circulation Research* **110**.

Cioffi DL, Wu S, Chen H, Alexeyev M, St Croix CM, Pitt BR, Uhlig S & Stevens T. (2012b). Orai1 Determines Calcium Selectivity of an Endogenous TRPC Heterotetramer Channel. *Circ Res*.

Cohen R, Torres A, Ma H, Holowka D & Baird B. (2009). Ca2+ Waves Initiate Antigen-Stimulated Ca2+ Responses in Mast Cells. *J Immunol* **183,** 6478-6488.

Coutinho-Silva R, Perfettini JL, Persechini PM, Dautry-Varsat A & Ojcius DM. (2001). Modulation of P2Z/P2X(7) receptor activity in macrophages infected with Chlamydia psittaci. *Am J Physiol Cell Physiol* **280,** C81-89.

Crabtree GR & Olson EN. (2002). NFAT signaling: choreographing the social lives of cells. *Cell* **109 Suppl,** S67-79.

Crowley MT, Costello PS, FitzerAttas CJ, Turner M, Meng FY, Lowell C, Tybulewicz VLJ & DeFranco AL. (1997). A critical role for Syk in signal transduction and phagocytosis mediated by Fc gamma receptors on macrophages. *Journal of Experimental Medicine* **186,** 1027-1039.

Da Silva CA & Frossard N. (2005). Regulation of stem cell factor expression in inflammation and asthma. *Mem Inst Oswaldo Cruz* **100 Suppl 1,** 145-151.

Dardano A, Falzoni S, Caraccio N, Polini A, Tognini S, Solini A, Berti P, Di Virgilio F & Monzani F. (2009). 1513A>C polymorphism in the P2X7 receptor gene in patients with papillary thyroid cancer: correlation with histological variants and clinical parameters. *J Clin Endocrinol Metab* **94,** 695-698.

Davies LC, Jenkins SJ, Allen JE & Taylor PR. (2013). Tissue-resident macrophages. *Nat Immunol* **14,** 986-995.

Dayam RM, Saric A, Shilliday RE & Botelho RJ. (2015). The Phosphoinositide-Gated Lysosomal Ca(2+) Channel, TRPML1, Is Required for Phagosome Maturation. *Traffic*.

DeHaven WI, Jones BF, Petranka JG, Smyth JT, Tomita T, Bird GS & Putney JW. (2009). TRPC channels function independently of STIM1 and Orai1. *Journal of Physiology-London* **587,** 2275-2298.

DeHaven WI, Smyth JT, Boyles RR, Bird GS & Putney JW. (2008). Complex actions of 2-aminoethyldiphenyl borate on store-operated calcium entry. *J Biol Chem* **283,** 19265-19273.

DeHaven WI, Smyth JT, Boyles RR & Putney JW. (2007). Calcium inhibition and calcium potentiation of Orai1, Orai2, and Orai3 calcium release-activated calcium channels. *Journal of Biological Chemistry* **282,** 17548-17556.

Derler I, Schindl R, Fritsch R, Heftberger P, Riedl MC, Begg M, House D & Romanin C. (2013). The action of selective CRAC channel blockers is affected by the Orai pore geometry. *Cell Calcium* **53,** 139-151.

Dey A, Allen J & Hankey-Giblin PA. (2014). Ontogeny and polarization of macrophages in inflammation: blood monocytes versus tissue macrophages. *Front Immunol* **5,** 683.

Di Capite J & Parekh AB. (2009). CRAC channels and Ca2+ signaling in mast cells. *Immunol Rev* **231,** 45-58.

Di Sabatino A, Rovedatti L, Kaur R, Spencer JP, Brown JT, Morisset VD, Biancheri P, Leakey NA, Wilde JI, Scott L, Corazza GR, Lee K, Sengupta N, Knowles CH, Gunthorpe MJ,

McLean PG, MacDonald TT & Kruidenier L. (2009). Targeting gut T cell Ca2+ release-activated Ca2+ channels inhibits T cell cytokine production and T-box transcription factor T-bet in inflammatory bowel disease. *J Immunol* **183,** 3454-3462.

Di Virgilio F, Meyer BC, Greenberg S & Silverstein SC. (1988). Fc receptor-mediated phagocytosis occurs in macrophages at exceedingly low cytosolic Ca2+ levels. *J Cell Biol* **106,** 657-666.

Di Virgilio F, Steinberg TH & Silverstein SC. (1990). Inhibition of Fura-2 sequestration and secretion with organic anion transport blockers. *Cell Calcium* **11,** 57-62.

Dietrich A, Fahlbusch M & Gudermann T. (2014). Classical Transient Receptor Potential 1 (TRPC1): Channel or Channel Regulator? *Cells* **3,** 939-962.

Dietrich A & Gudermann T. (2007). TRPC6. *Handb Exp Pharmacol***,** 125-141.

Dietrich A, Mederos y Schnitzler M, Emmel J, Kalwa H, Hofmann T & Gudermann T. (2003). N-linked protein glycosylation is a major determinant for basal TRPC3 and TRPC6 channel activity. *J Biol Chem* **278,** 47842-47852.

Dietrich A, Mederos y Schnitzler M, Kalwa H, Storch U & Gudermann T. (2005). Functional characterization and physiological relevance of the TRPC3/6/7 subfamily of cation channels. *Naunyn Schmiedebergs Arch Pharmacol* **371,** 257-265.

Dijstelbloem HM, van de Winkel JG & Kallenberg CG. (2001). Inflammation in autoimmunity: receptors for IgG revisited. *Trends Immunol* **22,** 510-516.

Ding L, Dolgachev V, Wu Z, Liu T, Nakashima T, Ullenbruch M, Lukacs NW, Chen Z & Phan SH. (2013). Essential role of stem cell factor-c-Kit signalling pathway in bleomycin-induced pulmonary fibrosis. *J Pathol* **230,** 205-214.

Dolmetsch R, Lewis R, Goodnow C & Healy J. (1997). Differential activation of transcription factors induced by Ca2+ response amplitude and duration. *Nature* **386,** 855-858.

Donnelly-Roberts DL, Namovic MT, Han P & Jarvis MF. (2009). Mammalian P2X7 receptor pharmacology: comparison of recombinant mouse, rat and human P2X7 receptors. *Br J Pharmacol* **157,** 1203-1214.

Downey GP, Botelho RJ, Butler JR, Moltyaner Y, Chien P, Schreiber AD & Grinstein S. (1999). Phagosomal maturation, acidification, and inhibition of bacterial growth in nonphagocytic cells transfected with FcgammaRIIA receptors. *J Biol Chem* **274,** 28436-28444.

Du J, Ma X, Shen B, Huang Y, Birnbaumer L & Yao X. (2014). TRPV4, TRPC1, and TRPP2 assemble to form a flow-sensitive heteromeric channel. *FASEB J* **28,** 4677-4685.

Dunn PM & Blakeley AG. (1988). Suramin: a reversible P2-purinoceptor antagonist in the mouse vas deferens. *Br J Pharmacol* **93,** 243-245.

Eccleston E, Leonard BJ, Lowe JS & Welford HJ. (1973). Basophilic leukaemia in the albino rat and a demonstration of the basopoietin. *Nat New Biol* **244,** 73-76.

Eischen A, Vincent F, Bergerat JP, Louis B, Faradji A, Bohbot A & Oberling F. (1991). Long term cultures of human monocytes *in vitro*. Impact of GM-CSF on survival and differentiation. *J Immunol Methods* **143,** 209-221.

Eltom S, Dale N, Raemdonck KR, Stevenson CS, Snelgrove RJ, Sacitharan PK, Recchi C, Wavre-Shapton S, McAuley DF, O'Kane C, Belvisi MG & Birrell MA. (2014). Respiratory infections cause the release of extracellular vesicles: implications in exacerbation of asthma/COPD. *PLoS One* **9,** e101087.

Eltom S, Stevenson CS, Rastrick J, Dale N, Raemdonck K, Wong S, Catley MC, Belvisi MG & Birrell MA. (2011). P2X7 receptor and caspase 1 activation are central to airway inflammation observed after exposure to tobacco smoke. *PLoS One* **6,** e24097.

Ennis M. (1991). Current techniques of histamine determination., pp. 31-38. Handbook Exp Pharmacol.

Estacion M, Li S, Sinkins WG, Gosling M, Bahra P, Poll C, Westwick J & Schilling WP. (2004). Activation of human TRPC6 channels by receptor stimulation. *J Biol Chem* **279,** 22047-22056.

Estacion M, Sinkins WG, Jones SW, Applegate MA & Schilling WP. (2006). Human TRPC6 expressed in HEK 293 cells forms non-selective cation channels with limited Ca2+ permeability. *J Physiol* **572,** 359-377.

Evans RJ, Lewis C, Buell G, Valera S, North RA & Surprenant A. (1995). Pharmacological characterization of heterologously expressed ATP-gated cation channels (P2x purinoceptors). *Mol Pharmacol* **48,** 178-183.

Fairbairn IP, Stober CB, Kumararatne DS & Lammas DA. (2001). ATP-mediated killing of intracellular mycobacteria by macrophages is a P2X(7)-dependent process inducing bacterial death by phagosome-lysosome fusion. *Journal of Immunology* **167,** 3300-3307.

Faouzi M, Hague F, Potier M, Ahidouch A, Sevestre H & Ouadid-Ahidouch H. (2011). Down-regulation of Orai3 arrests cell-cycle progression and induces apoptosis in breast cancer cells but not in normal breast epithelial cells. *J Cell Physiol* **226,** 542-551.

Faouzi M, Kischel P, Hague F, Ahidouch A, Benzerdjeb N, Sevestre H, Penner R & Ouadid-Ahidouch H. (2013). ORAI3 silencing alters cell proliferation and cell cycle progression via c-myc pathway in breast cancer cells. *Biochim Biophys Acta* **1833,** 752-760.

Feng C, Mery AG, Beller EM, Favot C & Boyce JA. (2004). Adenine nucleotides inhibit cytokine generation by human mast cells through a Gs-coupled receptor. *J Immunol* **173,** 7539-7547.

Feng YH, Li X, Wang L, Zhou L & Gorodeski GI. (2006). A truncated P2X7 receptor variant (P2X7-j) endogenously expressed in cervical cancer cells antagonizes the full-length P2X7 receptor through hetero-oligomerization. *J Biol Chem* **281,** 17228-17237.

Fernando SL, Saunders BM, Sluyter R, Skarratt KK, Goldberg H, Marks GB, Wiley JS & Britton WJ. (2007). A polymorphism in the P2X7 gene increases susceptibility to extrapulmonary tuberculosis. *Am J Respir Crit Care Med* **175,** 360-366.

Fernando SL, Saunders BM, Sluyter R, Skarratt KK, Wiley JS & Britton WJ. (2005). Gene dosage determines the negative effects of polymorphic alleles of the P2X7 receptor on adenosine triphosphate-mediated killing of mycobacteria by human macrophages. *J Infect Dis* **192,** 149-155.

Ferrari D, Chiozzi P, Falzoni S, DalSusino M, Melchiorri L, Baricordi OR & DiVirgilio F. (1997a). Extracellular ATP triggers IL-1 beta release by activating the purinergic P2Z receptor of human macrophages. *Journal of Immunology* **159,** 1451-1458.

Ferrari D, Chiozzi P, Falzoni S, Hanau S & Di Virgilio F. (1997b). Purinergic modulation of interleukin-1 beta release from microglial cells stimulated with bacterial endotoxin. *J Exp Med* **185,** 579-582.

Feske S. (2009). ORAI1 and STIM1 deficiency in human and mice: roles of store-operated Ca2+ entry in the immune system and beyond. In *Immunol Rev*, pp. 189-209. Denmark.

Feske S, Gwack Y, Prakriya M, Srikanth S, Puppel SH, Tanasa B, Hogan PG, Lewis RS, Daly M & Rao A. (2006). A mutation in Orai1 causes immune deficiency by abrogating CRAC channel function. *Nature* **441,** 179-185.

Feske S, Picard C & Fischer A. (2010). Immunodeficiency due to mutations in ORAI1 and STIM1. In *Clin Immunol*, pp. 169-182. 2008 Elsevier Inc, United States.

Feske S, Skolnik EY & Prakriya M. (2012). Ion channels and transporters in lymphocyte function and immunity. *Nat Rev Immunol* **12,** 532-547.

Feske S, Wulff H & Skolnik EY. (2015). Ion channels in innate and adaptive immunity. *Annu Rev Immunol* **33,** 291-353.

Fierro L & Parekh AB. (1999). Fast calcium-dependent inactivation of calcium release-activated calcium current (CRAC) in RBL-1 cells. *J Membr Biol* **168,** 9-17.

Finney-Hayward TK, Popa MO, Bahra P, Li S, Poll CT, Gosling M, Nicholson AG, Russell RE, Kon OM, Jarai G, Westwick J, Barnes PJ & Donnelly LE. (2010). Expression of transient receptor potential C6 channels in human lung macrophages. *Am J Respir Cell Mol Biol* **43,** 296-304.

Flannagan RS, Jaumouillé V & Grinstein S. (2012). The cell biology of phagocytosis. *Annu Rev Pathol* **7,** 61-98.

Fleetwood AJ, Lawrence T, Hamilton JA & Cook AD. (2007). Granulocyte-macrophage colony-stimulating factor (CSF) and macrophage CSF-dependent macrophage phenotypes display differences in cytokine profiles and transcription factor activities: implications for CSF blockade in inflammation. *J Immunol* **178,** 5245-5252.

Foster RR, Zadeh MA, Welsh GI, Satchell SC, Ye Y, Mathieson PW, Bates DO & Saleem MA. (2009). Flufenamic acid is a tool for investigating TRPC6-mediated calcium signalling in human conditionally immortalised podocytes and HEK293 cells. *Cell Calcium* **45,** 384-390.

Franchi L, Kanneganti TD, Dubyak GR & Núñez G. (2007). Differential requirement of P2X7 receptor and intracellular K+ for caspase-1 activation induced by intracellular and extracellular bacteria. *J Biol Chem* **282,** 18810-18818.

Fredericks GJ, Hoffmann FW, Rose AH, Osterheld HJ, Hess FM, Mercier F & Hoffmann PR. (2014). Stable expression and function of the inositol 1,4,5-triphosphate receptor requires palmitoylation by a DHHC6/selenoprotein K complex. *Proc Natl Acad Sci U S A* **111,** 16478-16483.

Freichel M, Almering J & Tsvilovskyy V. (2012). The Role of TRP Proteins in Mast Cells. *Frontiers in immunology* **3,** 150-150.

Funk CD. (2001). Prostaglandins and leukotrienes: advances in eicosanoid biology. *Science* **294,** 1871-1875.

Galli SJ, Nakae S & Tsai M. (2005). Mast cells in the development of adaptive immune responses. *Nat Immunol* **6,** 135-142.

Galli SJ & Tsai M. (2012). IgE and mast cells in allergic disease. *Nat Med* **18,** 693-704.

Gao ZG, Ding Y & Jacobson KA. (2010). P2Y(13) receptor is responsible for ADP-mediated degranulation in RBL-2H3 rat mast cells. *Pharmacol Res* **62,** 500-505.

Gao ZG, Wei Q, Jayasekara MP & Jacobson KA. (2013). The role of P2Y(14) and other P2Y receptors in degranulation of human LAD2 mast cells. *Purinergic Signal* **9,** 31-40.

Garcia RL & Schilling WP. (1997). Differential expression of mammalian TRP homologues across tissues and cell lines. *Biochem Biophys Res Commun* **239,** 279-283.

Garcia-Guzman M, Soto F, Gomez-Hernandez JM, Lund PE & Stühmer W. (1997). Characterization of recombinant human P2X4 receptor reveals pharmacological differences to the rat homologue. *Mol Pharmacol* **51,** 109-118.

Gargett CE & Wiley JS. (1997). The isoquinoline derivative KN-62 a potent antagonist of the P2Z-receptor of human lymphocytes. *Br J Pharmacol* **120,** 1483-1490.

Gautier EL, Shay T, Miller J, Greter M, Jakubzick C, Ivanov S, Helft J, Chow A, Elpek KG, Gordonov S, Mazloom AR, Ma'ayan A, Chua WJ, Hansen TH, Turley SJ, Merad M, Randolph GJ & Consortium IG. (2012). Gene-expression profiles and transcriptional regulatory pathways that underlie the identity and diversity of mouse tissue macrophages. *Nat Immunol* **13,** 1118-1128.

Gessner JE, Heiken H, Tamm A & Schmidt RE. (1998). The IgG Fc receptor family. *Annals of Hematology* **76,** 231-248.

Gilfillan AM, Austin SJ & Metcalfe DD. (2011a). MAST CELL BIOLOGY: Introduction and Overview. In *Mast Cell Biology: Contemporary and Emerging Topics*, ed. Gilfillan AM & Metcalfe DD, pp. 2-12. Springer-Verlag Berlin, Berlin.

Gilfillan AM, Austin SJ & Metcalfe DD. (2011b). Mast cell biology: introduction and overview. *Adv Exp Med Biol* **716,** 2-12.

Gilfillan AM & Beaven MA. (2011). Regulation of mast cell responses in health and disease. *Crit Rev Immunol* **31,** 475-529.

Gilfillan AM & Tkaczyk C. (2006). Integrated signalling pathways for mast-cell activation. *Nature Reviews Immunology* **6,** 218-230.

Gomez Perdiguero E, Klapproth K, Schulz C, Busch K, Azzoni E, Crozet L, Garner H, Trouillet C, de Bruijn MF, Geissmann F & Rodewald HR. (2015). Tissue-resident macrophages originate from yolk-sac-derived erythro-myeloid progenitors. *Nature* **518,** 547-551.

González-Cobos JC, Zhang X, Zhang W, Ruhle B, Motiani RK, Schindl R, Muik M, Spinelli AM, Bisaillon JM, Shinde AV, Fahrner M, Singer HA, Matrougui K, Barroso M, Romanin C & Trebak M. (2013). Store-independent Orai1/3 channels activated by intracrine leukotriene C4: role in neointimal hyperplasia. *Circ Res* **112,** 1013-1025.

Goodridge HS, Underhill DM & Touret N. (2012). Mechanisms of Fc receptor and dectin-1 activation for phagocytosis. *Traffic* **13,** 1062-1071.

Gordon S. (2007). The macrophage: Past, present and future. *European Journal of Immunology* **37,** S9-S17.

Grace MS, Baxter M, Dubuis E, Birrell MA & Belvisi MG. (2014). Transient receptor potential (TRP) channels in the airway: role in airway disease. *Br J Pharmacol* **171,** 2593-2607.

Gu BJ, Rathsam C, Stokes L, McGeachie AB & Wiley JS. (2009). Extracellular ATP dissociates nonmuscle myosin from P2X(7) complex: this dissociation regulates P2X(7) pore formation. *Am J Physiol Cell Physiol* **297,** C430-439.

Gu BJ, Saunders BM, Jursik C & Wiley JS. (2010). The P2X7-nonmuscle myosin membrane complex regulates phagocytosis of nonopsonized particles and bacteria by a pathway attenuated by extracellular ATP. *Blood* **115,** 1621-1631.

Gu BJ, Saunders BM, Petrou S & Wiley JS. (2011). P2X(7) is a scavenger receptor for apoptotic cells in the absence of its ligand, extracellular ATP. *J Immunol* **187,** 2365-2375.

Gu BJ, Sluyter R, Skarratt KK, Shemon AN, Dao-Ung LP, Fuller SJ, Barden JA, Clarke AL, Petrou S & Wiley JS. (2004). An Arg307 to Gln polymorphism within the ATP-binding site causes loss of function of the human P2X7 receptor. *J Biol Chem* **279,** 31287-31295.

Gu BJ, Zhang W, Worthington RA, Sluyter R, Dao-Ung P, Petrou S, Barden JA & Wiley JS. (2001). A Glu-496 to Ala polymorphism leads to loss of function of the human P2X7 receptor. *J Biol Chem* **276,** 11135-11142.

Guhl S, Babina M, Neou A, Zuberbier T & Artuc M. (2010). Mast cell lines HMC-1 and LAD2 in comparison with mature human skin mast cells--drastically reduced levels of tryptase and chymase in mast cell lines. *Exp Dermatol* **19,** 845-847.

Guilliams M, Bruhns P, Saeys Y, Hammad H & Lambrecht BN. (2014). The function of Fcγ receptors in dendritic cells and macrophages. *Nat Rev Immunol* **14,** 94-108.

Guo C, Masin M, Qureshi OS & Murrell-Lagnado RD. (2007). Evidence for functional P2X4/P2X7 heteromeric receptors. *Mol Pharmacol* **72,** 1447-1456.

Guth AM, Janssen WJ, Bosio CM, Crouch EC, Henson PM & Dow SW. (2009). Lung environment determines unique phenotype of alveolar macrophages. *Am J Physiol Lung Cell Mol Physiol* **296,** L936-946.

Hardie RC & Minke B. (1992). The trp gene is essential for a light-activated Ca2+ channel in Drosophila photoreceptors. *Neuron* **8,** 643-651.

Hishikawa T, Cheung JY, Yelamarty RV & Knutson DW. (1991). Calcium transients during Fc receptor-mediated and nonspecific phagocytosis by murine peritoneal macrophages. *J Cell Biol* **115,** 59-66.

Hoffmann A, Kann O, Ohlemeyer C, Hanisch UK & Kettenmann H. (2003). Elevation of basal intracellular calcium as a central element in the activation of brain macrophages (microglia): suppression of receptor-evoked calcium signaling and control of release function. *J Neurosci* **23,** 4410-4419.

Hofmann T, Obukhov AG, Schaefer M, Harteneck C, Gudermann T & Schultz G. (1999). Direct activation of human TRPC6 and TRPC3 channels by diacylglycerol. *Nature* **397,** 259-263.

Hofmann T, Schaefer M, Schultz G & Gudermann T. (2002). Subunit composition of mammalian transient receptor potential channels in living cells. *Proc Natl Acad Sci U S A* **99,** 7461-7466.

Hong JH, Li Q, Kim MS, Shin DM, Feske S, Birnbaumer L, Cheng KT, Ambudkar IS & Muallem S. (2011). Polarized but Differential Localization and Recruitment of STIM1, Orai1 and TRPC Channels in Secretory Cells. *Traffic* **12,** 232-245.

Honore P, Donnelly-Roberts D, Namovic M, Zhong C, Wade C, Chandran P, Zhu C, Carroll W, Perez-Medrano A, Iwakura Y & Jarvis MF. (2009). The antihyperalgesic activity of a selective P2X7 receptor antagonist, A-839977, is lost in IL-1alphabeta knockout mice. *Behav Brain Res* **204,** 77-81.

Honore P, Donnelly-Roberts D, Namovic MT, Hsieh G, Zhu CZ, Mikusa JP, Hernandez G, Zhong C, Gauvin DM, Chandran P, Harris R, Medrano AP, Carroll W, Marsh K, Sullivan JP, Faltynek CR & Jarvis MF. (2006). A-740003 [N-(1-{[(cyanoimino)(5-quinolinylamino) methyl]amino}-2,2-dimethylpropyl)-2-(3,4-

dimethoxyphenyl)acetamide], a novel and selective P2X7 receptor antagonist, dose-dependently reduces neuropathic pain in the rat. *J Pharmacol Exp Ther* **319,** 1376-1385.

Hoth M. (1995). Calcium and barium permeation through calcium release-activated calcium (CRAC) channels. *Pflugers Arch* **430,** 315-322.

Hoth M & Niemeyer BA. (2013). The neglected CRAC proteins: Orai2, Orai3, and STIM2. *Curr Top Membr* **71,** 237-271.

Hoth M & Penner R. (1992). DEPLETION OF INTRACELLULAR CALCIUM STORES ACTIVATES A CALCIUM CURRENT IN MAST-CELLS. *Nature* **355,** 353-356.

Hoth M & Penner R. (1993). CALCIUM RELEASE-ACTIVATED CALCIUM CURRENT IN RAT MAST-CELLS. *Journal of Physiology-London* **465,** 359-386.

Hou X, Pedi L, Diver MM & Long SB. (2012). Crystal structure of the calcium release-activated calcium channel Orai. *Science* **338,** 1308-1313.

Huang GN, Zeng W, Kim JY, Yuan JP, Han L, Muallem S & Worley PF. (2006). STIM1 carboxyl-terminus activates native SOC, I-crac and TRPC1 channels. *Nature Cell Biology* **8**.

Huang Z, Hoffmann FW, Fay JD, Hashimoto AC, Chapagain ML, Kaufusi PH & Hoffmann PR. (2012). Stimulation of unprimed macrophages with immune complexes triggers a low output of nitric oxide by calcium-dependent neuronal nitric-oxide synthase. *J Biol Chem* **287,** 4492-4502.

Humphreys BD & Dubyak GR. (1996). Induction of the P2z/P2X(7) nucleotide receptor and associated phospholipase D activity by lipopolysaccharide and IFN-gamma in the human THP-1 monocytic cell line. *Journal of Immunology* **157,** 5627-5637.

Hundley TR, Gilfillan AM, Tkaczyk C, Andrade MV, Metcalfe DD & Beaven MA. (2004). Kit and FcepsilonRI mediate unique and convergent signals for release of inflammatory mediators from human mast cells. *Blood* **104,** 2410-2417.

Hussell T & Bell TJ. (2014). Alveolar macrophages: plasticity in a tissue-specific context. *Nat Rev Immunol* **14,** 81-93.

Ingersoll MA, Spanbroek R, Lottaz C, Gautier EL, Frankenberger M, Hoffmann R, Lang R, Haniffa M, Collin M, Tacke F, Habenicht AJ, Ziegler-Heitbrock L & Randolph GJ. (2010). Comparison of gene expression profiles between human and mouse monocyte subsets. *Blood* **115,** e10-19.

Inoue R, Okada T, Onoue H, Hara Y, Shimizu S, Naitoh S, Ito Y & Mori Y. (2001). The transient receptor potential protein homologue TRP6 is the essential component of vascular alpha(1)-adrenoceptor-activated Ca(2+)-permeable cation channel. *Circ Res* **88,** 325-332.

Jacobson KA, Jarvis MF & Williams M. (2002). Purine and pyrimidine (P2) receptors as drug targets. *J Med Chem* **45,** 4057-4093.

Jaguin M, Houlbert N, Fardel O & Lecureur V. (2013). Polarization profiles of human M-CSF-generated macrophages and comparison of M1-markers in classically activated macrophages from GM-CSF and M-CSF origin. *Cell Immunol* **281,** 51-61.

Jardin I, Lopez JJ, Salido GM & Rosado JA. (2008). Orai1 mediates the interaction between STIM1 and hTRPC1 and regulates the mode of activation of hTRPC1-forming Ca2+ channels. *J Biol Chem* **283,** 25296-25304.

Jiang LH, Kim M, Spelta V, Bo X, Surprenant A & North RA. (2003). Subunit arrangement in P2X receptors. *J Neurosci* **23,** 8903-8910.

Joshi T, Ganesan LP, Cheney C, Ostrowski MC, Muthusamy N, Byrd JC & Tridandapani S. (2009). The PtdIns 3-kinase/Akt pathway regulates macrophage-mediated ADCC against B cell lymphoma. *PLoS One* **4,** e4208.

Jung S, Mühle A, Schaefer M, Strotmann R, Schultz G & Plant TD. (2003). Lanthanides potentiate TRPC5 currents by an action at extracellular sites close to the pore mouth. *J Biol Chem* **278,** 3562-3571.

Kalesnikoff J & Galli SJ. (2008). New developments in mast cell biology. *Nat Immunol* **9,** 1215-1223.

Kang J, Park KH, Kim JJ, Jo EK, Han MK & Kim UH. (2012). The role of CD38 in Fcγ receptor (FcγR)-mediated phagocytosis in murine macrophages. *J Biol Chem* **287,** 14502-14514.

Katsnelson MA, Rucker LG, Russo HM & Dubyak GR. (2015). K+ Efflux Agonists Induce NLRP3 Inflammasome Activation Independently of Ca2+ Signaling. *J Immunol* **194,** 3937-3952.

Kaur R, Sloan LA, Blanchard AD, Smith JL, Churcher I, Wayne GJ & Ludbrook SB. (2013). A phenotypic screening approach in cord blood-derived mast cells to identify anti-inflammatory compounds. *J Biomol Screen* **18,** 1223-1233.

Kawai T & Akira S. (2010). The role of pattern-recognition receptors in innate immunity: update on Toll-like receptors. *Nature Immunology* **11,** 373-384.

Kawasaki T, Lange I & Feske S. (2009). A minimal regulatory domain in the C terminus of STIM1 binds to and activates ORAI1 CRAC channels. In *Biochem Biophys Res Commun*, pp. 49-54. United States.

Kawate T, Michel JC, Birdsong WT & Gouaux E. (2009). Crystal structure of the ATP-gated P2X(4) ion channel in the closed state. *Nature* **460,** 592-598.

Kim JY, Zeng W, Kiselyov K, Yuan JP, Dehoff MH, Mikoshiba K, Worley PF & Muallem S. (2006). Homer 1 mediates store- and inositol 1,4,5-trisphosphate receptor-dependent translocation and retrieval of TRPC3 to the plasma membrane. *J Biol Chem* **281,** 32540-32549.

Klein M, Klein-Hessling S, Palmetshofer A, Serfling E, Tertilt C, Bopp T, Heib V, Becker M, Taube C, Schild H, Schmitt E & Stassen M. (2006). Specific and redundant roles for

NFAT transcription factors in the expression of mast cell-derived cytokines. *J Immunol* **177,** 6667-6674.

Kraft R & Harteneck C. (2005). The mammalian melastatin-related transient receptor potential cation channels: an overview. *Pflugers Arch* **451,** 204-211.

Kruskal BA & Maxfield FR. (1987). Cytosolic free calcium increases before and oscillates during frustrated phagocytosis in macrophages. *J Cell Biol* **105,** 2685-2693.

Kårehed K, Dimberg A, Dahl S, Nilsson K & Oberg F. (2007). IFN-gamma-induced upregulation of Fcgamma-receptor-I during activation of monocytic cells requires the PKR and NFkappaB pathways. *Mol Immunol* **44,** 615-624.

Laidlaw TM, Steinke JW, Tinana AM, Feng CL, Xing W, Lam BK, Paruchuri S, Boyce JA & Borish L. (2011). Characterization of a novel human mast cell line that responds to stem cell factor and expresses functional Fc is an element of RI. *Journal of Allergy and Clinical Immunology* **127,** 815-U499.

Lambrecht G, Friebe T, Grimm U, Windscheif U, Bungardt E, Hildebrandt C, Bäumert HG, Spatz-Kümbel G & Mutschler E. (1992). PPADS, a novel functionally selective antagonist of P2 purinoceptor-mediated responses. *Eur J Pharmacol* **217,** 217-219.

Lammas DA, Stober C, Harvey CJ, Kendrick N, Panchalingam S & Kumararatne DS. (1997). ATP-induced killing of mycobacteria by human macrophages is mediated by purinergic P2Z(P2X7) receptors. *Immunity* **7,** 433-444.

Laskin DL. (2009). Macrophages and inflammatory mediators in chemical toxicity: a battle of forces. *Chem Res Toxicol* **22,** 1376-1385.

Lee BH, Hwang DM, Palaniyar N, Grinstein S, Philpott DJ & Hu J. (2012). Activation of P2X(7) Receptor by ATP Plays an Important Role in Regulating Inflammatory Responses during Acute Viral Infection. *Plos One* **7,** 13.

Lee KP, Yuan JP, So I, Worley PF & Muallem S. (2010). STIM1-dependent and STIM1-independent Function of Transient Receptor Potential Canonical (TRPC) Channels Tunes Their Store-operated Mode. *J Biol Chem* **285,** 38666-38673.

Lees MP, Fuller SJ, McLeod R, Boulter NR, Miller CM, Zakrzewski AM, Mui EJ, Witola WH, Coyne JJ, Hargrave AC, Jamieson SE, Blackwell JM, Wiley JS & Smith NC. (2010). P2X7 receptor-mediated killing of an intracellular parasite, Toxoplasma gondii, by human and murine macrophages. *J Immunol* **184,** 7040-7046.

Leuner K, Kazanski V, Müller M, Essin K, Henke B, Gollasch M, Harteneck C & Müller WE. (2007). Hyperforin--a key constituent of St. John's wort specifically activates TRPC6 channels. *FASEB J* **21,** 4101-4111.

Lew PD & Stossel TP. (1980). Calcium transport by macrophage plasma membranes. *J Biol Chem* **255,** 5841-5846.

Lewis A, Wan J, Baothman B, Monk P, Suvarna S & Peachell P. (2013a). Heterogeneity in the responses of human lung mast cells to stem cell factor. *Clin Exp Allergy* **43,** 50-59.

Lewis A, Wan J, Baothman B, Monk PN, Suvarna SK & Peachell PT. (2013b). Heterogeneity in the responses of human lung mast cells to stem cell factor. *Clin Exp Allergy* **43,** 50-59.

Li J, McKeown L, Ojelabi O, Stacey M, Foster R, O'Regan D, Porter KE & Beech DJ. (2011). Nanomolar potency and selectivity of a Ca²⁺ release-activated Ca²⁺ channel inhibitor against store-operated Ca²⁺ entry and migration of vascular smooth muscle cells. *Br J Pharmacol* **164,** 382-393.

Liang X, Samways DS, Wolf K, Bowles EA, Richards JP, Bruno J, Dutertre S, DiPaolo RJ & Egan TM. (2015). Quantifying Ca2+ current and permeability in ATP-gated P2X7 receptors. *J Biol Chem* **290,** 7930-7942.

Liao Y, Erxleben C, Yildirim E, Abramowitz J, Armstrong DL & Birnbaumer L. (2007). Orai proteins interact with TRPC channels and confer responsiveness to store depletion. *Proc Natl Acad Sci U S A* **104,** 4682-4687.

Liao YY, Plummer NW, George MD, Abramowitz J, Zhu MX & Birnbaumer L. (2009). A role for Orai in TRPC-mediated Ca2+ entry suggests that a TRPC:Orai complex may mediate store and receptor operated Ca2+ entry. *Proc Natl Acad Sci U S A* **106,** 3202-3206.

Lievremont JP, Bird GS & Putney JW. (2005). Mechanism of inhibition of TRPC cation channels by 2-aminoethoxydiphenylborane. *Molecular Pharmacology* **68,** 758-762.

Lindemann O, Umlauf D, Frank S, Schimmelpfennig S, Bertrand J, Pap T, Hanley PJ, Fabian A, Dietrich A & Schwab A. (2013). TRPC6 regulates CXCR2-mediated chemotaxis of murine neutrophils. *J Immunol* **190,** 5496-5505.

Liou J, Fivaz M, Inoue T & Meyer T. (2007). Live-cell imaging reveals sequential oligomerization and local plasma membrane targeting of stromal interaction molecule 1 after Ca2+ store depletion. *Proc Natl Acad Sci U S A* **104,** 9301-9306.

Liou J, Kim M, Heo W, Jones J, Myers J, Ferrell J & Meyer T. (2005). STIM is a Ca(2+) sensor essential for Ca(2+)-store-depletion-triggered Ca(2+) influx. *Current Biology* **15,** 1235-1241.

Lis A, Peinelt C, Beck A, Parvez S, Monteilh-Zoller M, Fleig A & Penner R. (2007). CRACM1, CRACM2, and CRACM3 are store-operated Ca2+ channels with distinct functional properties. *Curr Biol* **17,** 794-800.

Liu X, Wang W, Singh BB, Lockwich T, Jadlowiec J, O'Connell B, Wellner R, Zhu MX & Ambudkar IS. (2000). Trp1, a candidate protein for the store-operated Ca(2+) influx mechanism in salivary gland cells. *J Biol Chem* **275,** 3403-3411.

Lockwich TP, Liu X, Singh BB, Jadlowiec J, Weiland S & Ambudkar IS. (2000). Assembly of Trp1 in a signaling complex associated with caveolin-scaffolding lipid raft domains. *J Biol Chem* **275,** 11934-11942.

Lommatzsch M, Cicko S, Mueller T, Lucattelli M, Bratke K, Stoll P, Grimm M, Duerk T, Zissel G, Ferrari D, Di Virgilio F, Sorichter S, Lungarella G, Virchow JC & Idzko M. (2010). Extracellular Adenosine Triphosphate and Chronic Obstructive Pulmonary Disease. *American Journal of Respiratory and Critical Care Medicine* **181,** 928-934.

Lucattelli M, Cicko S, Müller T, Lommatzsch M, De Cunto G, Cardini S, Sundas W, Grimm M, Zeiser R, Dürk T, Zissel G, Sorichter S, Ferrari D, Di Virgilio F, Virchow JC, Lungarella G & Idzko M. (2011). P2X7 receptor signaling in the pathogenesis of smoke-induced lung inflammation and emphysema. *Am J Respir Cell Mol Biol* **44,** 423-429.

Lundequist A & Pejler G. (2011). Biological implications of preformed mast cell mediators. *Cellular and Molecular Life Sciences* **68,** 965-975.

Ma H, Peng Z, Hiragun T, Iwaki S, Gilfillan A & Beaven M. (2008). **Canonical transient receptor potential 5 channel in conjunction with Orai1 and STIM1 allows Sr2+ entry, optimal influx of Ca2+, and degranulation in a rat mast cell line.**, pp. 2233-2239. J Immunol.

Ma W, Korngreen A, Weil S, Cohen EB, Priel A, Kuzin L & Silberberg SD. (2006). Pore properties and pharmacological features of the P2X receptor channel in airway ciliated cells. *J Physiol* **571,** 503-517.

Ma X, Cao J, Luo J, Nilius B, Huang Y, Ambudkar IS & Yao X. (2010). Depletion of intracellular Ca2+ stores stimulates the translocation of vanilloid transient receptor potential 4-c1 heteromeric channels to the plasma membrane. *Arterioscler Thromb Vasc Biol* **30,** 2249-2255.

Ma X, Cheng KT, Wong CO, O'Neil RG, Birnbaumer L, Ambudkar IS & Yao X. (2011a). Heteromeric TRPV4-C1 channels contribute to store-operated Ca(2+) entry in vascular endothelial cells. In *Cell Calcium*, pp. 502-509. 2011 Elsevier Ltd, Netherlands.

Ma X, Cheng KT, Wong CO, O'Neil RG, Birnbaumer L, Ambudkar IS & Yao X. (2011b). Heteromeric TRPV4-C1 channels contribute to store-operated Ca(2+) entry in vascular endothelial cells. *Cell Calcium* **50,** 502-509.

Mackenzie AB, Young MT, Adinolfi E & Surprenant A. (2005). Pseudoapoptosis induced by brief activation of ATP-gated P2X7 receptors. *J Biol Chem* **280,** 33968-33976.

Malaviya R, Ikeda T, Ross E & Abraham SN. (1996). Mast cell modulation of neutrophil influx and bacterial clearance at sites of infection through TNF-alpha. *Nature* **381,** 77-80.

Malik ZA, Denning GM & Kusner DJ. (2000). Inhibition of Ca(2+) signaling by Mycobacterium tuberculosis is associated with reduced phagosome-lysosome fusion and increased survival within human macrophages. *J Exp Med* **191,** 287-302.

Marchi LF, Sesti-Costa R, Ignacchiti MD, Chedraoui-Silva S & Mantovani B. (2014). *In vitro* activation of mouse neutrophils by recombinant human interferon-gamma: increased phagocytosis and release of reactive oxygen species and pro-inflammatory cytokines. *Int Immunopharmacol* **18,** 228-235.

Maroto R, Raso A, Wood TG, Kurosky A, Martinac B & Hamill OP. (2005). TRPC1 forms the stretch-activated cation channel in vertebrate cells. *Nat Cell Biol* **7,** 179-185.

Marquardt DL & Walker LL. (2000). Dependence of mast cell IgE-mediated cytokine production on nuclear factor-kappaB activity. *J Allergy Clin Immunol* **105,** 500-505.

Martinez FO, Gordon S, Locati M & Mantovani A. (2006). Transcriptional profiling of the human monocyte-to-macrophage differentiation and polarization: new molecules and patterns of gene expression. *J Immunol* **177,** 7303-7311.

Marwick JA, Adcock IM & Chung KF. (2010). Overcoming reduced glucocorticoid sensitivity in airway disease: molecular mechanisms and therapeutic approaches. *Drugs* **70,** 929-948.

Maródi L, Schreiber S, Anderson DC, MacDermott RP, Korchak HM & Johnston RB. (1993). Enhancement of macrophage candidacidal activity by interferon-gamma. Increased phagocytosis, killing, and calcium signal mediated by a decreased number of mannose receptors. *J Clin Invest* **91,** 2596-2601.

McHugh SM, Roman S, Davis B, Koch A, Pickett AM, Richardson JC, Miller SR, Wetten S, Cox CJ, Karpe F, Todd JA & Bullmore ET. (2012). Effects of genetic variation in the P2RX7 gene on pharmacodynamics of a P2X(7) receptor antagonist: a prospective genotyping approach. *Br J Clin Pharmacol* **74,** 376-380.

McIvor RA. (2015). Emerging therapeutic options for the treatment of patients with symptomatic asthma. *Ann Allergy Asthma Immunol*.

McNally BA, Somasundaram A, Yamashita M & Prakriya M. (2012). Gated regulation of CRAC channel ion selectivity by STIM1. *Nature* **482,** 241-245.

McNally BA, Yamashita M, Engh A & Prakriya M. (2009). Structural determinants of ion permeation in CRAC channels. *Proc Natl Acad Sci U S A* **106,** 22516-22521.

McNeil PL, Swanson JA, Wright SD, Silverstein SC & Taylor DL. (1986). Fc-receptor-mediated phagocytosis occurs in macrophages without an increase in average [Ca++]i. *J Cell Biol* **102,** 1586-1592.

Medic N, Desai A, Olivera A, Abramowitz J, Birnbaumer L, Beaven MA, Gilfillan AM & Metcalfe DD. (2013). Knockout of the Trpc1 gene reveals that TRPC1 can promote recovery from anaphylaxis by negatively regulating mast cell TNF-α production. *Cell Calcium* **53,** 315-326.

Mellor JD, Brown MP, Irving HR, Zalcberg JR & Dobrovic A. (2013). A critical review of the role of Fc gamma receptor polymorphisms in the response to monoclonal antibodies in cancer. *J Hematol Oncol* **6,** 1.

Mery L, Strauss B, Dufour JF, Krause KH & Hoth M. (2002). The PDZ-interacting domain of TRPC4 controls its localization and surface expression in HEK293 cells. *J Cell Sci* **115,** 3497-3508.

Metcalfe DD, Baram D & Mekori YA. (1997). Mast cells. *Physiol Rev* **77,** 1033-1079.

Michaelis M, Nieswandt B, Stegner D, Eilers J & Kraft R. (2015). STIM1, STIM2, and Orai1 regulate store-operated calcium entry and purinergic activation of microglia. *Glia* **63,** 652-663.

Mignen O, Thompson JL & Shuttleworth TJ. (2008). Orai1 subunit stoichiometry of the mammalian CRAC channel pore. *J Physiol* **586,** 419-425.

Miller M, Rosenthal P, Beppu A, Mueller JL, Hoffman HM, Tam AB, Doherty TA, McGeough MD, Pena CA, Suzukawa M, Niwa M & Broide DH. (2014). ORMDL3 transgenic mice have increased airway remodeling and airway responsiveness characteristic of asthma. *J Immunol* **192,** 3475-3487.

Miller M, Shi J, Zhu Y, Kustov M, Tian JB, Stevens A, Wu M, Xu J, Long S, Yang P, Zholos AV, Salovich JM, Weaver CD, Hopkins CR, Lindsley CW, McManus O, Li M & Zhu MX. (2011). Identification of ML204, a novel potent antagonist that selectively modulates native TRPC4/C5 ion channels. *J Biol Chem* **286,** 33436-33446.

Minke B & Cook B. (2002). TRP channel proteins and signal transduction. *Physiol Rev* **82,** 429-472.

Moffatt MF, Kabesch M, Liang L, Dixon AL, Strachan D, Heath S, Depner M, von Berg A, Bufe A, Rietschel E, Heinzmann A, Simma B, Frischer T, Willis-Owen SA, Wong KC, Illig T, Vogelberg C, Weiland SK, von Mutius E, Abecasis GR, Farrall M, Gut IG, Lathrop GM & Cookson WO. (2007). Genetic variants regulating ORMDL3 expression contribute to the risk of childhood asthma. *Nature* **448,** 470-473.

Monet M, Francoeur N & Boulay G. (2012). Involvement of phosphoinositide 3-kinase and PTEN protein in mechanism of activation of TRPC6 protein in vascular smooth muscle cells. *J Biol Chem* **287,** 17672-17681.

Montell C. (2005). TRP channels in Drosophila photoreceptor cells. *J Physiol* **567,** 45-51.

Montell C & Rubin GM. (1989). Molecular characterization of the Drosophila trp locus: a putative integral membrane protein required for phototransduction. *Neuron* **2,** 1313-1323.

Mortaz E, Braber S, Nazary M, Givi ME, Nijkamp FP & Folkerts G. (2009). ATP in the pathogenesis of lung emphysema. *European Journal of Pharmacology* **619,** 92-96.

Mosser DM. (2003). The many faces of macrophage activation. *Journal of Leukocyte Biology* **73,** 209-212.

Muik M, Frischauf I, Derler I, Fahrner M, Bergsmann J, Eder P, Schindl R, Hesch C, Polzinger B, Fritsch R, Kahr H, Madl J, Gruber H, Groschner K & Romanin C. (2008). Dynamic coupling of the putative coiled-coil domain of ORAI1 with STIM1 mediates ORAI1 channel activation. *J Biol Chem* **283,** 8014-8022.

Murgia M, Hanau S, Pizzo P, Rippa M & Di Virgilio F. (1993). Oxidized ATP. An irreversible inhibitor of the macrophage purinergic P2Z receptor. *J Biol Chem* **268,** 8199-8203.

Murray PJ & Wynn TA. (2011). Protective and pathogenic functions of macrophage subsets. *Nat Rev Immunol* **11,** 723-737.

Musson RA. (1983). Human monocyte maturation/differentiation during *in vitro* culture. *Surv Immunol Res* **2,** 246-251.

Nawa Y, Kiyota M, Korenaga M & Kotani M. (1985). Defective protective capacity of W/Wv mice against Strongyloides ratti infection and its reconstitution with bone marrow cells. *Parasite Immunol* **7,** 429-438.

Nelson DW, Gregg RJ, Kort ME, Perez-Medrano A, Voight EA, Wang Y, Grayson G, Namovic MT, Donnelly-Roberts DL, Niforatos W, Honore P, Jarvis MF, Faltynek CR & Carroll WA. (2006). Structure-activity relationship studies on a series of novel, substituted 1-benzyl-5-phenyltetrazole P2X7 antagonists. *J Med Chem* **49,** 3659-3666.

Ng LC, O'Neill KG, French D, Airey JA, Singer CA, Tian H, Shen XM & Hume JR. (2012). TRPC1 and Orai1 interact with STIM1 and mediate capacitative Ca(2+) entry caused by acute hypoxia in mouse pulmonary arterial smooth muscle cells. *Am J Physiol Cell Physiol* **303,** C1156-1172.

Ng SW, di Capite J, Singaravelu K & Parekh AB. (2008). Sustained activation of the tyrosine kinase Syk by antigen in mast cells requires local Ca2+ influx through Ca2+ release-activated Ca2+ channels. *J Biol Chem* **283,** 31348-31355.

Nicke A. (2008). Homotrimeric complexes are the dominant assembly state of native P2X7 subunits. *Biochem Biophys Res Commun* **377,** 803-808.

Nimmerjahn F & Ravetch JV. (2007). Fc-receptors as regulators of immunity. *Adv Immunol* **96,** 179-204.

Nimmerjahn F & Ravetch JV. (2008a). Fc gamma receptors as regulators of immune responses. *Nature Reviews Immunology* **8,** 34-47.

Nimmerjahn F & Ravetch JV. (2008b). Fcgamma receptors as regulators of immune responses. *Nat Rev Immunol* **8,** 34-47.

North RA. (2002). Molecular physiology of P2X receptors. *Physiol Rev* **82,** 1013-1067.

North RA & Jarvis MF. (2013). P2X receptors as drug targets. *Mol Pharmacol* **83,** 759-769.

North RA & Surprenant A. (2000). Pharmacology of cloned P2X receptors. *Annual Review of Pharmacology and Toxicology* **40,** 563-580.

Nunes P & Demaurex N. (2010). The role of calcium signaling in phagocytosis. In *J Leukoc Biol*, pp. 57-68. United States.

Nörenberg W, Sobottka H, Hempel C, Plötz T, Fischer W, Schmalzing G & Schaefer M. (2012). Positive allosteric modulation by ivermectin of human but not murine P2X7 receptors. *Br J Pharmacol* **167,** 48-66.

O'Neill LA, Golenbock D & Bowie AG. (2013). The history of Toll-like receptors - redefining innate immunity. *Nat Rev Immunol* **13,** 453-460.

Okada T, Inoue R, Yamazaki K, Maeda A, Kurosaki T, Yamakuni T, Tanaka I, Shimizu S, Ikenaka K, Imoto K & Mori Y. (1999). Molecular and functional characterization of a novel mouse transient receptor potential protein homologue TRP7. Ca(2+)-permeable cation channel that is constitutively activated and enhanced by stimulation of G protein-coupled receptor. *J Biol Chem* **274,** 27359-27370.

Okada T, Shimizu S, Wakamori M, Maeda A, Kurosaki T, Takada N, Imoto K & Mori Y. (1998). Molecular cloning and functional characterization of a novel receptor-activated TRP Ca2+ channel from mouse brain. *J Biol Chem* **273,** 10279-10287.

Okayama Y, Okumura S, Sagara H, Yuki K, Sasaki T, Watanabe N, Fueki M, Sugiyama K, Takeda K, Fukuda T, Saito H & Ra C. (2009). FcepsilonRI-mediated thymic stromal lymphopoietin production by interleukin-4-primed human mast cells. *Eur Respir J* **34,** 425-435.

Ong HL, Cheng KT, Liu X, Bandyopadhyay BC, Paria BC, Soboloff J, Pani B, Gwack Y, Srikanth S, Singh BB, Gill D & Ambudkar IS. (2007). Dynamic assembly of TRPC1-STIM1-Orai1 ternary complex is involved in store-operated calcium influx - Evidence for similarities in store-operated and calcium release-activated calcium channel components. *Journal of Biological Chemistry* **282**.

Ong HL, de Souza LB, Cheng KT & Ambudkar IS. (2014). Physiological functions and regulation of TRPC channels. *Handb Exp Pharmacol* **223,** 1005-1034.

Ong HL, de Souza LB, Zheng C, Cheng KT, Liu X, Goldsmith CM, Feske S & Ambudkar IS. (2015). STIM2 enhances receptor-stimulated Ca^{2+} signaling by promoting recruitment of STIM1 to the endoplasmic reticulum-plasma membrane junctions. *Sci Signal* **8,** ra3.

Oskeritzian CA, Zhao W, Min HK, Xia HZ, Pozez A, Kiev J & Schwartz LB. (2005). Surface CD88 functionally distinguishes the MCTC from the MCT type of human lung mast cell. *J Allergy Clin Immunol* **115,** 1162-1168.

Parekh AB & Penner R. (1997). Store depletion and calcium influx. *Physiol Rev* **77,** 901-930.

Parekh AB & Putney JW. (2005). Store-operated calcium channels. *Physiol Rev* **85,** 757-810.

Park CY, Hoover PJ, Mullins FM, Bachhawat P, Covington ED, Raunser S, Walz T, Garcia KC, Dolmetsch RE & Lewis RS. (2009). STIM1 clusters and activates CRAC channels via direct binding of a cytosolic domain to Orai1. *Cell* **136,** 876-890.

Peinelt C, Lis A, Beck A, Fleig A & Penner R. (2008). 2-Aminoethoxydiphenyl borate directly facilitates and indirectly inhibits STIM1-dependent gating of CRAC channels. *J Physiol* **586,** 3061-3073.

Peinelt C, Vig M, Koomoa DL, Beck A, Nadler MJS, Koblan-Huberson M, Lis A, Fleig A, Penner R & Kinet JP. (2006). Amplification of CRAC current by STIM1 and CRACM1 (Orai1). *Nature Cell Biology* **8,** 771-U231.

Pelegrin P & Surprenant A. (2006). Pannexin-1 mediates large pore formation and interleukin-1beta release by the ATP-gated P2X7 receptor. *EMBO J* **25,** 5071-5082.

Pelletier C, Varin-Blank N, Rivera J, Iannascoli B, Marchand F, David B, Weyer A & Blank U. (1998). Fc epsilon RI-mediated induction of TNF-alpha gene expression in the RBL-2H3 mast cell line: Regulation by a novel NF-kappa B-like nuclear binding complex. *J Immunol* **161,** 4768-4776.

Penna A, Demuro A, Yeromin AV, Zhang SYL, Safrina O, Parker I & Cahalan MD. (2008). The CRAC channel consists of a tetramer formed by Stim-induced dimerization of Orai dimers. *Nature* **456,** 116-U112.

Philipp S, Trost C, Warnat J, Rautmann J, Himmerkus N, Schroth G, Kretz O, Nastainczyk W, Cavalie A, Hoth M & Flockerzi V. (2000). TRP4 (CCE1) protein is part of native calcium release-activated Ca2+-like channels in adrenal cells. *J Biol Chem* **275,** 23965-23972.

Piccini A, Carta S, Tassi S, Lasiglié D, Fossati G & Rubartelli A. (2008). ATP is released by monocytes stimulated with pathogen-sensing receptor ligands and induces IL-1beta and IL-18 secretion in an autocrine way. *Proc Natl Acad Sci U S A* **105,** 8067-8072.

Putney JW. (2004). The enigmatic TRPCs: multifunctional cation channels. *Trends Cell Biol* **14,** 282-286.

Putney JW. (2010). Pharmacology of store-operated calcium channels. *Mol Interv* **10,** 209-218.

Py BF, Jin M, Desai BN, Penumaka A, Zhu H, Kober M, Dietrich A, Lipinski MM, Henry T, Clapham DE & Yuan J. (2014). Caspase-11 controls interleukin-1β release through degradation of TRPC1. *Cell Rep* **6,** 1122-1128.

Qu Y, Franchi L, Nunez G & Dubyak GR. (2007). Nonclassical IL-1 beta secretion stimulated by P2X7 receptors is dependent on inflammasome activation and correlated with exosome release in murine macrophages. *J Immunol* **179,** 1913-1925.

Qu Y, Misaghi S, Newton K, Gilmour LL, Louie S, Cupp JE, Dubyak GR, Hackos D & Dixit VM. (2011). Pannexin-1 is required for ATP release during apoptosis but not for inflammasome activation. *J Immunol* **186,** 6553-6561.

Rana A, Yen M, Sadaghiani AM, Malmersjö S, Park CY, Dolmetsch RE & Lewis RS. (2015). Alternative splicing converts STIM2 from an activator to an inhibitor of store-operated calcium channels. *J Cell Biol* **209,** 653-669.

Rassendren F, Buell GN, Virginio C, Collo G, North RA & Surprenant A. (1997). The permeabilizing ATP receptor, P2X7. Cloning and expression of a human cDNA. *J Biol Chem* **272,** 5482-5486.

Reynolds G & Haniffa M. (2015). Human and Mouse Mononuclear Phagocyte Networks: A Tale of Two Species? *Front Immunol* **6,** 330.

Ricciotti E & FitzGerald GA. (2011). Prostaglandins and inflammation. *Arterioscler Thromb Vasc Biol* **31,** 986-1000.

Rice LV, Bax HJ, Russell LJ, Barrett VJ, Walton SE, Deakin AM, Thomson SA, Lucas F, Solari R, House D & Begg M. (2013). Characterization of selective Calcium-Release Activated Calcium channel blockers in mast cells and T-cells from human, rat, mouse and guinea-pig preparations. *European Journal of Pharmacology* **704,** 49-57.

Richter JM, Schaefer M & Hill K. (2014). Clemizole hydrochloride is a novel and potent inhibitor of transient receptor potential channel TRPC5. *Mol Pharmacol* **86,** 514-521.

Rivera J & Gilfillan AM. (2006). Molecular regulation of mast cell activation. *Journal of Allergy and Clinical Immunology* **117,** 1214-1225.

Roos J, DiGregorio PJ, Yeromin AV, Ohlsen K, Lioudyno M, Zhang SY, Safrina O, Kozak JA, Wagner SL, Cahalan MD, Velicelebi G & Stauderman KA. (2005). STIM1, an essential and conserved component of store-operated Ca2+ channel function. *Journal of Cell Biology* **169,** 435-445.

Rubel C, Miliani De Marval P, Vermeulen M, Isturiz MA & Palermo MS. (1999). Lipopolysaccharide enhances FcgammaR-dependent functions *in vivo* through CD11b/CD18 up-regulation. *Immunology* **97,** 429-437.

Saitoh S, Arudchandran R, Manetz TS, Zhang W, Sommers CL, Love PE, Rivera J & Samelson LE. (2000). LAT is essential for Fc(epsilon)RI-mediated mast cell activation. *Immunity* **12,** 525-535.

Salmon JE, Kapur S & Kimberly RP. (1987). Opsonin-independent ligation of Fc gamma receptors. The 3G8-bearing receptors on neutrophils mediate the phagocytosis of concanavalin A-treated erythrocytes and nonopsonized Escherichia coli. *J Exp Med* **166,** 1798-1813.

Sanchez-Miranda E, Ibarra-Sanchez A & Gonzalez-Espinosa C. (2010). Fyn kinase controls FcepsilonRI receptor-operated calcium entry necessary for full degranulation in mast cells. *Biochem Biophys Res Commun* **391,** 1714-1720.

Sanmugalingam D, Wardlaw AJ & Bradding P. (2000). Adhesion of human lung mast cells to bronchial epithelium: evidence for a novel carbohydrate-mediated mechanism. *J Leukoc Biol* **68,** 38-46.

Saunders BM, Fernando SL, Sluyter R, Britton WJ & Wiley JS. (2003). A loss-of-function polymorphism in the human P2X7 receptor abolishes ATP-mediated killing of mycobacteria. *J Immunol* **171,** 5442-5446.

Schaefer M, Plant TD, Obukhov AG, Hofmann T, Gudermann T & Schultz G. (2000). Receptor-mediated regulation of the nonselective cation channels TRPC4 and TRPC5. *J Biol Chem* **275,** 17517-17526.

Schleifer H, Doleschal B, Lichtenegger M, Oppenrieder R, Derler I, Frischauf I, Glasnov TN, Kappe CO, Romanin C & Groschner K. (2012). Novel pyrazole compounds for

pharmacological discrimination between receptor-operated and store-operated Ca(2+) entry pathways. *Br J Pharmacol* **167,** 1712-1722.

Schneider C, Nobs SP, Kurrer M, Rehrauer H, Thiele C & Kopf M. (2014). Induction of the nuclear receptor PPAR-γ by the cytokine GM-CSF is critical for the differentiation of fetal monocytes into alveolar macrophages. *Nat Immunol* **15,** 1026-1037.

Schroder K, Hertzog PJ, Ravasi T & Hume DA. (2004). Interferon-gamma: an overview of signals, mechanisms and functions. *J Leukoc Biol* **75,** 163-189.

Sel S, Rost BR, Yildirim AO, Sel B, Kalwa H, Fehrenbach H, Renz H, Gudermann T & Dietrich A. (2008). Loss of classical transient receptor potential 6 channel reduces allergic airway response. *Clinical and Experimental Allergy* **38,** 1548-1558.

Sellge G, Barkowsky M, Kramer S, Gebhardt T, Sander LE, Lorentz A & Bischoff SC. (2014). Interferon-gamma regulates growth and controls Fc gamma receptor expression and activation in human intestinal mast cells. *Bmc Immunology* **15**.

Seo K, Rainer PP, Hahn VS, Lee D-i, Jo S-H, Andersen A, Liu T, Xu X, Willette RN, Lepore JJ, Marino JP, Jr., Birnbaumer L, Schnackenberg CG & Kass DA. (2014a). Combined TRPC3 and TRPC6 blockade by selective small-molecule or genetic deletion inhibits pathological cardiac hypertrophy. *Proceedings of the National Academy of Sciences of the United States of America* **111,** 1551-1556.

Seo K, Rainer PP, Shalkey Hahn V, Lee DI, Jo SH, Andersen A, Liu T, Xu X, Willette RN, Lepore JJ, Marino JP, Birnbaumer L, Schnackenberg CG & Kass DA. (2014b). Combined TRPC3 and TRPC6 blockade by selective small-molecule or genetic deletion inhibits pathological cardiac hypertrophy. *Proc Natl Acad Sci U S A* **111,** 1551-1556.

Shi J, Mori E, Mori Y, Mori M, Li J, Ito Y & Inoue R. (2004). Multiple regulation by calcium of murine homologues of transient receptor potential proteins TRPC6 and TRPC7 expressed in HEK293 cells. *J Physiol* **561,** 415-432.

Shim AH, Tirado-Lee L & Prakriya M. (2015). Structural and functional mechanisms of CRAC channel regulation. *J Mol Biol* **427,** 77-93.

Siraganian R. (1975). Refinements in automated fluorometric histamine analysis system. *J Immunol Methods* **7,** 283-289.

Smart ML, Gu B, Panchal RG, Wiley J, Cromer B, Williams DA & Petrou S. (2003). P2X7 receptor cell surface expression and cytolytic pore formation are regulated by a distal C-terminal region. *J Biol Chem* **278,** 8853-8860.

Smrž D, Bandara G, Beaven MA, Metcalfe DD & Gilfillan AM. (2013). Prevention of F-actin assembly switches the response to SCF from chemotaxis to degranulation in human mast cells. *Eur J Immunol* **43,** 1873-1882.

Smyth JT, Hwang SY, Tomita T, DeHaven WI, Mercer JC & Putney JW. (2010). Activation and regulation of store-operated calcium entry. In *J Cell Mol Med*, pp. 2337-2349. No claim to original US government works Journal compilation 2010 Foundation for Cellular and Molecular Medicine/Blackwell Publishing Ltd., England.

Soboloff J, Spassova MA, Dziadek MA & Gill DL. (2006a). Calcium signals mediated by STIM and Orai proteins--a new paradigm in inter-organelle communication. *Biochim Biophys Acta* **1763,** 1161-1168.

Soboloff J, Spassova MA, Hewavitharana T, He LP, Xu W, Johnstone LS, Dziadek MA & Gill DL. (2006b). STIM2 is an inhibitor of STIM1-mediated store-operated Ca2+ Entry. *Curr Biol* **16,** 1465-1470.

Solle M, Labasi J, Perregaux DG, Stam E, Petrushova N, Koller BH, Griffiths RJ & Gabel CA. (2001). Altered cytokine production in mice lacking P2X(7) receptors. *Journal of Biological Chemistry* **276,** 125-132.

Soltoff SP, McMillian MK & Talamo BR. (1989). Coomassie Brilliant Blue G is a more potent antagonist of P2 purinergic responses than Reactive Blue 2 (Cibacron Blue 3GA) in rat parotid acinar cells. *Biochem Biophys Res Commun* **165,** 1279-1285.

Sperlágh B, Haskó G, Németh Z & Vizi ES. (1998). ATP released by LPS increases nitric oxide production in raw 264.7 macrophage cell line via P2Z/P2X7 receptors. *Neurochem Int* **33,** 209-215.

Stathopulos PB, Zheng L, Li GY, Plevin MJ & Ikura M. (2008). Structural and mechanistic insights into STIM1-mediated initiation of store-operated calcium entry. *Cell* **135,** 110-122.

Steinberg BE, Huynh KK & Grinstein S. (2007). Phagosomal acidification: measurement, manipulation and functional consequences. *Biochem Soc Trans* **35,** 1083-1087.

Steinckwich N, Schenten V, Melchior C, Bréchard S & Tschirhart EJ. (2011). An essential role of STIM1, Orai1, and S100A8-A9 proteins for Ca2+ signaling and FcγR-mediated phagosomal oxidative activity. *J Immunol* **186,** 2182-2191.

Stenmark H. (2009). Rab GTPases as coordinators of vesicle traffic. *Nat Rev Mol Cell Biol* **10,** 513-525.

Stokes AJ, Shimoda LM, Koblan-Huberson M, Adra CN & Turner H. (2004). A TRPV2-PKA signaling module for transduction of physical stimuli in mast cells. *J Exp Med* **200,** 137-147.

Storch U, Forst AL, Philipp M, Gudermann T & Schnitzler MMY. (2012). Transient Receptor Potential Channel 1 (TRPC1) Reduces Calcium Permeability in Heteromeric Channel Complexes. *Journal of Biological Chemistry* **287,** 3530-3540.

Surprenant A, Rassendren F, Kawashima E, North RA & Buell G. (1996). The cytolytic P-2Z receptor for extracellular ATP identified as a P-2X receptor (P2X(7)). *Science* **272,** 735-738.

Suurmond J, Dorjée AL, Knol EF, Huizinga TW & Toes RE. (2015). Differential TLR-induced cytokine production by human mast cells is amplified by FcεRI triggering. *Clin Exp Allergy* **45,** 788-796.

Suzuki R, Liu X, Olivera A, Aguiniga L, Yamashita Y, Blank U, Ambudkar I & Rivera J. (2010a). Loss of TRPC1-mediated Ca2+ influx contributes to impaired degranulation in Fyn-deficient mouse bone marrow-derived mast cells. *Journal of Leukocyte Biology* **88,** 863-875.

Suzuki R, Liu X, Olivera A, Aguiniga L, Yamashita Y, Blank U, Ambudkar I & Rivera J. (2010b). Loss of TRPC1-mediated Ca2+ influx contributes to impaired degranulation in Fyn-deficient mouse bone marrow-derived mast cells. In *J Leukoc Biol*, pp. 863-875. United States.

Sweeney ZK, Minatti A, Button DC & Patrick S. (2009). Small-molecule inhibitors of store-operated calcium entry. *ChemMedChem* **4,** 706-718.

Tang J, Lin Y, Zhang Z, Tikunova S, Birnbaumer L & Zhu MX. (2001). Identification of common binding sites for calmodulin and inositol 1,4,5-trisphosphate receptors on the carboxyl termini of trp channels. *J Biol Chem* **276,** 21303-21310.

Taylor PR, Martinez-Pomares L, Stacey M, Lin HH, Brown GD & Gordon S. (2005). Macrophage receptors and immune recognition. In *Annual Review of Immunology*, pp. 901-944. Annual Reviews, Palo Alto.

Thiel M, Lis A & Penner R. (2013). STIM2 drives Ca2+ oscillations through store-operated Ca2+ entry caused by mild store depletion. *J Physiol* **591,** 1433-1445.

Thompson JL & Shuttleworth TJ. (2013). How many Orai's does it take to make a CRAC channel? *Sci Rep* **3,** 1961.

Torres GE, Egan TM & Voigt MM. (1999). Hetero-oligomeric assembly of P2X receptor subunits. Specificities exist with regard to possible partners. *J Biol Chem* **274,** 6653-6659.

Tsien RY, Rink TJ & Poenie M. (1985). Measurement of cytosolic free Ca2+ in individual small cells using fluorescence microscopy with dual excitation wavelengths. *Cell Calcium* **6,** 145-157.

Tsiokas L. (2009). Function and regulation of TRPP2 at the plasma membrane. *Am J Physiol Renal Physiol* **297,** F1-9.

Uehara K. (2005). Localization of TRPC1 channel in the sinus endothelial cells of rat spleen. *Histochem Cell Biol* **123,** 347-356.

Vaeth M, Zee I, Concepcion AR, Maus M, Shaw P, Portal-Celhay C, Zahra A, Kozhaya L, Weidinger C, Philips J, Unutmaz D & Feske S. (2015). Ca2+ Signaling but Not Store-Operated Ca2+ Entry Is Required for the Function of Macrophages and Dendritic Cells. *J Immunol*.

Vallabhapurapu S & Karin M. (2009). Regulation and function of NF-kappaB transcription factors in the immune system. *Annu Rev Immunol* **27,** 693-733.

van der Laan LJ, Döpp EA, Haworth R, Pikkarainen T, Kangas M, Elomaa O, Dijkstra CD, Gordon S, Tryggvason K & Kraal G. (1999). Regulation and functional involvement

of macrophage scavenger receptor MARCO in clearance of bacteria *in vivo*. *J Immunol* **162,** 939-947.

Vannier B, Peyton M, Boulay G, Brown D, Qin N, Jiang M, Zhu X & Birnbaumer L. (1999). Mouse trp2, the homologue of the human trpc2 pseudogene, encodes mTrp2, a store depletion-activated capacitative Ca2+ entry channel. *Proc Natl Acad Sci U S A* **96,** 2060-2064.

Venkatachalam K & Montell C. (2007). TRP channels. *Annu Rev Biochem* **76,** 387-417.

Venkatachalam K, Zheng F & Gill DL. (2003). Regulation of canonical transient receptor potential (TRPC) channel function by diacylglycerol and protein kinase C. *J Biol Chem* **278,** 29031-29040.

Vennekens R & Nilius B. (2007). Insights into TRPM4 function, regulation and physiological role. *Handb Exp Pharmacol***,** 269-285.

Verma S, Hoffmann FW, Kumar M, Huang Z, Roe K, Nguyen-Wu E, Hashimoto AS & Hoffmann PR. (2011). Selenoprotein K knockout mice exhibit deficient calcium flux in immune cells and impaired immune responses. *J Immunol* **186,** 2127-2137.

Verreck FA, de Boer T, Langenberg DM, Hoeve MA, Kramer M, Vaisberg E, Kastelein R, Kolk A, de Waal-Malefyt R & Ottenhoff TH. (2004). Human IL-23-producing type 1 macrophages promote but IL-10-producing type 2 macrophages subvert immunity to (myco)bacteria. *Proc Natl Acad Sci U S A* **101,** 4560-4565.

Vig M, Beck A, Billingsley JM, Lis A, Parvez S, Peinelt C, Koomoa DL, Soboloff J, Gill DL, Fleig A, Kinet JP & Penner R. (2006a). CRACM1 multimers form the ion-selective pore of the CRAC channel. *Current Biology* **16,** 2073-2079.

Vig M & Kinet JP. (2009). Calcium signaling in immune cells. *Nat Immunol* **10,** 21-27.

Vig M, Peinelt C, Beck A, Koomoa DL, Rabah D, Koblan-Huberson M, Kraft S, Turner H, Fleig A, Penner R & Kinet JP. (2006b). CRACM1 is a plasma membrane protein essential for store-operated Ca2+ entry. *Science* **312,** 1220-1223.

Virginio C, Church D, North RA & Surprenant A. (1997). Effects of divalent cations, protons and calmidazolium at the rat P2X7 receptor. *Neuropharmacology* **36,** 1285-1294.

Virginio C, North RA & Surprenant A. (1998). Calcium permeability and block at homomeric and heteromeric P2X2 and P2X3 receptors, and P2X receptors in rat nodose neurones. *J Physiol* **510 (Pt 1),** 27-35.

Vogel DY, Glim JE, Stavenuiter AW, Breur M, Heijnen P, Amor S, Dijkstra CD & Beelen RH. (2014). Human macrophage polarization *in vitro*: maturation and activation methods compared. *Immunobiology* **219,** 695-703.

Vogelpoel LT, Baeten DL, de Jong EC & den Dunnen J. (2015). Control of cytokine production by human fc gamma receptors: implications for pathogen defense and autoimmunity. *Front Immunol* **6,** 79.

Wang J, Chen Y, Lin C, Jia J, Tian L, Yang K, Zhao L, Lai N, Jiang Q, Sun Y, Zhong N, Ran P & Lu W. (2014a). Effects of chronic exposure to cigarette smoke on canonical transient receptor potential expression in rat pulmonary arterial smooth muscle. *Am J Physiol Cell Physiol* **306,** C364-373.

Wang S, Zhao J, Wang H, Liang Y, Yang N & Huang Y. (2015). Blockage of P2X7 attenuates acute lung injury in mice by inhibiting NLRP3 inflammasome. *Int Immunopharmacol* **27,** 38-45.

Wang X, Wang Y, Zhou Y, Hendron E, Mancarella S, Andrake MD, Rothberg BS, Soboloff J & Gill DL. (2014b). Distinct Orai-coupling domains in STIM1 and STIM2 define the Orai-activating site. *Nat Commun* **5,** 3183.

Wareham K, Vial C, Wykes RCE, Bradding P & Seward EP. (2009). Functional evidence for the expression of P2X1, P2X4 and P2X7 receptors in human lung mast cells. *Br J Pharmacol* **157,** 1215-1224.

Washburn DG, Holt DA, Dodson J, McAtee JJ, Terrell LR, Barton L, Manns S, Waszkiewicz A, Pritchard C, Gillie DJ, Morrow DM, Davenport EA, Lozinskaya IM, Guss J, Basilla JB, Negron LK, Klein M, Willette RN, Fries RE, Jensen TC, Xu X, Schnackenberg CG & Marino JP, Jr. (2013). The discovery of potent blockers of the canonical transient receptor channels, TRPC3 and TRPC6, based on an anilino-thiazole pharmacophore. *Bioorganic & Medicinal Chemistry Letters* **23,** 4979-4984.

Webb TE, Simon J, Krishek BJ, Bateson AN, Smart TG, King BF, Burnstock G & Barnard EA. (1993). Cloning and functional expression of a brain G-protein-coupled ATP receptor. *FEBS Lett* **324,** 219-225.

Weinstein AG. (2015). Improving adherence to asthma therapies. *Curr Opin Pulm Med* **21,** 86-94.

Wen RR, Jou ST, Chen YH, Hoffmeyer A & Wang DM. (2002). Phospholipase C gamma 2 is essential for specific functions of Fc epsilon R and Fc gamma R. *Journal of Immunology* **169,** 6743-6752.

Wijngaarden S, van de Winkel JG, Bijlsma JW, Lafeber FP & van Roon JA. (2008). Treatment of rheumatoid arthritis patients with anti-TNF-alpha monoclonal antibody is accompanied by down-regulation of the activating Fcgamma receptor I on monocytes. *Clin Exp Rheumatol* **26,** 89-95.

Wiley JS, Dao-Ung LP, Li C, Shemon AN, Gu BJ, Smart ML, Fuller SJ, Barden JA, Petrou S & Sluyter R. (2003). An Ile-568 to Asn polymorphism prevents normal trafficking and function of the human P2X7 receptor. *J Biol Chem* **278,** 17108-17113.

Winn MP, Conlon PJ, Lynn KL, Farrington MK, Creazzo T, Hawkins AF, Daskalakis N, Kwan SY, Ebersviller S, Burchette JL, Pericak-Vance MA, Howell DN, Vance JM & Rosenberg PB. (2005). A mutation in the TRPC6 cation channel causes familial focal segmental glomerulosclerosis. *Science* **308,** 1801-1804.

Woodbury RG, Miller HR, Huntley JF, Newlands GF, Palliser AC & Wakelin D. (1984). Mucosal mast cells are functionally active during spontaneous expulsion of intestinal nematode infections in rat. *Nature* **312,** 450-452.

Wu X, Eder P, Chang B & Molkentin JD. (2010). TRPC channels are necessary mediators of pathologic cardiac hypertrophy. *Proc Natl Acad Sci U S A* **107,** 7000-7005.

Wykes RCE, Lee M, Duffy SM, Yang W, Seward EP & Bradding P. (2007). Functional transient receptor potential melastatin 7 channels are critical for human mast cell survival. *J Immunol* **179,** 4045-4052.

Wynn TA, Chawla A & Pollard JW. (2013). Macrophage biology in development, homeostasis and disease. *Nature* **496,** 445-455.

Xiang Z & Burnstock G. (2005). Expression of P2X receptors on rat microglial cells during early development. *Glia* **52,** 119-126.

Xu L, Chen Y, Yang K, Wang Y, Tian L, Zhang J, Wang EW, Sun D, Lu W & Wang J. (2014). Chronic hypoxia increases TRPC6 expression and basal intracellular Ca2+ concentration in rat distal pulmonary venous smooth muscle. *PLoS One* **9,** e112007.

Xu S, Huo J, Lee KG, Kurosaki T & Lam KP. (2009). Phospholipase Cgamma2 is critical for Dectin-1-mediated Ca2+ flux and cytokine production in dendritic cells. *J Biol Chem* **284,** 7038-7046.

Xu SZ & Beech DJ. (2001). TrpC1 is a membrane-spanning subunit of store-operated Ca(2+) channels in native vascular smooth muscle cells. *Circ Res* **88,** 84-87.

Yarova PL, Stewart AL, Sathish V, Britt RD, Thompson MA, P Lowe AP, Freeman M, Aravamudan B, Kita H, Brennan SC, Schepelmann M, Davies T, Yung S, Cholisoh Z, Kidd EJ, Ford WR, Broadley KJ, Rietdorf K, Chang W, Bin Khayat ME, Ward DT, Corrigan CJ, T Ward JP, Kemp PJ, Pabelick CM, Prakash YS & Riccardi D. (2015). Calcium-sensing receptor antagonists abrogate airway hyperresponsiveness and inflammation in allergic asthma. *Sci Transl Med* **7,** 284ra260.

Ye Y, Huang X, Zhang Y, Lai X, Wu X, Zeng X, Tang X & Zeng Y. (2012a). Calcium influx blocked by SK&F 96365 modulates the LPS plus IFN-gamma-induced inflammatory response in murine peritoneal macrophages. *International Immunopharmacology* **12,** 384-393.

Ye Y, Huang X, Zhang Y, Lai X, Wu X, Zeng X, Tang X & Zeng Y. (2012b). Calcium influx blocked by SK&F 96365 modulates the LPS plus IFN-γ-induced inflammatory response in murine peritoneal macrophages. *Int Immunopharmacol* **12,** 384-393.

Yeromin AV, Zhang SL, Jiang W, Yu Y, Safrina O & Cahalan MD. (2006). Molecular identification of the CRAC channel by altered ion selectivity in a mutant of Orai. *Nature* **443,** 226-229.

Yildirim E, Carey MA, Card JW, Dietrich A, Flake GP, Zhang Y, Bradbury JA, Rebolloso Y, Germolec DR, Morgan DL, Zeldin DC & Birnbaumer L. (2012). Severely blunted allergen-induced pulmonary Th2 cell response and lung hyperresponsiveness in

type 1 transient receptor potential channel-deficient mice. *American Journal of Physiology-Lung Cellular and Molecular Physiology* **303,** L539-L549.

Young JD, Ko SS & Cohn ZA. (1984). The increase in intracellular free calcium associated with IgG gamma 2b/gamma 1 Fc receptor-ligand interactions: role in phagocytosis. *Proc Natl Acad Sci U S A* **81,** 5430-5434.

Yuan JP, Zeng W, Huang GN, Worley PF & Muallem S. (2007). STIM1 heteromultimerizes TRPC channels to determine their function as store-operated channels. *Nature Cell Biology* **9**.

Zagranichnaya TK, Wu XY & Villereal ML. (2005). Endogenous TRPC1, TRPC3, and TRPC7 proteins combine to form native store-operated channels in HEK-293 cells. *Journal of Biological Chemistry* **280**.

Zanoni I & Granucci F. (2012). Regulation and dysregulation of innate immunity by NFAT signaling downstream of pattern recognition receptors (PRRs). *Eur J Immunol* **42,** 1924-1931.

Zeng WZ, Yuan JP, Kim MS, Choi YJ, Huang GN, Worley PF & Muallem S. (2008). STIM1 Gates TRPC Channels, but Not Orai1, by Electrostatic Interaction. *Mol Cell* **32,** 439-448.

Zhang D, Spielmann A, Wang L, Ding G, Huang F, Gu Q & Schwarz W. (2012). Mast-cell degranulation induced by physical stimuli involves the activation of transient-receptor-potential channel TRPV2. *Physiol Res* **61,** 113-124.

Zhang SL, Yeromin AV, Zhang XH, Yu Y, Safrina O, Penna A, Roos J, Stauderman KA & Cahalan MD. (2006). Genome-wide RNAi screen of Ca(2+) influx identifies genes that regulate Ca(2+) release-activated Ca(2+) channel activity. *Proc Natl Acad Sci U S A* **103,** 9357-9362.

Zhang SL, Yu Y, Roos J, Kozak JA, Deerinck TJ, Ellisman MH, Stauderman KA & Cahalan MD. (2005). STIM1 is a Ca2+ sensor that activates CRAC channels and migrates from the Ca2+ store to the plasma membrane. *Nature* **437,** 902-905.

Zhou Y, Meraner P, Kwon HT, Machnes D, Oh-hora M, Zimmer J, Huang Y, Stura A, Rao A & Hogan PG. (2010). STIM1 gates the store-operated calcium channel ORAI1 *in vitro*. *Nat Struct Mol Biol* **17,** 112-116.

Zhu X, Chu PB, Peyton M & Birnbaumer L. (1995). Molecular cloning of a widely expressed human homologue for the Drosophila trp gene. *FEBS Lett* **373,** 193-198.

Zhu X, Jiang M, Peyton M, Boulay G, Hurst R, Stefani E & Birnbaumer L. (1996). trp, a novel mammalian gene family essential for agonist-activated capacitative Ca2+ entry. *Cell* **85,** 661-671.

Ziegler SF, Roan F, Bell BD, Stoklasek TA, Kitajima M & Han H. (2013). The biology of thymic stromal lymphopoietin (TSLP). *Adv Pharmacol* **66,** 129-155.

Zimmerli S, Majeed M, Gustavsson M, Stendahl O, Sanan DA & Ernst JD. (1996). Phagosome-lysosome fusion is a calcium-independent event in macrophages. *J Cell Biol* **132,** 49-61.

Zitt C, Obukhov AG, Strübing C, Zobel A, Kalkbrenner F, Lückhoff A & Schultz G. (1997). Expression of TRPC3 in Chinese hamster ovary cells results in calcium-activated cation currents not related to store depletion. *J Cell Biol* **138,** 1333-1341.

Zitt C, Zobel A, Obukhov AG, Harteneck C, Kalkbrenner F, Lückhoff A & Schultz G. (1996). Cloning and functional expression of a human Ca2+-permeable cation channel activated by calcium store depletion. *Neuron* **16,** 1189-1196.

ZWEIFACH A & LEWIS R. (1995). SLOW CALCIUM-DEPENDENT INACTIVATION OF DEPLETION-ACTIVATED CALCIUM CURRENT - STORE-DEPENDENT AND STORE-INDEPENDENT MECHANISMS. *Journal of Biological Chemistry* **270,** 14445-14451.